THE UNIVERSITY OF
SYDNEY

The Role of HOSCN in the Oxidation of Proteins and Cellular Damage in Atherosclerosis

Dominic Thomas Love

A thesis submitted in fulfilment of the requirements for the award of the degree of Doctor of Philosophy

November 2015

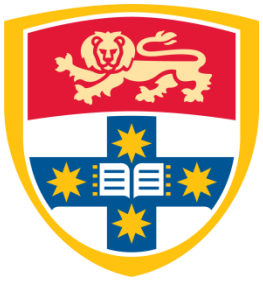

THE UNIVERSITY OF SYDNEY

Declaration

The work contained in this Thesis is original work conducted by the author at the Heart Research Institute and The University of Sydney. It has not been submitted to any other institution for a higher degree and does not contain any materials previously published or written by another person, except where due reference is made in the text.

Dominic Thomas Love BSc (Biology) (Hons)

“The risk I took was calculated, but man, am I bad at math.”

Author, Unknown.

Acknowledgements

First and foremost, none of this could have been done without Professor Clare Hawkins. Clare, for the past three and a half years, you've been a mentor, a role-model and a boss, but most importantly, you've been a friend. Thank you for listening to me ramble about nothing for hours, upon hours over the course of this project and thanks for laughing with me too. Your ideas, input and help is what made this project possible. If I can be half the scientist you are, then I'll be proud. Thank you for taking a chance on me to be your student.

Dr. David Pattison, thank you for all your help over the past three and a half years, but most importantly, thanks for your easy going nature, working with you made hard times seem easier. Thanks for laughing with me when no-one else thought it was appropriate to laugh. Not only that, but your knowledge about all things chemistry got me through some of the hardest parts of my project, and without that, I'd probably be a bumbling mess.

I want to say thanks to Professor Michael Davies, thank you for your insight that has, on more than one occasion, turned a failing experiment into a success. Thank you for your help and guidance.

I also want to thank everyone at the Heart Research Institute, for taking me in and always making me feel welcome. Thank you to all the people in fundraising for making all the crazy experiments come to life. Thank you to everyone in the Inflammation group and the Free Radical group; you've all become my family over these past three and a half years.

To Dr. Liz Carter and Dr. Joon Lee, thanks for putting up with me during the last legs of my Thesis, I really appreciate the friendship and help you've both given to me. I owe you both coffees.

Mum and Dad, I don't have enough space to write everything I have to thank you for. You two are awesome, and even though I haven't lived with you in years, it feels like you're still raising me. Thanks for all the dinners, and lunches, and groceries. I love you both, and hopefully you'll still buy groceries for me. Jordy, you're meant to be my younger brother, but for the past few years I've felt like you're the eldest, mainly because you've grown taller than me, but also because you drive me into work when I can't be bothered to catch the train. Thanks for all your support.

Finally, my best friend in the whole wide world, to the moon and back, forever and ever. Fuki, you've been nothing less than supportive these past three years and I owe you so much.

I can’t put into words how much you’ve helped me get through this; this PhD is as much yours as it is mine. Thank you, I love you.

Abstract

Myeloperoxidase (MPO) forms the reactive oxidants hypochlorous acid (HOCl) and hypothiocyanous acid (HOSCN) in inflammatory environments *in vivo*. HOCl is highly reactive, causing extensive damage to biomolecules and has been implicated in the progression of numerous inflammatory conditions. In contrast, HOSCN reacts preferentially with protein thiols, and can form a number of reversibly oxidised products. The targeting of thiols can lead to protein inactivation and inhibition, which has led to HOSCN being implicated in the alteration of cellular redox signaling pathways. Gaining an understanding of the reactivity of HOSCN *in vivo* has been limited by the lack of a specific biomarker for this oxidant. Indirect evidence supports a role of HOSCN in promoting inflammation and disease. However, the role of HOSCN in biological systems is currently debated, with evidence also for a protective role of this oxidant, preventing cellular damage from MPO by removal of the more damaging HOCl.

The studies in Chapter 3 compare the ability of both HOCl and HOSCN to form reversibly oxidsed cysteine products in J774A.1 macrophages after treatment. In these studies, the ability of these oxidants to reduce the intracellular thiol pool was examined using the fluorescent thiol probe, ThioGlo-1, where it was shown that HOSCN depleted cellular thiols to a greater extent than HOCl under comparable conditions. Evidence for reversible protein thiol modification in macrophages exposed to HOSCN but not HOCl, was obtained using the thiol alkylating agent 5-iodoacetamidofluorescein (IAF), which was supported by studies with sulfenic acid probes and antibodies recognizing glutathionylated proteins. In contrast, HOCl is believed to form irreversible cysteine oxidation products. Subcellular fractionation studies revealed that HOSCN targeted thiol-containing proteins in both the cytosol and mitochondria on exposure to macrophages.

HOSCN is a bacteriostatic agent, inhibiting bacterial cell growth and proliferation, and its ability to inhibit these bacterial processes is attributed to its action on the glycolytic pathways. Studies on isolated proteins and in vitro have linked HOSCN with the inactivation of proteins such as glyceraldehyde 3-phosphate dehydrogenase (GAPDH) and creatine kinase (CK), which are involved in metabolism of glucose in mammalian cells. Chapter 4 explored the functional effects of HOSCN-induced oxidation of J774A.1 macrophages on the glycolytic pathway. Exposure of cells to HOSCN resulted in the inhibition of glycolysis as determined by a functional glycolysis assay using the Seahorse XF bioanalyser and by assaying the glycolytic end-product, lactate. The results of this Chapter also showed that the inhibition of glycolysis

was not due to an inhibitory effect on the glucose uptake proteins, or because of a reduction in cell viability, but was consistent with HOSCN-induced targeting and oxidation of proteins involved in glycolysis, including GAPDH, aldolase and triosephosphate isomerase.

The experiments performed in Chapter 5 studied the effects of mitochondrial thiol oxidation and the reduced substrate formation from glycolysis on mitochondrial respiration. Exposure of macrophages to HOSCN resulted in a significant loss in mitochondrial respiration, and changes consistent with damage to the electron transport chain. Moreover, HOSCN induced a loss in mitochondrial membrane permeability and reduction in intracellular ATP concentration, which could be mitigated to some extent by pre-treatment with the mitochondrial permeability transition inhibitor cyclosporin A.

In Chapters 6 and 7, Fourier transform infra-red spectroscopy (FTIR) and Raman spectroscopy were employed as a novel and alternate method to quantify and visualise the oxidative damage caused by HOSCN and HOCl in J774A.1 cells. The results of these studies determined that HOSCN and HOCl, collectively, were able to interact with a multitude of biomolecules including proteins, lipids and nucleic acids. These studies also corroborated data from the previous Chapters, by showing that HOSCN influenced the intracellular concentrations and locations of carbohydrates, glucose, lactate and NADH, a by-product of glycolysis.

In summary, the studies of this Thesis provide valuable information relating to the action and functional effect of HOSCN on the targeting and oxidation products formed on cellular proteins in macrophages, particularly mitochondrial proteins and proteins involved in the metabolism of glucose and production of ATP. The observation that HOSCN has a significant role in the inhibition of key cellular bioenergetic processes provides new insight into the potential role of HOSCN in the induction of macrophage dysfunction, which may contribute to the progression of lesion development and instability in the inflammatory disease atherosclerosis. This may be particularly significant for smokers, who have elevated plasma thiocyanate, the precursor to HOSCN and are at greater risk of developing atherosclerosis and complications from this disease.

List of Figures

List of Tables

List of Abbreviations

Aldolase	**Fructose 1, 6-bisphosphate aldolase**
ApoA-1	Apolipoprotein A-1
ApoB-100	Apolipoprotein B-100
ATP	Adenosine triphosphate
BCA	Bicinchoninic acid
Br^-	Bromide ion
BSA	Bovine serum albumin
3-Br-Tyr	3-bromotyrosine
CCCP	Carbonyl cyanide m-chlorophenyl hydrazone
CF	Cystic fibrosis
CFTR	Cystic fibrosis transmembrane conductance regulator
CHAPS	3-[(3-Cholamidopropyl)dimethylammonio]-1-propanesulfonate
CK	Creatine kinase
Cl^-	Chloride ion
3-Cl-tyr	3-chlorotyrosine
CsA	Cyclosporin A
δ	Bending – asymmetric (as) or symmetric (s)
DAz-2	4-(3-azidopropyl)-3,5-dioxocyclohexane-1,3-dione
DCP-Bio1	3-(2,4-dioxocyclohexyl)propyl 5-((3aR,6S,6aS)-hexahydro-2-oxo-1H-thieno[3,4-d]imidazol-6-yl)pentanoate
dHOSCN	Decomposed hypothiocyanous acid
DMEM	Dulbecco's modified Eagle medium
DMSO	Dimethyl sulfoxide
DNA	Deoxyribonucleic acid

DTNB	5,5'-dithiobis-2-nitrobenzoic acid
DTT	Dithiothreitol
ε	Extinction coefficient
ECL	Enhanced chemiluminescence
EDTA	Ethylenediaminetetraacetic acid
EPO	Eosinophil peroxidase
ERK	Extracellular signal-regulated kinase
ETC	Electron transport chain
FCCP	Carbonyl cyanide-4-(trifluoromethoxy)phenylhydrazone
FTIR	Fourier transform infra-red spectroscopy
GAPDH	Glyceraldehyde 3-phosphate dehydrogenase
GPx	Glutathione peroxidase
GR	Glutathione reductase
Grx	Glutaredoxin
GSH	Glutathione
GSSG	Oxidised glutathione
HBSS	Hank's buffered salt solution
HCAEC	Human coronary artery endothelial cells
HDL	High-density lipoprotein
HEPES	4-(2-hydroxyethyl)-1-piperazineethanesulfonic acid
HMDM	Human monocyte-derived macrophages
$HO^{\bullet}$	Hydroxyl radical
HUVEC	Human umbilical vein endothelial cells
HRP	Horse radish peroxidase
H_2O_2	Hydrogen peroxide

HOBr	Hypobromous acid
HOCl	Hypochlorous acid
HOSCN	Hypothiocyanous acid
IAF	5-Iodoacetamidofluorescein
IR	Infra-red
LDH	Lactate dehydrogenase
JNK	c-Jun N-terminal kinase
LDL	Low-density lipoprotein
LPO	Lactoperoxidase
MAPK	Mitogen-activated protein kinases
MPO	Myeloperoxidase
MPTP	Mitochondrial permeability transition pore
NAD^+/NADH	Nicotinamide adenine dinucleotide
NADPH	Nicotinamide adenine dinucleotide phosphate
NEM	*N*-ethylmaleimide
NF-κB	Nuclear factor kappa-light-chain-enhancer of activated B cells
npH_2O	Nano-pure water
$^1O_2$	Singlet oxygen
O_2	Oxygen

$O_2^{\bullet-}$	Superoxide radical
oxLDL	Oxidised low-density lipoprotein
p-biotin	Phosphine-biotin
PBS	Phosphate-buffered saline
PBST	Phosphate-buffered saline Tween-20
PCA	Principal component analysis
Prx	Peroxiredoxin
PSSG	Protein S-glutationylation
PTP	Protein tyrosine phosphatase
PVDF	Polyvinylidene difluoride
RNA	Ribonucleic acid
RNS	Reactive nitrogen species
ROS	Reactive oxygen species
RSOH	Sulfenic acid
RSO_2H	Sulfinic acid
RSO_3H	Sulfonic acid
RSSCN	Sulfenyl thiocyanate
RuBPS	Ruthenium(II)tris(bathophenantrolinedisulfonate)
SCN^{--}	Thiocyanate ion
SDS-PAGE	Sodium dodecyl sulfate polyacrylamide gel electrophoresis

SERCA	Sarco/endoplasmic reticulum Ca^{2+}-ATPase
SPO	Salivary peroxidase
TNB	5-thio-2-nitrobenzoic acid
TPI	Triosephosphate isomerase
Tris	Tris(hydroxymethyl)aminomethane
Trx	Thioredoxin
UFA	Unsaturated fatty acid
v	Stretching – asymmetric (as) or symmetric (s)
VC	Vehicle control
XF	Extracellular flux

Publications and presentations arising from this Thesis

Invited Review

Rayner, B.S., Love, D.T., Hawkins, C.L.

Comparative reactivity of myeloperoxidase-derived oxidants with mammalian cells.

Free Radical Biology & Medicine, 2014 Jun;71:240-55

Research Paper

Love, D.T., Barrett, T.J., White, M.Y., Cordwell, S.J., Davies, M.J., Hawkins, C.L.

Cellular targets of the myeloperoxidase-derived oxidant hypothiocyanous acid (HOSCN) and its role in the inhibition of glycolysis in macrophages.

Free Radical Biology & Medicine, 2016

Conference Presentations (Posters)

Love, D.T., Barrett, T.J, Pattison, D.I., Davies, M.J., Hawkins, C.L.

Cellular targets of the myeloperoxidase derived oxidants hypothiocyanous acid (HOSCN) and hypochlorous acid (HOCl): A comparative study.

Society for Free Radical Research, Australasia, 2012, Brisbane, AU.

Love, D.T., Pattison, D.I., Davies, M.J., Hawkins, C.L.

The MPO-derived oxidant HOSCN in mitochondrial dysfunction in macrophages.

8th International Peroxidase Meeting, 2013, Sydney, AU.

Love, D.T., Pattison, D.I., Davies, M.J., Hawkins, C.L.

The MPO-derived oxidant HOSCN in mitochondrial dysfunction in macrophages.

20th annual meeting of the Society for Redox Biology and Medicine, 2013, San Antonio, USA.

Love, D.T., Barrett, T.J., White, M.Y., Cordwell, S.J., Davies, M.J., Hawkins, C.L.

The myeloperoxidase-derived oxidant HOSCN and glycolytic inhibition in macrophages.

21st annual meeting of the Society for Redox Biology and Medicine, 2014, Seattle USA.

Love, D.T., Pattison, D.I., Davies, M.J., Hawkins, C.L.

The MPO-derived oxidant HOSCN in mitochondrial dysfunction in macrophages.

21st annual meeting of the Society for Redox Biology and Medicine, 2014, Seattle USA.

Conference Presentations (Oral presentations)

Love, D.T., Pattison, D.I., Davies, M.J., Hawkins, C.L.

The MPO-derived oxidant HOSCN in mitochondrial dysfunction in macrophages.

6th joint Meeting of SFRR(A) and SFRR(J), 2013, Sydney, AU.

Love, D.T., Pattison, D.I., Davies, M.J., Hawkins, C.L.

The MPO-derived oxidant HOSCN in mitochondrial dysfunction in macrophages.

7th annual meeting of the Society for Free Radical Research, Australasia, 2014, Melbourne, AU.

1 Introduction

1.1 Oxidative stress

Oxidative stress can be defined as the imbalance between the creation of reactive oxygen species (ROS) in biological systems and the inability of the system to detoxify/remove these reactive intermediates or repair the damage caused by ROS [1]. ROS refer to radical and non-radical chemical species that contain oxygen (O_2) derivatives. Chemically, radicals can be formed by a number of routes, such as by the loss of a single electron from a non-radical, or on the other hand, the gain of an electron by a non-radical. Non-radical oxidants, such as hydrogen peroxide (H_2O_2) and peroxynitrite, can be formed via many processes, particularly *in vivo* by the action of peroxidases [2].

Inflammation is a major initiator of ROS formation, inflammatory stimuli recruit leukocytes to the site of injury, where they are activated and release enzymes from intracellular granules, resulting in the generation of superoxide ($O_2^{\bullet-}$) and H_2O_2, which is driven by membrane NADPH complexes [3, 4]. Another source of ROS is from the leakage of electrons from the electron transport chain (ETC), which reduce O_2, forming $O_2^{\bullet-}$ [5]. $O_2^{\bullet-}$ is a weak base, that does not appear to react readily with biomolecules, but its role seems to be involved in the formation of more potent oxidising agents [6]. The formation of $O_2^{\bullet-}$ can lead to the formation of numerous ROS, such as H_2O_2 which is formed via the addition of an electron, either enzymatically (by superoxide dismutase) or spontaneously [7, 8]. H_2O_2 is a non-radical oxidant that plays a role in various cell signalling pathways, and is involved in the oxidation of halide and (pseudo)halide ions [9-11]. The donation of another electron to H_2O_2 via Fenton chemistry with Fe^{2+}, results in the formation of the hydroxyl radical ($HO^{\bullet}$), an extremely reactive and short-lived species that can react with nearly all types of biological molecules, including lipids, nucleic acids, proteins and carbohydrates at diffusion-controlled rates [12]. An important of ROS in biological systems are the hypohalous acids (HOX) (hypochlorous; HOCl, hypobromous; HOBr, and hypothiocyanous; HOSCN), formed by lactoperoxidase (LPO), eosinophil peroxidase (EPO) and myeloperoxidase (MPO), enzymes that catalyse the reaction between H_2O_2 and halide anions (Cl^-, Br^- and SCN^-) [11]. The properties of these oxidants differ, which influences their roles in a biological setting and determines their role in the formation of further oxidants.

Thus, in the past few decades, excessive ROS production has been associated with detrimental biological effects in terms of playing a role in cellular dysfunction and disease. However, ROS are also formed via a myriad of normal physiological and cellular processes, such as by the ETC [13]. These processes create ROS as intermediates or by-products of

reactions in healthy cells, where they can play an important role in redox cell signalling in response to external stimuli such as infection [14]. Given the increasing importance of oxidative stress in the propagation of disease, significant research has been dedicated to understanding the cellular pathways modulated by ROS to be able to reverse the production and/or the damage caused by oxidants, particularly in the context of inflammatory disorders [15].

1.2 Inflammation

Inflammation is a complex process, which is defined as the biological response of body tissues to damaging stimuli, such as irritants and invading pathogens [16]. A hallmark of inflammation is the infiltration and subsequent extravasation of leukocytes [17]. Neutrophils are a key inflammatory leukocyte, which once at the site of inflammation will release MPO from azurophilic granules into their phagosomal compartment or extracellularly [18]. MPO catalyses the formation of hypohalous acids, which are potent antimicrobial agents, by utilising H_2O_2 [19]. However, excessive production of these oxidants, or the production of them at inappropriate times or locations, can lead to tissue damage [20]. Because of this reason, hypohalous acids, especially HOCl have been implicated in chronic inflammatory diseases [21, 22]. It has been hypothesised that the cellular damage during chronic inflammation is associated with the reaction of HOCl, HOBr and HOSCN with a multitude of biological molecules, particularly targeting a number of protein residues, which causes a change in the tertiary structure of proteins, thereby influencing their activity [23].

It has also been postulated that inflammation is associated with a change in the proper function of cellular energy producing pathways within the cytosol and the mitochondria [24-26]. In the cytosol, it has been shown that hypoxia (deficiency in O_2 in the cellular environment) enhances the glycolytic flux of macrophages together with an increase in pro-inflammatory activity [26] and glucose transporter 1 (GLUT1) mediated increases in glycolysis also drive inflammatory phenotypes in macrophages [27]. In the mitochondria, it is proposed that electron leak via the ETC, leads to the incidental liberation of ROS and subsequent increase in cellular concentrations of ROS [28]. It has been postulated that this release of ROS induces damage to major constituents of the mitochondria, which include the thousands of copies of mitochondrial DNA within each cell [29]. This link between an increase in cellular ROS, a decrease in mitochondrial function and a reduced ability to remove ROS has therefore

been hypothesised as a cause of inflammatory disorders and diseases [30-32] including, but not limited to, cancer, rheumatoid arthritis and cardiovascular disease [33, 34].

1.2.1 Immune Response

Leukocytes are the cells involved in the immune response and are largely responsible for protecting the body from harmful infections and foreign invaders. MPO is particularly useful in bacterial cell killing, while EPO (localised within granules of eosinophils) is largely used in defense against parasitic infection and LPO (secreted from salivary and mucosal glands) is an antibacterial agent in saliva, milk and tears [11, 35, 36]. Studies have shown that MPO, H_2O_2 and halide ions are able to effectively kill bacteria *in vitro* [37] and to serve as potent innate immune cells neutrophils are packed with these cytotoxic granules. Peroxidase positive granules (positive MPO content) [38] that are activated via increases in intracellular Ca^{2+} levels or various inflammatory stimuli release vesicles that express vesicle-associated membrane protein 2 (VAMP-2) into the extracellular environment [39, 40].

1.3 Haem Peroxidases

Peroxidases are a family of enzymes that catalyse the general reaction (Reaction 1.1):

$ROOR' + 2e^- + 2H^+ \rightarrow ROH + R'OH$ **Reaction 1.1**

The optimal substrate for these enzymes is H_2O_2 and haem peroxidases contain haem cofactors at their active sites [11]. The role of many human peroxidases, including MPO, LPO and EPO is the utilization of H_2O_2 to form further oxidising chemical species such as HOSCN, HOBr and the well-documented HOCl [41-43].

These particular peroxidases have genes that originate from chromosome 17 with similar exon and intron patterns [44], with each playing an important role in the innate arm of the human immune system, by synthesising powerful antimicrobial oxidants. The haem contained within the active site of MPO can react with H_2O_2, the original Fe^{3+} form of the haem becomes Fe^{5+}, also referred to as Compound I. Compound I is now able to undergo a two-electron reduction reaction known as the "halogenation cycle", returning back to its native Fe^{3+} state. This allows for the oxidation of halides and thiocyanate into their respective hypohalous acids [45]. Compound I is also able to undergo two sequential one-electron reactions, known as the "peroxidase cycle" to regenerate its native Fe^{3+} state, through the

creation of an intermediate known as “Compound II”, which forms oxidising radical species in the process. Finally, Compound II can react with H_2O_2 to bring about an inactive form of MPO, Compound III. Native MPO can also react with $O_2^{\bullet-}$ to form Ferrous MPO, which subsequently reacts with molecular O_2 to form Compound III (Figure 1.1).

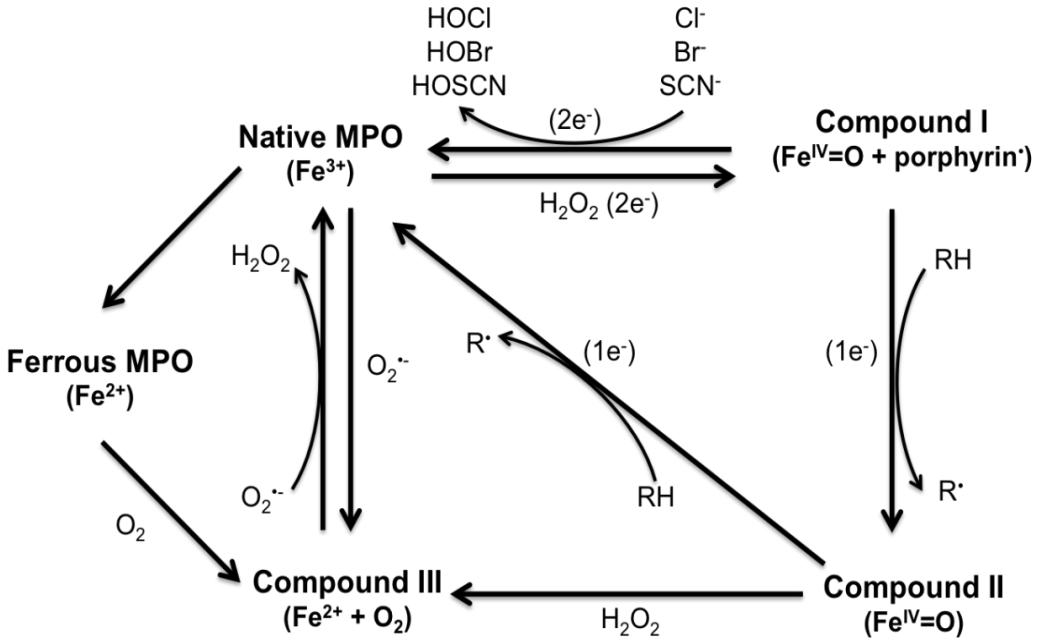

Figure 1.1: Catalytic cycle of peroxidases including MPO, EPO and LPO.

Using MPO as an example, oxidation of MPO by H_2O_2 forms Compound I, which can undergo a two-electron reduction with halide or pseudohalide ions to form the pseudo and hypohalous acids (halogenation cycle). Compound I can also undergo two successive one-electron reductions (peroxidation cycle), forming radicals via Compound II and returning to the native state. Compound III can be formed via a reaction of native MPO with $O_2^{\bullet-}$ via Ferrous MPO.

With MPO, during the peroxidase cycle, organic substrates can be converted to radicals via a one-electron oxidation by Compound I to Compound II, or by Compound II to native MPO (Figure 1.1). MPO has a ride range of substrates for peroxidation including tyrosine, ascorbate, steroidal hormones, as well as various xenobiotics and drugs, including paracetamol [46, 47].

When considering the peroxidases, their substrates and their possible physiological roles, many conditions and variables must be identified. At physiological pH and halide concentrations, MPO preferentially generates both HOCl and HOSCN, despite the large difference in plasma concentrations of the parent halides (and pseudohalides). Plasma concentrations of Cl^- are ca. 100 - 150 mM and SCN^- is typically 50 – 100 μM [48]. However, SCN^- has a higher specificity for MPO than Cl^- (rate constants, *k* of 9.6×10^6 M^{-1} s^{-1} for SCN^-, cf. 2.5×10^4 M^{-1} s^{-1} for Cl^- and 1.1×10^6 M^{-1} s^{-1} for Br^- and specificity constants 730:1:60, respectively) due in part to the lower standard reduction potential for the $2e^-$ HOSCN/SCN^- redox couple [48, 49]. Thus, at physiological pH and concentrations of the parent anions in plasma, it is estimated that 50 % of the H_2O_2 utilised by MPO is used to create HOSCN [48]. EPO preferentially generates HOBr (plasma Br^-, 100 μM) and LPO preferentially generates HOSCN [11].

1.4 Hypohalous acids

The hypohalous acids have been studied extensively due to their role in the innate arm of the human immune response [50-52], and are much more reactive and bactericidal than H_2O_2 [42, 53-56]. The most studied of these oxidants is HOCl, a powerful oxidant created by MPO that exists with hypochlorite (OCl^-, its conjugate base) in equilibrium at physiological pH (pK_a, 7.59) [57]. At physiologically relevant temperature and pH, HOBr is prevalent when compared to its conjugate base hypobromite (pK_a, 8.7) [58], while on the other hand hypothiocyanite ($OSCN^-$) rather than HOSCN is the predominate species under physiological conditions (pK_a, 5.3) [57, 59]. From here on, the terms HOCl, HOBr and HOSCN, will be used to represent physiological mixtures of acids and their conjugate bases.

1.4.1 Hypochlorous and hypobromous acids

HOCl and HOBr are both strong oxidants that are also capable of performing halogenation reactions *in vivo* [11]. At acidic pH and with excess amounts of Cl^- and Br^- ions, HOCl and HOBr exist in equilibrium with molecular chlorine (Cl_2) and bromine (Br_2) [60]. It has been suggested that these species exist within the phagosomes and that they contribute to peroxidase–mediated damage [60, 61].

HOCl and HOBr can avidly react with biomolecules that contain amines, organic compounds or functional groups that contain nitrogen with lone pairs, and amides to create *N*-chlorinated or *N*-brominated species [62, 63]. The species derived from amines are known as "halamines" (chloramines, RR'NCl and bromamines, RR'NBr). Primary halamines can react further with either HOCl or HOBr to create dihalamines (RNX_2, X = Cl, Br) [64]. Reaction of these oxidants with amides forms "halamides" (chloramides, RC(O)N(R')Cl and bromamides, RC(O)N(R')Br) [62-67]. These halamines and halamides can be generated on a variety of biological molecules such as the α-amino groups of proteins and certain residues that contain nucleophilic nitrogens such as, arginine (Arg), lysine (Lys) and histidine (His) and DNA bases [41, 65, 68].

1.4.1.1 Halamines

Halamines and halamides are major products of the reaction between HOCl/HOBr and biological molecules, which can preserve the oxidising capacity of the parent oxidant [69]. In some cases, these reactive intermediates can induce further reactions, some of which restore the amine/amide, owing to a transfer of the halogen [41, 67, 70]. Halamines and halamides can also dissociate the nitrogen-halide (N-X) bond, producing nitrogen-centred radicals, which can undergo further reactions to damage biomolecules [71].

1.4.2 Hypothiocyanous acid

HOSCN is not a hypohalous acid in the classical sense of the term, though it shares many common traits, and is therefore referred to as a (pseudo)hypohalous acid. It is theorised that SCN^- is either oxidised to HOSCN directly by peroxidases (Reaction 1.2) [72-74] or that thiocyanogen ($(SCN)_2$) is hydrolysed to HOSCN (Reaction 1.3) [75, 76], However, recent evidence suggests that thiocyanogen may not be formed at physiological pH [77]. SCN^- is

derived from the ingestion of foods, such as cassava and cruciferous vegetables [78, 79]. SCN^- is also derived from rhodanese, a protein that catalyses the detoxification of plasma cyanide (CN^-) and thiosulfate [80]. Instead, a prime source of SCN^- is from the detoxification of hydrogen cyanide via cigarette smoke inhalation [81, 82]. In non-smokers, plasma concentrations of SCN^- are usually between 10 – 100 μM [42], but plasma SCN^- levels in smokers have been reported to reach and exceed 300 μM [80, 82, 83].

$$SCN^- + H_2O_2 \rightarrow OSCN^- + H_2O \qquad \textbf{Reaction 1.2}$$

$$(SCN)_2 + H_2O \rightarrow HOSCN + H^+ + SCN^- \qquad \textbf{Reaction 1.3}$$

Debate exists about the exact nature of the oxidant formed from SCN^- by peroxidases [84-86]**.** Data suggest that numerous oxidising species can be formed such as CN^-, cyanate (OCN^-), cyanosulfurous (HO_2SCN) and/or cyanosulfuric (HO_3SCN) acid on decomposition of HOSCN [42]. In addition, certain studies support the formation of radical species including $SCN^\bullet$ and $OSCN^{-\bullet}$ [86-88]. HOSCN is not only formed by peroxidases, as HOCl, HOBr or secondary oxidants such as chloramines may oxidise SCN^- directly [89, 90]. This mechanism has been suggested to occur as both a protective mechanism and as a harmful factor in certain inflammatory situations [89, 91, 92].

HOSCN decomposes into numerous products at physiological pH and temperature, with much debate about the mechanisms involved and the intermediates formed, owing to their instability [93]. It has been shown that at neutral pH, the final products formed from the decomposition of HOSCN are anions such as SCN^-, SO_3^{2-}, SO_4^{2-} and OCN^- [77]. A number of reactive intermediates have been proposed, including $(SCN)_2$ (Reaction 1.4), HO_2SCN (Reaction 1.5), HO_3SCN (Reaction 1.6), HCN (Reaction 1.7) and trithiocyanate $(SCN)_3^-$ (Reaction 1.8) [55, 72, 73, 75, 85, 94]. However, no direct evidence exists for the formation of some of these species due to the lack of stability, rather, their formation is inferred from the ratio of the final products.

$$H_2O_2 + 2H^+ + 2SCN^- \rightarrow 2H_2O + (SCN)_2 \qquad \textbf{Reaction 1.4}$$

$$2HOSCN \rightarrow HO_2SCN + H^+ + SCN^- \qquad \textbf{Reaction 1.5}$$

$$HOSCN + HO_2SCN \rightarrow HO_3SCN + H^+ + SCN^- \qquad \textbf{Reaction 1.6}$$

$$HO_3SCN + H_2O \rightarrow HCN + H_2SO_4 \qquad \textbf{Reaction 1.7}$$

$$(SCN)_2 + SCN^- \rightarrow (SCN)_3 \qquad \textbf{Reaction 1.8}$$

HOSCN is generally classified as a weak oxidant, while HOCl and HOBr are strong oxidants, but the difference in chemistry and reactivity between HOCl/HOBr and HOSCN is seen in the number of their targets. HOCl and HOBr will react readily with lipids, nucleic acids and numerous amino acids, while HOSCN will preferentially oxidise cysteine (Cys) thiols and few others.

1.5 Hypohalous acid induced damage to cellular constituents

Hypohalous acids, *in vivo*, can cause damage to biomolecules, in addition to affording protection against bacteria and a multitude of pathogens [11]. The susceptibility of individual substrates to the damaging effects of hypohalous acids are defined by: 1) the location of the substrate in comparison to the oxidant, 2) the concentration of the substrate, 3) the second order reaction rate between the substrate and the oxidant and, 4) the concentration of antioxidants in particular biological compartments.

1.5.1 Proteins

Proteins exist in nearly every biological compartment and are favourable targets due to their abundance and high reactivity with hypohalous acids [95]. Kinetically, hypohalous acids preferentially react with the side chains of amino acids rather than the backbone amide sites [49, 68, 95, 96]. For example, HOCl will react with Cys thiols to a greater extent than the backbone amines and will only react with glutamine (Gln) or aspartic acid (Asp) to a limited extent (Met > Cys >Cystine ≈ His > Trp > Lys > Tyr ≈ Arg > backbone amines > Gln ≈ Asp) [96], a similar order of reactivity has been noted for HOBr (Cys > Trp ≈ Met ≈ His > Cystine > Lys ≈ Tyr > Arg > backbone amines > Glu) [68]. In comparison, HOSCN is extremely selective, reacting almost exclusively with thiol containing amino acids (Cys), and selenols (seleno-cysteine and seleno-methionine) residues, with some evidence for the reaction of HOSCN with tryptophan (Trp) (Seleno-Cys > Cys > Seleno-Met > Trp) [95, 97-99]. There are a few factors that govern which of these α-amino side chains will make a suitable substrate, which include, ease of accessibility due to protein structure and the pK_a of the residue, which can also be affected by neighbouring amino acid residues [96].

Due to the diverse nature of proteins with almost countless combinations of amino acids, peptide chain length and tertiary structure, the individual sensitivity of particular proteins to

oxidation by hypohalous acids can be difficult to determine, even using computational models. Thus, the susceptibility of a specific protein to oxidation by HOCl, HOBr or HOSCN is best determined by quantifying the reactions between the hypohalous acid and the protein directly. For example, computational data predicted that at a ratio of 300:1 HOCl:LDL, 30 % of tryptophan (Trp) residues would be oxidised, while experimental data showing that under these conditions HOCl, 60 % of the Trp residues contained on LDL were oxidised [100].

1.5.1.1 Sulfur-containing amino acids (Cysteine and Methionine)

Organosulfur compounds containing a carbon-bonded sulfhydryl group are found on the α-amino residues Cys and methionine (Met). These groups are nucleophilic, as Cys in the presence of a base is readily oxidised to give the covalently-linked organic disulfide, cystine. Despite HOSCN having a reaction rate with thiols (k, in the range of $10^4 – 10^6$ M^{-1} s^{-1} [98]) that is significantly less than the rate between HOCl or HOBr, and thiols (k = 3×10^7 M^{-1} s^{-1} [68, 96]), under some conditions, HOSCN can induce more damage at susceptible sites on account of its reduced activity with other targets [84, 91].

The reaction between Cys and a hypohalous acid will yield the sulfenyl halide (RS-X, where X= Cl, Br, SCN) (Reaction 1.9) [101, 102]. These species can be hydrolysed to the reversible sulfenic acid (RS-OH) (Reaction 1.10), or to form a disulfide bridge with another Cys residue (RS-SR') (Reaction 1.11) [62]. It should be noted that these species are "reversibly oxidised", as they can be reduced back to the parent thiol. The formation of all these species is strongly dependent on the immediate environment and pK_a, which can be influenced by neighbouring amino acids.

RSH + HOX (X=Cl, Br, SCN) → RS-X + H_2O **Reaction 1.9**

RS-X + H_2O → RS-OH + H^+ + X **Reaction 1.10**

RS-X + R'SH → RS-SR' + H^+ + X^- **Reaction 1.11**

The species described above can be reduced by the low-molecular mass thiol-containing tripeptide, glutathione (GSH) [103]. This results in the formation of a mixed disulfide (GS-SR) between GSH and the oxidised thiol (protein S-glutathionylation) [104]; GS-SR further reacts with glutaredoxin, recycling these species back to their original reduced thiol configuration (Reaction 1.12) [105]. These species are important in biological systems, as this action

between the oxidised thiols and GSH allow for the utilisation of cellular redox switches and various regulatory pathways [106].

$RS\text{-}OH + GSH \rightarrow GS\text{-}SR + H_2O$ **Reaction 1.12**

When thiols are exposed to strong oxidising agents, such as HOCl, they can yield higher oxyacids, or the "irreversibly oxidised" products such as sulfinic ($RS\text{-}O_2H$) (Reaction 1.13) and sulfonic ($RS\text{-}O_3H$) (Reaction 1.14) acids [42, 107]. The formation of these higher oxyacids can lead to irreversible enzyme inactivation and the possible failure of essential redox switches within the cell [9, 108-110].

$RS\text{-}OH + HOX \rightarrow RS\text{-}O_2H + H^+ + X^-$ **Reaction 1.13**

$RS\text{-}O_2H + HOX \rightarrow RS\text{-}O_3H + H^+ + X^-$ **Reaction 1.14**

Together with Cys, Met is another sulfur-containing α-amino acid and a major target of oxidation by HOCl and HOBr [68, 111]. Methionine residues are quite hydrophobic, and tend to exist close to or within the cell's lipid bilayer. Thus, the residues most exposed to the aqueous cytosol tend to be at greater risk of oxidation [112, 113]. Oxidation of Met by either HOCl or HOBr leads to the formation of methionine sulfoxide (Reaction 1.15), this species can be reduced back to the original Met by methionine sulfoxide reductases or can be further oxidised to methionine sulfone (Reaction 1.16) [111, 112, 114]. Currently, there is no evidence for the oxidation of Met by HOSCN [48, 115].

$RSCH_3 + HOCl \rightarrow RS(O)CH_3 + H^+ + Cl^-$ **Reaction 1.15**

$RS(O)CH_3 + HOCl \rightarrow RS(O)OCH_3 + H^+ + Cl^-$ **Reaction 1.16**

1.5.1.2 Tryptophan (Trp)

Trp is an essential amino acid in humans and the precursor to many biochemical-signalling molecules (e.g. serotonin) [116]. It is a favoured target of hypohalous acids [97] and the reaction between hypohalous acids (HOCl or HOBr) and Trp is determined by the environment surrounding the Trp residue, accessibility, pH and pK_a [117, 118]. When a hypohalous acid (either HOCl or HOBr) oxidises a Trp residue, two intermediate species are hypothesised to be formed, the 3-halo-indolenine and/or *N*-halo-indole [119]. These two species rapidly react to yield oxyindolyalanine and/or 2-hydroxytryptophan [120]. The

products of the reaction between HOSCN and Trp have yet to be wholly understood, though Hawkins *et al.* have provided evidence for the formation of oxindolyalanine via the formation of an SCN-indole intermediate and other related oxidation products [97]. Another study has shown that HOSCN may play an indirect role in lipid dysfunction via the oxidation of Trp residues within apolipoprotein A-1 (apoA-1) of high density lipoproteins (HDLs) [121]. The study noted that HOSCN-modified apoA-1 caused a reduced efflux of cholesterol from cholesterol-loaded macrophages, which is another important role in the progression of atherosclerosis [121]. However, more recently, the role of HOSCN in mediating Trp oxidation *in vivo* has been questioned, owing to the fact that significant Trp loss requires a low pH [122].

1.5.1.3 Tyrosine (Tyr)

Tyr is commonly found to exist in high levels within proteins and plays an important part in cell signalling cascades and transduction events and is probably the best characterised and documented substrate of hypohalous acids [123, 124]. HOCl and HOBr both undergo addition to the aromatic ring of Tyr to form 3-chlorotyrosine (3-Cl-Tyr) and 3-bromotyrosine (3-Br-Tyr), respectively [125, 126]. For years now, these species have been used extensively as biomarkers for hypohalous acid-mediated oxidative damage *in vivo*, as MPO is the only known enzyme to produce HOCl. Therefore, 3-Cl-Tyr production and detection *in vivo* is indicative of MPO specific oxidation. Secondary halogenation reactions result in the formation of 3,5-dichlorotyrosine or 3,5-dibromotyrosine (Figure 1.2) [127]. A major difference between HOCl and HOBr is the kinetics of the reaction with aromatic rings and double bonds, as seen by the difference between the halogenation of Tyr, with reports that bromination by HOBr occurs ≈5000-fold faster than the corresponding chlorination reactions [95]. These rate constants have been disputed recently; with a report describing a difference between HOBr and HOCl of only 250 fold, these differences in reactivities are most likely due to the slight differences in substrate composition and the pH at which the experiments were conducted [128].

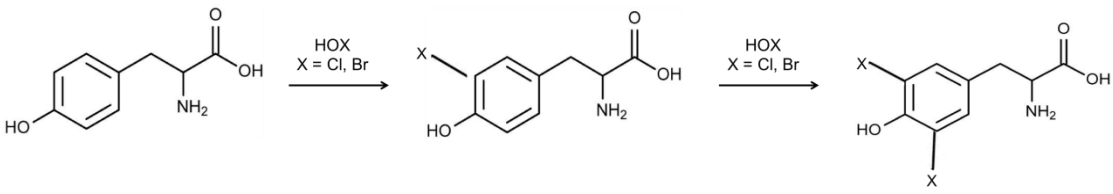

Figure 1.2: Formation of 3-chloro/bromotyrosine and 3,5-dichloro/dibromotyrosine after the halogenation of tyrosine by either hypochlorous or hypobromous acid.

Tyr modifications have also been noted on exposure of proteins to the LPO/H_2O_2/SCN^- system, however, the reaction is hypothesised to be caused by $(SCN)_2$ rather than HOSCN [107]. Another report has also noted that a lack in reactivity between HOSCN and Tyr in the absence of LPO [97].

1.5.1.4 Histidine (His)

Histidine is an amino acid with an imidazole functional group, that can react with HOCl and HOBr to form halamines [62, 67, 129]. The reactivity of the imidazole group with hypohalous acids is dependent on the protein environment [96]. The imidazole-derived halamines can rapidly transfer the Cl^- or Br^- to other amines, generating stable halamines with the regeneration of the parent compound [41].

The oxidation of His has been reported with both HOSCN and the LPO/H_2O_2/SCN^- system [130]. His has been reported to stabilise the oxidising amino thiocyanate (RN-SCN) product, lowering the concentration of HOSCN and inhibiting its decomposition. The RN-SCN product still maintains the oxidising potential of HOSCN, allowing for the transfer of the SCN^- to thiols [59].

1.5.1.5 Lysine (Lys)

As outlined in Section 1.4.1, amines such as ys are able to react with HOCl and HOBr to form reactive chloramines and bromamines, respectively, though bromamines are generally less stable than chloramines [69]. These oxidants can retain the oxidising ability of HOCl or HOBr, and are able to mediate secondary oxidative reactions [131]. Depending on their structure, chloramines can oxidise Cys and Met to form disulfides and sulfonic acids [96].

Lys is not thought to be a major target of HOSCN-induced oxidation, though RN-SCN species can be generated on Lys residues, they tend to be unstable at physiological pH [59].

1.5.2 DNA

Experimental evidence suggests that both HOCl and HOBr can target nucleic acids, resulting in modification of bases and strand cleavage [132, 133]. There is little to no evidence showing any reaction between HOSCN and nucleic acids. Even at concentrations exceeding 5-fold the concentration required to produce antibacterial effects in the human mouth, HOSCN is reported to pose no threat to the genetic material of host tissues [134].

HOCl reacts with DNA, RNA, free bases and nucleosides to form base-derived chloramines [71]. Initially, an unstable intermediate is formed after the reaction of HOCl with the heterocyclic ring NH groups of each nucleoside [66, 132]. The exocyclic NH_2 groups of guanosine, adenosine and cytidine ribonucleosides are also sensitive to HOCl-induced modification [135]. These products are quite unstable and once formed, undergo a secondary chlorination, where the chlorine is transferred to the ring carbons, to give stable chlorinated products. These secondary products include 8-chloro-2'(deoxy)guanosine, 5-chloro-2'(deoxy)cytidine, 8-chloro-2'(deoxy)adenosine and 5-chloro-uracil (a mutagenic thymine analog) (Figure 1.3) [136-139]. The formation of these products is theorised to cause the dissociation of the DNA double strand through a loss in Van der Waals force [135].

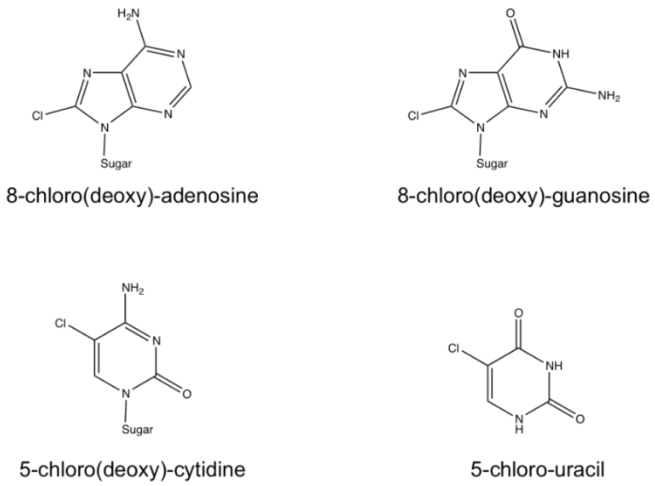

Figure 1.3: The stable chlorinated nucleoside products.

The products formed after the reaction of HOCl with various nucelosides (adenosine, guanosine and cytidine) and the nucleotide uracil (from top left to bottom right).

1.5.3 Lipids

Phospholipids, cholesterol, and free fatty acids, all of which are important in the integrity of cellular membranes, are susceptible to reaction with one or more of the hypohalous acids. Lipid oxidation can occur with both HOCl and HOBr, but evidence for reaction with HOSCN is limited. There are reports that the MPO/H_2O_2/SCN^- system is able to promote the peroxidation of plasma lipids (e.g. 17β-estradiol) suggesting that HOSCN may be able to play some part in the dysfunction of lipid transport [140] affecting arterial blood flow in women with coronary heart disease [141]. Recent evidence has also shown that HOSCN can oxidise low-density lipoprotein (LDL) cholesteryl esters to form F_2-isoprostanes, lipid hydroperoxides and 9-hydroxy-10, 12-octadecadienoic acid (9-HODE) [142]. This is postulated to contribute to the progression of atherosclerosis via macrophage oxidised LDL (oxLDL) accumulation and foam cell formation [142]. The role of HOCl is relatively more defined, HOCl can react with the double bond of unsaturated fatty acids to produce oxysterols, and α- and β-chlorohydrins [143]. A similar reaction also occurs upon the addition of HOBr to unsaturated fatty acids to produce bromohydrins [144] (Figure 1.4A). Chlorohydrins are also produced in the reaction between HOCl and the carbon-carbon double bonds of fatty acyl groups of phospholipids [145], and the reaction between HOCl and cholesterol has, in one report produced chlorohydrins and epoxides [146], with another report describing the production of epoxides and hydroxyl derivatives of cholesterol [147]. The resulting chlorohydrin (also known generally as a halohydrin) can lead to the dysfunction of the cell's lipid bilayer, increasing the cell's permeability and causing cell death [148, 149].

Plasmalogens are phospholipids that are augmented in numerous organ systems such as the nervous and especially the cardiovascular system, and have been shown to play a role in cellular protection against certain ROS [150-152]. Plasmalogens can be readily halogenated by HOCl and/or HOBr at their vinyl ether bond, where the major products are α-halo-fatty aldehydes, 2-chlorohexadecanals, and lysophosphatidylcholines (LPC) (Figure 1.4B). All of which can further react with HOCl, and possibly HOBr, to form halohydrin-LPC [153-155]. These products may have possible roles the progression of atherosclerotic plaques [156].

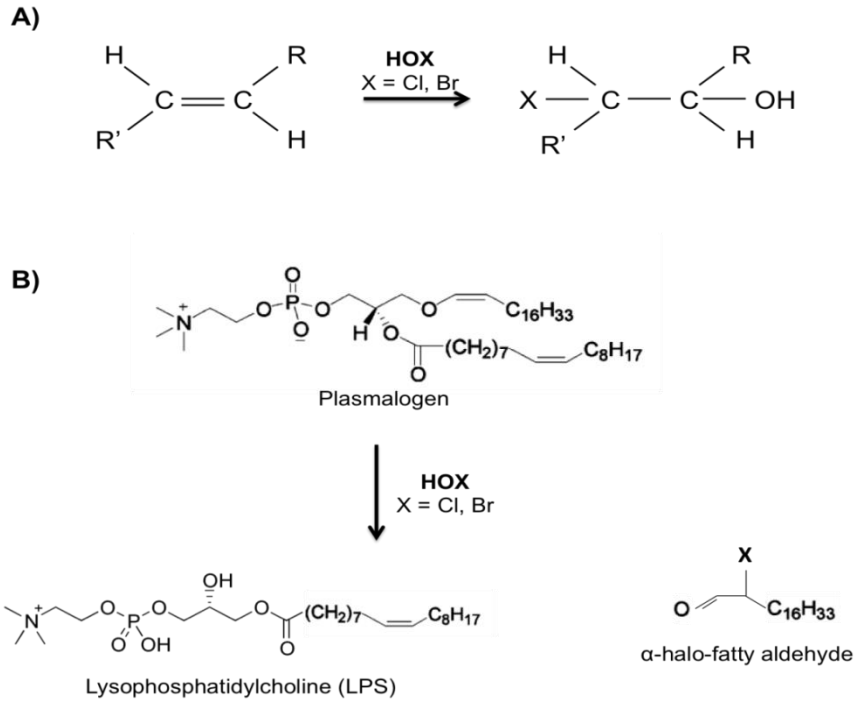

Figure 1.4: Products of the reactions between hypohalous acids and lipids.

(A) Reaction between hypohalous acids with the double bond of unsaturated fatty acids, producing the oxysterols, chlorohydrin or bromohydrin. (B) Reaction between hypohalous acids and plasmalogens, forming lysophosphatidylcholine and a α-halo-fatty aldehyde.

1.5.4 Carbohydrates

Carbohydrates have a number of roles in biology. Polysaccharides, such as starch and glycogen, are involved in energy storage, while the monosaccharide, ribose, is an important part of co-enzymes (ATP, NAD and FAD) [157]. Most importantly, monosaccharides, the smallest unit of carbohydrates, such as glucose, play an integral part in metabolism (glycolysis), where glucose is converted into pyruvate and the free energy of the reaction is used to create the high-energy compounds, adenosine triphosphate (ATP) and reduced nicotinamide adenine dinucleotide (NADH) [158, 159].

Compared to other biomolecules, less is known of the role of hypohalous acids in the oxidation of sugars, possibly due to less favourable reaction kinetics [95]. It has been reported that the reaction between HOCl with mannitol and ribose is quite slow [23, 135]. The reaction of HOCl with proteoglycans of the extracellular matrix has been shown to

liberate polysaccharides via the interaction of HOCl with glycosaminoglycan chains [160]. As HOCl has also been shown to preferentially react with the nitrogen side-chains of amines contained on glycosamines, these modifications to the extracellular matrix have effects on cell adhesion and proliferation. The oxidation of sugars of the extracellular matrix has been hypothesised to have an effect in disease states such as atherosclerosis, where the extracellular matrix is involved in lesion formation [160].

There is currently no data reporting reactions of sugars with HOSCN, though recently, monosaccharides have been modified into selenium-containing species to act as scavengers of hypohalous acids [161]. The results indicate that these selenium-sugars are potent scavengers of HOCl and HOBr oxidation (ca. 1×10^8 M^{-1} s^{-1} for HOCl, ca. 1.5×10^7 M^{-1} s^{-1} for HOBr), only being minimally slower than the reaction of HOCl/HOBr with the most reactive targets, such as Met, His, Tyr, Trp and Lys. The reaction of HOSCN with these selenium-sugars was considerably slower though (ca. 1×10^2 M^{-1} s^{-1}), but the results demonstrate that the modification of simple sugars, by the addition of moieties that are reactive with hypohalous acids are potential scavenging and antioxidant molecules [161].

1.6 Hypohalous acids and the cell

1.6.1 Hypohalous acids and cellular constituents

The interaction between hypohalous acids and cells can lead to a change in cellular homeostasis, either beneficially or detrimentally. Examples for the former include changes in immune status involved with the targeting and destruction of invading pathogens [51, 56]. On the other hand, excessive formation of hypohalous acids, especially in areas of inflammation can lead to the damage of otherwise healthy tissues [162].

1.6.2 Cell signalling

Calcium ions (Ca^{2+}) are important regulators in cell signalling, as Ca^{2+} exerts many regulatory effects on cytoplasmic proteins. This effect is the result of the activation of ion channels or due to Ca^{2+} as a secondary messenger [163]. Ca^{2+} signalling plays an important role in the heart during ventricular contraction, acting to maintain ventricular depolarisation and HOCl is able to reversibly disrupt cellular Ca^{2+} that is dependent on protein thiols in rabbit ventricular myocytes. The rise in cytosolic Ca^{2+} was from internal sources, which has been hypothesised to be a major factor contributing to the mechanical dysfunction of the myocardium [164, 165]. HOCl has also be shown to induce the release of Ca^{2+} by activating the sarcoplasmic reticulum Ca^{2+} release channel of skeletal muscles, implying a role of HOCl in the regulation of calcium signalling [166]. Furthermore, HOCl and HOSCN have been shown to increase intracellular Ca^{2+} concentrations, via the inhibition of sarco/endoplasmic reticulum Ca^{2+}-ATPases (SERCAs), which regulate the flux of Ca^{2+} between the sarco/endoplasmic reticulum and the cytosol [167]. By regulating the flux, SERCAs can mediate smooth, skeletal and cardiac muscle relaxation, growth and proliferation [168, 169]. HOCl and HOSCN, at concentrations as low as 10 µM, increase the intracellular Ca^{2+} levels of human coronary artery endothelial cells (HCAECs) via SERCA inhibition, leading to a loss of Ca^{2+} homeostasis, causing a stress response which is postulated to ultimately lead to cell death via apoptosis [170].

Mitogen-activated protein kinases (MAPK) are serine/threonine specific protein kinases [171] that are involved in the direct signalling responses of a multitude of different stimuli. Such stimuli include mitogens, heat shock and pro-inflammatory cytokines, and they regulate processes such as apoptosis, mitosis, proliferation, gene expression and differentiation [172,

173]. Data shows that HOSCN can influence cellular signalling in HUVECs, leading to an upregulation of various tissue factors and monocyte adhesion molecules which is attributed to the activation of the transcription factor NF-κB [174, 175]. The activation of NF-κB may be the result of protein tyrosine phosphatase (PTP) inactivation, resulting in the hyperphosphorylation of MAPK and various other signalling molecules [176]. Another group of signalling proteins are the extracellular signal-regulated kinases (ERK), ubiquitously expressed protein kinases that are involved in survival pathways, mitosis and meiosis with the disruption of ERK commonly noted in various cancers [177]. ERK has two major isoforms, p44 (ERK 1) and p42 (ERK 2) and it has been shown that HOCl can activate ERK1/2 in HUVEC and fibroblasts [173], which are known to play a role in cell growth and differentiation as well as cell survival pathways [172]. In a model of arthritis, chondrocytes were exposed to HOCl and increases were detected in the phosphorylation of ERK1/2, p38 (another major class of MAP kinases) and c-Jun N-terminal kinase (JNK), and while JNK activation remained at basal levels, ERK1/2 and p38 was increased after a 20 min treatment with 30 μM HOCl. These results indicated that HOCl treatment led to pro-survival mechanisms within the cell due to a loss in viability and decreases in ATP and GSH concentrations [178]. Similar results were also noted upon the treatment of HUVECs with HOSCN [175]. In the J774A.1 murine macrophage cell line, HOSCN activated ERK 2 and p38, which was attributed to a disruption in phosphorylation within the cell due to the inactivation of PTPs [179]; this has been attributed to the low p*Ka* active site Cys in PTPs, making them excellent targets for HOSCN oxidation. This oxidation by HOSCN and the inhibition of PTP is again similar to the effects of HOCl oxidation, in that the hyperphosphorylation of p38α, ERK1/2, MKK3/6 and MAPK signalling are the hallmarks of a survival/stress reaction which cause apoptotic cell death [179].

1.6.3 Hypohalous acids and cell death

Cell lysis has been observed upon exposure of erythrocytes, neutrophils, macrophages, endothelial cells and epithelial cells to HOCl [180-183]. HOCl-induced cell lysis can usually be attributed to the oxidation of membrane proteins, which attenuates the transport of molecules across the cell membrane, leading to cell swelling and lysis [184]. However, this seems to be cell-type specific [19], and there are multiple targets and pathways known to be activated by HOCl, as HOSCN induced cell lysis to a greater extent in J774A.1 macrophages

than HOCl or HOBr, while HOCl lysed human coronary endothelial cells to a greater extent than HOSCN [91, 185].

Apoptosis, also known as “programmed cell-death”, is a cascade of biological events that ultimately leads to cell death. This is in contrast to necrosis, a form of traumatic cell death due to an acute injury. It has been accepted that the treatment of many different cell types with hypohalous acids can result in apoptosis [186-188]. Apoptosis is usually described as having two distinct mechanisms, caspase-dependent and caspase-independent pathways [189].

HepG2 and human foetal liver cells undergo apoptosis after treatment with HOCl at low concentrations (60 μM) via an increase in mitochondrial membrane permeability and the ensuing cytochrome *c* release resulting in caspase activation [187]. However in macrophages, the concentration of HOCl required to cause mitochondrial permeability transition (MPT) pore opening, and cytochrome *c* release is much higher, which tended to cause necrotic cell death before apoptotic cell death [190]. The ryanodine receptor (RyR) has also been implicated in the process of HOCl-induced cell death, as pre-treatment of human monocyte-derived macrophages (HMDM) with dantrolene completely abolished HOCl-induced damage and cell death, implicating a strong connection between protein thiols and their control of intracellular Ca^{2+} in cell death [190]. In endothelial cells, it has been reported that if the caspases are inhibited, HOCl is unable to elicit apoptosis [191].

Lloyd *et al.* [91] provided a case for HOSCN-induced apoptosis. HOSCN (50 μM) was postulated to be pro-apoptotic, due to its selectivity in targeting important mitochondrial thiol-containing proteins [192]. The evidence provided has shown that HOSCN is able to cause apoptosis more efficiently than the corresponding hypohalous acids, despite HOCl and HOBr reacting indiscriminately with numerous targets, especially membrane-bound proteins (resulting in cell lysis).

The role of HOBr and HOSCN in apoptosis and necrosis has also been studied. H_2O_2 in the presence of SCN^- has been shown to inhibit apoptosis, while H_2O_2 in the presence of Br^- has been shown to induce apoptosis in HL-60 cells, SCN^- has also been shown to inhibit apoptosis induced by EPO in eosinophils [174, 193]. Various studies have shown that exposure of HCAECs to HOSCN induces both apoptosis and necrosis while the exposure of HUVECs to HOSCN has been shown to inhibit apoptosis via the inhibition of caspase 3 cleavage in

HUVECs, meaning that these cells become resistant to apoptosis, perhaps via survival pathways [92, 174].

These mixed results can be explained by differences in the cells used, and their unique reaction to the hypohalous acid, HOSCN. Another way these results can be rationalised is by the intrinsic differences in these studies such as treatment times, concentrations and media used. As explained previously, HOSCN is able to reversibly oxidise thiols, so lower concentrations, longer treatment periods and the replacing of treatment media with oxidant-free media, would allow for the repair of any damage.

1.6.4 Hypohalous acids and bioenergetics

1.6.4.1 Glycolysis

HOSCN has long been known to inhibit bacterial glycolysis [194, 195]. In milk and the oral cavity, the requirement for H_2O_2 in the catalysis of HOSCN in the LPO (or SPO)/SCN^-/H_2O_2 system is met by bacterial metabolism [196], as the addition of catalase inhibits the formation of HOSCN and allows for the growth of *Streptococcus cremoris* (strain 972) in milk or *Lactobacillus acidophilus* in saliva [196].

When washed, stationary phase *Streptococcus mutans* incubated with LPO/SCN^- and glucose had the utilisation of glucose inhibited by up to 90 %, [197]. This LPO/SCN^-/H_2O_2 system was shown to be more bactericidal than H_2O_2 alone [198], due to the product formed in the reaction, HOSCN. The product of the lactoperoxidase-catalysed oxidation of SCN^- was found to inhibit glycolysis in *strain 972 Streptococci* after a 30 min treatment at 30 °C. Analysis of the glycolytic enzymes revealed that hexokinase, aldolase and glucose 6-phosphate dehydrogenase were all inhibited to some degree [199]. The removal of LPO/SCN^-/H_2O_2 from *Streptococci* led to the restoration of these enzymes activities. Growth inhibition was hypothesised to occur via the incorporation of a product from the LPO/SCN^-/H_2O_2 system into protein thiols, removing these proteins from the functional pool, especially proteins involved in cell growth, glycolysis and glucose transport [200].

In regards to mammalian glycolytic proteins, HOCl has also been found to oxidise glyceraldehyde 3-phosphate dehydrogenase (GAPDH) in HCAECs, HUVECs and HMDMs after exposure, and it has been hypothesised that thiol targeting is the cause [103, 181, 185, 191]. Data have shown that HOSCN inhibits mammalian GAPDH and creatine kinase (CK) upon

exposure to cell lysates, and intact J774A.1 murine macrophages with evidence indicating the formation of sulfenyl thiocyanate species on these proteins, similar reactivity is reported with HOSCN and GAPDH in HCAECs [185, 201]. Exposure of erythrocytes to HOSCN resulted in the inactivation of glutathione S-transferases, ATPases and GAPDH, finding that the thiol specificity of HOSCN accounted for the deactivation, which for the ATPases, occurred 10 – 10,000 times more potently than HOCl [84].

1.6.4.2 The mitochondria

The mitochondria are organelles found within most eukaryotic cells and are commonly known as the "powerhouse of the cell", as they generate the majority of the ATP, the biologic energy currency [202]. However, the mitochondria are involved in multiple cellular pathways in addition to producing energy. Including roles in cellular signalling, differentiation, growth and death [203]. The role of mitochondria in these crucial mechanisms has implications for several disease processes, such as cardiomyopathy and ageing [32].

Many of the functional proteins and groups of the mitochondrial membrane are sensitive to modification by ROS, including complexes I (NADH dehydrogenase) and V (ATP synthase) [204]. Increases in the generation of ROS can cause damage to and cause alterations in mitochondrial proteins [205, 206]. Many mitochondrially-associated proteins contain critical thiols, such as iron-sulfur clusters, that could be oxidised by both HOSCN and HOCl, including aconitase 2, complexes I, II, III and V, and voltage-dependent anion channel 1 (VDAC-1) [207-215]. The oxidation of these proteins has multiple consequences on the cell, as published data has shown that HOSCN is able to induce mitochondrial dysfunction, as assessed by changes in mitochondrial membrane permeability, at 100 µM after 2 h in HCAECs while HOCl was able to induce mitochondrial dysfunction at concentrations as low as 25 µM (1 h) and 30 µM (20 min), respectively in HCAECs and HepG2s [185, 187].

1.7 Antioxidants and inhibitors of MPO

Molecules that inhibit or have the ability to reverse the oxidation of other molecules, particularly biomolecules, are called antioxidants. Antioxidant systems are a defence to protect organisms from the potentially deleterious effects of ROS, reactive nitrogen species (RNS), free radicals, hypohalous acids and various biological oxidants, all of which are normal

metabolic by-products. In humans, the antioxidant system can be divided up into 2 broad sections, enzymatic and non-enzymatic antioxidants [216, 217]. These antioxidants include, but are not restricted to, superoxide dismutase (SOD), catalase, glutathione (GSH), glutathione reductase (GR), glutaredoxin (Grx), glutathione peroxidase (GPx), thioredoxin (Trx), peroxiredoxin (Prx) ascorbate (vitamin C), α-tocopherol (vitamin E), β-carotene, uric acid and ubiquinol. Additionally, given the role of MPO-derived oxidants in disease, there is significant interest in the development of MPO inhibitors, to prevent hypohalous acid formation and hence mitigate damage.

1.7.1 Enzymatic antioxidants

1.7.1.1 Superoxide dismutase

SOD for a long time were known only as metalloproteins with unknown functions [218]. Now, SOD are recognised as a group of enzymes (CuZn-SOD and MnFe-SOD and Ni-SOD) that catalyse the dismutation of $O_2^{\bullet-}$ to H_2O_2 and O_2 [7]. The SOD-catalysed dismutation of $O_2^{\bullet-}$ may be written as (Reaction 1.17);

$$\mathbf{2O_2^{\bullet-} + 2H^+ + 2e^- \rightarrow H_2O_2 + O_2} \qquad \textbf{Reaction 1.17}$$

In eukaryotic cells, the most common type of SOD is the CuZn (Copper-Zinc) form of the enzyme, found in the cytosol of virtually all animal cells. In humans, 3 forms of the SOD enzyme exist, SOD1 (CuZn-SOD, dimer) is located in the cytosol, SOD2 (Mn-SOD, tetramer) exists in the mitochondria and SOD3 (CuZn-SOD, tetramer) is located extracellularly [7, 219, 220]. SOD is considered the major defensive antioxidant system against the damaging effects of $O_2^{\bullet-}$, and research has demonstrated that the cellular damage caused by $O_2^{\bullet-}$ can be exacerbated by the inactivation of SOD by HOCl and chloramines [221].

1.7.1.2 Catalase

Catalase is found in nearly every living organism that is exposed to oxygen. It catalyses the decomposition of H_2O_2 into water and molecular oxygen (Reaction 1.18) [222].

$$\mathbf{2H_2O_2 \rightarrow 2H_2O + O_2} \qquad \textbf{Reaction 1.18}$$

Catalase also has one of the highest k_{cat} of all enzymes known, converting ca. 5×10^6 of molecules of H_2O_2 to O_2 and H_2O per second [223]. H_2O_2 is a normal, but sometimes harmful by-product of cellular metabolism. Cells use catalase to yield less reactive molecules, removing an integral substrate from use by MPO to create hypohalous acids. In most eukaryotic cells, catalase is commonly found within peroxisomes [224], an organelle interestingly involved in the catabolism of long chain fatty acids, polypeptides, and in the biosynthesis of plasmalogens [225].

1.7.1.3 Glutathione antioxidant system

GSH, GR, Grx, GPx and NADPH make up the glutathione antioxidant system. GSH is a tripeptide, specifically noted due to its active Cys residue, which is important in its antioxidant role [226, 227]. GSH acts by reducing disulfide bonds formed between cytoplasmic proteins, to Cys, by acting as an electron donor. In this process, GSH is oxidised to glutathione disulfide (GS-SG), which can be reduced back to GSH, through the action of the enzyme, GR and NADPH, as an electron donor (Figure 1.5) [228].

GSH is a major antioxidant in cells, with concentrations varying between 0.1 – 10 mM in different cell types and it reacts directly with HOCl, with a rate constant in excess of 10^7 M^{-1} s^{-1}, making it an extremely good defence against oxidative onslaught [229]. These factors help to explain why a loss of macrophage and endothelial cell viability is only observed after treatment with HOCl on depletion of GSH [181, 230]. Other studies have noted that depending on the cell type being studied, GSH also seems to be able to protect membrane thiols from oxidation by HOCl [231, 232] and that it may be the primary antioxidant in preventing oxidation by HOCl in human monocyte-derived macrophages [103]. Not only is GSH a major target for HOCl, but also for HOBr and HOSCN [181, 232] as they are also reported to deplete intracellular GSH levels [91].

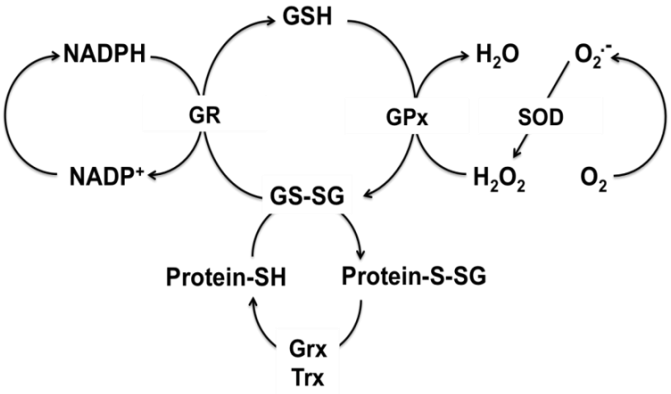

Figure 1.5: Interrelationship of various roles played by the GSH antioxidant system in cellular redox homeostasis.

Glutathione peroxidase (GPx) utilises GSH to catalyse the reduction of H_2O_2 to H_2O, and lipid hydroperoxides to their corresponding alcohols. Several isozymes exist, each varies in their compartmentalisation and specificity, but interestingly, several of these isozymes (GPx 1, 2, 3 and 4) contain seleno-cysteines in their active sites [233]. Reports have given evidence for the inactivation of GPx by HOSCN and HOCl via the rapid oxidation of seleno-cysteine residues important to the function of GPx [99, 234]. Protein S-glutathionylation occurs during times of increased oxidative stress, this is hypothesised to be a protective mechanism of the cell [235]. It is believed to protect key residues from becoming oxidised, while also reserving the pool of GSH in the cell, through their attachment to Cys residues. Glutaredoxin (Grx) is responsible for catalysing the removal of GSH groups from proteins, thus also implicating this enzyme in cellular redox state and signalling [106].

1.7.1.4 Peroxiredoxin antioxidant system

Peroxiredoxins (Prx) are a family of enzymes (3 classes; 2-Cys Prx, 1-Cys Prx and atypical 2-Cys Prx) that exist in many compartments of the cell such as the cytosol, mitochondria, plasma membranes and the peroxisomes [236]. Prx exhibit peroxidase activity that is dependent on the reduction status of GSH or thioredoxin and they exist as homodimers with an active site Cys (the peroxidatic Cys), that is oxidised to sulfenic acid after reaction with the ROS substrate [237]. The sulfenic acid is an intermediate that can react with the Cys of the other subunit, forming a disulfide that can be reduced by thioredoxin (Trx), regenerating the parent enzyme (Figure 1.6) [238].

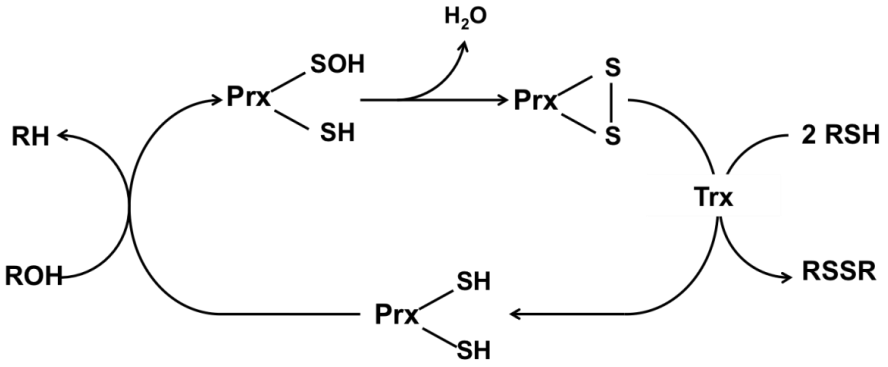

Figure 1.6: The mechanism of the Peroxiredoxin (Prx) antioxidant system, using the typical 2-Cys Prx as an example.

Work carried out by Stacey *et al.* showed that treatment of human umbilical vein endothelial cells (HUVEC) and Jurkat cells with HOCl led to the reversible oxidation of the active site, peroxidatic Cys residue of 2-Cys Prx [239, 240]. This work suggests that even at low levels of exposure, HOCl can modulate the redox status of Prx, possibly contributing to endothelial dysfunction in inflammatory states. While the effect of HOCl on Prx has been studied, little is known about the role of HOSCN in Prx modulation.

1.7.1.5 Thioredoxin

Thioredoxins (Trx) are a class of redox proteins that play a role in redox signalling and act as antioxidants by catalysing the reduction of protein Cys by thiol-disulfide exchange [241]. It reduces protein disulfides by attacking one of the sulfur atoms with a thiolate (S^-) within the Trx protein, and its action has been found to promote the differentiation of the anti-inflammatory M2 macrophage phenotype, offering protective effects against oxidative stress and cardiovascular disease [242-244].

Thioredoxins share many functions with Grx, but a major difference between them relates to the method by which they are reduced. Grx are reduced by GSH, while Trx is reduced by a reductase, the flavoenzyme thioredoxin reductase, in a reaction that is dependent on NADPH activity [245].

1.7.2 Non-enzymatic antioxidants

1.7.2.1 Ascorbate

Ascorbic acid (vitamin C), is a water-soluble antioxidant present in many tissues throughout the human body, and present in plasma at concentrations between 25 – 150 µM [246]. It is a naturally occurring compound, found in fruits including oranges (≈50 mg/100 g), with one of the highest known natural sources being the camu-camu fruit (2400-3000 mg/100 g) [247]. For almost all animals, uptake of ascorbic acid is not essential, as they are able to synthesise it enzymatically, using glucose as a substrate, whereas certain primates including humans, and other animals such as guinea pigs and bats require dietary sources of ascorbic acid [248, 249]. This can make it difficult when trying to study the effects of vitamin C supplementation in human disease. *In vitro*, ascorbate (the biologically active and dominant form of ascorbic acid) can scavenge $O_2^{\bullet-}$, peroxyl radicals, HOCl ($k \approx 2 \times 10^5\ M^{-1}\ s^{-1}$ [23]), and it can inhibit LDL oxidation (Figure 1.7) [250]. Under certain conditions, ascorbate can also behave as a "pro-oxidant". *In vitro*, it is capable of reducing transition metals, and the conversion from ascorbate to dehydroascorbate can generate ROS [251], though this may be limited in a biological system, as any transition metals would likely be chelated or bound to proteins [252].

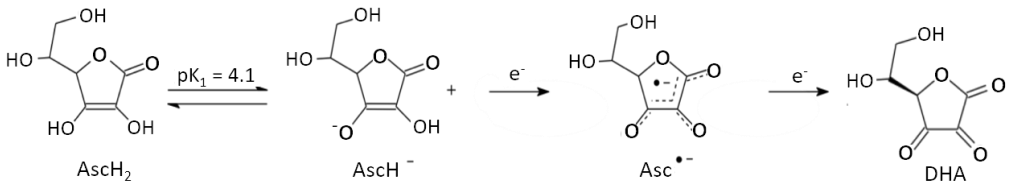

Figure 1.7: Different forms of ascorbate and their reducing ability. *AscH2, Ascorbic acid; AscH−, Ascorbate; Asc•−, Ascorbate radical; DHA, Dehydroascorbate.*

1.7.2.2 Urate

Uric acid is the final product of purine catabolism in humans, and is produced via the oxidation of hypoxanthine by xanthine oxidase and xanthine dehydrogenase. At physiological pH, the majority of uric acid exists as the urate anion. Urate exists in the blood plasma at concentrations ca. 300 µM [253] but is found in much lower concentrations inside

cells. Like ascorbate, urate is a strong reducing agent as it is attributed to over 50% of the antioxidant capacity in blood plasma [254].

Urate can directly react with singlet oxygen ($^1O_2$), $HO^{\bullet}$, and free radicals produced from peroxynitrite ($ONOO^-$) [253]. But more importantly, urate is able to bind transition metals [255], this ability of urate may be important in the prevention of LDL peroxidation in the vessel wall [256]. Once urate reacts with a 1e-oxidant, the urate radical is formed, which can then be reduced by ascorbate. Urate is also a substrate of MPO, it is oxidised by MPO and H_2O_2 to 5-hydroxyisourate, which decays to allantoin, a marker of oxidative stress, and has been implicated in the progression of inflammation and cardiovascular disease [257-259].

1.7.3 MPO inhibitors

MPO inhibitors are compounds used in an attempt to prevent hypohalous acid production and hence the pro-oxidative and inflammatory action of MPO. The inhibitors fall into three different classes, those that promote the accumulation of Compound II, irreversible inhibitors and those that bind reversibly to native MPO. The first two types of inhibitors act as alternative substrates that shift MPO away from its normal catalytic cycle and include chemicals such as dapsone, nitroxides, tryptophan analogues, 4-aminobenzoic acid hydrazide and 2-thioxanthines [260-265]. These methods of MPO inhibition are not necessarily effective, and research of late has preferred the use of reversible inhibitors, such as hydroxamate HX1, which competes with MPO substrates by filling the MPO haem binding pocket, blocking the oxidative capability of the enzyme without altering it permanently. Though the results indicate a drawback of these hydroxamates seems that they can be metabolised by MPO [266]. Moreover, because MPO is a haem peroxidase, with a strong oxidising ability, most of the inhibitors are oxidised by it, forming reactive radicals which can promote other potentially damaging reactions *in vivo* [267].

There is significant interest in the development of novel MPO inhibitors, as MPO and the oxidants formed by it are indicated to play a role in numerous diseases and disorders. The development of potent MPO-inhibitors would potentially therefore be an attractive therapeutic approach to prevent oxidant damage by MPO in inflammatory disease states, such as atherosclerosis and cystic fibrosis [22, 268, 269].

1.8 The beneficial role of MPO and hypohalous acids

1.8.1 Immune role and the destruction of invading pathogens

MPO has been studied extensively in relation to bacterial cell killing. MPO, H_2O_2 and halide ions are able to induce cell death after exposure to bacteria, though this is generally attributed to the formation of hypohalous acids [52, 270]. As mentioned previously, MPO is an important part of neutrophil-mediated defence against infectious agents, with evidence of MPO-deficient mice being increasingly prone to bacterial infection compared to wild-types [271, 272]. In addition, the use of peroxidase inhibitors affects the ability of peroxidase-positive neutrophils to destroy invading pathogens, but had little-to-no effect on peroxidase-negative neutrophils, indicating a major role of MPO in the process of bacterial clearing [270]. A major part of neutrophil-mediated cell killing is the formation of HOCl in the phagosome and the reaction of HOCl with bacterial proteins, causing bacterial cell death [51, 273]. Instead of causing cell death, HOSCN is widely considered to be a bacteriostatic agent, with the ability to reversibly modify bacterial cell proliferation and growth by interacting with critical thiols [56, 274]. Evidence for the bacteriostatic role of HOSCN is highlighted by observations of dysregulated or dysfunctional SCN^- efflux in the epithelial secretions of cystic fibrosis affected cells where these cells have an impaired ability to kill bacteria [275, 276]. The cystic fibrosis transmembrane conductance regulator (CFTR) is the mechanism by which SCN^- is transported into the airway epithelial mucosa. SCN^- is found in abundant levels within the mucosa, along with enzymatically active LPO, leading to favourable conditions for HOSCN formation [36, 277]. Despite HOSCN being formed at high concentrations within the airway mucosa, there is no apparent damage to the host tissue [277-279]. It has been suggested that SCN^- plays a protective role, preventing exposure of lung cells from the damaging effects of HOCl or H_2O_2, and that SCN^- can inhibit the cytotoxic effects by reacting with HOCl and removing it [280].

In spite of this evidence, it seems that humans deficient for MPO are not plagued by bacterial infections, and it has been argued that HOCl and HOSCN do not confer any advantage in bacterial cell killing [53, 281, 282]. However, evidence has shown that the MPO/H_2O_2/Cl^- system does play an integral role in the destruction of invading bacteria [283, 284], but the part of the system that specifically destroys invaders has yet to be fully elucidated.

1.8.2 Oral health

The predominate enzymes within the oral cavity are LPO and salivary peroxidase (SPO), which are closely related enzymes [73]. HOSCN plays a key role in maintaining oral health, with the formation of HOSCN determined by the availability of H_2O_2 and this requirement for H_2O_2 in the LPO (or SPO)/SCN^-/H_2O_2 system is met by bacterial metabolism [196]. Due to the high levels of SCN^- (ca. 1 mM) in saliva, HOSCN tends to be the main oxidant formed within the oral cavity, also because SCN^- is the preferred substrate for LPO/SPO [285].

The role of HOSCN in the mouth is to inhibit glucose metabolism in cariogenic bacteria, and by inhibiting glucose metabolism in these bacteria HOSCN reduces the formation of dental caries [286, 287]. HOSCN is formed in the mouth because of its apparent innocuity to the cells of the oral cavity. This is in contrast to the formation of other hypohalous acids within the oral cavity, such as HOCl formed during gingivitis, which can cause host tissue damage [288].

1.9 MPO, hypohalous acids and disease progression

MPO and hypohalous acids have been implicated to have a role in a wide number of non-infectious and inflammatory diseases. There is considerable evidence on the role of MPO and hypohalous acids in the progression of cystic fibrosis (CF), a chronic inflammatory disease characterised by fibrotic scarring, and abnormal Cl^- and Na^+ transport via the CFTR channel across airway epithelial cells [289, 290]. CF is associated with chronic inflammation and the formation of hypohalous acids, owing to the infiltration of macrophages into the pulmonary tract and the dysfunction of the cystic fibrosis transmembrane conductance regulator (CFTR) [22, 291]. Considerable levels of enzymatically active MPO are found within the sputum of CF patients [292], while 3-Cl-Tyr is detected at high concentrations in the sputum and bronchoalveolar lavage fluid of CF patients [293]. This implicates MPO and HOCl as a damaging oxidant that could incite further inflammation under these conditions.

SCN^- is also transported into the bronchi by the CFTR channel [294], and it has been noted that SCN^- is not released in cells without the CFTR channel [276], therefore it has been hypothesised that inflammation and damage to the pulmonary tract can be exacerbated by the reduction of SCN^-, which is postulated to scavenge the more damaging hypohalous acids, HOCl and HOBr [275, 276].

There is also evidence for the hypohalous acid-induced oxidation of DNA, that can cause mutations to various suppressor genes, which have been hypothesised as a beginning step in cancer progression, with various studies showing that chlorinated bases are able to be incorporated into genomic DNA [295-298]. An increase in the expression of MPO, along with the presence of the biomarkers for HOCl and HOBr induced damage (3-Cl-Tyr and 3-Br-Tyr) in diseased tissue, has also been linked to the progression of various neurodegenerative diseases such as Alzheimer's disease and Parkinson's disease, and atherosclerosis, consistent with the role of MPO in pathogenesis [165, 269, 299, 300].

1.9.1 Atherosclerosis

Evidence linking MPO with atherosclerosis is extensive. This disease is a major source of morbidity and mortality in the western world [301]. It is marked by the deposition of cholesterol and macrophages in medium and large sized arteries [302]. These depositions form "fatty streaks", and can be seen in otherwise healthy people [303]. The fatty streaks become enlarged over many years by causing cellular proliferation and the deposition begins to invade the vessel lumen, obstructing blood flow, becoming an atherosclerotic plaque/lesion. Rupture of the lesion can occur, leading to thrombosis and jeopardising oxygen supply to vital organs, especially the heart and brain [304].

There are a number of hypotheses postulated to explain the initiation and early stages of atherosclerosis. One being the oxidative modification hypothesis [305], that states that LDL is atherogenic once it has been modified or oxidised into a product that is readily internalised by macrophages [306]. The accumulation of this oxidised LDL (oxLDL) results in the formation of foam cells, a hallmark of atherosclerosis (Figure 1.8) [305, 307, 308]. MPO-derived oxidants are postulated to play a key role in this process, with the H_2O_2/MPO/Cl^- system known to be a promoter of LDL oxidation [309, 310]. Foam cells are fat-laden macrophages formed when macrophages are recruited to inflammatory areas, such as a lesion of a blood vessel, where oxLDL is recognised by scavenger receptors such as CD36 and SRB1, and oxidised by hypohalous acids, in an attempt to correct the inflammatory stimuli [142, 311, 312]. The foam cells then migrate into the subendothelial space, where they perpetuate the inflammatory situation [313].

Atherosclerotic lesions contain cells of an inflammatory nature, such as neutrophils, monocytes and tissue macrophages, all of which are known to release MPO upon activation

[314]. There is evidence that these cells release enzymatically active MPO in lesions of all grades in humans [269]. Lesion formation also induces the release and activation of other inflammatory mediators, such as, interleukin-1, tumour necrosis factor and interferon-γ [314, 315]. The MPO-derived oxidants are implicated in disease development owing to the detection of the HOCl biomarker, 3-Cl-Tyr in atherosclerotic lesions [299, 316]. Additionally, 3-Cl-Tyr and MPO have also been found to co-localise in atherosclerotic lesions, with MPO acting as a predictive marker for adverse cardiac events in patients with angina, with evidence showing those deficient in circulating MPO having lower chances of adverse cardiovascular events [21, 317, 318].

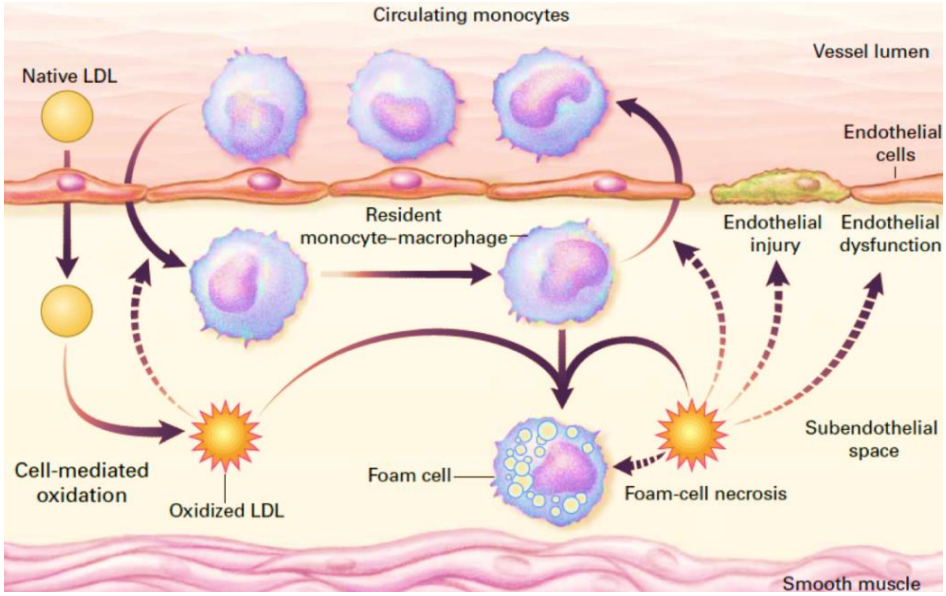

Figure 1.8: The oxidative modification hypothesis of atherosclerosis.

LDL becomes trapped and oxidised by smooth muscle cells, endothelial cells or macrophages, and oxidised LDL stimulates the recruitment of monocytes. Monocytes differentiate into macrophages which uptake oxidised LDL, becoming foam cells. Oxidised LDL can lead to foam cell necrosis, which causes the release of lysosomal enzymes, and endothelial damage. Taken from Diaz et al. [305].

There is also evidence that shows MPO co-localising with macrophages in atherosclerotic plaques, implicating MPO and its products as an important factor in plaque progression and/or plaque formation [269, 317]. Not only does the MPO/H_2O_2/Cl^- system and HOCl

promote LDL oxidation [131, 310], aggravating the problem in the vasculature, but MPO has also been reported to attenuate the protective effects of high density lipoproteins (HDL) via the modification of apoA-1 [319, 320]. The oxidation of apoA-1 directly affects HDL's ability to remove cholesterol from the circulation, accelerating the formation of lipid-laden foam cells [320, 321]. When analysed, the HDL-derived apoA-1 is found to contain 3-Cl-Tyr in elevated levels when compared against healthy samples, further increasing the evidence for HOCl involvement in the inflammatory process of atherosclerosis. [322].

Notwithstanding the wealth of knowledge about the role of HOCl, less is known about the mechanisms controlling MPO and HOSCN in the disease process. This is possibly due to the lack of a biomarker of HOSCN-specific oxidation; however evidence suggests that there is indeed a role for HOSCN in atherosclerosis. Serum SCN^- levels correlate with increased LDL deposition and fatty streak formation in the aorta, and levels of SCN^- increase in areas with MPO-induced damage to lipids and LDL [87, 140]. There is also evidence of HOSCN modifying Cys residues contained on apoB-100, and oxidising cholesteryl esters, resulting in formation of lipid hydroperoxides, 9-HODE and F_2-isoprostanes, resulting in macrophage lipid accumulation and foam cell formation [142].

There is further, indirect evidence that implicates HOSCN in the progression of atherosclerosis, such as elevated levels of homocitrulline, a carbamylated protein product of the reaction between OCN^- and Lys residues, have been detected within diseased arteries and used as an independent marker to predict future adverse events [81]. As OCN^- is a major breakdown product of HOSCN, HOSCN may be an important factor in the oxidation process, it has long been known that smokers are at an increased risk of developing many diseases, particularly atherosclerosis, coupled with evidence that smokers have high plasma SCN^- (up to 300 µM in excessive smokers), it implicates the MPO/H_2O_2/SCN^- system in the development/exacerbation of atherosclerosis [80, 82, 83].

1.9.1.1 Biomarkers for hypohalous acid detection

The role of HOCl in disease, such as atherosclerosis, is supported by the detection of elevated levels of a HOCl-specific marker of oxidative damage, 3-Cl-Tyr [125, 126, 299]. Similarly, 3-Br-Tyr has been employed as a biomarker for HOBr-induced damage [127]. However, there is no specific biochemical marker for HOSCN induced damage. Despite the evidence given, the destructive role of HOSCN in the disease process has only been evinced indirectly.

Homocitrulline formation has been suggested, as one of the decomposition products of HOSCN, OCN^-, can cause protein carbamylation [81]. But a problem arises when trying to detect homocitrulline formation in a cardiovascular disease setting, being that OCN^- is also elevated under uremic conditions, meaning that implicating HOSCN as responsible for tissue damage during cardiovascular disease is not absolute. HOSCN has been shown to oxidise Trp residues on proteins [97], so a biomarker based on a Trp oxidation product has been proposed. However, it has been noted that the HOSCN oxidation of Trp requires strongly acidic conditions, making it an unlikely candidate to detect HOSCN-induced oxidation *in vivo* [122]. Despite the drawbacks, the identification of a HOSCN-specific biomarker, or new methods to determine HOSCN-induced damage to biomolecules would allow further insights into the role played by HOSCN in disease.

1.10 Summary

The data compiled supports theories that explain the roles of haem peroxidases in normal cellular function and their roles in cellular dysfunction. The peroxidases are capable of oxidising halide anions (Cl^-, Br^- and SCN^-) into their respective hypohalous (HOCl and HOBr) and (pseudo)hypohalous (HOSCN) acids. With SCN^- being the preferred substrate for MPO, it is estimated that ca. 50% of the H_2O_2 consumed by MPO is utilised to create HOSCN. Considering this, less is known about the physiological role of HOSCN, other than its antimicrobial role in the human immune system. This warrants further investigations of HOSCN and its ability to cause cellular dysfunction, as published data has currently identified HOSCN as being as able to oxidise proteins related to glucose metabolism, but does not investigate the functional effect of HOSCN in regards to affecting the energy producing pathways such as glycolysis and oxidative phosphorylation. HOSCN is a chemical that oxidises thiols; therefore it has the potential to perturb the activity of several key thiol-dependent enzymes. Additionally, due to its reversible nature and similarity to other hypohalous acids, a biomarker for HOSCN-induced oxidation has not been identified. Therefore this Thesis explores the role of HOSCN in the induction of macrophage damage, which is relevant to the pathological process of atherosclerosis. It will also assess the utility of vibrational spectroscopy as a tool to determine the patterns of damage induced by HOSCN to cells.

1.11 Hypothesis

The oxidant, HOSCN, generated by MPO from SCN^- ions, targets critical thiol containing proteins, such as those related to glucose metabolism and mitochondrial respiration, modulating macrophage cell function in a detrimental manner. HOSCN attenuates the biologic process of energy production, more potently than HOCl via its specificity for thiol oxidation, which could promote the development of atherosclerosis.

1.12 Aims of this Thesis

Chapters 3 – 7 of this thesis will address the following experimental aims based on the projects hypothesis.

1) To determine the mode of oxidation and assess the ability of HOSCN and HOCl to target intracellular thiols in macrophages.
2) Identify, establish and understand the consequences of reversible thiol modifications on energy production, mitochondrial function and cellular function in HOSCN-oxidised macrophages.
3) To use novel methods to detect, identify and understand the damage caused by HOSCN.

2 Materials and Methods

2.1 General Information

This Chapter details the methods and materials used throughout the thesis. All concentrations noted are the final concentration unless stated otherwise.

The pH of all solutions was measured using a Radiometer Analytical PHM220 pH meter with a pHC2401 probe (Radiometer Analytical, France) calibrated with pH 4 and 7 or pH 7 and 10 standards.

Centrifugation was performed on all samples using an Eppendorf Refridgerated Micro-Centrifuge (Model 5215R, Eppendorf, Germany), unless stated otherwise.

Nanopure water, hereinafter referred to as npH_2O, was filtered through a four stage Milli-Q sysem (Millipore Water, Australia).

2.2 Materials

All chemicals and solutions were purchased commercially, were of the highest purity available and were stored and used as instructed by the manufacturer, unless stated otherwise. All aqueous solutions were prepared in npH_2O.

Table 2.1: Suppliers of Reagents

Reagent	Supplier
Acetone	Merck
Aldolase antibody (IgG)	Abcam
ATPlite Luminescence ATP Detection Assay System	Perkin Elmer
Bicinchoninic Acid (BCA) Reagent	Pierce
Bio-Spin 6 Columns in Tris Buffer	BioRad
p-Biotin	Cayman Chemical
Bovine Serum Albumin (BSA)	Sigma-Aldrich
Bradford Assay Reagent	BioRad
L-Buthionine Sulfoximine	Sigma-Aldrich
Carbonyl cyanide *m*-chlorophenyl hydrazone (CCCP)	Life Technologies
Catalase	Sigma-Aldrich
Cell Lytic M Cell Lysis Reagent	Sigma-Aldrich

Cell-Tak Cell and Tissue Adhesive	BD Bioscience
CHAPS	Sigma-Aldrich
COX-4 antibody (IgG)	Abcam
Complex II Enzyme Activity Microplate Assay Kit	Sapphire Bioscience
Coomassie Blue G-250 Dye	Sigma-Aldrich
DAz-2	Cayman Chemical
DCP-Bio1	Merck Millipore
5,5'-dithiobis-(2-nitrobenzoic acid) (DTNB)	Sigma-Aldrich
Dithiothreitol (DTT)	Sigma-Aldrich
Dulbecco's Modified Eagles Medium (DMEM)	JRH Biosciences
ECL-Plus, Enhanced Chemiluminescence Substrate	Perkin-Elmer
Ethylenediaminetetraacetic acid (EDTA)	Sigma-Aldrich
Foetal Calf Serum	Invitrogen
GAPDH antibody (IgG)	Abcam
Glucose Uptake Cell-Based Assay Kit	Cayman Chemical
Glutathione (Reduced) (GSH)	Sigma-Aldrich
Glycolysis Cell-Based Assay Kit	Cayman Chemical
GSH Antibody (IgG2a)	ViroGen Corp.
HEPES	Sigma-Aldrich
High Sensitivity Streptavidin-HRP	Thermo-Fisher
30% (v/v) Hydrogen Peroxide (H_2O_2)	Merck Millipore
5-Iodoacetamidofluorescein (IAF)	Invitrogen
JC-1 (5,5',6,6'-tetrachloro-1,1',3,3' - tetraethylbenzimidazolylcarbocyanine iodide)	Life Technologies
L-Lactate	Sigma-Aldrich
Lactoperoxidase (LPO)	Calbiochem
Lowry DC Protein Assay Reagents	Biorad
Mammalian Mitochondrial Isolation Kit	Thermo Fisher Scientific
N-ethylmalemide (NEM)	Sigma-Aldrich
Nicotinamide adenine dinucleotide (NADH), disodium salt	Roche
NuPAGE Novex 4-12% Bis-Tris Gel (1 mm, 10 well)	Invitrogen
Phenylmethylsulfonyl Fluoride (PMSF)	Sigma-Aldrich
Phosphate Buffered Saline (PBS)	Amresco
Protease Inhibitor (Complete)	Roche Diagnostics
RIPA Buffer	Sigma-Aldrich

Ruthenium(II)tris(bathophenantrolinedisulfonate) (RuBPS)	Jomar Bioscience
Seahorse XF Base Medium	In Vitro Technologies
Seahorse XF Calibrant Solution	In Vitro Technologies
Seahorse XF Mito Stress Test Kit	In Vitro Technologies
Seahorse XF Glycolysis Stress Test Kit	In Vitro Technologies
Skim Milk Powder	Bonlac Foods Ltd
Sodium Dodecyl Sulfate (SDS)	Sigma-Aldrich
10 – 15 % (v/v) Sodium Hypochlorite	Sigma-Aldrich
Sodium Diphosphate	Sigma-Aldrich
Sodium Monophosphate	Sigma-Aldrich
Sodium Pyruvate	Sigma-Aldrich
Sodium Thiocyanate	Sigma-Aldrich
ThioGlo-1	Berry & Associates Inc
Trichloroacetic acid (TCA)	Sigma-Aldrich
Tris	Sigma-Aldrich
Trisephosphate isomerase antibody (IgG)	Abcam
Triton X-100	Sigma-Aldrich
Tween 20	Sigma-Aldrich

2.3 Methods

2.3.1 Tissue Culture

2.3.1.1 J774A.1 Murine Macrophage Cells

The cell experiments performed in this Thesis were carried out using J774A.1 cells, a murine macrophage-like cell line. J774A.1 cells were obtained from the American Type Culture Collection (ATCC, USA) (cat. no TIB-67). Cells were cultured in Dulbecco's modified Eagle's medium (DMEM) supplemented with 10% v/v foetal bovine serum (FBS) and 2 mM L-glutamine that was warmed to 37 ˚C prior to use. During passaging cells were maintained in a 175 cm^2 flask under sterile conditions in an incubator of humidified 5% CO_2 at 37 ˚C. When cells had reached 80 - 90% confluency, cells were washed twice with DMEM, and then scraped from the flask into 10 mL of fresh DMEM, with 2 mL of the cell suspension then

transferred into a new flask and the total volume adjusted to 25 mL with DMEM. Cells reached confluency 3-4 days after splitting.

Prior to experiments (excluding experiments using the Seahorse XF24), cells were washed with fresh DMEM, followed by scraping from the flasks into 10 mL of DMEM and counted using a haemocytometer in the presence of 0.2% v/v trypan blue to exclude dead cells. Cells were then centrifuged in an Allegra X-15R centrifuge (Beckman Coulter) at 400 *g* for 5 min at 22 ˚C to form a cell pellet. The pellet was then resuspended in DMEM to the required density of cells (1×10^6 cells mL^{-1}) before being transferred to 12-well plates and incubated in a sterile environment, overnight at 5% CO_2 and 37 ˚C.

2.3.1.2 Oxidant treatment of J774A.1 cells

For the experiments detailed in this Thesis, cells were plated at a density of 1×10^6 cells mL^{-1} in DMEM into 12-well plates and allowed to adhere overnight in an incubator of humidified 5% CO_2 at 37 ˚C. The next day, cells were washed twice with HBSS prior to incubation with oxidant (at 22 ˚C). Following oxidant treatment, the oxidant was removed and the cells were again washed with HBSS to prevent confounding reactions resulting from residual oxidant or media components.

2.3.1.3 Mitochondrial isolation of J774A.1 cells

The mitochondrial isolation was performed using a mammalian mitochondrial isolation kit (Thermo Fisher Scientific). Before the isolation of J774A.1 mitochondria, protease inhibitors (1x) were added to the volumes of Reagent A and C to be used in the experiment. After the cells had been treated with oxidant (Section 2.3.1.2), 3 wells (1×10^6 cells/well) of cells were combined and then the consolidated cell suspension (3×10^6 cells) was pelleted by centrifugation at 900 *g* for 2 min at 4 ˚C. The supernatant was carefully removed and discarded before 800 µL of Reagent A was added and the mixture was vortexed at medium speed for 5 sec and incubated on ice for exactly 2 min. After the incubation, 10 µL of Reagent B was added, and the mixture was vortexed at high speed for 5 sec. The tube was then incubated on ice for 5 min, with vortexing at maximum speed for 5 sec every minute. After the final vortexing, 800 µL of Reagent C was added to the tube and it was inverted several

times to mix (being careful not to use the vortex again). The tube was then centrifuged at 700 *g* for 10 min at 4 ˚C. After centrifugation, the supernatant was removed, being careful not to disturb the pellet. The supernatant was transferred to a new tube and the pellet was discarded. The supernatant was then centrifuged at 3000 *g* for 15 min at 4 ˚C. After the centrifugation, the supernatant was a purified fraction of the cytosol, while the pellet contained the mitochondria. The supernatant was removed carefully and placed into new tubes to be stored on ice. The pellet was then washed with 1 mL of Reagent C and centrifuged at 12,000 *g* for 5 min at 4 ˚C. After centrifugation, the supernatant was removed and discarded, then the pellet was lysed in 75 µL mitochondrial lysis buffer (0.5% Triton X-100; 30 mM Tris, pH 7.4; 200 mM KCl; 5 mM Ethylenediaminetetraacetic acid [EDTA]; 0.5 mM phenylmethylsulfonyl fluoride [PMSF]; 1x protease inhibitors) with vigorous vortexing for 1 min, after which the samples were stored on ice. To determine the protein concentration of both the cytosolic and mitochondrial fractions, a DC Lowry protein assay was performed and concentration was determined against a BSA standard curve (Section 2.3.12.3).

2.3.2 Preparation and Quantification of Oxidants

2.3.2.1 Generation of HOSCN and decomposed HOSCN

HOSCN was produced enzymatically from the reaction of H_2O_2 with SCN^- in the presence of LPO [91]. 2 µM LPO was incubated with 7.5 mM NaSCN in 10 mM pH 6.6 potassium phosphate buffer. The solution was then left on ice and aliquots of H_2O_2 (3.75 mM) were added every minute for 5 min. The suspension was then left to incubate on ice for 10 min, prior to the addition of 200 IU of catalase for 5 min. The solution was then filtered through a 10 kDa molecular mass cut-off filter (Pall Corporation) by centrifugation 12,000 *g* for 5 min at 4 ˚C to remove the LPO and catalase from the solution. The concentration of HOSCN generated was quantified immediately by the TNB assay (Section 2.3.2.3) using the molar absorption coefficient (ε) ε_{412} = 14150 M^{-1} cm^{-1} [323].

Decomposed HOSCN (dHOSCN) was generated by producing HOSCN and leaving it in the dark for at least 24 h at 22 ˚C. This control is limited by the variability of HOSCN's breakdown products, and the individual chemicals and their concentrations can differ between samples, and the products added to the cell may vary slightly.

2.3.2.2 Preparation of HOCl

HOCl was prepared by diluting a concentrated stock solution of 1 M NaOCl into npH_2O to a final concentration of 1 mM. This solution was then diluted further into HBSS immediately prior to addition to the cells. The concentration of $^{-}$OCl in the stock solution was determined at pH 11 after the dilution into 0.1 M NaOH and measured using the optical absorbance at 292 nm, where ε_{292} = 350 $M^{-1}cm^{-1}$ [57].

2.3.2.3 TNB assay

The yellow coloured 5-thio-2-nitrobenzoic acid (TNB) reacts with hypohalous acids (HOX) and N-chloramines to produce a colourless dimer 5,5-dithio-bis(2-nitrobenzoic acid) (DTNB). The concentration of HOX can be determined by monitoring the consumption of TNB, noting the 1:2 stoichiometry as shown in Reaction 2.1 using the ε_{412}= 14150 $M^{-1}cm^{-1}$ [41].

HOX + 2 RSH → RSSR + H_2O + H^+ + X^- **Reaction 2.1**

The TNB reagent is prepared before each experiment by alkaline hydrolysis of DTNB. DTNB (0.4 mg mL^{-1}) was prepared in 50 mM NaOH and incubated in the dark for 10 min to produce a dark yellow stock TNB solution. The TNB was diluted 1:50 into 100 mM sodium phosphate buffer (pH 7.4) to attain a working solution with an optical absorbance of 0.4 – 0.5 at 412 nm. The oxidant (5 µL) was then added to the diluted TNB reagent (1 mL final volume), and incubated in the dark for 10 min. The absorbance was measured at 412 nm and the consumption of TNB was determined by comparison to a blank solution containing TNB and an identical volume of buffer [115].

The samples were pipetted into plastic cuvettes (1 cm path length) and the absorbance was measured on a UV-Vis spectrophotometer (Shimadzu).

2.3.3 Intracellular thiol quantification

2.3.3.1 ThioGlo-1 assay

Methyl-maleimidobenzochromenecarboxylate (ThioGlo-1) (Berry & Associates Inc) was used for the determination of the concentration of free thiols and reduced protein thiols in cell

lysate preparations via a fluorometric method [324]. ThioGlo-1 is a maleimide-based fluorescent dye that binds to thiols within a sample, resulting in an increase in fluorescence. A stock solution of ThioGlo-1 (2.4 mM) was prepared in acetonitrile and stored at 4 ˚C in the dark. Prior to addition to the sample cells were treated with oxidant (Section 2.3.1.2) and then lysed in npH_2O (1 mL). An equal volume (50 µL) of sample was added to a solution of ThioGlo-1, diluted 1:100 in PBS (pH 7.4). The resulting solutions were incubated in the dark for 5 min at 22 ˚C in a 96-well plate. Thiol concentrations were determined by fluorescence spectroscopy at λ_{ex} = 360 nm and λ_{em} = 530 nm using a SpectraMax M2e plate reader. The concentration of thiols in each sample was determined by constructing a GSH (0 – 10 µM) standard curve [324] and an N-Ethylmaleimide (NEM) (1 mM; 15 min) control to block available thiols in the sample and probe for any sample auto-fluorescence or non-thiol interactions that would cause fluorescence.

2.3.3.2 5-Iodoacetamidofluorescein (IAF) labelling

The thiol-reactive fluorescent probe, 5-iodoacetamidofluorescein (IAF) was used in conjunction with *N*-ethylmaleimide (NEM), a thiol reactive alkene, to probe oxidant treated samples for reversible protein thiol oxidation (Figure 2.1).

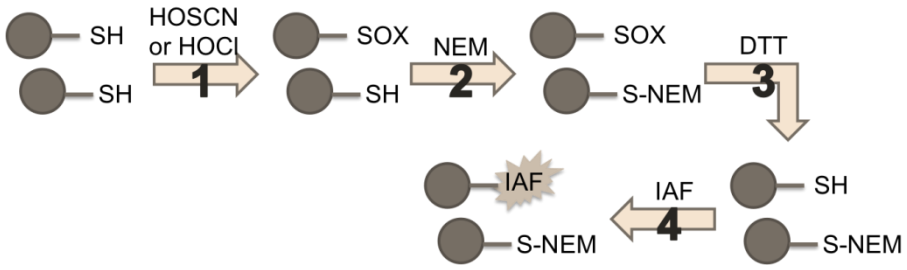

Figure 2.1: Using IAF to probe for reversible oxidation products.

The outline of the IAF labelling procedure used to probe J774A.1 proteins for reversible thiol oxidation. Beginning with reduced thiols (1) certain thiols are oxidised by treatment of J774A.1 cells with hypohalous acids. (2) After oxidation, residual reduced thiols were alkylated with NEM to block them from taking part in further reactions. (3) Oxidised thiols were then reduced using DTT and (4) alkylated with the fluorescent probe, IAF.

Cells were plated at a density of 1 × 10^6 cells mL^{-1} and exposed to oxidant (Figure 2.1, Step 1). After oxidant treatment, cells were lysed in 225 µL of labelling buffer (35 mM HEPES, 0.1% Triton X, 100 mM NEM and 1 × Roche complete protease inhibitor), scraped with a syringe plunger and left to incubate on an orbital shaker for 30 min at 22 ˚C. NEM was present in the lysis buffer to alkylate any protein thiols that were in a reduced state (Figure 2.1, Step 2). After incubation, the lysate was centrifuged at 8000 *g* for 5 min at 4 ˚C. The supernatant was then passed through a Bio-Spin 6 spin column (BioRad) to remove excess NEM, according to the manufacturer's instructions. The solution that passed through the spin columns was then removed and transferred into new 1.5 mL tubes. Dithiothreitol (DTT) was then added to a final concentration of 1 mM and the samples were incubated for 10 min at 22 ˚C to reduce any thiols that had been reversibly oxidised (Figure 2.1, Step 3). Solutions were passed through Bio-Spin 6 spin columns to remove residual DTT, and IAF (80 mM in DMSO) was added to the sample solution (to a final concentration of 100 µM) and left to react with reduced thiols for 10 min at 22 ˚C in the dark (Figure 2.1, Step 4) [325]. The protein concentration was determined at this time using the Bradford protein assay (Section 2.3.12.1). Protein precipitation was performed via the addition of TCA (10% w/v) to the sample, followed by incubation for 20 min at -20 ˚C. Protein was pelleted by centrifugation at 8000 *g* for 15 min at 4 ˚C. The supernatant was then removed and the protein pellet was washed with ice-cold acetone (80% v/v) and stored either overnight or for 2 h at -20 ˚C. Following the incubation, samples were centrifuged at 10000 *g* for 15 min at 4 ˚C and the acetone was removed. The protein pellet was then dissolved in lithium dodecyl sulfate (LDS) sample buffer (Invitrogen, CA) for gel loading. The pellets were dissolved in various volumes of PBS to ensure equal protein loading onto the gel (800 µg mL^{-1}) [185, 326].

2.3.3.3 DAz-2 derivatisation

DAz-2 is a cell permeable probe used to detect protein sulfenic acid formation [327, 328]. Modification of protein cysteines and sulfenic acid formation can result in the modification of protein function, with these species reported to act as molecular switches, responsible for activating or deactivating enzyme activity [109, 329]. Cells (1 × 10^6 cells mL^{-1} in a 12-well tissue culture plate) were loaded with DAz-2 in DMSO (to a final concentration of 500 µM) or a vehicle control (DMSO – 1% v/v) in DMEM (1 mL) for 1 h at 37 ˚C and 5% CO_2. After incubation with DAz-2, the cells were washed three times with HBSS and treated with HOSCN or HOCl for 1 h at 22 ˚C (Section 2.3.1.2). Following treatment, the cells were washed three

times with HBSS and then lysed with 100 µL cold lysis buffer (50 mM Tris pH 8.0, 150 mM NaCl, 1% NP-40, 2 × Roche complete protease inhibitor), scraped with a syringe plunger and incubated on an orbital shaker for 20 min at 4 ˚C. Lysates were centrifuged 10000 *g* for 20 min at 4 ˚C to remove insoluble cell debris and the supernatant was collected. Protein concentration was determined at this time using the BCA protein assay (Section 2.3.12.2). Following the incorporation of DAz-2 into the cellular proteins, the DAz-2 azide-tagged proteins were ligated to p-Biotin via the click reaction [330]. The lysate was incubated with p-Biotin (200 µM) and DTT (5 mM) for 2 h at 37 ˚C while being shaken. The reaction was then quenched by protein precipitation with ice-cold acetone (1 mL) and the samples were incubated for 2 h at -20 ˚C or overnight at -80 ˚C. Following incubation, the samples were collected and centrifuged at 10000 *g* for 20 min at 4 ˚C to pellet the proteins. The pellets were washed once again and centrifuged before being dissolved in LDS sample buffer (Invitrogen) (assuming complete recovery after acetone-precipitation). The protein pellets were dissolved in various volumes to ensure equal protein loading onto the gel (800 µg mL^{-1}).

2.3.3.4 DCP-Bio1 derivitisation

DCP-Bio1 is a cell permeable probe, similar to DAz-2, in that it displays specificity for sulfenic acid formation. However, the DCP-Bio1 is already conjugated to biotin, which removes the need to perform a click reaction. Cells (1×10^6 cells mL^{-1} in a 12-well tissue culture plate) were loaded with DCP-Bio1 in DMSO (to a final concentration of 500 µM) or a vehicle control (DMSO) in DMEM (1 mL) for 1 h at 37 ˚C and 5% CO_2. After incubation with DCP-Bio1, the cells were washed three times with HBSS and treated with HOSCN (0, 50, 100 or 200 µM) for 1 h at 22 ˚C (Section 2.3.1.2). After oxidant treatment, the cells were washed three times in HBSS and then mitochondrial isolation was performed (Section 2.3.1.3). After mitochondrial isolation and protein concentration determination, the samples were prepared in LDS sample buffer (Invitrogen) and reducing buffer (Invitrogen) to a volume of 40 µL and a protein concentration of 800 µg mL^{-1} before being loaded onto the gel.

2.3.4 SDS-PAGE

2.3.4.1 Gel electrophoresis

SDS-PAGE was used to separate proteins and was carried out using either 10- or 12-well pre-cast mini-format 4-12% acrylamide Bis-Tris gels (Life Technologies). Samples were loaded into wells and separated at 80 V until the dye front reached the gel interface (typically 15 min); samples were then run at 120 V for 1 h or until the dye front reached the bottom of the gel. Gels which were used to separate samples labelled with IAF were run in the dark. The running buffer contained 50 mM Tris, 0.38 M glycine and 0.1% (w/v) SDS, pH 7.4.

2.3.4.2 IAF visualisation

Following electrophoresis, gels were transferred to npH_2O and then scanned for IAF fluorescence at λ_{ex} = 488 nm and λ_{em} = 530 nm on the PharosFX system (BioRad, USA). The gels were then fixed in 200 mL of 30% (v/v) methanol and 10% (v/v) acetic acid for 4 h at 22 ˚C.

2.3.4.3 Protein staining

The protein loading was assessed after fixing the gels in gel-fixing solution (30% (v/v) methanol and 10% (v/v) acetic acid in npH_2O) overnight at 4 ˚C in the dark. Gels were stained in a solution of 200 nM ruthenium (II) tris (bathophenantroline disulfonate) (RuBPS), 30 % (v/v) methanol and 10 % (v/v) acetic acid, overnight at 22 ˚C in the dark. Gels were then washed in npH_2O for 10 min in the dark, prior to measuring RuBPS fluorescence at λ_{ex} = 532 nm and λ_{em} = 605 nm, by scanning the gel on the PharosFX system (BioRad, USA).

2.3.5 Western blotting

Following electrophoresis, proteins were transferred to polyvinylidene fluoride (PVDF) membranes (iBlot transfer stacks, Life Technologies) using an iBlot 2 transfer device (Invitrogen). The transfer occurred for 7 min (program 0), prior to blocking of the membrane as described below.

2.3.5.1 DAz-2, DCP-Bio1 derivatisation and biotinylated proteins

The membrane was blocked in 3 % (w/v) BSA in PBS containing Tween 20 (PBST, 0.1 % v/v Tween 20) overnight at 4 ˚C. The membrane was then washed with PBST (3 × 10 min) and incubated with 1:10000 horseradish peroxidase (HRP)-streptavidin in 3 % (w/v) BSA-PBST for 1 h at 22 ˚C. The membrane was then washed with PBST (3 × 10 min) and immunodetection was performed using ECL Plus chemiluminescence reagents (Perkin-Elmer, USA), and detected by a ChemiDoc XRS (BioRad, USA).

2.3.5.2 S-Glutathionylated proteins

Membranes were blocked for 1 h at 22 ˚C in 3 % (w/v) BSA in PBST containing 2.5 mM NEM (to alkylate any thiol contaminates present in the BSA solution). Membranes were incubated overnight at 4 ˚C with 1:1000 anti-GSH IgG (ViroGen) in PBST. Prior to washing with PBST (3 × 10 min), and incubation with 1:1000 anti-mouse rabbit IgG (Cell Signalling) in 3 % BSA (w/v) in PBST. Finally, the membranes were washed with PBST (3 × 10 min) before immunodetection was performed using ECL Plus chemiluminescence reagents (Perkin-Elmer, USA), and detected by a ChemiDoc XRS (BioRad, USA).

2.3.5.3 Housekeeping proteins

β-actin, GAPDH, trisephosphate isomerase, fructose-bisphosphate aldolase and COX-4 antibodies were used to determine the protein loading in experiments involving DCP-Bio1 (Section 2.3.3.4). PVDF membranes were incubated with their respective loading control antibody at 1:1500 in 3 % (w/v) BSA-PBST for 1 h at 22 ˚C. The PVDF membranes were then washed with PBST (3 × 10 min), then incubated with 1:1000 anti-mouse rabbit IgG (Cell Signalling) in 3 % BSA (w/v) in PBST. The membrane was then washed with npH_2O and dried before being immunodetection was performed using ECL Plus chemiluminescence reagent (Perkin-Elmer, USA), and detected by a ChemiDoc XRS (BioRad, USA).

2.3.5.4 Protein staining of membranes

Protein staining of the PVDF membranes was carried out to confirm equal protein loading. Membranes were incubated with 0.05% (w/v) Coomassie R-250 (Sigma-Aldrich) in isopropanol/acetic acid/npH_2O (50:20:30) for 2 h. The membrane was then destained for 1 h in isopropanol/acetic acid/npH_2O (13:10:77), and washed with npH_2O, dried, before being immunodetection was performed using ECL Plus chemiluminescence reagents (Perkin-Elmer, USA), and detected by a ChemiDoc XRS (BioRad, USA).

2.3.5.4.1 Determining band density and analysis

After gel or PVDF membrane imaging was performed, the detected bands were analysed using Image J software. The images were opened in the software and the bands were selected using the "Select Lane Tool" (Figure 2.2A). The image was then processed and the band intensities were plotted, with each lane being plotted on separate graphs (peaks display each bands intensity within a specific lane) (Figure 2.2B). To integrate the peaks, the "Line Tool" was used to create a rolling ball integration (Figure 2.2C), which was done separately for each protein lane. Finally, the "Wand Tool" was used to determine the area under each peak of a lane (Figure 2.2D, example of Lane 1), which was then summed to give the total density of detected product in each lane, which was expressed as Area (Pixels).

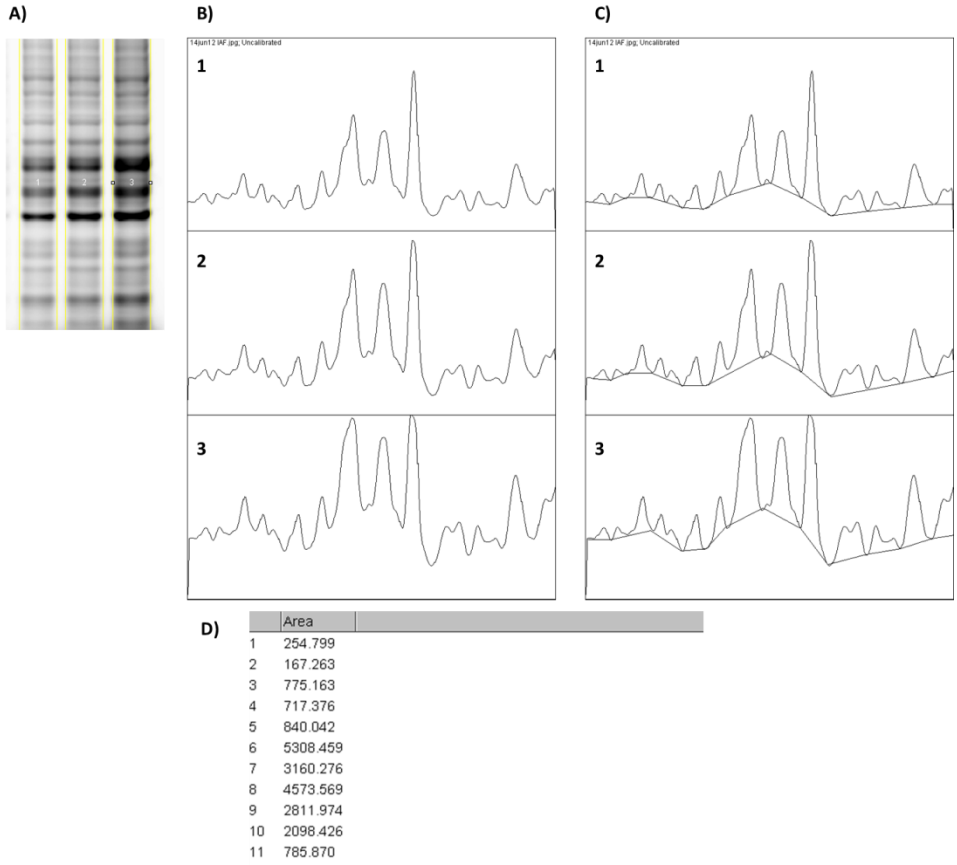

Figure 2.2: Using Image J to analyse protein band densities.

An example of protein density analysis using Image J. The scanned gel or membrane with detectable proteins was scanned and the image is loaded into the program. (A) An example of a typical scanned gel with Lane 1; 0 µM HOSCN, Lane 2; 50 µM HOSCN and Lane 3; 100 µM HOSCN being selected using the lane selection tool. (B) An intensity plot of the selected lanes (numbers correspond with lanes). (C) Peaks after using a rolling ball method of integration. (D) Using the "Wand Tool" the area of the peaks is determined (example of Lane 1 results).

2.3.6 Seahorse XF24 extracellular flux assays

Extracellular flux analysers probe energy producing pathways of the cell in real time. The XF24 analyser determines oxygen consumption rates (OCR) and extracellular acidification rates (ECAR) in cellular extracellular media to determine the functions of oxidative phosphorylation and glycolysis. The analyser measures OCR and ECAR by isolating small volumes of media above a cellular monolayer. Oxidative phosphorylation and glycolysis cause almost instantaneous and measureable changes to the dissolved oxygen and free

protons in the media and it is these changes that allow for the determination of respiratory and glycolytic activity of cells.

2.3.6.1 Plate and cartridge preparation

To maintain cell adhesion during the flux assay, the XF24-well cell plate was prepared with BD Cell-Tak adhesive (BD Biosciences). The Cell-Tak adhesive was added to the XF24 plate (0.28 cm^2/well) at a density of 3.5 µg/cm^2 in $NaHCO_3$. Cell-Tak (20 µL) was added to each well and the plate was left for 30 min at 22 ˚C in a sterile environment. The Cell-Tak solution was removed and 300 µL npH_2O was added to the plate and it was left for 5 min at 22 ˚C. The npH_2O was then removed and the plate was left to dry in a sterile environment for 30 min at 22 ˚C. Once dry, the plate could be stored for up to 7 days at 4 ˚C.

Prior to running the Seahorse XF24, the XF24 probes on the cartridge were rehydrated with 1 mL XF calibrant solution (Seahorse Bioscience, USA) and left to incubate in a CO_2-free environment overnight at 37 ˚C (Figure 2.3).

Figure 2.3: XF24 probe cartridge and cell culture plate.

A profile view of the XF24 probe cartridge (green) containing the wells to place inhibitors, and the XF24 cell culture plate which was coated with Cell-Tak adhesive and plated with J774A.1 macrophages.

2.3.6.2 Preparation of cells

The media was removed from the J774A.1 cells in 175 cm^2 flasks and the cells were washed 3 times with HBSS before the media was replaced with XF base medium (Seahorse

Bioscience, USA), containing 2 mM L-glutamine, 40 mM sodium pyruvate and 10 mM glucose (glucose was excluded if the glycolysis assay was to be performed). The cells were then scraped from the flask and a small volume (10 µL) of cell suspension was removed for counting in the presence of 0.2% (w/v) trypan blue (10 µL) to exclude dead cells. Cells were then centrifuged in an Allegra X-15R centrifuge (Beckman Coulter) at 400 *g* for 5 min at 22 ˚C to form a cell pellet. The pellet was then resuspended in the XF base medium and the cells were plated on the XF24 plate at 7.5×10^4 cells/well. Cells were excluded from 4 wells on the XF24 plate as they served as background wells (as per the manufacturer's instruction). The plate was then left to incubate in a CO_2-free incubator at 37 ˚C for 45 min.

2.3.6.3 Baseline Glycolysis

Before treating the cells with oxidant, the rehydrated probe cartridge was prepared with 100 mM glucose (50 µL) pipetted into PORT A (Figure 2.4A), to be injected during the stress test. The rehydrated probe cartridge was then placed into the Seahorse XF analyser to undergo a 15 min calibration. The cells (7.5×10^4 cells/well) were then treated with HOSCN (10, 25, 50, 100 µM) or a pH 6.6 potassium phosphate buffer control in the base medium (no glucose) (final volume = 450 µL) and the cell plate was placed directly into the XF24 analyser. Extracellular acidification rate (ECAR) was monitored over a period of 13 cycles (Equilibrate, Loop (3 ×), Shake (3 min), Wait (3 min), Measure (3 min), End Loop, Inject PORT A, Loop (10 ×), Shake (3 min), Wait (3 min), Measure (3 min), End Loop). After the experiment had concluded the cells were removed from the analyser, media on the cells was removed and the cells were lysed in 25 µL RIPA buffer and glycolytic activity was normalised to cell protein after quantification using the DC Lowry protein assay (Section 2.3.12.3).

2.3.6.4 Glycolysis stress test

After incubation in the CO_2-free incubator at 37 ˚C for 45 min, the cells were treated with HOSCN (10, 25, 50, 100 µM) or a pH 6.6 potassium phosphate buffer control in the base medium (no glucose) (final volume = 300 µL) for 1 h at 22 ˚C. While the cells were being treated, the rehydrated probe cartridge was prepared with the glycolysis inhibitors to be injected during the stress test. Glucose (50 µL, 100 mM) was pipetted into PORT A, Oligomycin (50 µL, 13.5 µM) was pipetted into PORT B and 2-deoxyglucose (50 µL, 1 M) was

pipetted into PORT C (Figure 2.4B). The cartridge was then placed into the Seahorse XF24 analyser to undergo a 15 min calibration. After treatment, the cell plate was placed into the XF24 analyser and the glycolysis stress test was performed. The experimental protocol to observe ECAR was setup in the following order: Equilibrate, Loop (3 ×), Shake (3 min), Wait (3 min), Measure (3 min), End Loop, Inject PORT A, Loop (3 ×), Shake (3 min), Wait (3 min), Measure (3 min), End Loop, Inject PORT B, Loop (3 ×), Shake (3 min), Wait (3 min), Measure (3 min), End Loop, Inject PORT C, Loop (3 ×), Shake (3 min), Wait (3 min), Measure (3 min), End Loop. After the experiment had concluded, the cells were removed from the analyser, media on the cells was removed and the cells were lysed in 25 µL RIPA buffer and glycolytic activity was normalised to cell protein after quantification using the DC Lowry protein assay (Section 2.3.12.3).

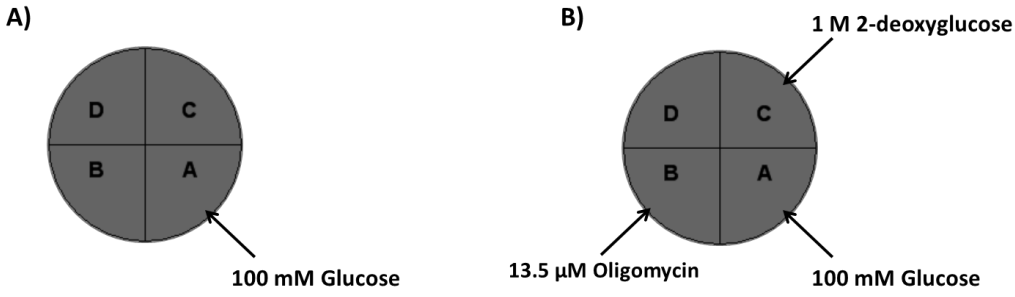

Figure 2.4: XF24 probe cartridge port layout for baseline glycolysis and glycolysis stress test experiments.

2.3.6.5 Baseline mitochondrial respiration

Before treating the cells with oxidant, the rehydrated probe cartridge was prepared by placing it in the Seahorse XF24 analyser to undergo a 15 min calibration. The cells were treated with HOSCN (50, 75, 100, 150 µM) or a pH 6.6 potassium phosphate buffer control in the base medium (final volume = 500 µL) and the cell plate was placed directly into the XF24 analyser and baseline oxygen consumption rate (OCR) was monitored over a period of 10 cycles (Equilibrate, Loop (10 x) Shake (3 min), Wait (3 min), Measure (3 min), End Loop). After the experiment had concluded the cells were removed from the analyser, media on the cells was removed and the cells were lysed in 25 µL RIPA buffer and glycolytic activity was

normalised to cell protein after quantification using the DC Lowry protein assay (Section 2.3.12.3).

2.3.6.6 Mitochondrial stress test

After incubation, the cells were treated with HOSCN or a pH 6.6 potassium phosphate buffer control in the base medium (final volume = 500 µL) for 1 h at 22 ˚C. While the cells were being treated, the cartridge was prepared with the mitochondrial inhibitors to be injected during the stress test. Oligomycin (55 µL, 15 µM) was pipetted into PORT A of the cartridge, FCCP (61 µL, 5 µM) was pipetted into PORT B and a cocktail of antimycin A (5 µM) and rotenone (5 µM) (68 µL) was pipetted into PORT C (Figure 2.5). The cartridge was then placed into the Seahorse XF24 analyser to calibrate. After treatment, the cell plate was then placed into the XF24 analyser and the mitochondrial stress test was performed. The experimental protocol to observe OCR was setup in the following order: Equilibrate, Loop (3 ×), Shake (3 min), Wait (3 min), Measure (3 min), End Loop, Inject PORT A, Loop (3 ×), Shake (3 min), Wait (3 min), Measure (3 min), End Loop, Inject PORT B, Loop (3 ×), Shake (3 min), Wait (3 min), Measure (3 min), End Loop, Inject PORT C, Loop (3 ×), Shake (3 min), Wait (3 min), Measure (3 min), End Loop. After the experiment had concluded the cells were removed from the analyser, media on the cells was removed and the cells were lysed in 25 µL RIPA buffer and metabolic activity was normalised to cell protein after quantification using the DC Lowry protein assay (Section 2.3.12.3).

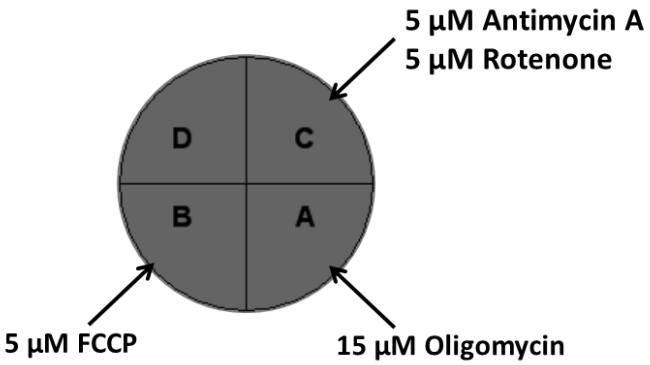

Figure 2.5: XF24 probe cartridge port layout for the mitochondrial stress test experiment.

2.3.7 Determination of mitochondrial membrane potential

JC-1 (Life Technologies) is a membrane permeable dye that exhibits potential-dependent accumulation in the mitochondria. In the mitochondria JC-1 becomes a red fluorescent J-aggregate which can leak out into the cytosol with changes in membrane potential, where the aggregates are lost and JC-1 fluoresces green [331, 332]. This ability allows for the determination of mitochondrial membrane potential after the treatment of cells with oxidant. JC-1 experiences an emission shift from green (λ_{em} = 529 nm) in the cytosol to red (λ_{em} = 590 nm) in the mitochondria due to the formation of these J-aggregates. Therefore, mitochondrial depolarisation is indicated by a decrease in the red/green fluorescence intensity ratio. After oxidant treatment, the media was removed from the cells and they were washed twice with HBSS, before adding 1 mL of HBSS to each well of cells, and scraping them from the plate. Pipetting was then performed to ensure that the cells were mixed homogeneously throughout the HBSS. The cells were pipetted into flow cytometry tubes and labelled with 2 µM JC-1 and left to incubate for 15 min in an incubator of humidified 5% CO_2 at 37 ˚C. Positive controls were treated with 5 µM of the mitochondrial uncoupler, CCCP, for 10 min in an incubator of humidified 5% CO_2 at 37 ˚C. When complete the cells were analysed using a BD flow cytometer scanning both the emission shift from 590 nm to 530 nm, indicating a leak of the JC-1 from inside to mitochondria (red) to the cytosol (green). This leak is viewed as a percentage of the total counts (10, 00 counts), that is then expressed as a ratio (red/green), with a decrease in the ratio indicating an increase in the permeability of the mitochondrial permeability transition pore (MPTP).

2.3.8 ATP assays

Intracellular adenosine triphosphate (ATP) is a marker for cell viability as ATP is required by and present in all metabolically active cells [333]. The concentration of ATP declines rapidly in cells undergoing failure in the mechanisms that synthesise ATP, such as glycolysis or oxidative phosphorylation. The ATPlite assay (Perkin Elmer) is based on the production of white light via the reaction between ATP, luciferase and D-luciferin (Reaction 2.2).

$$\text{ATP + D-luciferin + } O_2 \xrightarrow[Mg^{2+}]{\text{Luciferase}} \text{ADP + } PP_i + CO_2 + \text{oxyluciferin + light} \qquad \text{Reaction 2.2}$$

Cells (1×10^6 cells/well) were treated with HOSCN (0, 25, 50, 75, 100, 150 and 200 µM) for 1 h at 22 ˚C. After oxidant treatment, the oxidant was removed and the cells were washed with HBSS 3 times. 1 mL of HBSS was pipetted onto the cells and they were scraped from the wells of the 12-well culture plate before pipetting 100 µL of the cell suspension into a 96-well white-walled plate. Mammalian cell lysis solution (50 µL) was added to the wells containing the cell suspension and the plate was shaken on an orbital shaker for 5 min at 22 ˚C. After shaking, 50 µL of the substrate solution was added to the wells and the plate was shaken again on the orbital shaker for 5 min at 22 ˚C. Finally, the plate was removed from the shaker and incubated in the dark for 10 min at 22 ˚C before the luminescence was recorded at 570 nm (10 sec integration) using a SpectraMax L luminescence plate reader (SpectraMax). ATP concentration was determined using ATP standards that were included with the ATPlite luminescence ATP detection kit (Perkin Elmer). The results were normalised to cellular protein concentration using a BCA protein assay to quantify protein in the lysate from the cell suspensions (Section 2.3.12.2).

2.3.9 Lactate dehydrogenase assays

Lactate dehydrogenase (LDH) is a ubiquitous cytoplasmic protein that catalyses the reduction of pyruvate to lactate, using NADH as a co-factor. Viable cells are able to prevent the diffusion of LDH into the extracellular milieu, therefore, the LDH assay is a reliable measure of cell viability as a loss in viability is correlated with LDH release into the media.

$$\text{Pyruvate + NADH} \rightarrow \text{L-Lactate + } NAD^+$$

Reaction 2.3: The conversion of pyruvate to lactate by lactate dehydrogenase using NADH as a co-factor.

Thus the extent of cell lysis can be quantified by measuring LDH activity in the media as a proportion of the total LDH activity (intracellular and extracellular). After oxidant treatment, the media on the cells is removed and kept on ice. Then 1 mL of npH_2O is added to the cells, they are lysed using a syringe plunger and left to incubate for 20 min at 4 ˚C. After incubation, 10 µL of sample (media and lysate) are added into separate wells on a 96-well plate along with 200 µL of the reaction buffer (0.15 mg/mL NADH and 2.5 mM sodium pyruvate in PBS). The plate is mixed briefly and the absorbance is recorded at 340 nm every 5 min for 7 cycles on an M2e plate reader (SpectraMax) to determine the rate of change of NADH absorbance as a measure of LDH activity (Reaction 2.3). The cellular viability is then determined using Equation 1.

$$Viability\ (\%) = \frac{\Delta\ Intracellular\ LDH}{\Delta\ Intracellular\ LDH + \Delta\ Extracellular\ LDH} \times 100$$

Equation 1: Lactate dehydrogenase viability equation.

2.3.10 Lactate assays

Lactate is an end product of glycolysis, which is released into the extracellular environment; its levels are directly correlated with intracellular glycolytic activity [334, 335]. The glycolysis cell-based assay kit (Cayman) allows for the determination of lactate concentration in the extracellular media of cells in culture. The cells (1×10^6 cells/well in a 12-well plate) were treated with HOSCN (0, 10, 25, 50 and 100 µM) as well as decomposed HOSCN (dHOSCN) for 1 h at 22 ˚C. After treatment, the cell plate is centrifuged at 1000 *g* for 5 min before 10 µL of the media on top of the cells is removed and pipetted into the well of a 96-well plate. Next, 90 µL of assay buffer is pipetted into the well containing the sample and finally 100 µL of the reaction solution is pipetted into each well. The plate was then incubated on a plate shaker for 30 min at 22 ˚C before absorbance was read at 490 nm on an M2e plate reader (SpectraMax). The lactate concentration was determined using L-lactate standards included in the kit (0 – 1 mM).

For further time points, all the media above the cells was removed and replaced with HBSS before the cells were incubated in a humidified 5% CO_2 environment at 37 ˚C for a further 1 h. At the end of the second hour, 10 µL of the media on top of the cells was removed and

pipetted into the well of a new 96-well plate, where the assay was performed as described above.

2.3.11 Glucose uptake assay

Glucose uptake is a process achieved by the action of glucose transporters, which move glucose down a concentration gradient. This is a highly regulated and dynamic process, which is dictated by environmental conditions [336]. These experiments were performed to determine whether the effect of HOSCN on glycolysis was influenced by changes to glucose uptake into the cell.

2.3.11.1 Plate reader assay

For the plate reader assay, cells were plated directly into clear bottom 12-well plates (1×10^6 cells/well) in 1 mL DMEM and left to incubate overnight in an incubator of humidified 5% CO_2 at 37 ˚C. The next day the media in the plate was aspirated and the cells washed with PBS (glucose-free) twice before being treated with 1 mL HOSCN (0, 25, 50, 100, 200 µM) supplemented with 500 µM 2-(*N*-(7-Nitrobenz-2-oxa-1,3-diazol-4-yl)Amino)-2-Deoxyglucose (2-NBDG) in PBS for 1 h at 22 ˚C. Cells were also treated with 50 µM Apigenin, which is a flavonoid that inhibits glucose uptake, and supplemented with 500 µM 2-NBDG in 1 mL PBS for 20 min at 22 ˚C as a positive control. The plate was then centrifuged for 5 min at 400 *g* and the PBS was aspirated. The cells were washed twice with 500 µL cell-based assay media (item no. 10009322, Cayman chemical), being careful not to disturb the cells. The assay media was aspirated once more before being replaced with 500 µL of cell-based assay media and analysis using the M2e plate reader (SpectraMax) (λ_{ex} = 485 nm, λ_{em} = 535 nm centre focus).

2.3.11.2 Fluorescence microscopy

After plating and overnight incubation (1×10^6 cells/well) (as Section 2.3.11.1), cells were washed with PBS (glucose-free) twice and then treated with 1 mL HOSCN (0, 50, 100 µM) supplemented with 500 µM 2-NBDG in PBS for 1 h at 22 ˚C. Cells were also treated with 50

μM Apigenin supplemented with 500 μM 2-NBDG in PBS for 20 min at 22 ˚C served as a positive control. The plate was then centrifuged for 5 min at 400 *g* and the media was aspirated. The cells were washed twice with 1 mL cell-based assay media as above (Section 2.3.11.1). The assay media was aspirated once more, before being replaced with 500 μL of cell-based assay media and anlysis using a fluorescent microscope (λ_{ex} = 485 nm, λ_{em} = 535 nm).

2.3.12 Protein concentration assays

2.3.12.1 Bradford protein assay

The Bradford protein assay was used to determine the protein concentration in samples containing IAF to be separated by SDS-PAGE, as it is compatible with the various components present in the cell lysis buffer (with the exception of samples treated with DAz-2 or DCP-Bio-1, the BCA assay was used in this case). The Bradford assay is based on the direct binding of Coomassie brilliant blue G-250 dye (CBBG) to proteins at Arg, Trp, Tyr, His, and Phe residues [337, 338]. Anionic CBBG binds to these residues producing an absorbance maximum at 595 nm, whilst the free dye in solution has an absorbance maximum at 470 nm. The assay measures the CBBG complex with the protein, which results in an absorption peak shift at 595 nm.

The Bradford reagent solution (BioRad) was diluted 1:5 in npH_2O, and passed through filter paper to remove insoluble particles of dye prior to use. The assay was performed by the addition of 200 μL of the Bradford reagent to 10 μL of protein sample or standard on a 96-well plate, in triplicate. Solutions were mixed by gentle shaking, followed by 5 min incubation at 22 ˚C. The absorbance was recorded at 595 nm on an M2e plate reader (SpectraMax), and the protein concentration was determined by the inclusion of protein standards prepared with BSA (0.05 – 1.0 mg mL^{-1}).

2.3.12.2 Bicinchoninic acid protein assay

Cellular protein concentration was measured using a Bicinchoninic acid (BCA) assay. The BCA assay measures the formation of Cu^{+} from Cu^{2+} by the Biuret complex in alkaline solutions of proteins using BCA, which has a strong absorbance at 562 nm [339, 340]. The BCA assay reagent was prepared by mixing BCA solution A (Pierce, 0.1 g sodium bicinchoninate, 2.0 g $Na_2CO_3{\cdot}H_2O$, 0.16 g sodium tartrate, 0.4 g NaOH, 0.95 g $NaHCO_3$ made up to 100 mL) and 4% $CuSO_4$ (w/v) in a 50:1 ratio. 200 µL of the BCA working reagent was mixed with 10 µL of samples and standards, on a 96-well plate, in triplicate. Solutions were mixed by gently shaking, followed by a 30 min incubation at 60 ˚C. The absorbance was recorded at 562 nm on an M2e plate reader (SpectraMax), and the protein concentration was determined by the inclusion of protein standards prepared with BSA (0.05 – 1.0 mg mL^{-1}).

2.3.12.3 DC Lowry protein assay

The Lowry DC assay (BioRad) was used to measure protein content within the cell populations that had undergone the Seahorse XF extracellular flux assay. It was chosen as it was a method compatible with the lysis buffer used and allowed for the quick determination of protein concentration without the need for incubation at 60 ˚C. The reaction measures the formation of Cu^{+} by the Biuret complex, the reaction of Cu^{2+} with peptide bonds in alkaline solutions produces a colour change which can be measured at 750 nm [341]. The DC Lowry working reagent was prepared by mixing solution A (alkaline copper taltrate) and solution S (surfactant solution) in a 49:1 ratio. 125 µL of the A+S solution was added to 25 µL of the cell lysate in the XF24 plate and mixed, then 1 mL of solution B (Folin reagent) was added. This solution was then mixed thoroughly on an orbital shaker and incubated for 15 min at 22 ˚C. 200 µL of sample was then added to a 96-well plate before the absorbance was recorded at 750 nm on a M2e plate reader (SpectraMax). The protein concentration was determined by the inclusion of protein standards prepared with BSA (0.1 – 2.0 mg mL^{-1}).

2.3.13 Statistical analysis

Statistical analyses were performed to compare the effect of oxidant treatment on J774A.1 cells, cellular enzymes and cell function versus the untreated control. All analyses were carried out using one-way ANOVA with a Tukey's post-hoc test, two-way ANOVA was used to compare multiple treatment conditions or differences over time. All statistical analyses were performed using GraphPad Prism 6.0 (GraphPad Software, San Diego, USA), with $p < 0.05$ taken as significant. Details of the significance or changes to statistical methods for each experiment are outlined where relevant.

3 The Effect of Hypohalous Acids on Cellular Protein Thiols

3.1 Introduction

The production of the hypohalous acids, HOSCN and HOCl is catalysed by the peroxidase enzymes MPO, LPO and EPO, which are all important elements of the human innate immune system [11, 342-344]. HOCl is a chemical that is primarily involved in bacterial cell killing, which has the ability to cause cell lysis in a wide number of different cell types [180, 184]. HOCl is not particularly specific in respect to the targets that it oxidises, reacting readily with most biological molecules, particularly proteins, owing to rapid rate constants for reaction with many amino acids, including methionine, cysteine, histidine, tryptophan and lysine [96]. HOCl can also react rapidly with a range of other substrates including DNA, lipids or plasmalogens to form various chlorinated and oxidised products [143, 153-155]. Thus, HOCl can cause wide spread damage upon exposure to cells [66, 70, 183, 324, 345]. In contrast, HOSCN is a bacteriostatic agent, and it is reported that rather than causing cell death, HOSCN inhibits bacterial cell growth and proliferation [197, 199]. This action is attributed to the ability of HOSCN to almost exclusively target protein thiols contained on the cysteine residues of various proteins [95, 98]. It has been demonstrated that thiol proteins essential to glycolysis within bacteria are key targets [198-200, 274]. HOSCN forms reversible oxidised cysteine products on these proteins including sulfenyl products, disulfides and mixed disulfides, which can be reduced by various mechanisms to restore function and permit bacterial cell growth [56, 199].

HOCl also reacts readily with thiols, with a higher rate constant that reported for HOSCN with cysteine residues (HOCl: $k = 3 \times 10^7$ M^{-1} s^{-1} compared to HOSCN: k = ca. 7.8×10^4 M^{-1} s^{-1}) [96, 98]. The reaction of thiols with either HOCl or HOSCN yields a sulfenyl halide (RS-X, where X= Cl or SCN) [101, 102]. With HOSCN, this results in the formation of a sulfenyl thiocyanate, which can then be hydrolysed to a sulfenic acid (RS-OH) or react with another cysteine to form a disulfide bridge (RS-SR'), both of which are reversible species that can be reduced to the original thiol [62]. When thiols are exposed to HOCl, which is a stronger oxidising agent, the resulting sulfenyl chloride (RS-Cl) can then be further oxidised to higher oxyacid products and irreversibly oxidised products, such as sulfinic (RS-O_2H) and sulfonic acids (RS-R_3H) [346]. The formation of reversibly oxidised sulfur-species within a cell can be important, as oxidant-induced damage can be potentially reversed, thereby avoiding permanent enzyme inactivation [56]. Furthermore, these modifications are critical in redox signalling processes [347, 348]. The repair of HOSCN-modified protein modifications resulting in the restoration of enzyme function has been reported on isolated proteins, including creatine kinase (CK)

and GAPDH, after HOSCN exposure with subsequent reduction with dithiothreitol (DTT) [201]. Direct evidence for repair of thiol modifications within mammalian cells is rather limited, but is known to occur in bacteria [56, 199]. The formation of higher cysteine oxyacids, such as those formed upon HOCl treatment, can lead to irreversible enzyme activation and the failure of essential redox switches within the cell [9, 109, 349], which has been postulated to be a cause of cell death [162, 180, 187]. Targeting of critical thiol proteins has been proposed to be the cause for the inhibition of various cellular processes, though very few studies have reported or characterised the post-translational modifications induced by HOSCN compared to HOCl within cells. The specificity of HOSCN for thiols has been shown to cause more damage to susceptible sites than the non-specific reactions of HOCl [84, 91]. However, whether sulfenic acids and other reversible thiol products are also formed in cells exposed to HOCl is not well established. Comparative studies of thiol oxidation on proteins in cells exposed to HOCl and HOSCN have shown different results, which are dependent on the cell type. With macrophages, a greater extent of thiol loss was seen with HOSCN, whereas in endothelial cells, HOCl induced a greater loss in the thiol concentration under analogous reaction conditions [91, 185].

3.2 Aim

The aim of the studies in this Chapter is to assess the ability of HOSCN and HOCl to target protein thiols, and form reversible oxidation products in J774A.1 murine macrophages, using a thiol specific probe to assess reversible modifications. The nature of the reversible oxidation products formed in each case will be examined using a Western blotting approach with the sulfenic acid probes DAz-2 and DCP-Bio1, and an antibody raised against glutathionylated protein. The formation of reversible cysteine oxyforms in the mitochondria was also studied using a mitochondrial isolation kit to fractionate mitochondrial and cytosolic proteins.

3.3 Results

3.3.1 HOSCN and HOCl affect intracellular thiol concentrations

Initial studies were performed to explore whether there were differences in the extent of total thiol loss on exposure of J774A.1 murine macrophages to HOCl and HOSCN, as previous studies have shown that thiol-dependent enzymes can be readily inactivated by these oxidants [201]. J774A.1 cells (1×10^6 cells) were treated with HOSCN and HOCl (0 – 100 μM) for 1 h at 22 ˚C. These conditions were selected as a result of data in the literature showing that cells exposed to concentrations ≤ 200 μM HOSCN for 1 h showed very little cell lysis [91] but a decrease in enzyme activity and thiol loss is noted [201]. After treatment, intracellular thiol concentrations were determined with a fluorescence assay using ThioGlo-1. ThioGlo-1 is a maleimide derivative that contains a double bond that reacts readily with the thiol group of cysteine, which are targets of both HOSCN and HOCl oxidation, resulting in a change in fluorescence [324, 350]. This method is superior to other methods, such as the DTNB (5,5'-dithiobis-(2-nitrobenzoic acid)) assay, where the disulfide bond of the DTNB is cleaved by a thiol to give TNB^-, which has been performed previously on this cell type, as it is more sensitive and there is no confounding reaction of the oxidants with ThioGlo-1 in contrast to TNB [324, 350]. ThioGlo-1 is added to the cell lysate after the cells were oxidant-treated, washed and lysed in npH_2O, and the loss of thiols in the samples is determined via a proportional loss in ThioGlo-1 binding to available thiols. The concentration of thiols within the samples is determined by comparing the sample fluorescence against a GSH standard curve (0 – 10 μM).

Treatment of J774A.1 macrophages with HOSCN resulted in a dose-dependent decrease in the intracellular thiol concentration (Figure 3.1). The result was significant at concentrations above 50 μM HOSCN (Figure 3.1), while at 100 μM the effect begins to plateau, indicating there are thiols inaccessible or unreactive to HOSCN. In contrast, when the cells were treated with HOCl, no significant reduction in the concentration of intracellular thiols was observed unless a dose greater than 50 μM was employed. When the cells were treated with 100 μM HOCl, there was a decrease in the intracellular thiol concentration that was comparable to the 50 μM HOSCN treatment. In each case, the thiol concentration was normalised to protein concentration, to account for any thiol loss due to lysis. To confirm that the change in fluorescence was reflecting thiol concentration rather than a reaction of ThioGlo-1 with other intracellular targets to cause an artifactual increase in fluorescence, the cells were

treated with N-ethylmaleimide (NEM, 1 mM) prior to adding ThioGlo-1. NEM is an alkene, Michael acceptor that reacts with nucleophiles, such as thiols, producing a strong, almost irreversible C-S bond. Blocking the thiols in the samples with NEM prevents a reaction of the thiols with ThioGlo-1, allowing for the determination of background or non-specific fluorescence.

The results show that upon treatment with NEM, the ThioGlo-1 fluorescence is dramatically decreased, consistent with ThioGlo-1 reacting primarily with intracellular thiols. The difference in intracellular thiol concentrations after treatment with HOSCN or HOCl was then extended to examine the nature of the oxidation products formed, and whether the oxidation and subsequent thiol loss could be reversed.

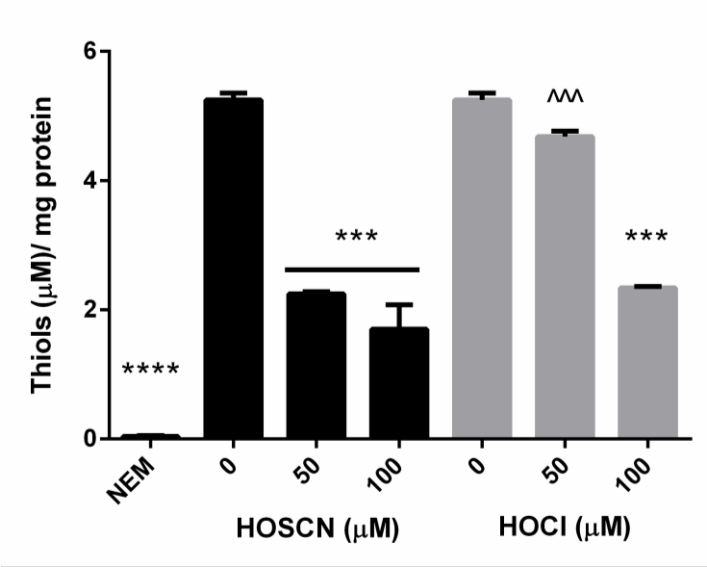

Figure 3.1: HOSCN and HOCl are able to oxidise intracellular thiols in J774A.1 cells.

*Loss of intracellular thiols by HOSCN (black bars) or HOCl (grey bars) occurs in a dose-dependent manner. J774A.1 (1×10^6) cells were treated with HOSCN or HOCl (0 – 100 μM) for 1 h at 22 ˚C. J774A.1 cells were also treated with NEM (1 mM) for 15 min instead of oxidant before the addition of ThioGlo-1, to probe for artifactual ThioGlo-1 fluorescence, due to non-specific binding. Thiol concentrations were determined by fluorescence spectroscopy at λ_{ex} = 360 nm and λ_{em} = 530 nm. Values of the results are the mean ± S.E.M (n = 3). *** and **** show a significant (p < 0.001 and 0.0001, respectively) decrease compared to the respective non-treated controls. ^^^ shows a significant (p < 0.001) difference between the oxidants at the same concentration by Repeated Measures two-way ANOVA with a post-hoc Tukey's test.*

3.3.2 Formation of reversible protein thiol modifications by HOSCN and HOCl

This study was performed to determine whether the intracellular oxidation products of HOSCN or HOCl formed on protein thiols are reversible. J774A.1 cells were treated with HOCl or HOSCN (0 – 100 μM) prior to washing to remove any residual oxidant and treatment with NEM (100 mM) to block any of the thiols that did not become oxidised (i.e. reduced thiols). The samples were then treated with DTT (1 mM) to reduce any reversibly oxidised thiols back to their original state. Finally, samples were treated with the fluorescent IAF probe (80 mM) to alkylate the newly reduced thiol groups. The cell protein samples were then separated using SDS-PAGE. In this case, an increase in IAF fluorescence is consistent with the production of reversible thiol products, which could include, but are not limited to, disulfide bridges, sulfenic acids and S-glutathionylated adducts.

Results show that exposure of the cells to 50 μM HOSCN results in the formation of reversible oxidation products upon treatment for 1 h at 22 ˚C, shown by an increase in IAF staining intensity (Figure 3.2A). This increase in the formation of reversible cysteine oxidation products is apparent at both the concentrations of HOSCN used (50 and 100 μM) with the densitometry showing that the apparent density of the bands is almost double at the highest concentration of oxidant (Figure 3.2C). In the HOSCN treated samples proteins with molecular mass ca. 70, 65, 60 and 35 kDa were particularly sensitive to modification, as the densities of these protein bands contributed to the majority of the total pixel area, which was assessed using Image J. The protein content of each sample was visualised using the RuBPS stain (Figure 3.2B), which showed equal loading of sample across all the gel lanes (Figure 3.2D). Thus, the increase in IAF staining is consistent with reversible thiol modification rather than increased protein loading on the gel.

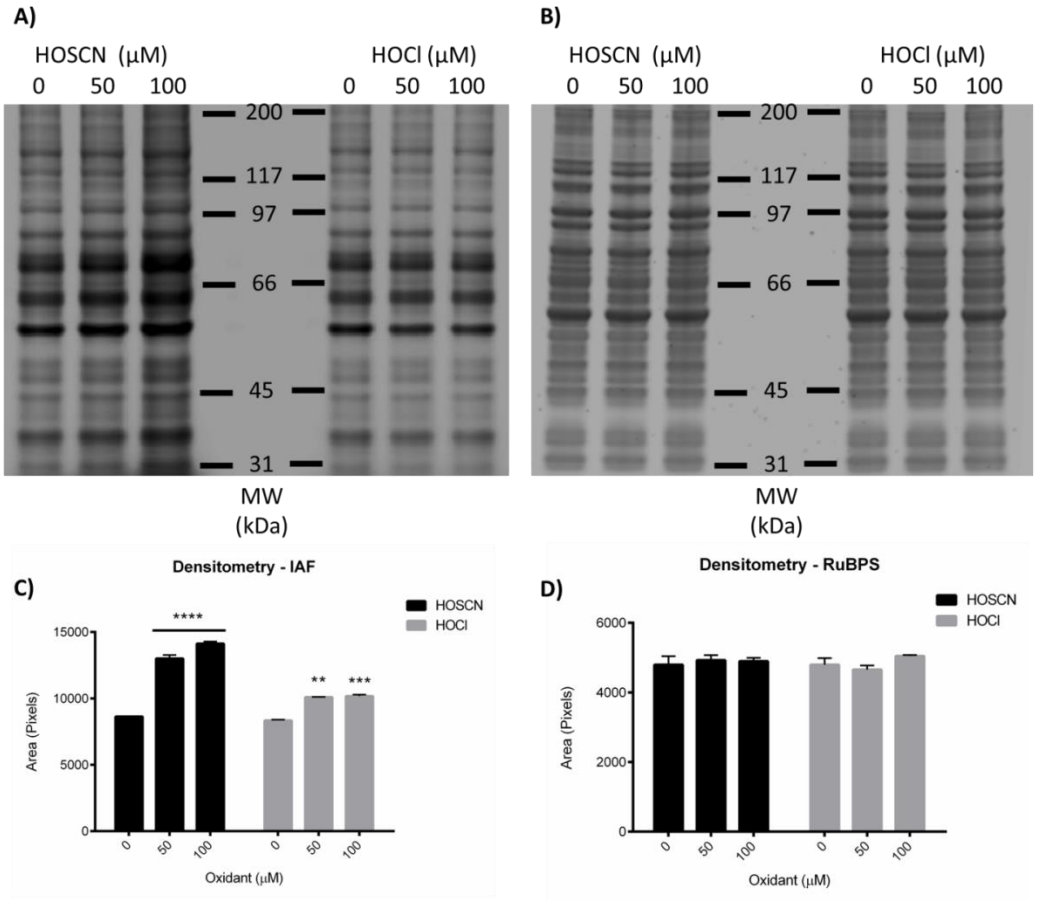

Figure 3.2: HOSCN and HOCl both promote the formation of reversible oxidation products on protein cysteines.

*J774A.1 (1 × 10^6 cells mL^{-1}) cells were treated with HOSCN or HOCl (0 – 100 μM) for 1 h at 22 ˚C, blocked with NEM, reduced with DTT and probed with IAF before the proteins separated via 1D SDS-PAGE (4-12%). (A) Protein cysteines probed with the fluorescent thiol probe IAF, with increases in intensity indicating an increase in the formation of reversible oxidation products when scanned at λ_{ex} = 488 nm and λ_{em} = 530 nm on the PharosFX system. (B) The gel is treated with the protein stain RuBPS to ensure equal protein loading by scanning the gel in the PharosFX system using λ_{ex} = 532 nm and λ_{em} = 605 nm lines. (C) The densitometry of the IAF bands for both HOSCN (black bars) and HOCl (grey bars) treated samples and (D) the densitometry of the RuBPS stained bands. The images are representative of 3 separate experiments. Values of the results are the mean ± S.E.M (n = 3). **, *** and **** show a significant (p < 0.01, 0.001 and 0.0001, respectively) increase compared to respective controls by Repeated Measures one-way ANOVA with a post-hoc Tukey's test.*

In contrast with HOCl, a less significant increase in IAF staining was observed, and the change in IAF fluorescence was not as marked as with HOSCN. This is consistent with a decreased extent of formation of reversible cysteine oxidation products (Figure 3.2A), and supports the reported differences in the chemistry and selectivity of these oxidants [49, 95]. Again, the difference in the formation of reversible thiol products is not a reflection of unequal loading of the protein samples, seen by RuBPS staining (Figure 3.2B & D), with densitometry performed using Image J software.

3.3.3 HOSCN, HOCl and the formation of protein sulfenic acids in J774A.1 macrophages

The formation of sulfenic acids has been demonstrated in J774A.1 macrophages after HOSCN treatment [201], but it is not clear whether these species are also formed in cells exposed to HOCl, which may be expected in light of the above finding showing some evidence for reversible thiol modification with IAF. To address this, additional studies were performed to examine the nature of the reversible modifications using the chemical probe DAz-2, a sulfenic acid specific dimedone containing molecule that contains an azido group, allowing conjugation to phosphine-biotin (p-biotin), as the phosphine is reactive towards azido groups (Staudinger ligation, click reaction) [328, 351]. Using DAz-2 and p-biotin allows for the detection of sulfenic acid formation using streptavidin-HRP to visualise the resulting biotinylated proteins. Prior to the exposure of J774A.1 cells to HOSCN, cells were treated with DAz-2 (500 μM) in DMSO (1% v/v) or a vehicle control of DMSO (1% v/v) in DMEM for 1 h at 37 ˚C. Cells (1×10^6 cells mL^{-1}) were then washed and treated with HOSCN or HOCl (0 – 150 μM) for 1 h at 22 ˚C before being lysed in npH_2O. The lysate was then incubated with p-Biotin to biotinylate any protein-bound DAz-2 (Figure 3.3) and the proteins were separated using SDS-PAGE and transferred to a PVDF membrane. The membrane was incubated with streptavidin-HRP and the protein bands visualised using ECL.

Under these conditions, evidence was obtained for the formation of sulfenic acids in macrophages upon treatment with concentrations above 50 μM of HOSCN (Figure 3.4A). The band density of biotinylated proteins was determined using Image J, where it was apparent that there was more than a doubling in the average total density between the control and the 150 μM HOSCN treatment group (Figure 3.5A) (red arrows indicate proteins that had more than a 100% increase in density between the control and 150 μM treatment groups).

These data are consistent with previous studies with isolated proteins and in cells [201]. There was a significant increase in the formation of cellular protein sulfenic acids at all the concentrations of HOSCN tested. After visualisation of sulfenic acid formation with streptavidin-HRP and ECL, the blots were stained with Coomassie R-250 to ensure equal protein loading across all samples (Figure 3.4C). Image J was used to measure the density of the protein bands and no change was observed in Coomassie staining, indicating equal protein loading (Figure 3.5B).

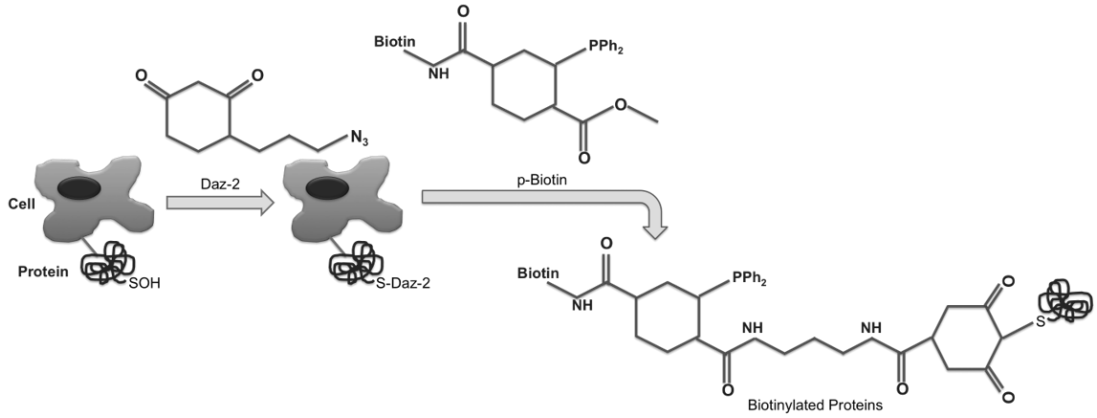

Figure 3.3: DAz-2 as a tag for sulfenic acid production in cells.

The figure outlines the steps taken to tag sulfenic acids with DAz-2, and the subsequent addition of p-biotin via a Staudinger ligation to form a complex that can be visualised using a Western blotting method and ECL.

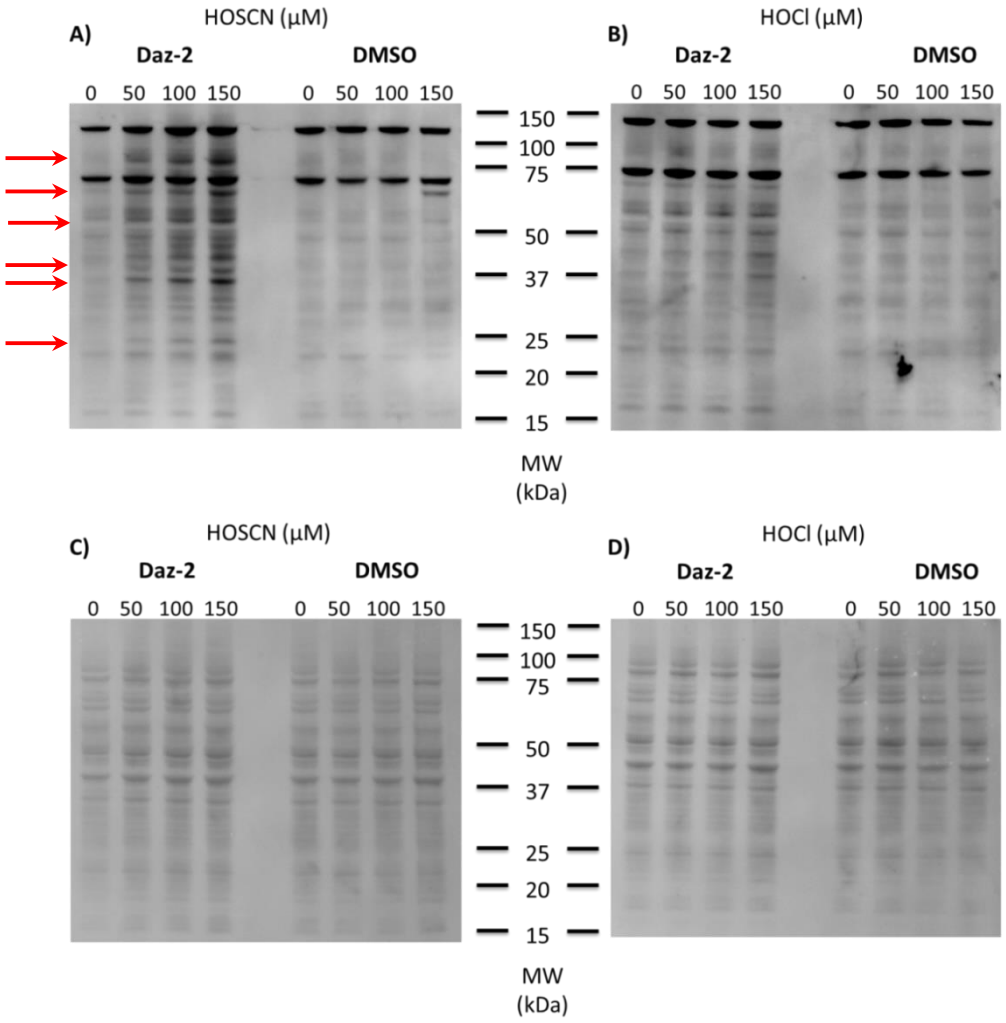

Figure 3.4: HOSCN promotes the formation of sulfenic acids on protein cysteine residues, while HOCl does not, following treatment of J774A.1 cells.

J774A.1 cells (1 x 10^6 cells mL^{-1}) were pre-treated with DAz-2 (500 μM) or DMSO (1% v/v) for 1 h at 37 ˚C prior to the addition of (A) HOSCN or (B) HOCl (0 – 150 μM) and further incubation for 1 h at 22 ˚C. Cells were then lysed, and Staudinger ligation was carried out with p-Biotin (200 μM) and DTT (5 mM) for 2 h at 37 ˚C. The reaction was quenched and proteins were separated via 1D SDS-PAGE (4-12%). Proteins were transferred to PVDF membranes and biotinylated proteins were detected by Western blotting with HRP-streptavidin. Coomassie R-250 was used to determine equal protein loading on both (C) HOSCN and (D) HOCl - treated samples. The images are representative of 3 separate experiments. Red arrows indicate bands that had more than a doubling in density between the control and 150 μM treatment groups.

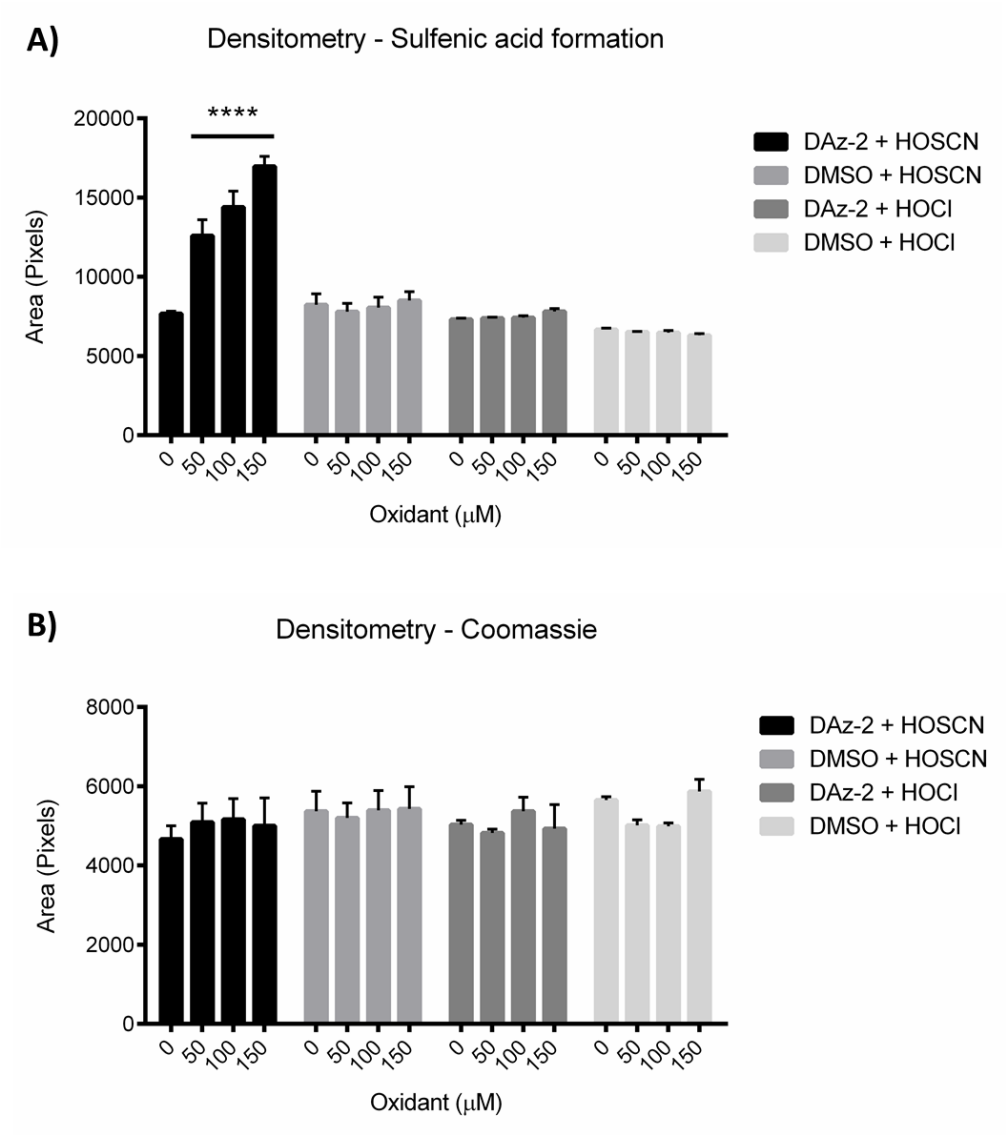

Figure 3.5: Changes in the band density of Daz-2 reactive sulfenic acid protein-residues.

*Densitometry analysis of the membranes was performed using ImageJ. (A) Density of the biotinylated bands detected via Western blot after DAz-2 derivitisation shows that HOSCN causes an increase in the formation in protein sulfenic acids as determined by an increase in biotinylated proteins. HOCl shows a trend towards increase but no significance was determined. (B) Density of the Coomassie R-250 stained protein bands shows no significant difference in the density of bands across all samples, indicating an equal load of proteins across all samples tested. Values of the results are the mean ± S.E.M (n = 3). **** shows a significant ($p < 0.0001$) increase when compared to the control by Repeated Measures one-way ANOVA with a post-hoc Tukey's test.*

In contrast, HOCl had a different effect on the cells, as the formation of sulfenic acids on cellular protein was not observed (Figure 3.4B). Thus, in this case, the formation of sulfenic acids was below the detection limit, with no statistical difference in the density between the control or the highest concentration of HOCl used (150 μM) (Figure 3.5A). After probing for biotinylated proteins, the membranes were again stained with Coomassie R-250 to determine protein loading (Figure 3.4C & D). The analysis of the band density showed that there was no statistical difference between the density of any of the protein bands (Figure 3.5B), indicating that the lack of sulfenic acid formation was not a result of reduced or unequal protein loading.

In the vehicle control treated samples (DMSO) (Figure 3.4A & B), there were only a few visible bands, with 2 prominent bands at ca. 70 and 120 kDa. This is attributed to proteins that are already biotinylated within the cell, that are not related to sulfenic acid formation. This is further supported by the observation that the band density in the DMSO treated samples remains constant, indicating that protein biotinylation in this case, occurs independently from HOSCN treatments (Figure 3.5A).

In summary, exposure of J774A.1 cells to HOSCN but not HOCl induces the formation of sulfenic acids on protein residues. Various bands within the HOSCN treated samples exhibited increases in sulfenic acid formation (shown by red arrows in Figure 3.4A) which suggests that HOSCN may exhibit specificity for particular cellular proteins or that particular proteins may be susceptible to sulfenic acid formation via HOSCN oxidation.

3.3.4 HOSCN and the formation of S-glutathionylated proteins in J774A.1 macrophages

Sulfenic acids are highly reactive and unstable intermediates that can react with other cysteine residues to form disulfides or mixed disulfides [352, 353]. The reaction of a protein-bound sulfenic acid with a molecule of GSH can lead to the formation of a particular type of mixed disulfide, an S-glutathionylated protein disulfide (PSSG). In recent years PSSG have been increasingly implicated in various cellular pathways and modification of protein function, including the protection of cysteine residues from over-oxidation into the higher, non-reversible oxyacids such as sulfinic and sulfonic acids [348, 354-356].

The formation of PSSG residues within J774A.1 cells after treatment with HOSCN or HOCl for 1 h at 22 ˚C was determined using an anti-GSH antibody (ViroGen, [357]). Due to the instability of the PSSG adducts, the cells were kept on ice, to reduce PSSG decomposition with an excess of NEM present throughout the entire experiment [358]. By alkylating any reduced thiols it was ensured that any thiols that were not originally oxidised during HOSCN or HOCl treatment would not become oxidised during further processing steps. To do this, after treatment the cells were lysed under alkylating conditions using NEM (100 mM) and the proteins were resuspended in LDS buffer containing NEM (100 mM). SDS-PAGE was also run under non-reducing conditions with running buffer containing NEM (100 mM). Results show that the samples treated with HOSCN show a consistent increase in PSSG formation in 3 separate experiments (Figure 3.6C), particularly in the bands located at ca. 40 kDa and another at 250 kDa (red arrows), after protein band density is analysed using Image J. Samples treated with HOCl also exhibited an increase in PSSG formation, in a similar fashion to the PSSG formation in HOSCN treated samples. In this case, the PSSG formation but tended to be more variable over the 3 independent experiments (Figure 3.6C). Protein bands which exhibited consistent increases in PSSG were proteins located at ca. 40, 90, 150 and 250 kDa (Figure 3.6A), indicating that HOCl may exhibit specificity for these particular proteins. With both HOSCN and HOCl, an increase in PSSG formation on cellular proteins only became significant at the highest treatment concentration (200 µM), primarily due to the high amount of PSSG observed in the control samples of both treatments. In most cases, the bands present in non-treated controls increased in intensity with increasing oxidant concentrations, while in others, very little, to no increase was observed. When the blots were stained with Coomassie R-250 (Figure 3.6B), no change was observed in the amount of protein loaded in each lane as indicated by the constant density across all the samples when analysed using ImageJ (Figure 3.6D). This demonstrates that the lack of consistency apparent on the PSSG blots is likely to be due to decomposition of the adducts rather than unequal loading of the protein sample.

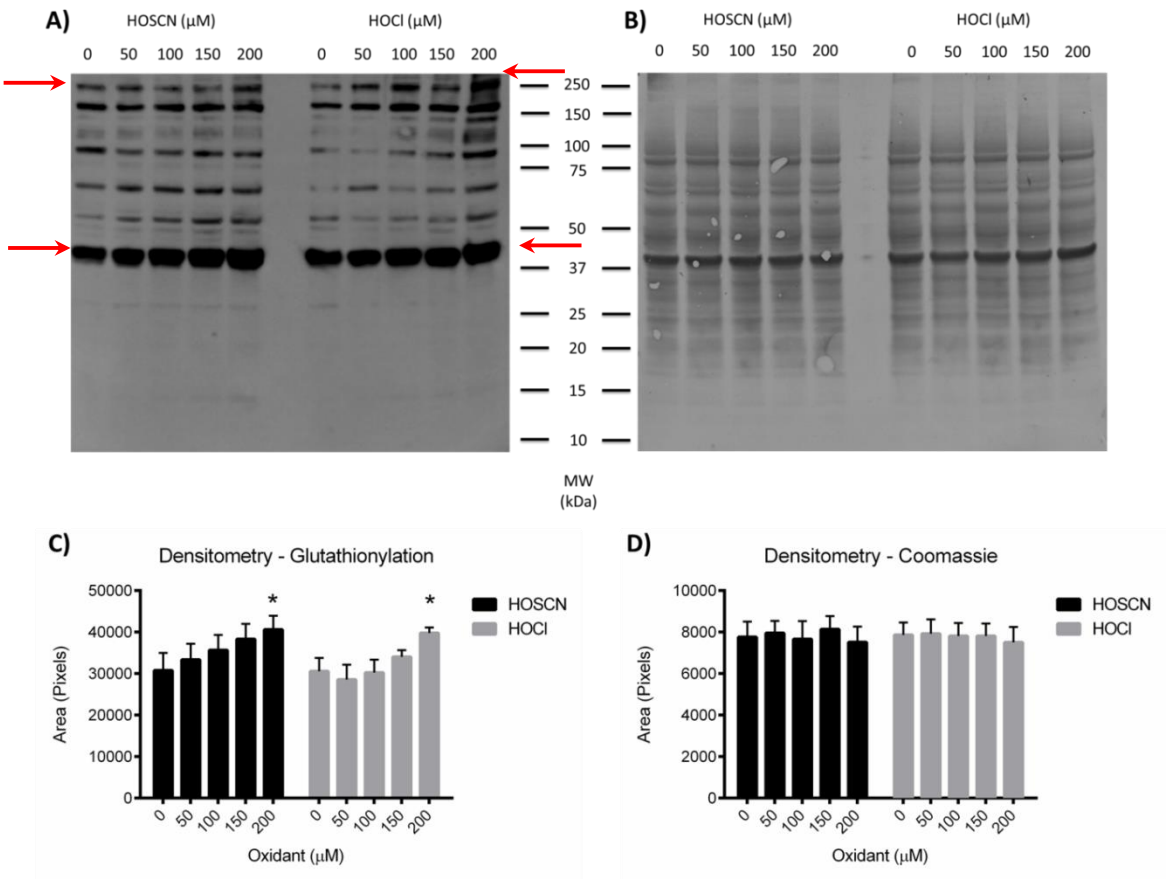

Figure 3.6: The formation of S-glutathionylated proteins in J774A.1 cells following treatment with HOSCN and HOCl.

*J774A.1 cells (1 x 10^6 cell mL^{-1}) were treated with HOSCN or HOCl (0 – 200 µM) for 1 h at 22 ˚C, before being lysed in an NEM-containing buffer, and proteins were separated by 1D gel electrophoresis under non-reducing conditions in media containing 100 mM NEM before being transferred to a PVDF membrane. (A) Glutathionylated proteins were detected using an anti-GSH antibody before being imaged using ECL-HRP. (B) The PVDF membranes were stained with Coomassie R-250 and used to determine equal protein loading. The images are representative of 3 separate experiments. Using ImageJ, the density of the (C) anti-GSH probed blots and the (D) Coomassie R-250 stained blots were determined by analysing all the bands contained in each lane. Values of the results are the mean ± S.E.M (n = 3). * shows a significant ($p < 0.05$) increase when compared to the respective controls by Repeated Measures one-way ANOVA with a post-hoc Tukey's test. Red arrows indicate proteins that showed consistent increases in density over the course of the 3 experiments.*

It is not clear why PSSG adducts are so readily formed in the non-treated control wells, whereas little sulfenic acid formation or reversible thiol oxidation is seen in comparable conditions. This may reflect PSSG formation under basal conditions, which may play a role in cellular signaling and in redox regulation of protein functions [104, 359], This may also reflect a lack of specificity of the anti-GSH antibody.

Due to the successful identification and formation of sulfenic acid adducts in the whole cell lysates after HOSCN treatment and a lack of consistency in the formation of PSSG after oxidant treatment, an experiment was devised to examine the susceptibility of cytosolic and mitochondrial proteins to sulfenic acid formation on HOSCN treatment.

3.3.5 HOSCN causes the formation of protein-bound sulfenic acids in the cytosol and mitochondria

3.3.5.1 Optimising protocols to detect sulfenic acid formation in mitochondria

Using the sulfenic acid probe DAz-2 with p-biotin and Staudinger ligation, it was shown that the treatment of J774A.1 macrophage cells with HOSCN is able to generate protein sulfenic acids within the cells. Initial studies were performed to examine sulfenic acid formation on mitochondrial proteins by loading the cells with DAz-2, then treating the cells with HOSCN. After oxidant treatment, a mitochondrial isolation was performed, before the mitochondrial fraction was lysed and p-biotin was added, and a Staudinger ligation reaction performed. The mitochondrial proteins were then separated using SDS-PAGE and the proteins were transferred to a PVDF membrane where they were incubated with HRP-streptavidin and imaged with ECL. However, upon imaging, no biotinylated proteins (except for 2 bands at ca. 70 and 100 kDa) were identified in any of the samples (Figure 3.7A), despite the identification of protein after staining the membranes with Coomassie R-250 (Figure 3.7B). This was attributed to the loss of the sulfenic acid adducts during the mitochondrial isolation procedure.

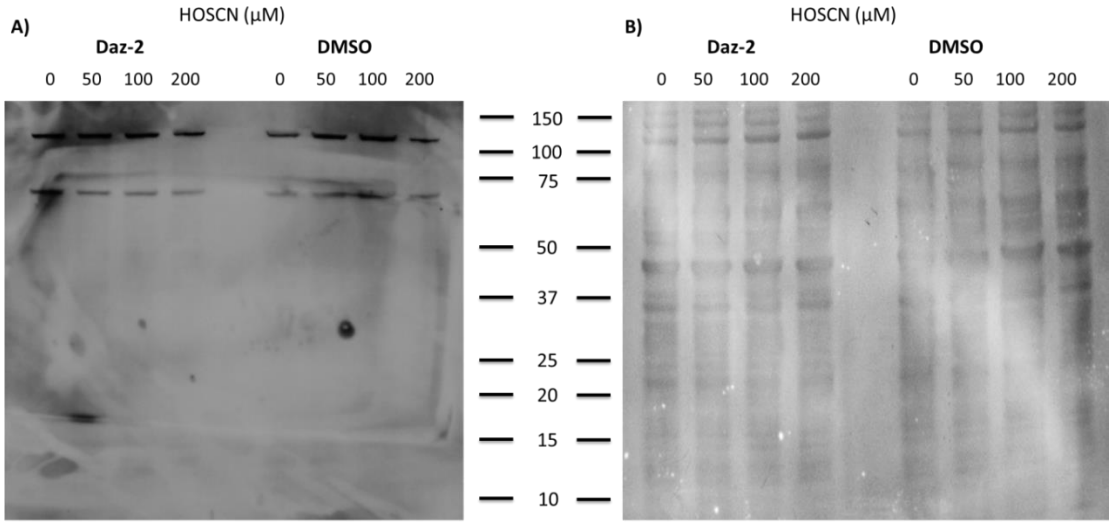

Figure 3.7: Using DAz-2 to identify sulfenic acid formation in J774A.1 mitochondria.

J774A.1 cells (1 x 10^6 cells mL^{-1}) were pre-treated with DAz-2 (500 μM) or DMSO (1% v/v) for 1 h at 37 ˚C prior to the addition of HOSCN (0 – 200 μM) and further incubation for 1 h at 22 ˚C. Mitochondrial isolation was performed, and Staudinger ligation carried out with p-Biotin (200 μM) and DTT (5 mM) for 2 h at 37 ˚C. The reaction was quenched and mitochondrial proteins were separated via 1D SDS-PAGE (4-12%). (A) Proteins were transferred to PVDF membranes and biotinylated proteins were detected by Western blotting with HRP-streptavidin and ECL. (B) Coomassie R-250 was used to determine equal protein loading and if protein was contained with mitochondrial samples.

After the unsuccessful result of the previous optimisation experiment, the cells were loaded with DAz-2 prior to HOSCN treatment and the p-biotin was added to the whole cells. After the Staudinger ligation, the mitochondria were isolated from the cells, and lysed before the proteins were separated using SDS-PAGE, transferred to a PVDF membrane and incubated with HRP-streptavidin and imaged with ECL. This was also unsuccessful, as no bands were detected, possibly because the p-biotin is more suited for use in lysates and not whole cells [360]. So another method was devised, which employed the use of a new sulfenic acid probe that did not require the need for Staudinger ligation to p-biotin, as the probe, called DCP-Bio1, is already biotin-linked. To compare the reactivity of DCP-Bio1 and DAz-2, cells were loaded with DCP-Bio1 before HOSCN treatment and after oxidant treatment the cells were lysed and the proteins were separated using SDS-PAGE before being transferred to a PVDF membrane and incubation with streptavidin-HRP before imaging using ECL. The formation

of sulfenic acids in cells exposed to increasing concentrations of HOSCN using DCP-Bio1 was then compared to that seen using DAz-2. No difference in sulfenic acid detection was observed between the DCP-Bio1 (Figure 3.9A) or DAz-2 (Figure 3.9B).

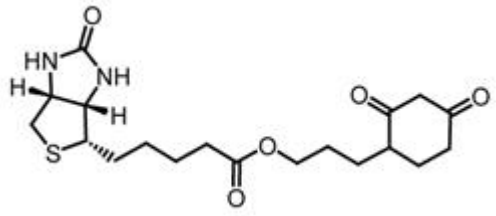

Figure 3.8: DCP-Bio1, a dimedone based sulfenic acid probe that contains a cleavable biotin tag.

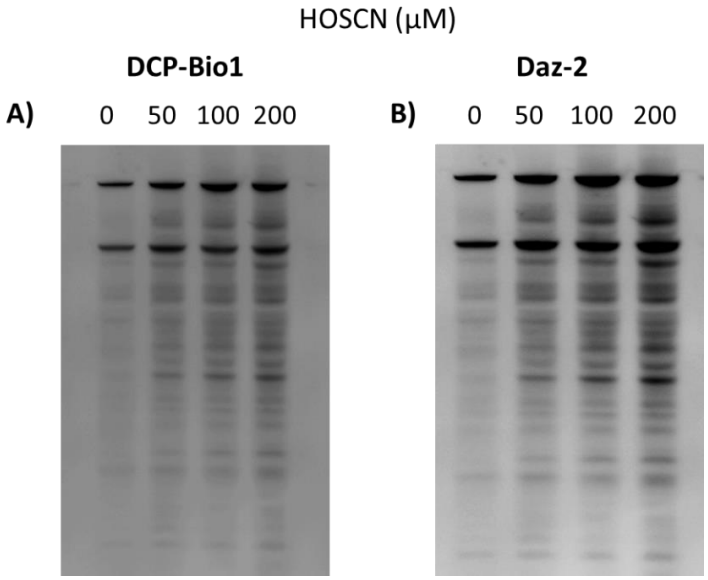

Figure 3.9: A comparison of the sulfenic acid probes DCP-Bio1 and DAz-2 in whole cell lysates

J774A.1 cells (1 x 10^6 cells mL^{-1}) were pre-treated with (A) DCP-Bio1 (500 µM) or (B) DAz-2 (500 µM) for 1 h at 37 ˚C prior to the addition of HOSCN (0 – 200 µM) and further incubation for 1 h at 22 ˚C. Cells were then lysed, and Staudinger ligation was carried out with p-Biotin (200 µM) and DTT (5 mM) for 2 h at 37 ˚C on the cells treated with the DAz-2 probe. The reaction was quenched and proteins were separated via 1D SDS-PAGE (4-12%). Proteins were transferred to PVDF membranes and biotinylated proteins were detected by Western blotting with HRP-streptavidin.

To determine whether sulfenic acids are formed on mitochondrial proteins in J774A.1 cells, the cells were loaded with DCP-Bio1, then treated with HOSCN before the mitochondria were isolated from the cytosolic fraction using a mammalian mitochondria isolation kit (Thermo Fisher). The mitochondria were lysed in mitochondrial lysis buffer and both the mitochondrial and cytosolic proteins were separated using SDS-PAGE. After electrophoresis the proteins were transferred to a PVDF membrane, and the membranes were incubated with HRP-streptavidin and imaged using ECL.

On separation of the cytosolic and mitochondrial fractions, it was shown that the cytosolic fraction gave results were similar to the results of the experiment with whole cell lysates (Figure 3.9A) but fewer bands were apparent when compared to the results of the DAz-2 or DCP-Bio1 probe with whole cell lysates. Treatment of the cells with HOSCN results in an increase in the formation of sulfenic acid adducts on proteins within the cytosol (Figure 3.10A), which is consistent with the results of the DAz-2 probing experiment. After imaging, the membrane was stripped and re-probed for β-actin and COX-4, which both act as a loading control and a means to determine mitochondrial contaminants in the cytosolic fractions (Figure 3.10A). Using ImageJ, analysis of the cytosolic fraction showed that the intensity of biotinylation increases by approximately 3-fold between 0 – 200 μM HOSCN treatments (Figure 3.11A), indicating an increase in biotinylation due to binding of the probe to sulfenic acids, formed by the increasing concentrations of HOSCN. Several bands within the cytosolic fraction became darker with increased oxidant treatment, such as bands located at ca. 100, ca. 160 kDa and ca. 37 kDa. After analysing the β-actin and COX-4 images using Image J, it was determined that equal protein was loaded between samples had no effect on the results (β-actin) (Figure 3.11E) and that there were no mitochondrial contaminants (COX-4) (Figure 3.11).

After HOSCN treatment, numerous proteins within the mitochondria are also oxidised to form sulfenic acids. Within non-treated, control samples, very few protein sulfenic acid residues are observed; whereas an increase in sulfenic acid production within the mitochondria is apparent with increasing concentrations of HOSCN (Figure 3.10B). The results also indicate that various proteins within the mitochondria (marked with red arrows) showed larger increases in sulfenic acid formation than others, indicating that there is possible protein-specific sulfenic acid formation in the mitochondria on exposure of cells to HOSCN. After analysing all the bands within each lane, using Image J, a trend towards an increase in protein sulfenic acid formation is identified in all the treated samples, which is

statistically significant at the 200 μM HOSCN treatment (Figure 3.11B). After imaging, the membrane was stripped and blotted for COX-4 and β-actin (Figure 3.10B). Data showed no variation in COX-4 intensity (Figure 3.11D), indicating that the results are not due to changes in protein loading. Within the mitochondrial fraction there was some β-actin recognition (Figure 3.11F), which may be an artifact of the mitochondrial isolation preparation or show residual cytosolic proteins in the mitochondrial preparation. However, the levels of β-actin in the mitochondria are very low compared to the cytosolic fraction, and the pattern of bands in the 2 fractions are quite different (red arrows; proteins with the largest increase in sulfenic acid formation), suggesting that different proteins are being oxidised by HOSCN in each case. This is consistent with the mitochondrial fraction containing primarily mitochondrial proteins, and the cytosol composed of cytosolic proteins.

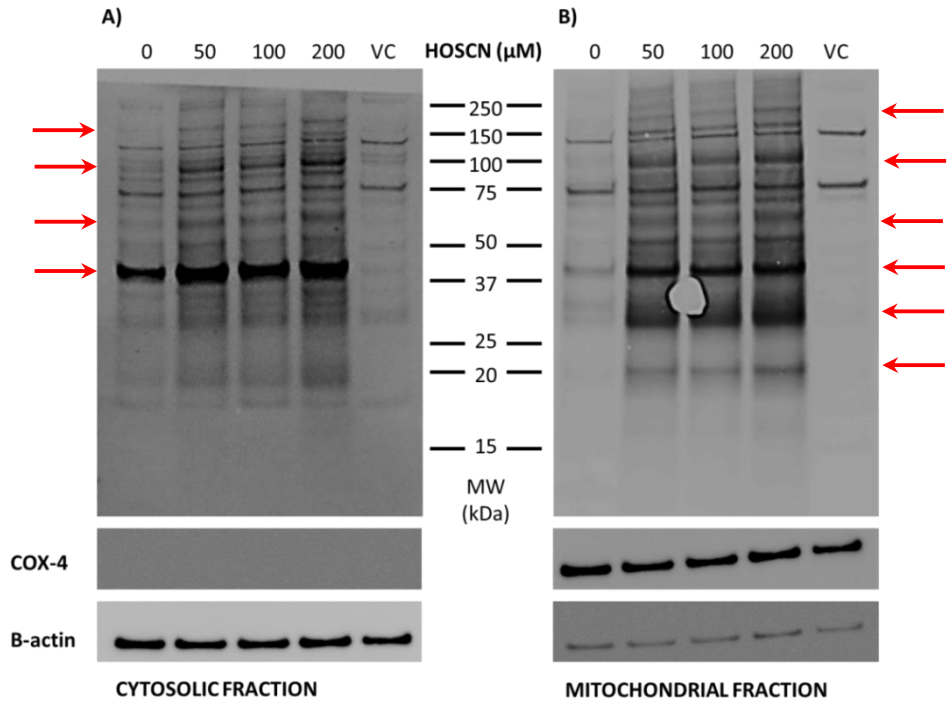

Figure 3.10: HOSCN causes the formation of sulfenic acids in both the cytosol and mitochondria of J774A.1 cells after treatment.

J774A.1 cells (1 x 10^6 cells mL^{-1}) were pre-treated with DCP-Bio1 (500 μM) or DMSO (1% v/v) as the vehicle control (VC) for 1 h at 37 ˚C prior to the addition of HOSCN (0 – 200 μM) before further incubation for 1 h at 22 ˚C. The (A) cytosol and (B) mitochondrial fractions were prepared using the mammalian mitochondrial isolation kit (Thermo Fisher Scientific) before the proteins were separated via 1D SDS-PAGE (4-12%). Proteins were transferred to PVDF membranes and biotinylated proteins detected by Western blotting with HRP-streptavidin. After imaging, the membranes were stripped before being probed with the loading control antibodies, COX-4 for mitochondrial protein detection and β-actin for cytosolic protein detection. The images are a representative of 3 separate experiments. Red arrows indicate bands that had more than a doubling in density between the control and 200 μM treatment groups.

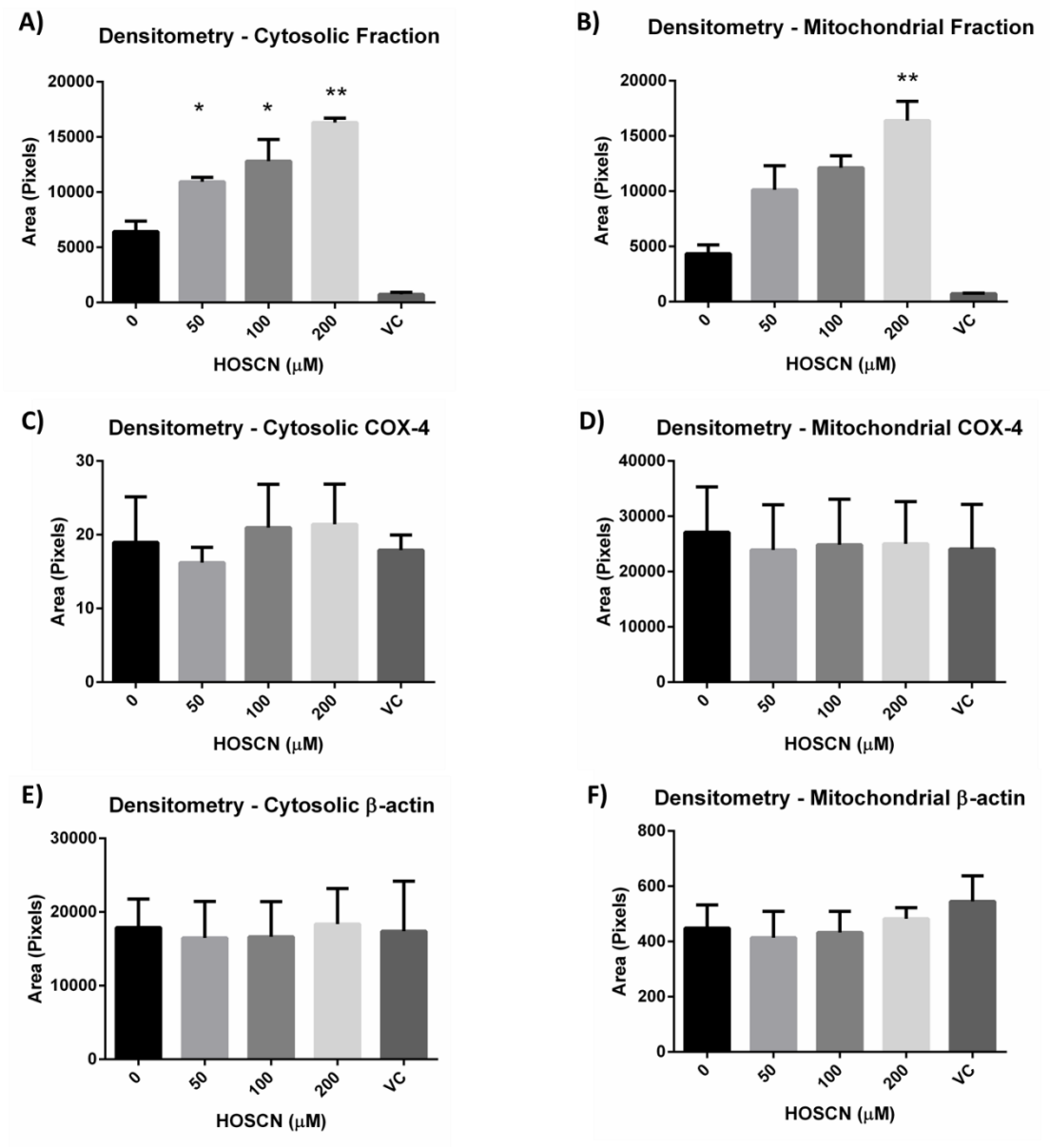

Figure 3.11: Changes in the band density of DCP-Bio1 reactive sulfenic acid protein-residues.

*Densitometry analysis of the membranes was performed using ImageJ, analysing each band in every lane. Density of the biotinylated bands was detected via Western blot after DCP-Bio1 derivitisation in the (A) cytosol and (B) mitochondria after treatment with HOSCN (0 – 200 μM) or DMSO (VC). After imaging each membrane was probed for loading controls of COX-4 (C & D) or β-actin (E & F). Values of the results are the mean ± S.E.M (n = 3). *, ** shows a significant ($p < 0.05$ or 0.01, respectively) increase when compared to the control by Repeated Measures one-way ANOVA with a post-hoc Tukey's test.*

3.4 Discussion

This Chapter examined the extent and pattern of reactivity of HOCl and HOSCN with intracellular thiols and the nature of the reversible protein thiol modifications. Exposure of J774A.1 macrophages to HOCl and HOSCN resulted in changes to intracellular thiol concentrations, with HOSCN reducing the intracellular thiol concentration to a greater extent than HOCl. The nature of the oxidised products of HOCl and HOSCN-induced protein thiol oxidation was probed using SDS-PAGE and Western blotting methods. The results indicate that HOCl and HOSCN are able to form reversible thiol oxidation products, though HOSCN was able to do this to a greater extent under analogous conditions. Evidence was obtained for the formation of sulfenic acids and S-glutathionylated adducts. In each case, a greater extent of product was seen with HOSCN compared to HOCl. It was also shown that HOSCN targeted both cytosolic and mitochondrial proteins on exposure to the cells, with sulfenic acids seen in each case following fractionation.

Exposure of J774A.1 cells to HOSCN results in a decrease in intracellular thiols in a dose-dependent manner. The decrease in thiols seen with HOSCN was greater than that seen in corresponding experiments with HOCl. This is attributed to the difference in selectivity between HOSCN and HOCl [49]. HOSCN reacts almost exclusively with protein thiols and low-molecular mass thiols such as GSH, whereas HOCl reacts with a wide range of biological targets [49, 91, 95, 96, 98, 345]. Thus, although HOSCN reacts with protein thiols at a rate in the range of $1 \times 10^4 – 7.6 \times 10^4$ M^{-1} s^{-1}, and with GSH at a rate of 2.5×10^4 M^{-1} s^{-1} at pH 7.4 [98], which is slower than the reaction of HOCl with thiols ($k = 3 \times 10^7$ M^{-1} s^{-1}) [96] the limited reactivity of HOSCN with other cellular targets means a greater loss in thiols is seen. These results compare well with previous studies reporting a greater targeting of HOSCN for thiols compared to HOCl in macrophages. For example, *Lloyd et al.* [91] reported that after 15 min oxidant treatment HOSCN reduced the intracellular GSH concentration to a greater extent than HOCl. HOSCN also oxidised protein thiols in J774A.1 macrophages to a greater extent than HOCl, as observed by a decrease in the binding of the IAF, indicating a reduced availability of free thiols. The ability of HOSCN to oxidise thiols in cellular models has been studied extensively in the past decade. One study, comparing the thiol oxidising abilities of HOSCN and HOCl showed that the selectivity of HOSCN for thiols led to an increased inactivation of membrane ATPases, and HOSCN could be up to 1000 times more efficient than HOCl at inhibiting ATPases [84]. It has also been shown that both HOCl and HOSCN could cause thiol loss in yeast alcohol dehydrogenase. Both oxidants caused protein thiol loss, but

it occurred at lower concentrations in samples treated with HOSCN compared to HOCl, most likely due to the differences in the number of targets between HOSCN and HOCl [361]. Similarly, HOSCN has been shown to oxidise free cysteines on LDL-apoB100 with greater efficiency than HOCl during a 30 min exposure [142].

Conversely, studies have shown that during a 15 min exposure to varying concentrations of HOSCN or HOCl, HOCl consistently depleted intracellular thiols and GSH with greater efficiency [185] in human coronary artery endothelial cells (HCAECs), though this may be due to reduced uptake of HOSCN into HCAEC's, as a slower rate of oxidant consumption is seen in this case. These data agree with previous studies of HOCl with HCAECs [362] and HUVECs [363], where depletion of thiols occur at low oxidant concentrations. There are other examples where HOCl depletes thiols to a similar or greater extent as HOSCN. When comparing the effect of HOSCN and HOCl on sarcoplasmic reticulum samples from rat hind-limb skeletal muscles, *Cook et al.* found no difference between HOCl or HOSCN induced thiol loss at 100 µM after 2 h treatments [170].

The results show that HOSCN causes the formation of more reversible thiol oxidation adducts than HOCl. Results indicate that a majority of the oxidation occurs at 50 µM HOSCN as an increase in staining is observed, but this response is seen to plateau at 100 µM HOSCN (Figure 3.2C), indicating that many of the reversible cysteine adducts are formed at lower HOSCN concentrations. The formation of reversible oxidative species by HOCl is less obvious (Figure 3.2A), as there seems to be less difference between the treatment groups. These results can be rationalised on the basis of the difference in chemistry between HOCl and HOSCN [49]. When thiols are exposed to stronger oxidising agents, such as HOCl, the sulfenyl chloride (RS-Cl) can be further oxidised to higher oxyacid products, such as sulfinic and sulfonic acids which are not readily reduced [108, 364]. The ability of HOCl to oxidise thiol proteins has been shown to be irreversible in cells and shown to occur on thiols on various proteins including GAPDH, PTPs and caspases, leading to enzyme inactivation or attenuation [91, 179, 181, 187]. Conversely, HOSCN is a weaker acid, and upon exposure to thiols can cause the formation of sulfenyl thiocyanate products, which can be hydrolysed to reversible products such as sulfenic acids [201].

This difference between HOCl and HOSCN is reflected in the formation of cellular sulfenic acids, with treatment of cells with HOSCN, but not HOCl, leading to the formation of sulfenic acids at all concentrations tested (Figure 3.4A). Cells treated with HOCl did not elicit a similar

response, with no significant increase in sulfenic acid formation noted at any of the concentrations tested (0 – 150 μM).

Many proteins have been identified as candidates for sulfenic acid formation (e.g. c-Jun, GAPDH) and the formation of sulfenic acids has been hypothesised to be a redox sensitive biochemical switch [364, 365]. The formation of sulfenic acids by HOSCN has also been shown to occur on the glycolysis-related enzymes GAPDH and CK, which results in a loss of activity [201]. Other studies have shown that various proteins involved in DNA repair, metabolism, nuclear transport, protein homeostasis and protein synthesis, redox homeostasis, signaling and cellular transport contain sulfenic acids in HeLa cells [328]. Another study showed the formation of sulfenic acids on Yap1, a transcriptional co-activator with proliferative and oncogenic activity, following exposure to H_2O_2 [366]. Studies have shown that the formation of sulfenic acids have effects on various proteins, such as phosphatases, including PTP-1B [367, 368], a protein involved in metabolism. The formation of sulfenic acids is crucial towards PTP-1B activity; oxidation of Cys215 to sulfenic acid prevents irreversible over-oxidation, indicating that sulfenic acids regulate PTP-1B activity. Previous studies have shown that HOSCN can inactivate PTPs which can result in the perturbation of the phosphorylation of MAPK proteins [179]. In light of the data in this Thesis, this may occur via the formation of sulfenic acids.

Protein S-glutathionylation is a cysteine specific post-translational modification that is stimulated by oxidative stress [106]. Not all thiols are equally susceptible to S-glutathionylation, but this modification can occur via reaction of sulfenic acids and GSH, and requires thiol accessibility and a cationic environment for the reaction to occur, which can play an important role in protein function [355, 369, 370]. Treatment of the J774A.1 cells with HOSCN and HOCl led to an increase in PSSG formation, though the formation of these species was inconsistent throughout 3 separate experiments and there were large amounts of PSSG detected in the control lanes.

The lack of reproducible protein S-glutathionylated products could be explained by the very strict and specific conditions required for S-glutathionylation to occur [371]. The cysteines need to be accessible for glutathionylation to occur; the environment requires cationic conditions as acidic environments will inhibit glutathionylation [106, 357, 359]. The addition of HOSCN or HOCl to the cells may therefore perturb the conditions required for glutathionylation to occur. The formation of PSSG adducts in cells exposed to HOSCN helps rationalise data from a previously published study, where HOSCN led to a loss in intracellular

GSH concentration, but this loss could not be accounted for by GSSG formation within J774A.1 cells [91]. In contrast, in isolated systems, GSSG is the only product formed on reaction of GSH with HOSCN [98]. This disparity may be explained by the formation of PSSG adducts on exposure of cells to HOSCN.

Formation of PSSG adducts after HOCl treatment of the cells was unexpected, as HOCl is a strong oxidant, and is perhaps more likely to oxidise protein thiols to sulfinic or sulfonic derivatives, which are irreversible and do not allow for the formation of PSSG. The formation of sulfinic or sulfonic acids on exposure of cells to HOCl could cause protein misfolding and aggregation [372], which may allow for the formation of PSSG adducts. After HOCl oxidation and the induction of protein misfolding, new neighbouring amino acids would play a greater effect on the environment of the cysteine residue. One possibility being a change in the pK_a of the environment surrounding the cysteine residue, the change in protein structure may affect S-glutathionylation via a loss in hydrogen-bonding between cysteine residues and residues such as serine and histidine, which would decrease the pK_a and allow PSSG formation [369]. Previous data has shown that extensive modification of cysteine residues can affect protein function and structure [373, 374], so if oxidation of proteins by HOCl yields changes in protein structure, this may affect the formation of protein S-glutathionylated species, but no previous data exists in relation to the formation of PSSG in response to HOCl, or indeed HOSCN.

The formation of PSSG in the control samples suggests that PSSG adducts are used in J774A.1 cellular signaling and redox regulation [104, 359], which may be perturbed on formation of PSSG in response to HOSCN and HOCl treatment. In response, the formation of the PSSG adducts is most likely a defensive mechanism, to prevent the over-oxidation of cysteine residues [106] in highly oxidative environments. But the formation of PSSG adducts, while protecting the cysteine residues from over oxidation, can lead to perturbation of protein function, and if the thiol is critical to protein function, the PSSG adduct will render the protein totally inactive [375-378].

However, the lack of reproducibility in this experiment is a limitation of this study, which could be a result of adducts being lost due to decomposition during the protocol. Moreover, the extensive glutathionylation in the non-treated controls could reflect a lack of specificity of the antibody used. Another method which could be employed to observe protein S-glutathionylation would involve using the thiol probe IAF, with use of glutaredoxin to remove GSH from the proteins, and a comparison between the IAF/DTT blot and the IAF/glutaredoxin

blot would allow for the visualisation of PSSG adduct formation in response to HOSCN or HOCl.

The reactivity of mitochondrial proteins with HOSCN was examined using DCP-Bio1 which gave comparable data to the DAz-2 experiment performed in whole cell lysates. The mitochondrial samples also showed increases in protein sulfenic acid formation in response to HOSCN treatment, consistent with the targeting of mitochondria by HOSCN.

The mitochondria would be a viable target for HOSCN, as previous data has shown that HOSCN can influence mitochondrial membrane potential in HCAECs [185] and the mitochondria contain numerous thiol containing proteins, especially those involved in the tricarboxylic acid (TCA) cycle and the electron transport chain (ETC). Proteins including aconitase 2, NADH dehydrogenase (Complex I), succinate dehydrogenase (Complex II) and cytochrome *c* — oxidoreductase (Complex III), all of which contain numerous Fe-S clusters, are viable targets of HOSCN-induced sulfenic acid formation [207-212]. Other proteins include ATP synthase (Complex V), which contains crucial thiol residues and voltage-dependent anion channel 1 (VDAC-1), which is located on the outer mitochondrial membrane and contains transmembrane cysteine residues. In both cases the cysteines are critical for protein function [213, 215]. Furthermore, caspase 3, which is a mitochondrial protein, has also been shown to be inhibited by HOSCN in HUVECs, which inhibited apoptosis, even in the presence of apoptotic stimuli [92]. Another report hypothesised that HOSCN was interacting with the mitochondria of J774A.1 macrophages by inducing a caspase-independent apoptotic pathway [91]. All of the proteins mentioned contain crucial cysteine residues that can possibly be oxidised by HOSCN, and the formation of sulfenic acids on these proteins could cause changes in protein conformation, inhibiting their activity, which would cause an inhibition of cellular proliferation and growth, much in the same way HOSCN affects bacterial cell growth and proliferation [198, 200, 379].

3.5 Summary

The studies in this Chapter have shown that HOSCN and HOCl can reduce the concentration of intracellular free thiols in J774A.1 cells by oxidising cysteine residues contained on proteins. The results show that both oxidants can cause reversible thiol modifications, but HOSCN is more potent. HOSCN, and not HOCl is able to cause the formation of sulfenic acids within the cell, and HOSCN is able to form these adducts within both the cytosol and the mitochondria. The formation of S-glutathionylated adducts was also investigated, and both oxidants were able to induce the formation of PSSG on cellular proteins, though HOSCN was more efficient. These data suggest that HOSCN may play a role in perturbing cellular homeostasis and protein-redox regulation. Further studies in this Thesis will investigate the functional consequences of HOSCN-induced thiol targeting of cytosolic and mitochondrial proteins by assessing changes that occur to glycolysis and oxidative phosphorylation in J774A.1 macrophages in response to HOSCN treatment.

4 The Effect of Hypothiocyanous Acid on Glycolysis

4.1 Introduction

The action of HOSCN, in a cellular setting, is primarily attributed to the oxidation of protein and low-molecular mass thiols [49, 95]. It was shown that exposure of J774A.1 cells to HOSCN results in the formation of reversible thiol oxidation products, including sulfenic acids, which may act as regulators of protein redox status and redox homeostasis. The formation of protein sulfenic acids has been reported previously, in both mammalian and bacterial cells, with the latter exposed to HOSCN via its production by the LPO system, which is present in milk and other biological fluids [11].

It was first hypothesised that the bactericidal activity of milk was due to agents termed "oxidising enzymes", as heat treatment inhibited the activity of these enzymes, later recognised as peroxidases, which in turn diminished the bactericidal effects [194, 195]. It was then determined that the peroxidases themselves had little direct effect on the bactericidal properties of milk; rather, other components, including the substrates thiocyanate (SCN^-) and hydrogen peroxide (H_2O_2) play a critical role. LPO catalyses the reaction between H_2O_2 and SCN^- to form HOSCN, which is the critical component in the antimicrobial action of this system [380]. In milk and similarly, the oral cavity, the requirement for H_2O_2 in the LPO (or SPO)/SCN^-/H_2O_2 system is met by bacterial metabolism [196], as the addition of catalase is able to prevent the system's ability to inhibit the growth of *Streptococcus cremoris* (strain 972) in milk or *Lactobacillus acidophilus* in saliva [196]. Data has shown that stationary phase *Streptococcus mutans* incubated with LPO/SCN^- had glucose utilisation inhibited by up to 90%, and if cells released H_2O_2 as a result of metabolism, into the media, which contained LPO and SCN^-, glucose utilisation was inversely proportional to the amount of H_2O_2 released indicating that the LPO/H_2O_2/SCN^- system is more bactericidal than H_2O_2 alone, due to the production of HOSCN [197, 198].

The product of the LPO-catalysed oxidation of SCN^- was also found to inhibit glycolysis in other studies with *strain 972 Streptococci* after a 30 min treatment at 30 °C [199]. Analysis of the glycolytic enzymes revealed that hexokinase, aldolase and glucose 6-phosphate dehydrogenase were all inhibited to some degree [199]. The removal of LPO/SCN^-/H_2O_2 from the *Streptococci* led to the restoration of enzyme activity, consistent with the reversible nature of HOSCN-induced oxidation. In related studies, growth inhibition of the bacteria was hypothesised to occur via the incorporation of a product from the LPO/SCN^-/H_2O_2 system into thiols of proteins involved in cell growth, glycolysis and glucose transport, removing these proteins from the functional pool [200]. A study investigating the action of HOSCN in

mammalian cells has shown that HOSCN can target GAPDH in HCAECs, and GAPDH and CK in J774A.1 macrophages, both important proteins involved in glucose metabolism, resulting in a loss of enzymatic activity, indicating that HOSCN can also oxidise non-bacterial proteins, influencing their activity [92, 185, 201].

However, the consequences of the perturbation of GAPDH activity, and potentially other metabolic enzymes, by HOSCN have not been studied in detail. During inflammatory conditions, where neutrophil activation leads to the increased production of MPO-derived oxidants, this may be an important pathway to cell dysfunction. This is particularly important to smokers who are at an increased risk of developing inflammatory diseases, including cardiovascular diseases and stroke, and have elevated plasma SCN^-, hence producing greater yields of HOSCN [83, 304, 381].

The study performed in this Chapter will determine whether HOSCN-induced oxidation of protein thiols influences glycolysis in J774A.1 macrophages, as predicted on account of the known targeting of GAPDH, and the effects of this oxidant on glycolysis in bacterial cells.

4.2 Aims

The aim of the studies presented in this Chapter is determine whether HOSCN perturbs the metabolism of glucose in J774A.1 macrophages, resulting in decreased energy production using a series of functional glycolysis assays. Whether the effect of HOSCN on the cellular glycolytic pathways occurs in a reversible manner will also be assessed.

4.3 Results

4.3.1 HOSCN targets glycolytic enzymes

It has been shown previously that HOSCN targets glycolytic enzymes in different cell types [56, 199, 379]. Evidence has been presented for sulfenic acid formation on GAPDH and CK in macrophages exposed to HOSCN [201]. In addition, a proteomic analysis to measure reversible thiol modification indicated that fructose-bisphosphate aldolase and triose-phosphate isomerase (TPI) are also targets of HOSCN *(Tessa Barrett, PhD Thesis, 2012)*. Initial studies were performed to examine whether sulfenic acids were formed on key glycolytic enzymes within cells after exposure to HOSCN. J774A.1 cells (1×10^6 cells) were treated with DCP-Bio1 for 1 h at 37 ˚C before being treated HOSCN (0 – 200 µM) for 1 h at 22 ˚C. After the mitochondrial isolation, the cytosolic fraction was sampled and the proteins were separated using SDS-PAGE. The proteins were transferred to membranes and were probed with anti-GAPDH, anti-aldolase or anti-TPI antibodies, before being incubated with streptavidin-HRP and imaged using ECL.

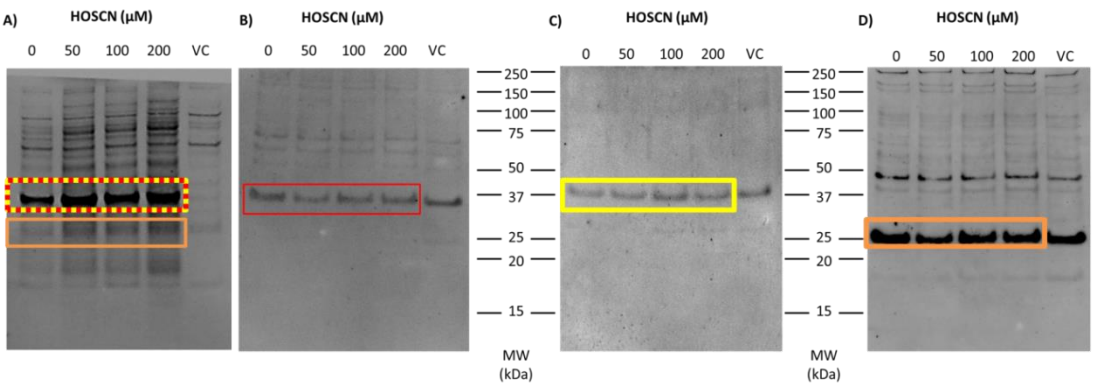

Figure 4.1: Western blots identifying the location of glycolytic enzymes.

J774A.1 cells (1 x 10^6 cells mL^{-1}) were pre-treated with DCP-Bio1 (500 µM) or DMSO (1% v/v) (VC) for 1 h at 37 ˚C prior to the addition of HOSCN (0 – 200 µM) before further incubation for 1 h at 22 ˚C. Cells were then prepared and the cytosol was probed for (A) sulfenic acids (B) GAPDH, (C) fructose-bisphosphate aldolase or (D) TPI. These blots were then compared against the blots of DCP-Bio1 probed samples. Boxes indicate which bands lined up with bands from both the DCP-Bio1 probed cytosol samples. The images are a representative of 3 separate experiments.

The results show that the molecular weight and position some of the bands in the DCP-Bio1 blot align with the position of GAPDH, aldolase and TPI from this experiment (Figure 4.1). The data are consistent with previous studies using IAF and 2D SDS-PAGE to probe for reversible thiol modifications in J774A.1 cells exposed to HOSCN *(Tessa Barrett, PhD Thesis, 2012)*. As IAF does not identify the specific type of reversible modification, these results indicate that the reversible modifications previously identified are possibly sulfenic acids. There are various limitations to using Western blot analysis to identify proteins tagged with the DCP-Bio1 probe, and further analysis, such as LC-MS/MS, is required to fully characterise the identification of the DCP-Bio1 labelled proteins.

Further studies were performed to determine whether HOSCN has a functional effect on glycolysis in J774A.1 macrophages.

4.3.2 Determining the effect of HOSCN on glycolysis using the Seahorse XF analyser

To determine the effect of HOSCN oxidation of the function of glycolysis in J774A.1 cells a Seahorse XF bioanalyser was used. The analyser can measure two variables, oxygen consumption rate (OCR), which is a measure of mitochondrial respiration, and extracellular acidification rate (ECAR), which is largely the result of the glycolytic pathway. Glycolysis is a process that causes the release of protons from the cell as a by-product. The release of protons from the cell causes the extracellular media to acidify, decreasing the pH, which can be analysed by the XF bioanalyser by isolating small volumes of the media directly above a cellular monolayer (ca. 100 – 200 microns) by solid state probes. By analysing the changes in pH above the cells, proton efflux from the cells can be determined, and by using specific inhibitors of mitochondrial respiration and glycolysis, the 2 processes can be directly measured. To properly determine glycolysis in cells, two prerequisites must be met, firstly; the cells must adhere in a monolayer to ensure an even release of protons from the sample into the media. Secondly; the cells must be in an environment of media that has no buffering capacity as to properly determine the flux of protons from the cell, as a change in the pH of the media must occur, if the media has a buffering capacity, glycolysis cannot be properly determined by this method.

Seahorse bioscience supplies a non-buffering DMEM media that also contains no glucose, L-glutamine, sodium pyruvate or growth factors, which has been used in all of the glycolysis and mitochondrial analysis experiments in this Thesis and will be called “basal DMEM” throughout.

A glycolytic stress test is performed by measuring the release of protons from the cell into the media. First, the glycolytic state of the cells in glucose-free media is recorded, then glucose (10 mM) is injected, activating the glycolytic pathway and the basal glycolytic state is recorded. After baseline glycolysis is recorded, oligomycin (1.5 µM) is injected; inhibiting mitochondrial ATP synthesis and this inhibition of ATP synthase induces the glycolytic capacity, an increase in the metabolism of glucose in an attempt to maintain ATP production. Finally, the hexokinase inhibitor 2-deoxyglucose (100 mM, 10 × excess compared to glucose) is injected, halting glycolysis and allowing for the quantification of non-glycolytic proton producing pathways. This reading is subtracted from all previous recordings, allowing for an accurate determination of glycolytic flux. From this point, the glycolytic reserve can be calculated, which is the difference between the glycolytic capacity and baseline glycolysis (Figure 4.2).

4.3.2.1 Cell culture density

Before performing the glycolytic stress test as a functional measure of glycolysis (Figure 4.2), an optimal cell number needed to be determined. The optimal cell number to be used was determined by finding a balance between a viable cell monolayer within each well of the plate and the required number of cells to cause a measurable change in ECAR (ca. 10 – 20 mpH/min/mg protein). Because the plate is shaken between readings, the cells were plated to the wells (0.28 cm^2/well) using Cell-Tak adhesive (3.5 µg/cm^2), to ensure the cells remain attached to the plate.

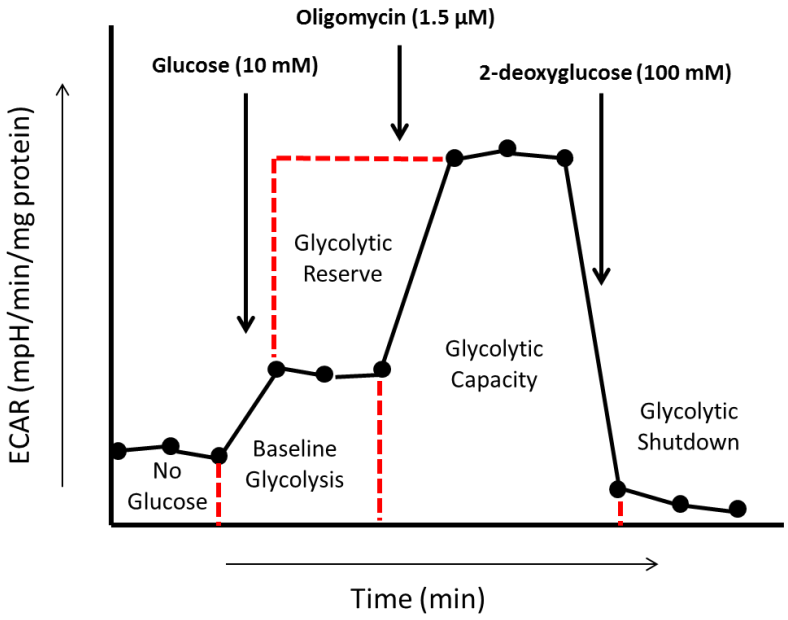

Figure 4.2: The glycolytic stress test profile.

The glycolytic stress test is made of 4 distinct parts. A no glucose glycolysis response, then the injection of 10 mM glucose allows recording of baseline glycolysis. After the baseline readings, 1.5 µM oligomycin is injected and the glycolytic capacity (maximum glycolysis) can be determined. 2-deoxyglucose (2-DG) is injected which inhibits hexokinase, halting glycolysis, allowing for the determination of background proton releasing processes to non-glycolytic pathways.

For this experiment, the cells were plated in basal DMEM containing 10 mM glucose (glucose is typically injected once the experiment has begun, but in this test a 'no glucose reading' was not needed), at varying cell densities, before being placed in the Seahorse XF analyser and baseline glycolysis was monitored for ca. 1 h. Results show that 2.5×10^4 cells and 5.0×10^4 cells gave similar ECAR readings, both of which were below 10 mpH/min/mg protein (Figure 4.3). Cells plated at a density of 7.5×10^4 cells/well resulted in a steady and continuous signal for the duration of the experiment (ca. 17 mpH/min/mg protein), while cells at densities above this did not actually improve or increase the signal substantially. Instead, higher cell densities led to a decrease in ECAR throughout the experiment, upon further inspection, the cells had not formed a strong monolayer, which caused cells to be shaken off, confounding the analysis.

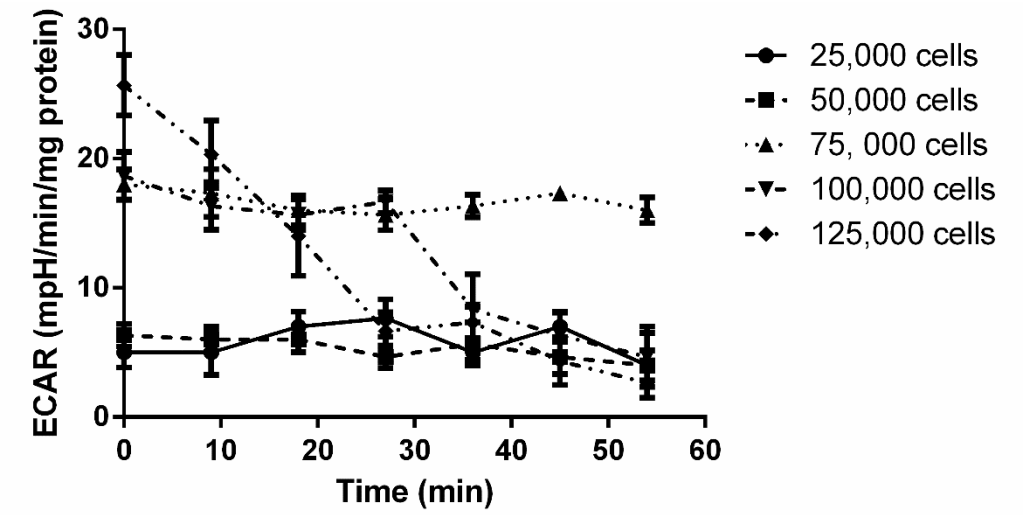

Figure 4.3: Optimisation of cell number used in the glycolytic stress test.

J774A.1 cells were plated in XF24 cell culture plates at various densities 2.5 × 10^4 (●), 5.0 × 10^4 (■), 7.5 × 10^4 (▲), 1.0 × 10^5 (▼) and 1.25 × 10^5 (◆) in basal DMEM containing 10 mM glucose. The cells were then left placed into the Seahorse bioanalyser and their baseline ECAR was measured for 7 cycles (ca. 1 h). The results indicate that 7.5 × 10^4/ well had the highest and most consistent measurements throughout. The results are the average of 1 experiment run with triplicate treatments ± S.E.M.

4.3.2.2 Oligomycin injection concentration

The next step was to optimise the concentration of the ATP synthase inhibitor, oligomycin. Oligomycin inhibits the formation of ATP by ATP synthase during oxidative phosphorylation; this causes the cells to respond by increasing their glycolytic activity to compensate [382, 383], enabling the determination of the maximum glycolytic capacity of the cell to be determined. Two prerequisites were set to determine which concentration of oligomycin would be used; firstly, the response must be substantial compared to the baseline. Secondly, of the concentrations that are substantial, the lowest concentration of them would be chosen as high concentrations can be toxic [384].

J774A.1 cells were plated at a density of 7.5 × 10^4 cells/well before being placed in the Seahorse analyser and equilibrated for 10 min before baseline glycolysis (ECAR) was measured for 3 cycles. Oligomycin was then injected and the ECAR response was measured for another 3 cycles. The optimisation assay showed that low concentrations (0.5 µM and

1.0 μM) oligomycin did not induce an increase in the ECAR of J774A.1 cells (Figure 4.4), while higher concentrations (2.5 μM and 3.0 μM) of oligomycin led to unsteady and variable readings. The results indicated that both 1.5 μM and 2.0 μM oligomycin caused a doubling in the ECAR from baseline readings, and both caused very similar and steady responses, leading to the choice of 1.5 μM oligomycin being the concentration to be used for the stress test as it was the lower of the two.

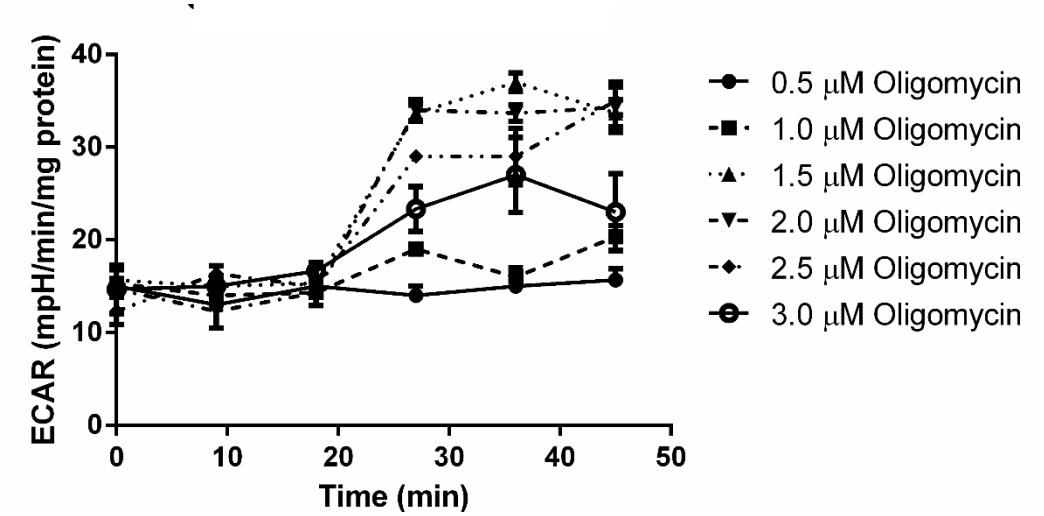

Figure 4.4: Oligomycin concentration optimisation using J774A.1 cells.

J774A.1 cells (7.5 × 10^4 cells) were seeded into an XF24 cell culture plate and placed into the Seahorse XF bioanalyser where increasing concentrations 0.5 (●), 1.0 (■), 1.5 (▲), 2.0 (▼), 2.5 (◆) and 3.0 (○) μM of the ATP synthase inhibitor, oligomycin were injected and the ECAR response was recorded. The results are the average of 1 experiment run with triplicate treatments ± S.E.M.

4.3.3 HOSCN inhibits the glycolytic ability of J774A.1 macrophages

The functional effect of HOSCN on the glycolytic activity of J774A.1 macrophages was examined initially using the Seahorse analyser to measure changes in ECAR on stimulation of cells with glucose. J774A.1 cells (7.5×10^4 cells) were treated with HOSCN (0 – 100 μM) in the XF24-well Seahorse plate in the presence of XF basal DMEM, which contained no glucose. Glucose is initially excluded from the media to determine the baseline measurement in the absence of glucose. After HOSCN treatment, the XF24 plate was placed into the Seahorse analyser to equilibrate, and then glycolytic activity was recorded by determining ECAR.

Results indicate that HOSCN has a significant effect on the ECAR measurements following the injection of glucose into the media (Figure 4.5). In this experiment, the cells were exposed to HOSCN (0 – 100 μM) and immediately placed in the analyser, and changes in glycolysis were recorded for 13 cycles (ca. 1 h). Interestingly, it appears that the effect of HOSCN on glycolysis is almost immediate, as glycolysis is affected at the very first glucose positive recording, indicating the effects of HOSCN occur in the first ca. 20 min. Treatment with HOSCN has a dose-dependent inhibitory effect on ECAR measurements following injection of glucose to promote glycolysis, with untreated cells performing glycolysis 4 times more efficiently than cells treated with 100 μM HOSCN (Figure 4.5). This change in ECAR was only observed in the presence of active HOSCN, with no reduction in ECAR seen in experiments with decomposed HOSCN (dHOSCN). For the functional assays in this experiment, dHOSCN was employed to determine that the result observed was due to the oxidative ability of HOSCN and not due to the non-oxidative by-products of HOSCN decomposition, excess SCN^- or a result of any buffer effect.

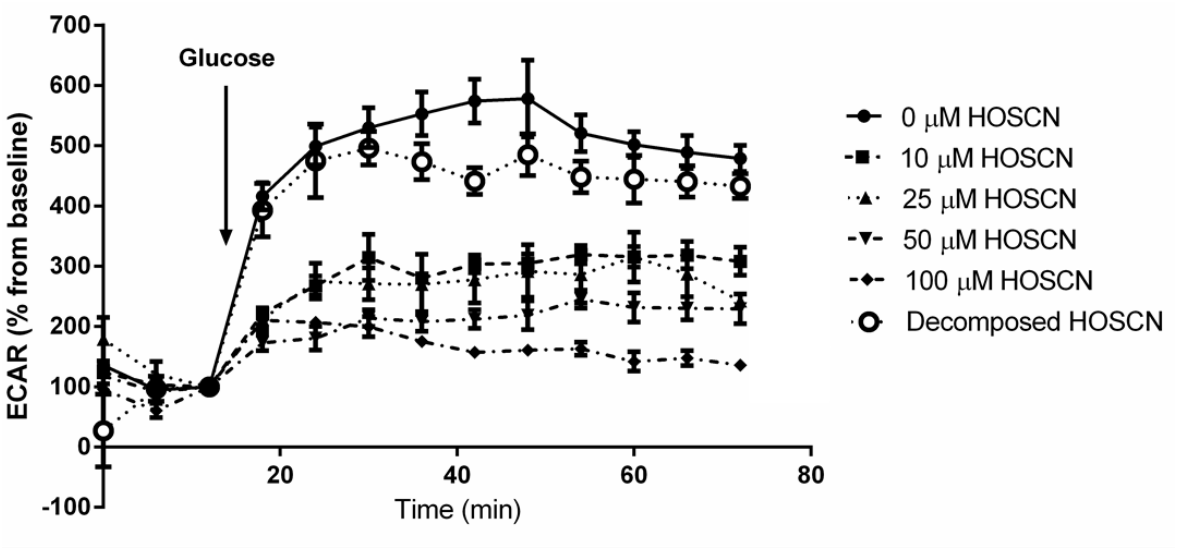

Figure 4.5: J774A.1 baseline glycolysis is affected by the oxidative ability of HOSCN

*Treatment of J774A.1 cells (7.5 × 10^4 cells) with 0 (●), 10 (■), 25 (▲), 50 (▼), 100 (◆) μM HOSCN or decomposed HOSCN (○) for 1 h at 37 ℃ led to the attenuation of baseline glycolysis. Cells were treated with HOSCN and were immediately placed into the Seahorse analyser to be analysed for the duration of the treatment. Results **s**how that under basal conditions (10 mM glucose injection only) glycolysis is clearly attenuated at even low levels of HOSCN exposure when compared against baseline wells. Results are the average of 3 independent experiments ± S.E.M.*

After recording the baseline glycolytic activity of J774A.1 cells, the functional effect of HOSCN on glycolysis was examined in more detail by performing a glycolytic stress test. Cells (7.5 × 10^4 cells) were treated with HOSCN (0 – 100 μM) or decomposed HOSCN for 1 h at 22˚C. After treatment, the cells were placed into the Seahorse analyser and the test was performed (Figure 4.6). The background ECAR readings were first recorded for 3 cycles in the absence of glucose before 10 mM glucose was injected into each well and baseline glycolysis was recorded. The baseline closely mirrors the results from the previous experiment (Figure 4.5), with increasing concentrations of HOSCN impairing the ability of the cells to perform glycolysis (Figure 4.6).

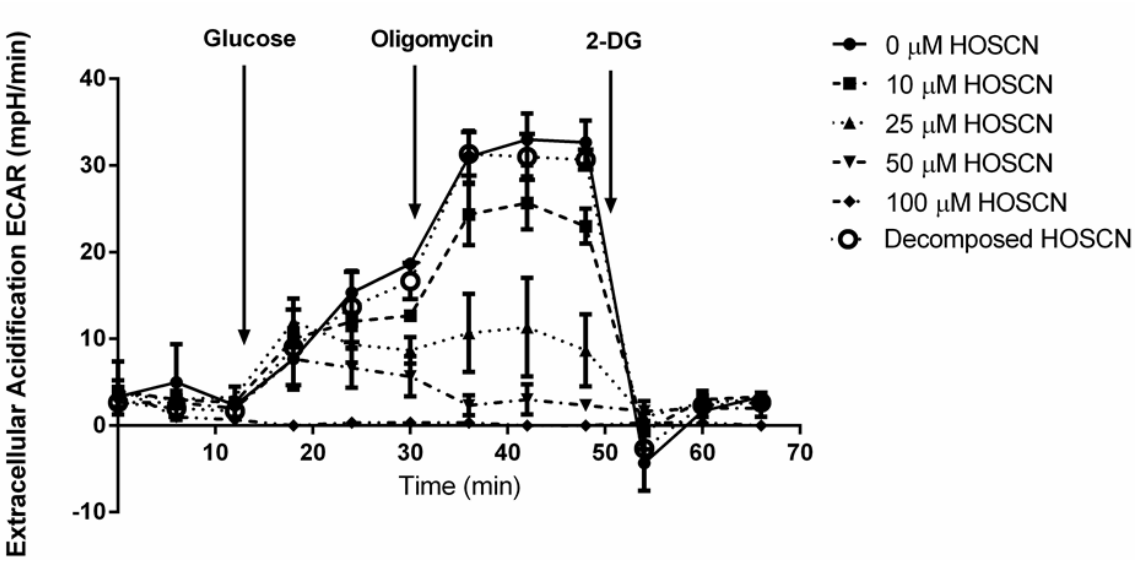

Figure 4.6: HOSCN affects the glycolytic profile of J774A.1 cells

Treatment of J774A.1 cells (7.5 × 10^4 cells) with 0 (●), 10 (■), 25 (▲), 50 (▼), 100 (◆) μM HOSCN or decomposed HOSCN (○) for 1 h at 22 ℃ led to the attenuation of the glycolytic profile of the cells, decreased basal glycolysis, glycolytic capacity and reserve. The cells were markedly affected by HOSCN treatment at all stages of glycolysis. Results are the average of 3 independent experiments ± S.E.M.

After baseline glycolysis was recorded, 1.5 μM oligomycin was injected into the media of the cells to measure glycolytic capacity (Figure 4.7B). Results indicate that HOSCN inhibits the glycolytic capacity of the cells, compared to that observed with non-treated control cells or cells exposed to dHOSCN. Thus, HOSCN leaves the cells unable to meet their bioenergetic needs, with increasing concentrations of HOSCN causing a decrease in the glycolytic capacity of the J774A.1 cells that was significant at every concentration tested. Results also indicate that cells treated with concentrations of ≥ 50 μM HOSCN are unable to increase glycolytic capacity in response to oligomycin, with the ECAR measurements of 50 and 100 μM HOSCN treated cells falling below their baseline glycolysis readings.

After determining baseline glycolysis and glycolytic capacity, cellular glycolytic reserve was determined (Figure 4.7C). Glycolytic reserve is the difference between glycolytic capacity and baseline, and is measured after the injection of 2-deoxyglucose (100 mM), which is used to inhibit glycolysis, and confirm that changes to ECAR in the experiment are related to glycolysis, rather than background proton producing processes within the cell. The

measurement of glycolytic reserve, therefore acts as a determinant of glycolytic stress. Exposure of J774A.1 cells to HOSCN resulted in a dose-dependent decrease in glycolytic reserve which was significant at concentrations ≥ 25 µM HOSCN. These data indicate that HOSCN promotes a significant increase in glycolytic stress, which renders the cells unable to respond to the stress placed on the glycolytic pathway. Changes in baseline glycolysis, glycolytic capacity and glycolytic reserve were not observed in the analogous experiments with dHOSCN showing that the response is due to the oxidative ability of HOSCN and not due to any of the non-oxidative by-products of HOSCN decomposition.

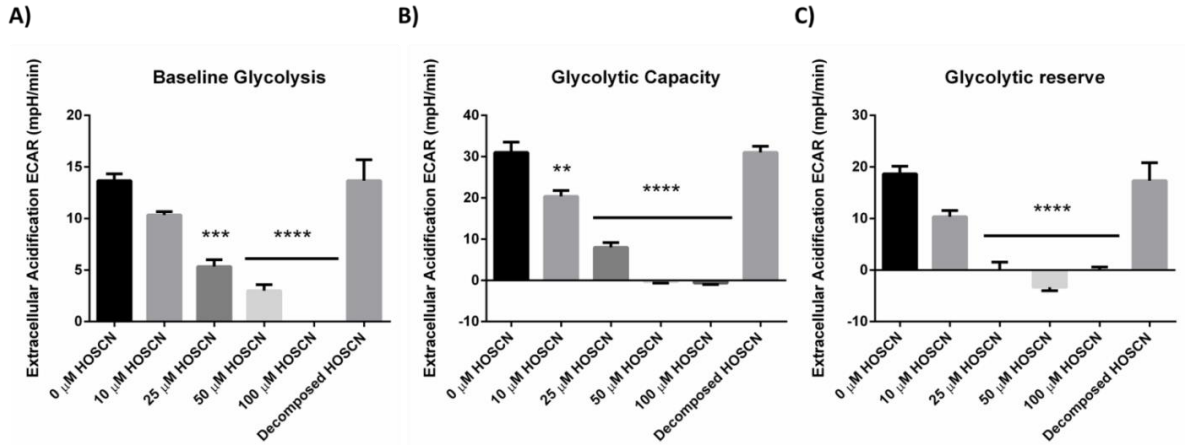

Figure 4.7: Changes in the glycolytic profile of J774A.1 cells exposed to HOSCN.

*Analysis of the glycolytic stress test performed on J774A.1 macrophages (7.5 × 10^4 cells/well) treated with HOSCN (0 – 100 µM) or decomposed HOSCN. (A) Baseline glycolysis, which describes the effect of HOSCN on basal glycolysis after the injection of 10 mM glucose. (B) The maximum glycolytic output is described by the glycolytic capacity, following the injection of oligomycin (1.5 µM). (C) Glycolytic reserve is the glycolytic capacity minus basal glycolysis, and it indicates that HOSCN causes 'glycolytic stress' at sub-pathological concentrations. All data are the average of 3 separate experiments ± S.E.M. Significance was defined using one-way ANOVA with post-hoc Tukey's multiple comparisons test (** = p <0.01, *** = p <0.001, **** = p <0.0001).*

A limitation of this study was the requirement for incubation of the cells in non-buffered cell media rather than a balanced salt solution that has been used in previous experiments. HOSCN could react with media components which may influence its reactivity. For this reason, it was not possible to perform a direct comparison of HOSCN with HOCl, as HOCl reactivity was quenched by media components when tested (data not shown). Studies were therefore extended to examine the effect of HOSCN on glycolysis by measuring lactate release, an end-point measurement of glycolysis which allowed for the testing of cells in HBSS, and also provided a means of comparing the effects of HOSCN and HOCl.

After analysing the results of the Seahorse assay, an experiment was devised to determine if the treatment of J774A.1 cells with HOSCN led to a decrease in the formation of glycolytic end-products, and if these end-products could be easily measured and correlated back to the data obtained by the glycolytic stress test.

4.3.4 Extracellular release of lactate from J774A.1 macrophages is reduced by HOSCN

Lactate is produced from the conversion of pyruvate via LDH and is considered an end-product of glycolysis, which is released into the extracellular environment, with extracellular lactate levels being proportionally correlated to intracellular glycolytic activity [334]. A lactate assay was performed to determine if HOSCN exposure to J774A.1 macrophages led to a decrease in glycolytic end-products. J774A.1 cells (1×10^6 cells) were treated with HOSCN (0 – 100 µM) or decomposed HOSCN for 1 h at 22 ˚C, before removal of the oxidant solution, which was replaced with oxidant-free HBSS containing 10 mM glucose. The lactate concentration was measured in the supernatant at 1 and 2 h post treatment (Figure 4.8 & Figure 4.9).

Exposure of cells to HOSCN for 1 h caused a significant decrease in the concentration of lactate secreted by the cells, with a significant decrease noted at the first treatment concentration (10 µM) (Figure 4.8A) and at further time points (Figure 4.8B & C). Treatment of cells with the decomposed HOSCN did not lead to a decrease in lactate release from J774A.1 cells, indicating that the loss is due to the oxidative action of HOSCN and not a decomposition by-product, with the results mirroring the basal ECAR measurements of the glycolytic baseline and stress test experiments.

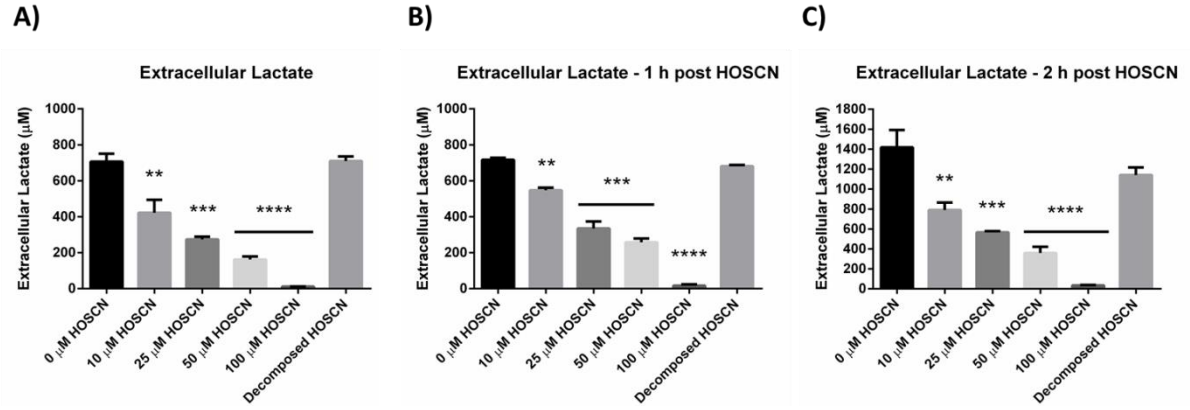

Figure 4.8: HOSCN attenuates the extracellular release of lactate from J774A.1 cells.

*(A) Treatment of J774A.1 cells (1 × 10^6 cells) with HOSCN (0 – 100 µM) or decomposed HOSCN for 1 h at 22 ℃ led to a decrease in lactate release. Cell media was replaced and cells incubated at 22 ℃ for another (B) 1 h and (C) 2 h before lactate concentration was determined using an M2e plate reader reading absorbance at 490 nm. Values of the results are the mean ± S.E.M (n = 3). **, *** and **** show a significant (p < 0.01, 0.001 and 0.0001, respectively) decrease compared to respective controls by Repeated Measures one-way ANOVA with a post-hoc Tukey's test.*

A second hypothesis was also tested, as data has shown that the removal of LPO/H_2O_2/SCN^- from bacterial cultures led to the restoration of the glycolytic enzyme activity [200], indicating that HOSCN damage may be reversible. After measuring the lactate concentration in the extracellular media, the oxidant solution was removed and replaced with fresh HBSS (10 mM glucose). The cells were then left to metabolise the glucose in the media for another hour, to examine whether HOSCN-induced changes to lactate production is reversible. Results show that over the next 2 hours, the untreated cells and dHOSCN treated cells continued to release lactate into the media, at similar rate to that observed during the treatment time (Figure 4.8A). In the 1 h after treatment, there was a non-significant increase but still reduced extent of lactate release with the HOSCN-treated cells. During the second hour, non-treated and dHOSCN treated cells roughly doubled the concentration of lactate in the supernatant while cells treated with 10 and 25 µM HOSCN saw a significant, but still

reduced increase in extracellular lactate release compared to the treatment and 1 h post time points (Figure 4.9). Cells treated with ≥ 50 µM HOSCN saw no increases in the rate of lactate release over the 2 hours. These results indicate that treatment with 10 and 25 µM HOSCN may be reversible, though extent of reversibility is limited.

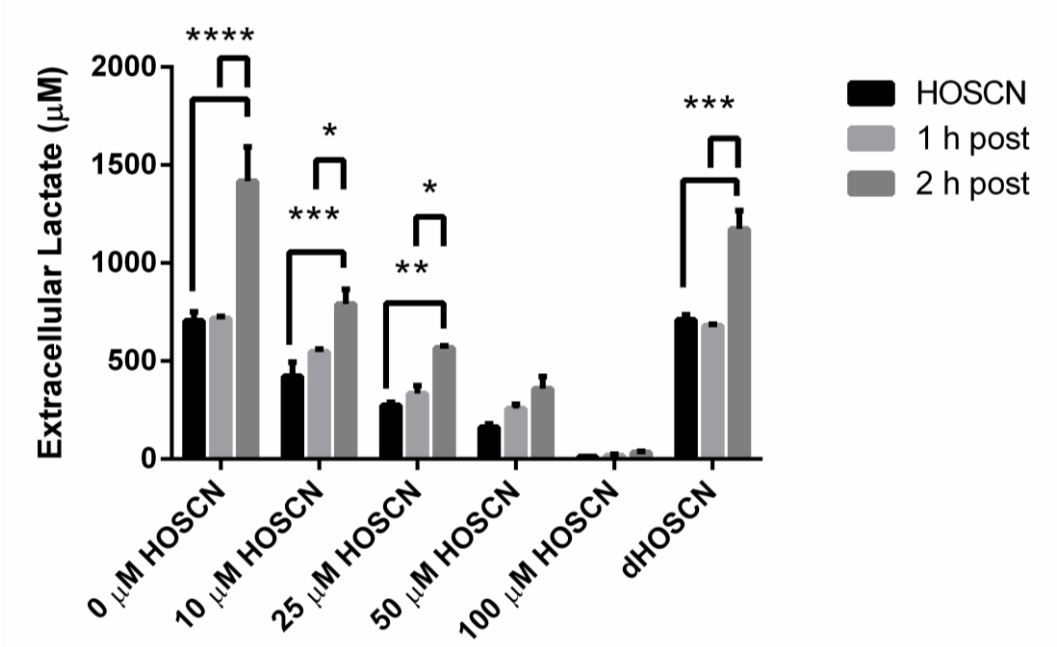

Figure 4.9: Comparison of lactate release against time.

*Treatment of J774A.1 cells (1 × 10^6 cells) with HOSCN (0 – 100 µM) or decomposed HOSCN for 1 h at 22 ℃, comparing each concentration separately over the 3 h experiment. Results indicate that HOSCN induced damage can be repaired to a certain extent. Values of the results are the mean ± S.E.M (n = 3). *, **, *** and **** show a significant (p < 0.05, 0.01, 0.001 and 0.0001, respectively) increase compared to respective time-points by Repeated Measures two-way ANOVA with a post-hoc Tukey's test.*

4.3.4.1 HOCl does not reduce the concentration of extracellular lactate

An extracellular lactate assay was performed to determine if HOCl was able to inhibit lactate formation in J774A.1 cells and allow a comparison of the data to the results obtained after treating cells with HOSCN.

J774A.1 cells were treated for 1 h with HOCl (0 – 100 µM) at 22 ˚C, before analysing, the extracellular media was tested for lactate. Results indicate that HOCl was unable to cause a reduction in the concentration of extracellular lactate at any of the concentrations tested (Figure 4.10), suggesting that HOCl, unlike HOSCN, is unable to inhibit glycolytic enzymes in J774A.1 cells.

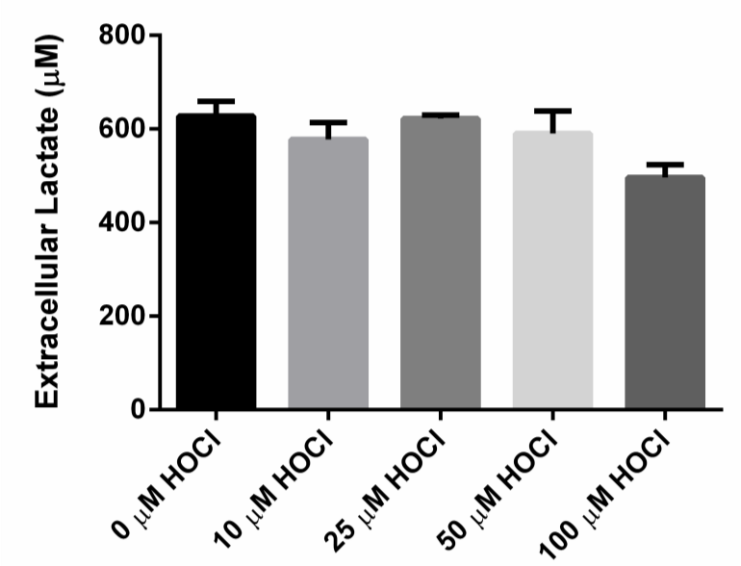

Figure 4.10: HOCl is unable to inhibit the release of lactate into the extracellular media.

J774A.1 cells (1 × 10^6 cells) were treated with HOCl (0 – 100 µM) for 1 h at 22 ˚C before lactate concentration was determined using an M2e plate reader and reading absorbance at 490 nm. HOCl did not induce a decrease in lactate release at any of the concentrations tested, indicating that HOCl does not play a part in the inhibition of glycolytic activity. Values of the results are the mean ± S.E.M (n = 3). Data were analysed using Repeated Measures one-way ANOVA with a post-hoc Tukey's test.

4.3.4.2 Glucose uptake is unaffected by HOSCN treatment

Experiments were performed to assess the effect of HOSCN on glucose uptake, which may also influence the capacity of the cells to undergo glycolysis. This is important because HOSCN may inactivate glucose transport proteins on the cell membrane; this has been reported previously in bacterial cells, including *S. galactiae* [385] Glucose uptake was measured using the fluorescent glucose analog, 2-deoxy-2-[(7-nitro-2,1,3-benzoxadiazol-4-yl) amino]-D-glucose (2-NBDG).

J774A.1 cells (1×10^6 cells mL^{-1}) were treated with HOSCN (0 – 200 μM) in PBS (does not contain glucose) for 1 h at 22˚C or the glucose uptake inhibitor, apigenin (50 μM), for 20 min, while being supplemented with 500 μM 2-NBDG for 1 h. After treatment, the media was removed and replaced with PBS before being imaged using a fluorescence microscope. The results clearly show that non-treated control cells readily take up the fluorescent 2-NBDG, consistent with active glucose uptake. HOSCN has no effect on the uptake of 2-NBDG into J774A.1 cells at 50 and 100 μM while cells treated with the positive control, apigenin (50 μM), had an observable reduction in 2-NBDG fluorescence indicating an inhibition of glucose uptake proteins.

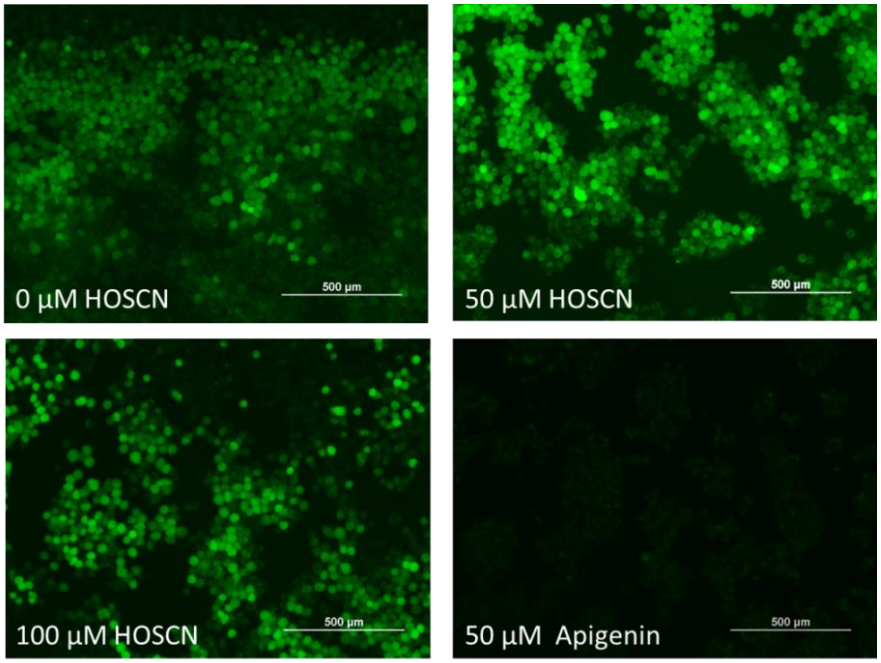

Figure 4.11: HOSCN does not affect the ability of J774A.1 macrophages to uptake glucose.

Representative images of cells exposed to HOSCN (0 – 100 µM) or the positive control, apigenin (50 µM), a flavonoid that inhibits glucose uptake. Images show that HOSCN has little to no effect on the fluorescence of 2-NBDG within the cell using a fluorescent microscope (λ_{ex} = 485 nm, λ_{em} = 535 nm). Results indicate that glucose uptake is unaffected by HOSCN treatment while cells treated with apigenin show a marked decrease in intracellular 2-NBDG fluorescence, indicating an inhibition of glucose uptake. The results are representative of 1 experiment with samples run in triplicate.

A plate reader assay was also performed, to quantify the change in 2-NBDG fluorescence after HOSCN exposure of the J774A.1 cells. Cells (1×10^6 cells/well) were treated with HOSCN (0 – 200 µM) for 1 h or apigenin (50 µM) for 20 min at 22 ˚C in the presence of 500 µM 2-NBDG in PBS. After treatment the cells were washed with PBS and the fluorescence was determined using an M2e plate reader at λ_{ex} = 485 nm, λ_{em} = 535 nm.

The results are consistent with the microscopy results, showing that HOSCN does not inhibit the ability of the cells to take up 2-NBDG at any of the concentrations tested (Figure 4.12). In contrast, apigenin caused a significant decrease in the ability of cells to uptake 2-NBDG. These data suggest that HOSCN plays no role in the inhibition of glucose uptake under the

conditions employed in this study. Thus, the effect of HOSCN on cellular glycolysis is attributed to the inhibition of glycolytic enzymes within the cytosol, rather than the oxidation of thiols or other modifications of membrane glucose transporters. However, it is important to confirm that extensive cell death is not responsible for the changes in glycolysis.

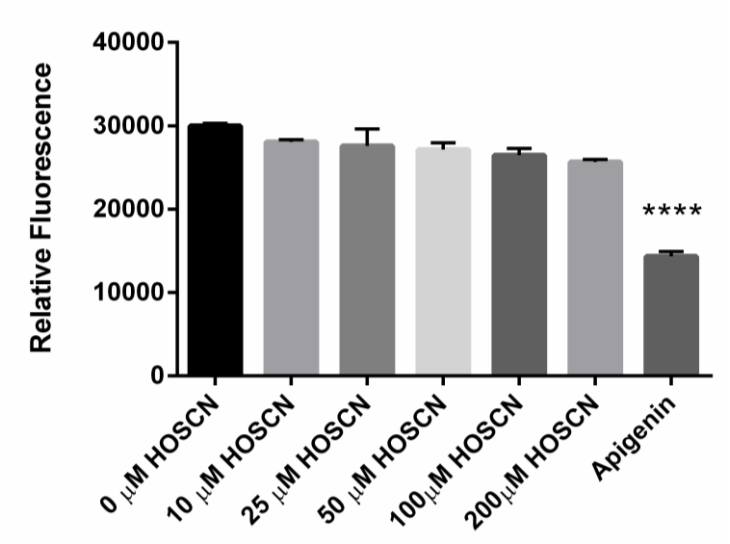

Figure 4.12: HOSCN treatment has no effect on glucose uptake in J774A.1 cells exposed to 2-NBDG.

*Cells (1×10^6 cells) were treated with HOSCN (0 – 200 µM) for 1 h or apigenin (50 µM) for 20 min at 22 ˚C before the media was removed and replaced with PBS. In place of glucose, 2-NBDG, a fluorescent glucose analogue was used to determine whether or not the cells are able to uptake glucose using a M2e plate reader (λ_{ex} = 485 nm, λ_{em} = 535 nm). Results indicate that HOSCN does not have the ability to inhibit glucose uptake, while apigenin significantly reduced glucose uptake in J774A.1 cells. Values of the results are the mean ± S.E.M (n = 3). **** shows a significant ($p < 0.0001$) increase when compared to the control by Repeated Measures one-way ANOVA with a post-hoc Tukey's test.*

Therefore, an experiment was performed to confirm that HOSCN did not perturb glycolysis via the induction of cell lysis and release of cellular contents into the media.

4.3.4.3 The inhibition of glycolysis is not due a decrease in cell viability

Lactate dehydrogenase (LDH) catalyses the reversible reaction of pyruvate to lactate when oxygen is in short supply in the environment [386]. LDH release is commonly used as a test for cellular viability, as LDH activity can be readily measured in the extracellular milieu as cells lyse. Activity is measured following the addition of NADH and pyruvate, in excess, to ensure that the rate-limiting factor is LDH concentration. This assay was performed to confirm that the effect of HOSCN on glycolysis was not influenced by cellular lysis, as predicted on the basis of previously published data [91]. The experiment was performed under identical conditions to the Seahorse XF glycolysis stress test, except that cells were treated in HBSS, rather than the basal DMEM. Cells were treated with the same concentration of HOSCN used in the glycolytic stress test (0 – 100 µM) or decomposed HOSCN in HBSS for 1 h at 22 ˚C and for 2 h, with the second hour at 37 ˚C.

Results of the LDH assay indicated that HOSCN did induce some cell lysis (20 % loss in viability) at the highest concentration of HOSCN used (100 µM) at the 1 h time point (Figure 4.13A) with increases in the LDH activity apparent in the extracellular media, while little to no LDH activity was observed in the media of non-treated cells and cells treated with lower concentrations. At the 2 h time point, a greater degree of lysis was observed, which was significant on exposure of the cells to 50 and 100 µM HOSCN (Figure 4.13B). These results indicate that HOSCN-induced oxidation induces lysis at the higher treatment concentrations, while lysis did not occur in the samples treated with decomposed HOSCN, indicating that lysis is caused by the oxidative ability of HOSCN and not SCN^- or a decomposition product of HOSCN (Figure 4.13A & B). These results indicate that the significant perturbation of glycolysis, seen at concentrations where no cell lysis is observed, is not due to a loss in cell viability.

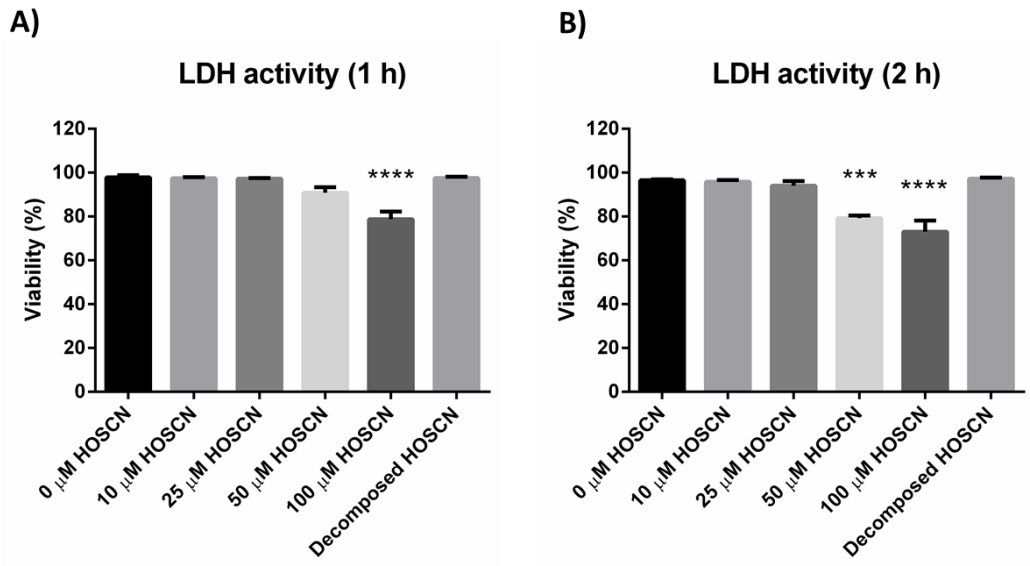

Figure 4.13: Cell lysis and LDH release into the extracellular milieu is induced by HOSCN treatment.

*J774A.1 cells (1 × 10^6 cells) were treated with HOSCN (0 – 100 µM) or decomposed HOSCN for (A) 1 h or (B) 2 h at 22 ℃ for the first hour and at 37 ℃ for the second hour to emulate the conditions of the glycolysis assay. The activity of LDH was measured in the extracellular milieu and within the cells using an M2e plate reader, recording the absorbance at 340 nm every 5 min for 30 min, to determine the extent of cellular lysis. Values of the results are the mean ± S.E.M (n = 3). *** and **** show a significant (p < 0.001 and 0.0001, respectively) decrease compared to respective controls by Repeated Measures one-way ANOVA with a post-hoc Tukey's test.*

4.4 Discussion

The results of this Chapter support the hypothesis that HOSCN targets glycolytic enzymes, causing an attenuation of glycolysis in J774A.1 cells. The Seahorse assay confirmed that the oxidative ability of HOSCN causes a decrease in the glycolytic capabilities of the macrophages. The results also indicate that the production of the glycolytic end-product, lactate, is reduced in HOSCN-treated cells. This was not observed in cells treated with HOCl, consistent with HOCl having less effect on glycolysis under the treatment conditions in this study. The results are consistent with the inhibitory effects of HOSCN on glycolysis being due to the targeting and inhibition of cytosolic glycolysis proteins, rather than the inactivation of glucose transport proteins or cell lysis.

Aldolase, TPI together with GAPDH have been shown to be targeted by HOSCN in proteomic experiments *(Tessa Barrett, PhD Thesis, 2012)*. These data are supported by the Western blots in this Chapter showing the co-migration of proteins labelled with the sulfenic acid probe, DCP-Bio1, with these glycolytic proteins following exposure of the cells to HOSCN. Aldolase converts fructose 1,6-bisphosphate into the triose phosphates, dihydroxyacetone phosphate and glyceraldehyde 3-phosphate, and has been shown previously to be partially inhibited in *Streptococci cremoris 972* exposed to the LPO/H_2O_2/SCN^- system for 30 min [199]. GAPDH catalyses the conversion of glyceraldehyde 3-phosphate to D-glycerate 1,3-bisphosphate, and has been shown to be inhibited by HOSCN in both bacterial and mammalian cells [84, 92, 201]. These glycolytic enzymes span the end of the preparatory phase and the beginning of the pay-off phase of glycolysis (Scheme 4.1). Modification of these enzymes by HOSCN is likely to have impact on the extent of glycolysis and ATP levels in the cells, because of the locations of these proteins (aldolase, TPI and GAPDH) in the pathway, the cells will have consumed 2 ATP molecules in the preparatory phase to create fructose 1,6-bisphosphate. From this point, no further glycolysis is occurring in cells treated with HOSCN, as the enzymes required to form D-glycerate 1,3-bisphosphate are inhibited, which also means a loss in the net formation of 2 ATP molecules for the cell.

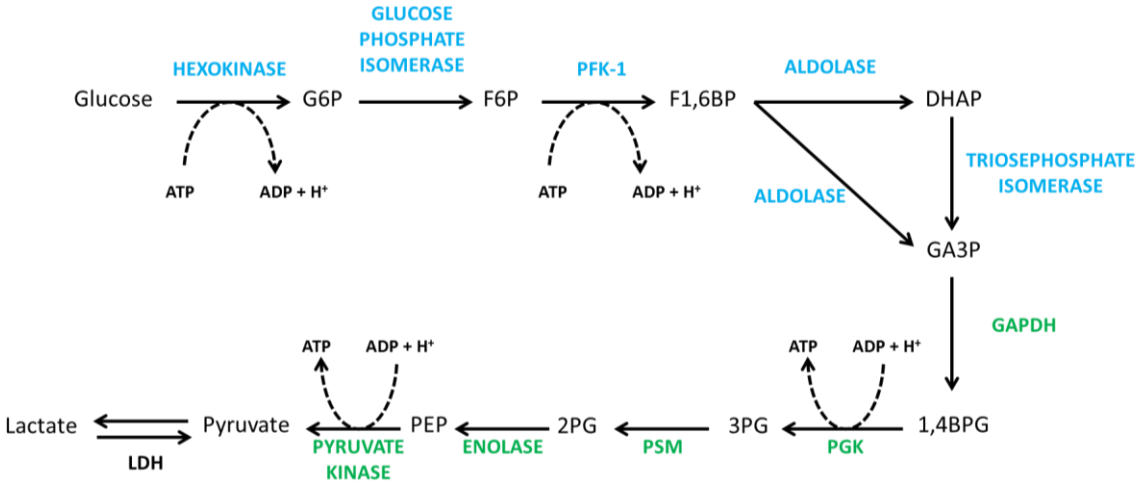

Scheme 4.1: The glycolytic pathway.

Glycolysis is a highly conserved pathway involved in the production of ATP from glucose. The pathway consists of 10 steps and can be divided into 2 parts. The preparatory phase (blue); involves the use of 2 ATP molecules to break glucose down into glyceraldehyde 3-phosphate and the pay-off phase (green); where 4 ATP molecules are produced to net a total of 2 ATP molecules per molecule of glucose. Pyruvate, the glycolytic end-product can be converted to lactate by LDH and vice versa. G6P, glucose-6-phosphate; F6P, fructose-6-phosphate, PFK-1, phosphofructokinase-1; F1,6BP, fructose 1,6-bisphosphate; DHAP, dihydroxyacetone phosphate; GA3P, glyceraldehyde 3-phosphate; GAPDH, glyceraldehyde 3-phosphate dehydrogenase; 1,3BPG, 1,3-bisphosphoglycerate; PGK, phosphoglycerate kinase; 3PG, 3-phosphoglycerate; PSM, phosphoglycerate mutase; 2PG, 2-phosphoglycerate; PEP, phosphoenolpyruvate; LDH, lactate dehydrogenase.

The ability of HOSCN to affect glycolysis in J774A.1 macrophages was examined using the Seahorse Extracellular Flux analyser. The analyser allows for the detection of changes in the pH of the extracellular milieu of cells. As cells undergo glycolysis, the surrounding media becomes increasingly acidic, which allows for the determination of glycolytic flux. Results indicated that HOSCN has a profound effect on the ability of J774A.1 cells to perform glycolysis, with low concentrations of the oxidant (25 µM) leading to a significant attenuation of glycolytic activity. These results were confirmed by determining the concentration of lactate released into the media by cells treated with HOSCN. It was shown that HOSCN inhibits the formation of lactate, a glycolytic end-product, in J774A.1 cells. The lactate assay also allowed for the determination of the effect of HOCl on glycolysis in J774A.1 cells, as the

experiment could be performed in a balanced salt solution rather than the basal DMEM required for use in the Seahorse assay, which immediately quenched the HOCl. In contrast to HOSCN, HOCl did not inhibit the formation of lactate in J774A.1 cells, indicating that HOCl does not attenuate glycolysis.

Glucose transport in cells exposed to HOSCN was also interrogated, given the effects of this oxidant on glycolysis, and that previous data have shown that HOSCN can inhibit glucose uptake in *Streptococcus agalactiae* [385]. Results of the studies in this Chapter indicate that HOSCN does not influence that ability of the cells to uptake glucose. This suggests that HOSCN is unable to oxidise glucose uptake proteins on the cellular membrane of J774A.1 macrophages, in contrast to previous studies where HOSCN inhibits glucose uptake in bacterial cells [379]. Similarly, no evidence for significant cell death was obtained under conditions where perturbations in glycolysis and lactate release are observed.

Lloyd et al. published results indicating that HOSCN induced significant cell lysis in J774A.1 cells [91], under comparable oxidant doses, but over a longer incubation time (3 h), using a different lysis assay, measuring DNA release. DNA release requires the lysis of both the cellular membrane and the nuclear envelope [387], while the LDH assay only requires the lysis of the cellular membrane [388, 389]. The LDH activity assay was not performed by *Lloyd et al*. owing to the ability of HOCl to inhibit LDH activity, causing an underestimation of damage caused by the oxidant to the cells [91, 183]. In this Thesis, the mode of death was not studied, but Lloyd et al. showed that in J774A.1 cells, with comparable HOSCN concentrations at 1-2 h that cell death occurs by apoptosis [91]. The results of this Chapter indicate that a possible trigger for this apoptosis is the perturbation of glycolysis in J774A.1 cells.

The results imply that HOSCN alters glycolysis by directly interacting with cellular enzymes. The formation of sulfenic acids may play a role given the overlay of the DCP-Bio1 Western blots with aldolase, TPI and GAPDH. The activities of thiol-dependent enzymes have been known to be critical to glycolysis for many years now [198, 390]. Data show the inhibition of GAPDH and aldolase in *Clostridium perfringens* correlates with a loss in reduced thiols and a loss in the growth of *C. perfringens*, with the inhibition postulated to be caused by an interaction of the treatment with reactive sulfhydryl groups, which could include sulfenic acids [391]. The inhibition of growth and metabolism may be a result of HOSCN-induced thiol oxidation in bacteria, though in many cases no significant loss in bacterial viability is noted.

Moreover, in some cases, HOSCN-induced damage in regard to glycolysis is reversible once the oxidant is removed from *Streptococci* [199, 392].

Glucose uptake in J774A.1 macrophages was not affected by HOSCN-induced oxidation, in contrast to data showing that HOSCN can attenuate the ability of bacterial cells to transport glucose into the cytosol, for it to be catabolised [200, 379, 385]. In bacteria there are numerous systems involved in glucose uptake, a well characterised system is the phosphoenolpyruvate (PEP) group translocation, also known as the phosphotransferase system (PTS), first described in 1966 [393]. The PTS is responsible for transporting many carbohydrates into bacteria such as mannose, fructose and glucose, after phosphorylating the carbohydrates at the expense of phosphoenolpyruvate (PEP). The PTS is a group of phosphoproteins, mainly enzyme I and Histidine protein (HPr); the proteins which transfer the phospho-group from PEP to the sugar, which contains an essential cysteine residue that acts as a proton donor during catalysis [394]. The second group of the PTS is enzyme II; the enzyme responsible for glucose transport across the cell membrane, which requires the transfer of a phosphoryl group to a cysteine residue contained within the protein [395, 396]. Mammalian cells employ a different system, using Na^+ - dependent co-transporters and simple facilitative uniporters; GLUT proteins. These proteins are not required to modify the carbohydrate to move it across the cell membrane, and only need to move the substrate down the concentration gradient, as the concentration within the cell is modified by modifying the concentration of glucose in the cells environment e.g. the bloodstream or extracellular fluids [397, 398].

The functional differences between bacterial and mammalian glucose transporters may help to explain that HOSCN has a differential effect on glucose transport in bacterial cells compared to macrophages. The PTS system requires cysteines, the major target of HOSCN, which are important in the transfer of phosphoryl-groups from PEP to the carbohydrate via the action of enzyme I and HPr [395, 396]. The PTS is also responsible for the transfer of the phosphorylated sugars through the cell membrane, which requires a subsequent transfer of a phosphoryl group to the cysteine residue of enzyme II [395, 396]. Mammalian cells are less reliant on cysteines and only require the facilitative movement of glucose down the concentration gradient, making them less susceptible to HOSCN induced damage and inhibition.

The HOSCN-induced inhibition of glycolysis has numerous implications for the J774A.1 cells, which bear some similarities to the behaviour of HOSCN-treated bacterial cells. While not

necessarily causing cell death, HOSCN-induced oxidation of glycolytic proteins is likely to result in an inhibition in growth and proliferation, as these pathways require ATP, the energetic end-product of glycolysis. Interestingly, because of the location of aldolase, TPI and GAPDH within the glycolytic pathway, inhibition of these enzymes would cause a significant loss in ATP formation. Studies investigating male rat fertility have shown that the inhibition of GAPDH and TPI has a dramatic effect on the formation of ATP within sperm cells without causing cell death [399]. The rationale for this is that these enzymes appear in the glycolytic pathways at the end of the preparatory phase, when the cell has expended 2 molecules of ATP per glucose molecule, but before the pay-off phase where there is a net gain of 2 ATP molecules per glucose molecule [158, 400], and without the formation of ATP, cells reduce their use of ATP by only performing processes vital for survival.

Lactate is also important in terms of glycolysis and cell survival, as lactate is formed by LDH in a reversible reaction from pyruvate [401]. The inhibition of glycolysis by HOSCN will therefore reduce pyruvate production and cause a loss in energetic substrates for the electron transport chain (ETC). Another consequence of HOSCN-induced attenuation of lactate formation is the loss of NAD^+. When lactate is formed by LDH, NAD^+ is regenerated, which is used in concert with GAPDH to oxidise glyceraldehyde 3-phosphate to D-glycerate 1,3-bisphosphate. This loss in the glycolytic capacity is then fed back into the pathway, further reducing the ability of key glycolytic enzymes to form the energetic substrates needed for proper cellular function [402].

4.5 Summary

The studies in this Chapter demonstrated that the addition of exogenously-added HOSCN has the ability to inhibit glycolysis in real-time in J774A.1 macrophages at physiologically relevant concentrations (≥ 25 μM). This is especially relevant to cigarette smokers, as the parent ion of HOSCN (SCN^-) is found in plasma at concentrations up to and exceeding exceed 300 μM [80, 82, 83]. Data are consistent with the formation of sulfenic acids on the glycolytic proteins GAPDH, TPI and aldolase in cells exposed to HOSCN, rather than the oxidation and inhibition of glucose uptake proteins on the cellular membrane or significant cell lysis. Lactate release from the J774A.1 cells was also inhibited in cells treated with HOSCN, validating the results of the real-time glycolytic assay showing that HOSCN inhibits glycolysis and the formation of glycolytic end-products, while HOCl was unable to inhibit lactate release. Further studies were performed to examine whether the inhibitory effects of HOSCN on glycolysis and the decreased production of energetic substrates affects oxidative phosphorylation and the integrity of mitochondria of J774A.1 cells.

5 Hypothiocyanous Acid Induces Mitochondrial Dysfunction in J774A.1 macrophages

5.1 Introduction

In a biological setting, the hypohalous acids play a role in innate immune defence. While HOCl is primarily responsible for bacterial cell killing, HOSCN has a bacteriostatic effect. HOSCN reversibly oxidises bacterial protein thiols, with a major target of this reversible oxidation being bacterial glycolytic proteins [56, 197, 199, 379]. The results of the previous Chapter showed that HOSCN can also attenuate glycolysis in mammalian J774A.1 macrophages.

HOSCN affects glycolysis by oxidising critical enzymes along the glycolytic pathway, leading to a decrease in the availability of pyruvate, the glycolytic end-product. Pyruvate is then dehydrogenated by pyruvate dehydrogenase to form acetyl-CoA, which is shuttled toward the mitochondria to participate in the citric acid cycle (or tricarboxylic acid cycle; TCA cycle) [403]. This cycle is important in aerobic metabolism as the product is NADH, a critical co-factor, is fed into the electron transport chain and is required for oxidative phosphorylation, mitochondrial respiration and ATP production [404, 405]. For this reason, cellular NADH concentrations have been used as a marker of mitochondrial and cellular bioenergetic health [406]. Changes in the formation of glycolytic end-products not only have various effects on the energetic status of the cell but can also affect cellular growth [407], much in the same way HOSCN affects bacterial cell growth. Additionally, HOCl has also been shown to perturb mitochondrial function [187], though the results of the previous Chapter indicate that HOSCN may be more potent given its effects on glycolysis.

Mitochondrial electron transport chain enzymes contain critical thiols and iron-sulfur clusters, which play an important role in the regulation and activity of the TCA cycle and mitochondrial oxidative phosphorylation [408, 409]. Proteins such as aconitase 2, complex I, complex II, complex III and complex V all contain viable targets for HOSCN oxidation [207-213], and the oxidation of these proteins is predicted to lead to a decrease in the efficiency of the electron transport chain (ETC). Another protein that is critical for the function of the ETC, but is not directly involved in the shuttling of electrons across the pathway is VDAC-1, which also contains thiol residues and is located on the outer mitochondrial membrane [214, 215].

Interestingly, the inhibition of mitochondrial respiration has numerous consequences for the mitochondria. As ATP production is reduced, either via a reduction in the formation of glycolytic end-products or by the oxidation of ETC proteins, the mitochondrial permeability

transition pores (MPTP) are formed. The induction of MPTP increases the permeability of mitochondria, causing a depolarization of the mitochondria, which allows for the movement of small molecules across the mitochondrial membrane, including protons [410, 411]. The free movement of protons across the mitochondrial membrane means a loss in the electrochemical gradient that is needed to produce the proton-motive force required for the production of ATP and the viability of the cell [412, 413]. The induction of the MPTP also causes the leakages of pro-apoptotic factors, such and cytochrome *c* into the cytosol, triggering cell death by apoptosis [414].

5.2 Aim

The aim of this Chapter is to determine if HOSCN is able to inhibit J774A.1 macrophage-mitochondrial respiration and induce mitochondrial dysfunction. HOSCN-induced changes to the mitochondria and electron transport chain will be probed by using real-time mitochondrial respiration assays, probing the mitochondria for changes in the membrane potential and ATP, the end-product of the bioenergetic pathway, will be quantified.

5.3 Results

5.3.1 The effect of HOSCN on J774A.1 mitochondrial respiration

To determine the effect of HOSCN on mitochondrial respiration and oxidative phosphorylation in J774A.1 cells, the Seahorse XF bioanalyser was used. In these experiments the analyser was used to measure the oxygen consumption rate (OCR) of the cells. OCR is a measure of mitochondrial respiration, as cells respire, the concentration of dissolved O_2 in the extracellular milieu changes directly above the cells. By using solid state sensor probes, the change (flux) in O_2 concentrations can be determined, which is directly correlated to the activity of the electron transport chain of mitochondria. The result is a real-time graph displaying changes to the respiratory profile of the cell.

To obtain the respiratory profile, the cells are allowed to metabolise glucose (10 mM), which in turn allows for the baseline respiration to be determined. Then oligomycin is injected into the cell media, inhibiting ATP synthase and attenuating oxidative phosphorylation so the ATP coupler response (proton leak) can be observed. Next FCCP, an ionophore which shuttles protons through the mitochondrial membrane, is injected, disrupting the proton gradient, causes the mitochondria to increase their O_2 consumption, with no ATP formation, so the ETC accelerator response can be observed. Finally, a mixture of rotenone and antimycin A are injected, causing a complete shutdown of the mitochondrial ETC, so non-mitochondrial O_2 consumption can be determined. This result is then deducted from all previous observations.

After the experiment, two more mitochondrial states can then be determined. The first is the spare respiratory capacity, which describes the stress of the mitochondria, is calculated as the ratio between the ETC accelerator response and the baseline respiration. Finally, the coupling efficiency, the ratio between the baseline respiration and the ATP coupling response, is a measurement of the efficiency of ATP formation.

Before performing the glycolytic stress tests, the optimal cell number and oligomycin concentration was optimised (Section 4.3.2.1 and 4.3.2.2). Here the concentrations of FCCP, antimycin A and rotenone were optimised, after doing this the baseline OCR and mitochondrial stress test experiments were performed to determine if HOSCN and its role in inhibiting glycolysis also attenuates mitochondrial respiration and energy production.

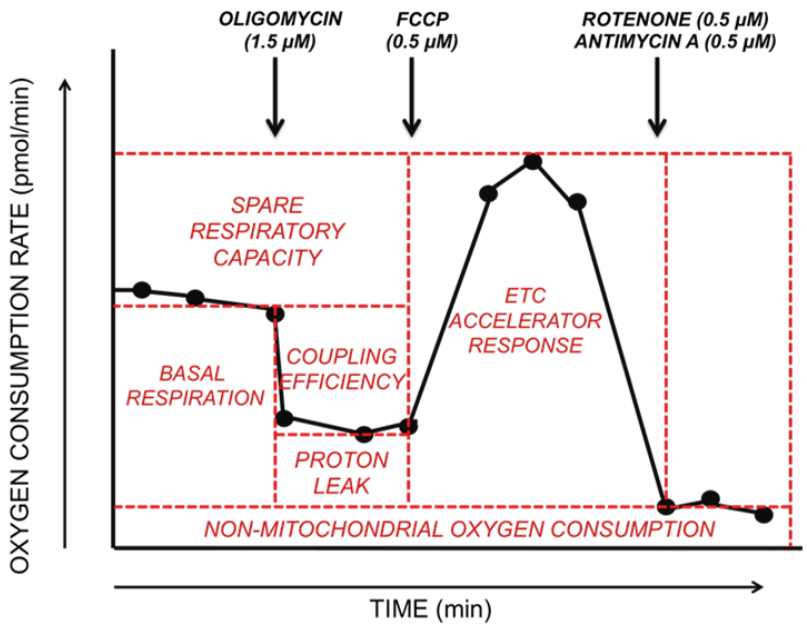

Figure 5.1: The mitochondrial respiratory profile.

The mitochondrial stress test consists of distinct 4 parts. Firstly, baseline respiration is taken while the cells are in 10 mM glucose media, analogous to the baseline glycolysis reading. The 1.5 µM oligomycin is injected and the ATP coupler response is recorded, determining the amount of proton leak. Then 0.5 µM FCCP is injected to determine the ETC accelerator response, the maximum O_2 consumption ability of the cell. Then 1.5 µM rotenone and antimycin A are injected, giving non-mitochondrial O_2 consumption. This allows for the determination of the spare respiratory capacity ratio; a measure of mitochondrial stress and coupling efficiency; a measure of how efficiently ATP is produced.

5.3.1.1 FCCP concentration optimisation

Before performing the mitochondrial stress test, the concentrations of the various inhibitors were determined. To determine which concentration would be used, the greatest response with the lowest amount of inhibitor was chosen, as high concentrations can be toxic or in the case of FCCP, can totally collapse the mitochondrial membrane potential. FCCP is an ionophore, and is used as an uncoupling agent in experiments analysing mitochondrial respiration. It disrupts ATP synthesis by transporting H^+ across the mitochondrial membrane, reducing the proton gradient before the protons can be used to provide energy for oxidative

phosphorylation, resulting in an increase in O_2 consumption to correct for the decrease in ATP formation.

The cells were plated into the XF24 cell culture plate (7.5×10^4 cells/well, based on the optimal number of cells to form a viable monolayer) (Section 4.3.2.1) and left to adhere to the plate for 20 min before being placed into the analyser where FCCP was injected from the probe cartridge after the cells were allowed to have their baseline OCR recorded for 3 cycles. The results indicate that 0.5 µM FCCP elicited the best response, increasing the OCR of the cells with the greatest efficiency (Figure 5.2). The lower concentration (0.1 µM) did not elicit a response, while 0.75, 1.0 and 1.5 µM did not perform as well as 0.5 µM FCCP, with lower overall OCR readings. The highest treatment of FCCP (3.0 µM) caused a decrease in OCR from baseline, indicating that the mitochondria had become completely uncoupled.

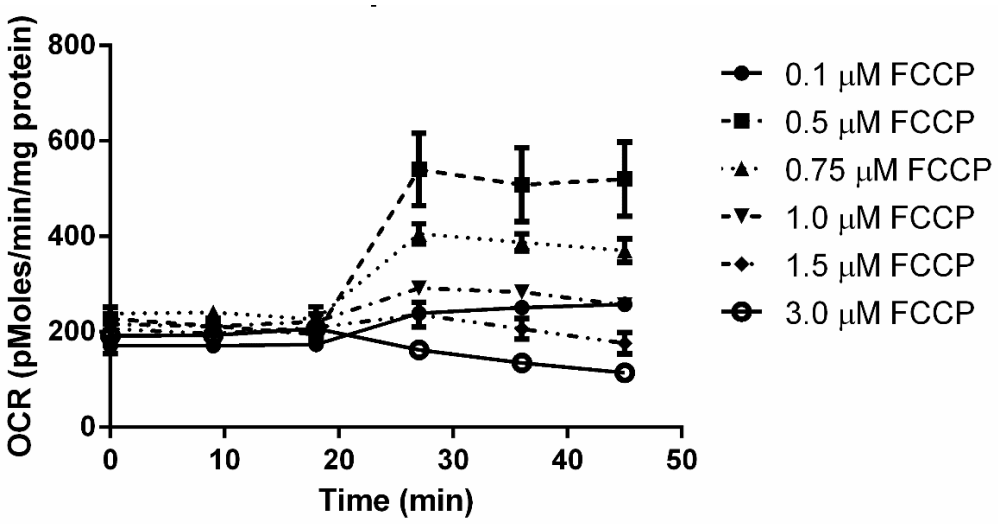

Figure 5.2: FCCP concentration optimisation using J774A.1 cells.

J774A.1 cells (7.5×10^4 cells) were seeded into an XF24 cell culture plate in XF basal DMEM (10 mM glucose) and placed into the Seahorse XF bioanalyser where increasing concentrations 0.1 (●), 0.5 (■), 0.75 (▲), 1.0 (▼), 1.5 (◆) and 3.0 (○) µM of the mitochondrial uncoupler, FCCP, were injected and the response was recorded. The results are the average of 1 experiment run with triplicate treatments ± S.E.M.

5.3.1.2 Antimycin A and rotenone concentration optimisation

It was also necessary to optimise the concentrations of rotenone, which inhibits complex I by inhibiting the transfer of its electrons to ubiquinone, and antimycin A, a complex III inhibitor which binds to the Qi site, attenuating the reduction of ubiquinone [415]. The inhibition of complex I and III in the last step of the experiment, results in the shutdown of the mitochondria, resulting in no mitochondrial consumption of O_2. This enables determination of background O_2-consuming processes in the cell.

The results of the mitochondrial inhibitor optimisation indicated that 0.5 µM antimycin A (Figure 5.3A) and 0.5 µM rotenone (Figure 5.3B) were the optimal concentrations to elicit a shutdown of the ETC in J774A.1 cells. When J774A.1 (7.5×10^4 cells) cells were treated with < 0.5 µM antimycin A, no decrease in the OCR was observed. The higher concentrations (1.0, 1.5 & 3.0 µM) caused a substantial decrease, with OCR that was close to 0 pM/min, consistent with the shutdown of mitochondrial utilisation of O_2 and other O_2 consuming processes.

The concentration that met the criteria needed for the experiments was 0.5 µM antimycin A, as its ability to cause mitochondrial shutdown was the same as the 0.75 µM treatment, while background oxygen consumption was still observed, indicating that the cells were still functional. A similar trend was observed after treating with the complex I inhibitor, rotenone. Treatment with 0.1 µM rotenone led to a decrease in OCR, but a greater extent of inhibition of respiration was seen with 0.5, 0.75 and 1.0 µM rotenone, with the ETC being almost completely inhibited while maintaining background oxygen consuming processes. Treatments with 1.5 and 3.0 µM rotenone led to an OCR close to 0 pM/min, indicating no oxygen consuming processes were taking place within the cell and that these concentrations may cause a loss in viability. Thus, a rotenone concentration of 0.5 µM was used in the mitochondrial stress test.

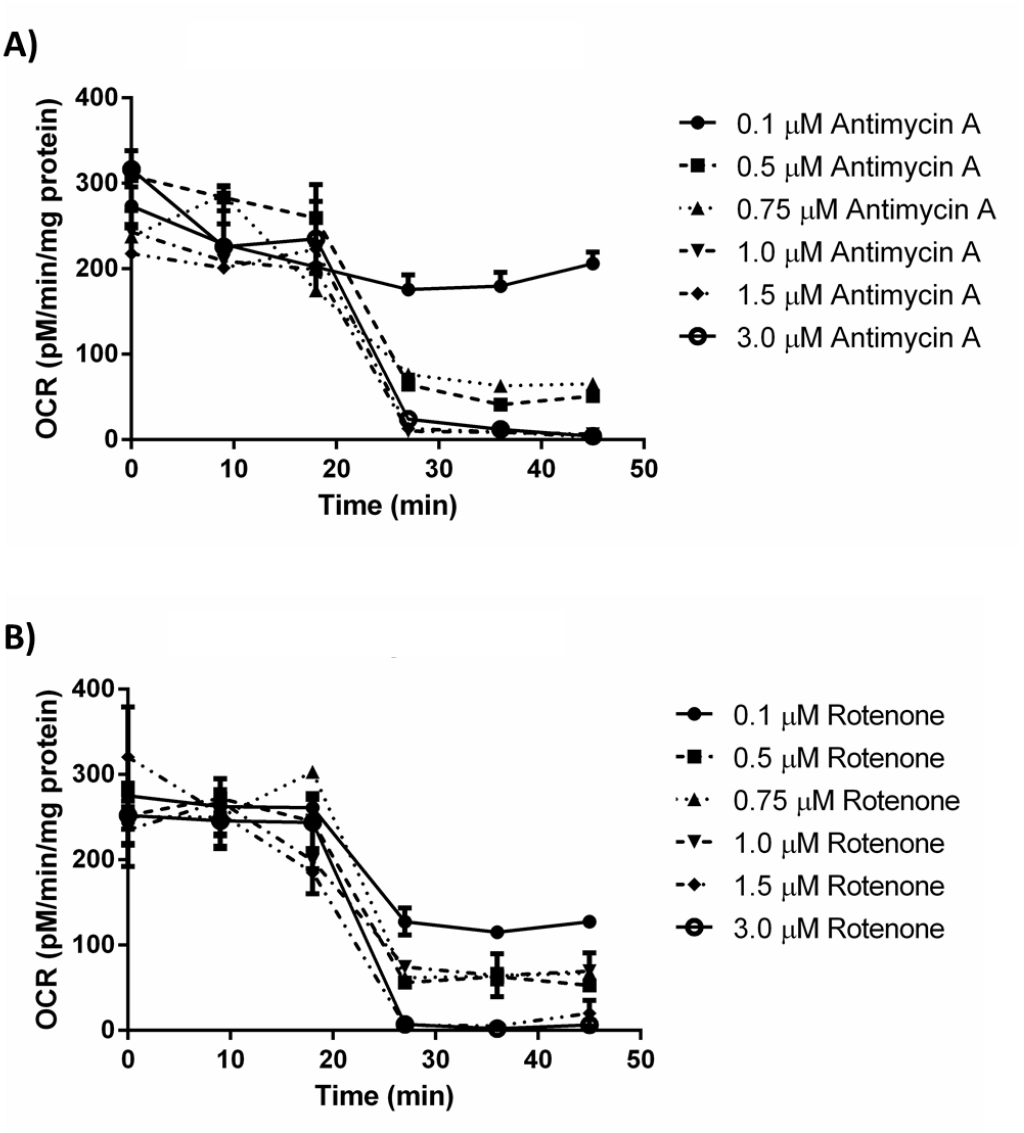

Figure 5.3: Optimisation of the mitochondrial inhibitors Antimycin A and Rotenone on J774A.1 cells.

J774A.1 cells (7.5 × 10^4 cells) were seeded into an XF24 cell culture plate in XF basal DMEM (10 mM glucose) and placed into the Seahorse XF bioanalyser where increasing concentrations 0.1 (●), 0.5 (■), 0.75 (▲), 1.0 (▼), 1.5 (◆) and 3.0 (○) μM of (A) *Antimycin A, a complex III inhibitor and* (B) *Rotenone, a complex I inhibitor were injected and the response was recorded. The results are the average of 1 experiment run with triplicate treatments ± S.E.M.*

5.3.2 HOSCN inhibits mitochondrial respiration in J774A.1 macrophages

The J774A.1 cells were plated (7.5×10^4 cells/well) in the XF24 cell culture plate and then treated with HOSCN (0 – 150 µM) in the XF basal DMEM. The Seahorse XF DMEM was used as it does not have a buffering capacity, unlike HBSS or PBS. Media with a buffering capacity does not allow for the determination of pH and O_2 flux of the media, which is required to determine the bioenergetic status of the cells. After the addition of HOSCN, the cells were transferred immediately into the analyser and their OCR was recorded for 1 h, not including a 15 min period at the beginning, where the cells and media were allowed to equilibrate. The results of baseline OCR readings in J774A.1 cells showed that HOSCN causes a decrease in cellular OCR, with concentrations of ≥ 100 µM HOSCN inducing a significant decrease in baseline OCR over the hour (Figure 5.4.).

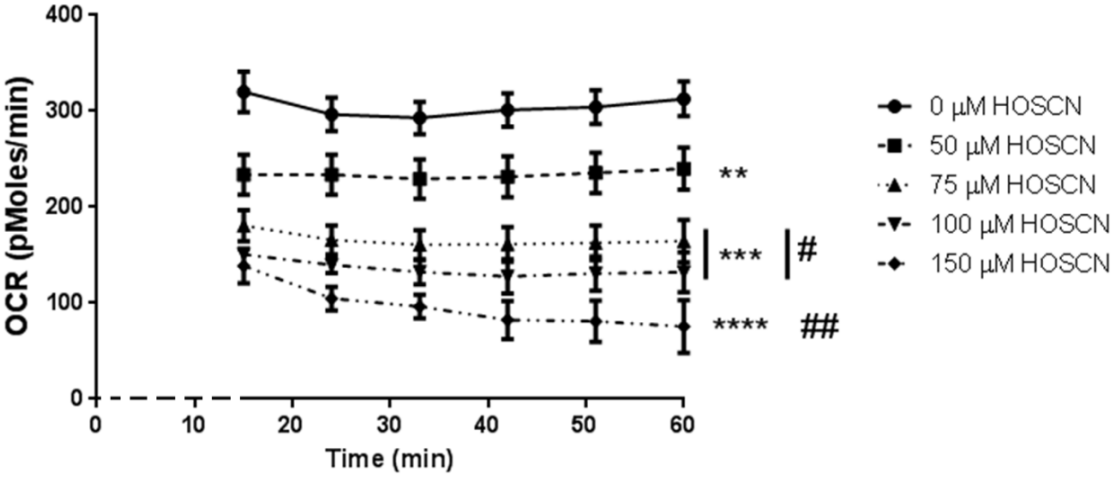

Figure 5.4: J774A.1 cells treated with HOSCN exhibit changes to baseline respiration.

*Treatment of J774A.1 cells (7.5×10^4 cells) with 0 (●), 50 (■), 75 (▲), 100 (▼) or 150 (◆) µM HOSCN in XF basal DMEM for 1 h at 37 ℃ led to the attenuation of baseline mitochondrial respiration. Cells were treated with HOSCN and were immediately placed into the Seahorse analyser for the duration of the treatment. The beginning of OCR recording occurs after a 15-minute equilibration phase. Results **s**how that under basal conditions, respiration is clearly attenuated at even low levels of HOSCN exposure when compared against baseline wells. Results are the average of 3 independent experiments ± S.E.M. **, *** and **** show a significant ($p < 0.01$, 0.001 and 0.0001, respectively) decrease compared to respective controls and #, ## show a significant ($p < 0.05$, 0.01, respectively) decrease over time by Repeated Measures two-way ANOVA with a post-hoc Tukey's test.*

The J774A.1 cells were plated in the wells of the XF24 cell culture plate (7.5×10^4 cells/well) and after leaving the cells to attach for 20 min at 37 ˚C and 5 % CO_2, they were treated with HOSCN (0 – 150 µM) for 1 h at 22 ˚C. The cells were then placed into the analyser where the media and cells were further equilibrated for 15 min at 37 ˚C. After equilibration, the mitochondrial stress test was performed (Figure 5.5). First, baseline OCR was recorded, which resulted in a similar inhibition of basal respiration compared to that seen in Figure 5.4 (Figure 5.6A), which supports HOSCN playing a role in inhibiting basal respiration. After the addition of oligomycin, which blocks the F_0 portion of ATP synthase and inhibits state 3 phosphorylating respiration, a decrease is observed in the ATP coupler response following HOSCN treatment (Figure 5.6B). After the FCCP injection, to stimulate maximum respiration and O_2 consumption, the ETC accelerator response is recorded. The result shows that HOSCN has a profound effect on the cells ability to funnel O_2 into the ETC, significantly inhibiting the ability of J774A.1 cells to increase oxygen consumption at every treatment concentration (Figure 5.6C).

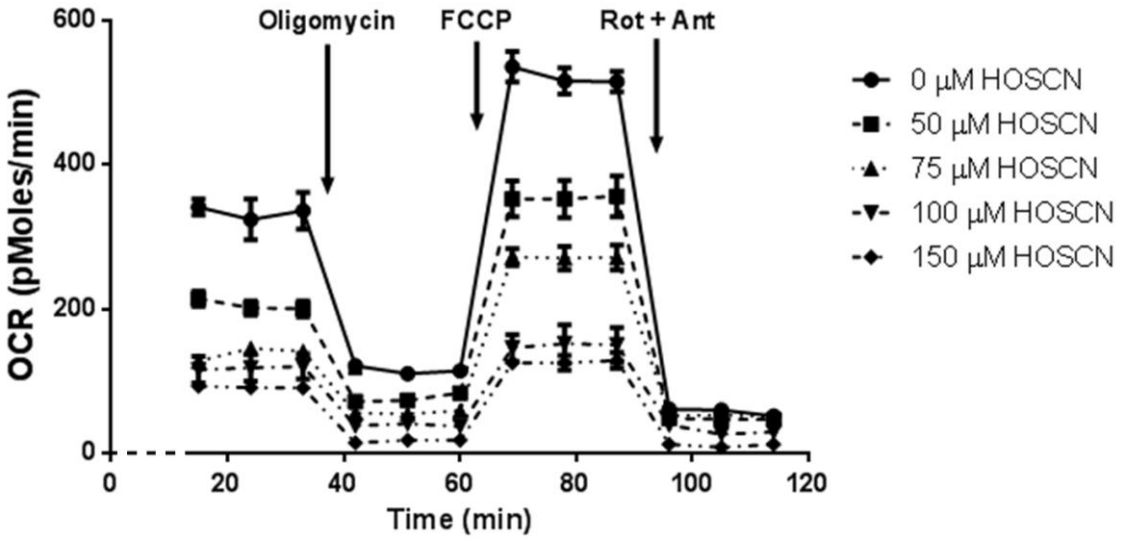

Figure 5.5: HOSCN causes the attenuation of the respiratory profile in J774A.1 cells.

J774A.1 cells (7.5×10^4 cells) were treated with 0 (●), 50 (■), 75 (▲), 100 (▼), 150 (◆) µM HOSCN in XF basal DMEM for 1 h at 22 ˚C before being placed into the analyser to be equilibrated for 15 min, then the stress test was performed. Baseline respiration, ATP coupler response, ETC accelerator response, coupling efficiency and spare respiratory capacity were recorded. The results show J774A.1 cells were markedly affected by HOSCN treatment at many stages of respiration. These results are the average of 3 independent experiments ± S.E.M.

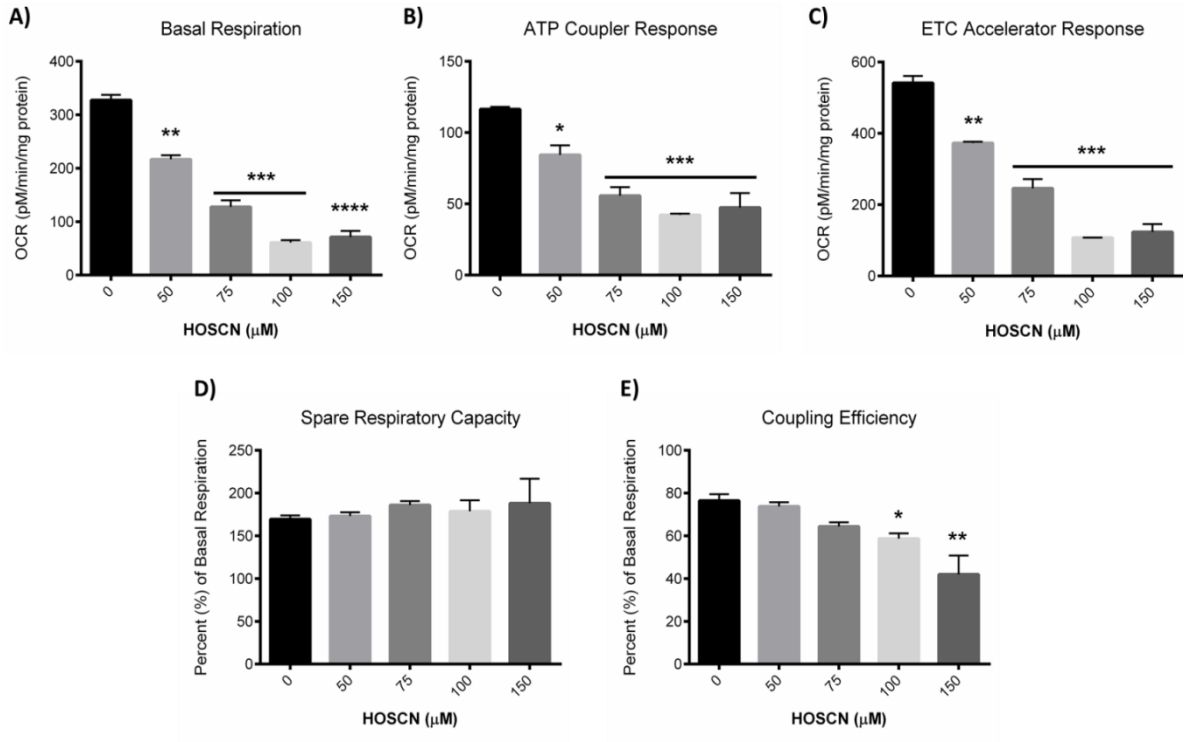

Figure 5.6: Changes in the respiratory profile of J774A.1 cells exposed to HOSCN.

*Analysis of the respiratory stress test performed on J774A.1 macrophages treated with HOSCN (0 – 150 μM). (A) Baseline respiration, which describes the effect of HOSCN on basal respiration. (B) ATP coupler response represents the minimum OCR reading in response to HOSCN and oligomycin. (C) The ETC accelerator response represents the highest possible OCR in response to HOSCN and FCCP. (D) The spare respiratory capacity provides details on the cells maximum ability to produce ATP while (E) coupling efficiency measures ATP turnover within the cell, describing the effect of HOSCN on baseline ATP production. Results are the average of 3 independent experiments ± S.E.M. *, **, *** and **** show a significant ($p < 0.05$, 0.01, 0.001 and 0.0001, respectively) decrease compared to respective controls by Repeated Measures one-way ANOVA with a post-hoc Tukey's test.*

When analysing the ratio of ETC accelerator response and basal respiration, spare respiratory capacity can be assessed, which is a measure of mitochondrial 'stress'. The results show that HOSCN does not influence spare respiratory capacity in J774A.1 cells (Figure 5.6D). No change was observed due to the ratiometric decrease in both the basal respiration and the ETC accelerator response. Thus, although HOSCN perturbs basal respiration and the ETC accelerator response, the changes remained equal between the two profiles, maintaining a ca. 150 % spare respiratory capacity.

Finally, when the ratio between the ATP coupler response and basal respiration is analysed, the coupling efficiency can be determined. Coupling efficiency describes how much of the total O_2 consumption is involved in the synthesis of ATP, while the rest is used to overcome the proton leak from the mitochondrial space. Results indicated that treating cells with HOSCN caused a loss in the efficiency at which ATP is formed (Figure 5.6E). At higher HOSCN concentrations (≥ 100 µM), a significant amount of O_2 is either lost or used to overcome the proton leak, leading to a loss in ATP production. This result indicates that HOSCN plays a direct role in altering the mitochondria, and is possibly acting on transition and pore proteins, causing a loss in mitochondrial membrane potential.

5.3.2.1 Cells treated with HOSCN are unable to maintain their ability to meet cellular energetic needs

After determining the changes to glycolysis (Chapter 4) and mitochondrial respiration after HOSCN treatment further analysis was performed to better understand the energetic state of the cells in response to HOSCN. To determine this, an OCR/ECAR ratio was calculated (Figure 5.7), which combined data from both the glycolytic stress test (Section 4.3.3) and the mitochondrial stress test (Figure 5.5), and allowed for the visualisation of both glycolysis and oxidative phosphorylation, and how these two processes interact.

The results of the OCR/ECAR analysis help to identify what is occurring within the J774A.1 cells after HOSCN treatment in regards to their bioenergetic status. Firstly, with increasing concentrations of HOSCN, the baseline OCR and ECAR is attenuated (Figure 5.7). Treatment of J774A.1 macrophages with HOSCN also inhibits their response to oligomycin treatment. This result is not surprising in regards to the OCR, as oligomycin inhibits ATP synthase. But in

response to oligomycin treatment, healthy cells are expected to increase their glycolytic activity to accommodate for the loss in ATP production by the mitochondria.

Thus, in the non-treated cells, the addition of oligomycin causes an increase in ECAR, with a decrease in OCR. However, with the addition of HOSCN, the oligomycin ECAR response falls below basal rate. Indicating that the cells treated with HOSCN are unable to increase the rate of glycolysis is response to ATP synthase inhibition by oligomycin. These results demonstrate that HOSCN is very efficient at inducing bioenergetic dysfunction in J774A.1 macrophages.

The results of the mitochondrial stress test indicate that HOSCN reduces the efficiency at which ATP is formed by the mitochondria. This reduced efficiency was hypothesised to be occurring as a response to proton leakage across the mitochondrial membrane. To test this hypothesis, mitochondrial membrane potential was studied using a fluorescent probe and flow cytometry, and assays to quantify cellular ATP levels were performed.

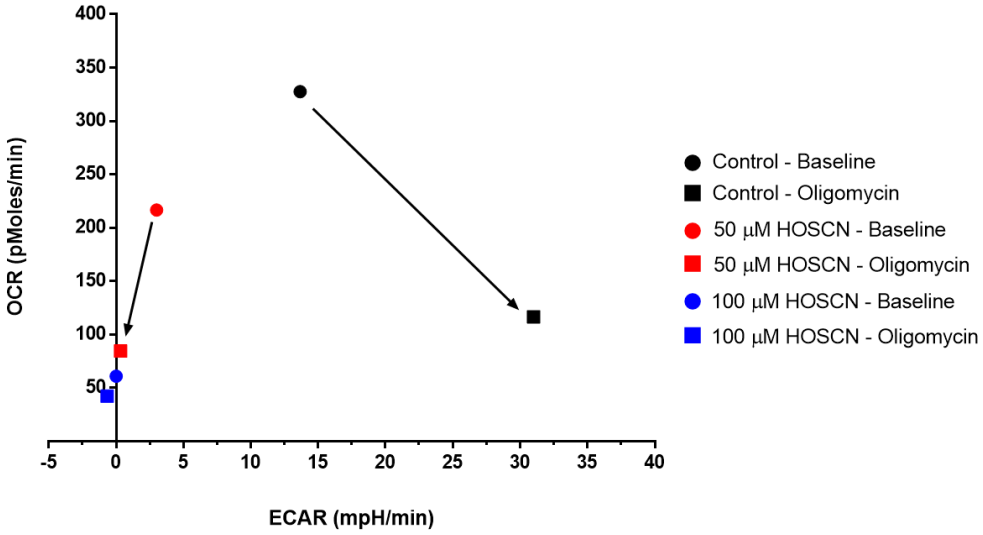

Figure 5.7: Cells treated with HOSCN are unable to maintain their ability to meet bioenergetic needs.

After performing both the glycolytic stress test and mitochondrial stress test, the condition of the J774A.1 cells was determined using an OCR/ECAR ratio. The OCR/ECAR ratios determined that in non-HOSCN treated cells (black), when oligomycin (black square) is added to basal state cells (black circle) and OCR is inhibited, ECAR can be increased to maintain the cells need for ATP. Treatment with 50 µM HOSCN (red) does not allow for increased glycolysis and ECAR to maintain energy production. 100 µM HOSCN (blue) affects glycolysis to a greater extent as it can no longer produce ATP.

5.3.3 HOSCN induces mitochondrial dysfunction by causing mitochondrial depolarisation

To determine if the reduction in ATP coupling efficiency is due to a proton leak caused by HOSCN, a flow cytometry method was employed to examine whether HOSCN caused a reduction in the mitochondrial membrane potential. If mitochondrial depolarisation was observed, it would be indicative that HOSCN causes, at least partially, a loss of ATP production by inducing a proton leak from the mitochondria.

To observe mitochondrial depolarisation, JC-1 was used. JC-1 is a cationic dye that accumulates within the mitochondria, where it forms J-aggregates, with broad excitation bands and an emission band at ca. 590 nm (red). As the mitochondria depolarise, the change in the membrane potential causes a 'leakage' of JC-1 into the cytosol, where the relative concentration is much lower, causing a dissociation of the J-aggregates and a shift in the emission spectra to ca. 530 nm (green). The formation of pores within the mitochondrial membrane, results in a decrease in the membrane potential to cause a leakage of JC-1 and a shift in the ratio of red:green fluorescence.

The cells were plated (1 x 10^6 cells/well) in a 12-well plate and exposed to HOSCN (0 – 200 µM) in HBSS for 1 h at 22 ˚C or CCCP, a positive control for mitochondrial depolarisation, for 10 min at 5 % CO_2 and 37 ˚C prior to the addition of JC-1. After incubation with JC-1, the cells were incubated for 15 min in an incubator of humidified 5 % CO_2 at 37 ˚C and then the red:green fluorescence ratio was determined using the flow cytometer. Results indicated that with increasing concentrations of HOSCN, an increase in green fluorescence occurred (Figure 5.8). This means that with increasing concentrations of HOSCN, the J-aggregates within the mitochondria (red) begin to dissociate due to the depolarisation of the mitochondria and leakage into the cytosol (green). The increase in green fluorescence indicates that HOSCN is responsible for the change in mitochondrial membrane potential, which causes small molecules within the mitochondria to leak into the cytosol. This depolarisation could also explain the loss in the efficiency at which ATP is formed in the mitochondria in response to HOSCN treatment. The results indicate that a significant decrease in the mitochondrial membrane potential also occurs with CCCP treatment, indicating the positive control induces mitochondrial depolarisation (Figure 5.9). HOSCN-induced a significant depolarisation of the mitochondria occurs at concentrations of HOSCN ≥ 75 µM (Figure 5.9). At lower oxidant concentrations, there is an observable, but non-significant decrease in the mitochondrial membrane potential. The results of this flow

cytometry experiment correlate well with the decrease in ATP production efficiency determined by the Seahorse XF mitochondrial stress test (Figure 5.6E).

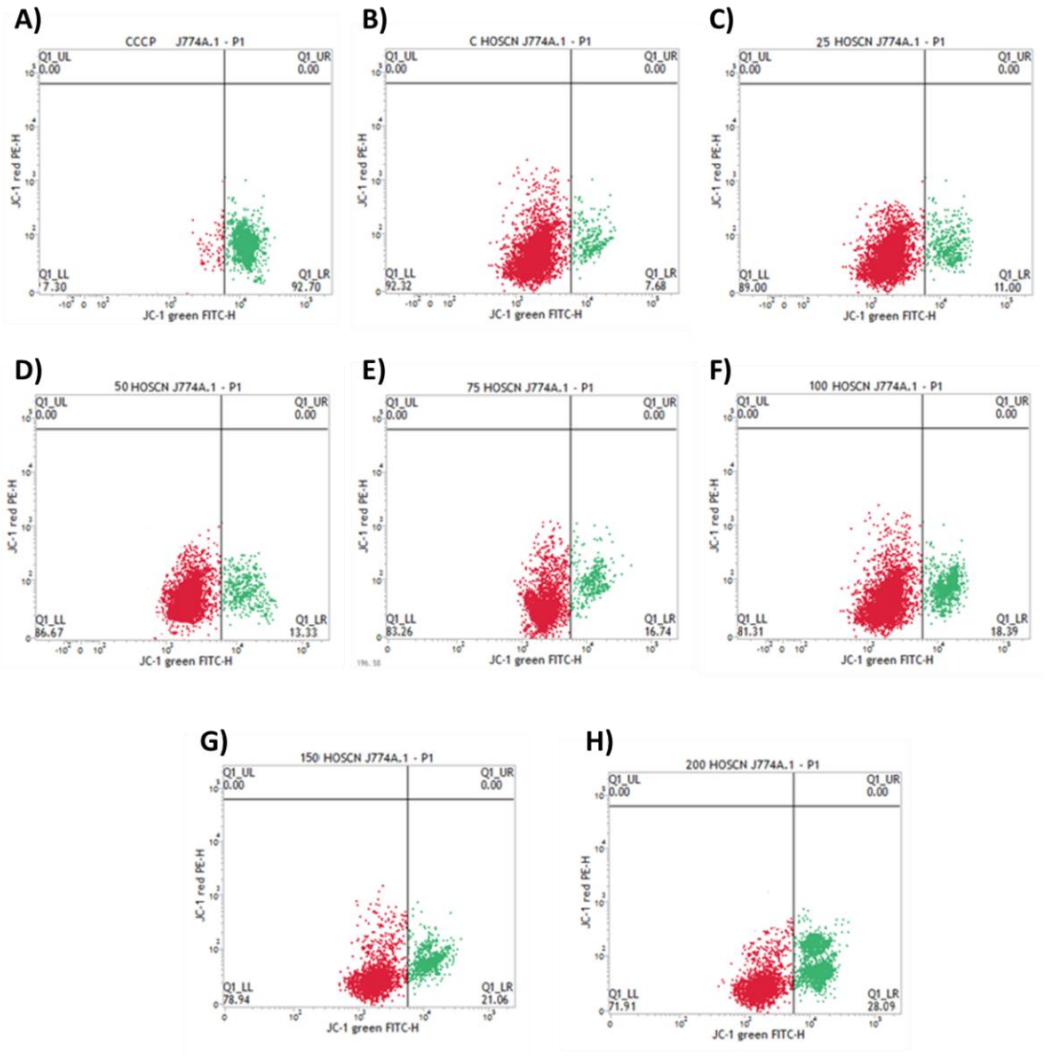

Figure 5.8: Mitochondrial depolarisation caused by HOSCN was probed using JC-1

J774A.1 cells (1 × 10^6 cells) were treated with (B) 0, (C) 25, (D) 50, (E) 75, (F) 100, (G) 150 or (H) 200 µM HOSCN for 1 h at 22 ˚C or (A) 5 µM CCCP for 10 min at 37 ˚C. The cells were then labelled with JC-1 (2 µM) and left to incubate for 15 min at 37 ˚C. The formation of J-aggregates in the mitochondria (red; λ_{em} = 590 nm) and the leak of these aggregates into the cytosol (green; λ_{em} = 529 nm) was analysed using flow cytometry. Results indicate that increasing concentrations of HOSCN decrease the mitochondrial membrane potential, with the increase in mitochondrial depolarisation causing the increased loss of J-aggregates from the mitochondria to the cytosol. The results pictured are a representation of data from 3 separate experiments.

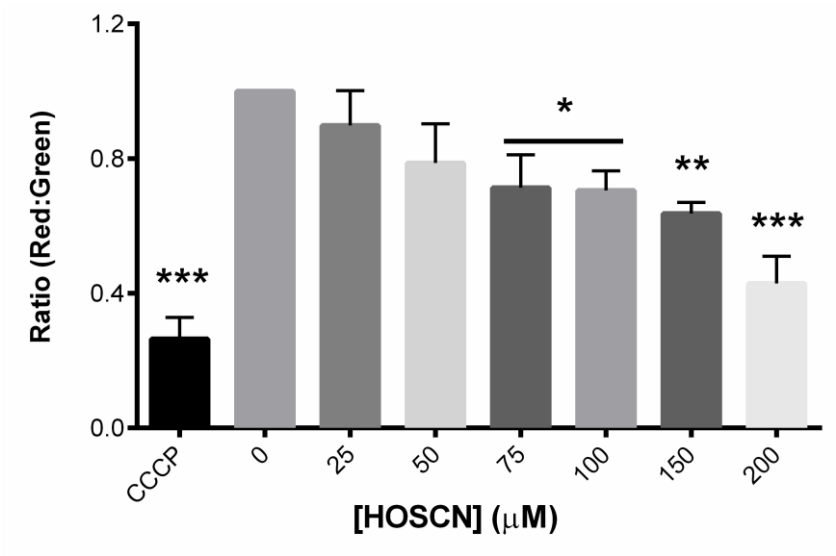

Figure 5.9: HOSCN causes mitochondrial depolarisation in J774A.1 cells.

*J774A.1 cells (1 × 10^6 cells) were treated with HOSCN (0 – 200 µM) for 1 h at 22 ˚C or 5 µM CCCP for 10 min at 37 ˚C. The cells were then labelled with JC-1 (2 µM) and left to incubate for 15 min at 37 ˚C. The formation of J-aggregates in the mitochondria (red; λ_{em} = 590 nm) and the leak of these aggregates into the cytosol (green; λ_{em} = 529 nm) was analysed using flow cytometry. Results are expressed as a ratio of red:green and indicate that HOSCN causes a decrease in the mitochondrial membrane potential, causing contents of the mitochondrial matrix to leak into the cytosol. Values of the results are the mean ± S.E.M (n = 3). *, ** and *** show a significant (p < 0.05, 0.01 and 0.001, respectively) decrease compared to the untreated control by Repeated Measures one-way ANOVA with a post-hoc Tukey's test.*

After determining that HOSCN is able to cause a loss in the mitochondrial membrane potential, an experiment was performed to determine if the changes occur through the mitochondrial permeability transition pore (MPTP), by assessing whether the damage caused by HOSCN could be attenuated by inhibiting the action of the MPTP.

5.3.3.1 HOSCN induced mitochondrial depolarisation can be reversed

To determine if the MPTP was involved in the HOSCN-induced attenuation of ATP synthesis, cyclosporin A (CsA) was used to inhibit the opening of MPTP and prevent depolarisation. The cells were plated (1 x 10^6 cells/well) in a 12-well plate and exposed to 1 µM CsA for 1 h at 5 % CO_2 and 37 ˚C. After treatment with CsA, the cells were washed three times with HBSS before being treated with HOSCN (0 – 200 µM) for 1 h at 22 ˚C or CCCP for 10 min at 5 % CO_2 and 37 ˚C prior to the addition of JC-1. The results show that pre-treating cells with CsA (1 µM) before HOSCN treatment prevented the loss of mitochondrial membrane potential at all of the HOSCN concentrations tested (Figure 5.10), while non-CsA treated cells were still affected by CCCP and HOSCN. These data are consistent with HOSCN playing a role in the opening of the MPTP and attenuation of ATP coupling in J774A.1 macrophages.

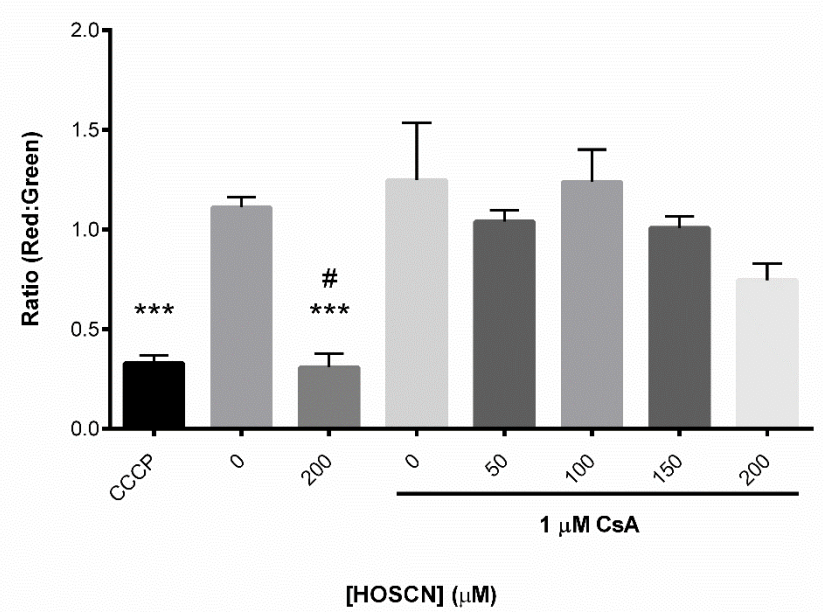

Figure 5.10: Cyclosporin A is able to inhibit the mitochondrial membrane depolarisation caused by HOSCN.

*J774A.1 cells (1 × 10^6 cells) were treated with CsA (1 µM) for 1 h before HOSCN (0 – 200 µM) treatment for 1 h at 22 ˚C or 5 µM CCCP for 10 min at 37 ˚C. The cells were then labelled with JC-1 (2 µM) and left to incubate for 15 min at 37 ˚C. The formation of J-aggregates in the mitochondria (red; λ_{em} = 590 nm) and the leak of these aggregates into the cytosol (green; λ_{em} = 529 nm) was analysed using flow cytometry and the results show that pre-treating J774A.1 cells with CsA protects against HOSCN-induced mitochondrial depolarisation at all the concentrations tested, indicating that HOSCN may interact with the MPTP. Values of the results are the mean ± S.E.M (n = 3). *** shows a significant ($p < 0.001$) decrease compared to the untreated control, # shows a significant ($p < 0.05$) decrease compared to CsA treated samples of the same HOSCN treatment concentration by Repeated Measures one-way ANOVA with a post-hoc Tukey's test.*

5.3.4 HOSCN induced oxidation of J774A.1 cells attenuated the synthesis of ATP

As HOSCN treatment of J774A.1 cells has been shown to attenuate glycolysis and mitochondrial respiration, experiments were performed to determine if the inhibition of these energy producing pathways had an effect on the formation of the final energetic substrate, ATP. Cells (1×10^6 cells/well) were treated with HOSCN (0 – 200 μM) in HBSS for 1 h at 22 ˚C before being scraped and pipetted into a 96-well plate, where they were lysed, and a D-luciferin and luciferase solution added. The D-luciferin is converted to oxyluciferin by luciferase at the expense of ATP; the amount of luminescent oxyluciferin created is directly related to the concentration of ATP in the sample. Luminescence was recorded at 570 nm and the results show that HOSCN decreased the intracellular ATP concentration in J774A.1 cells in a dose-dependent manner (Figure 5.11). A significant decrease in intracellular ATP concentration was observed at ≥ 50 μM HOSCN treatments. This result indicates that the attenuation of glycolysis and mitochondrial respiration by HOSCN reduces ATP production.

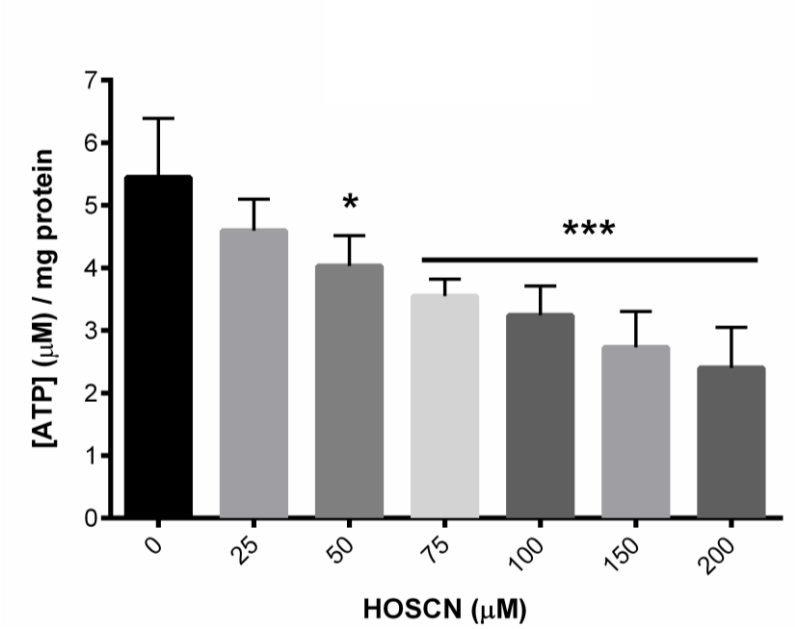

Figure 5.11: HOSCN reduces the concentration of intracellular ATP in J774A.1 cells.

*J774A.1 cells (1 × 10^6 cells) were treated with HOSCN (0 – 200 μM) for 1 h at 22 ˚C before being lysed and added to a solution of D-luciferin and luciferase. ATP from the cell lysate is consumed in the reaction which produces visible light (570 nm) allowing for the quantification of intracellular ATP concentration. Results show a dose-dependent decrease in intracellular ATP concentration with increases in HOSCN treatment concentration. Values of the results are the mean ± S.E.M (n = 3). * and *** show a significant (p < 0.05 and 0.001, respectively) decrease compared to the untreated control by Repeated Measures one-way ANOVA with a post-hoc Tukey's test.*

5.3.4.1 CsA treatment can help prevent the loss of intracellular ATP by HOSCN

After determining that HOSCN causes a decrease in the intracellular ATP concentration, and that CsA could inhibit the opening of the MPTP, an experiment was performed to determine if CsA could also prevent the decrease in intracellular ATP concentrations caused by HOSCN. Results showed that pre-treating J774A.1 cells with 1 µM CsA for 1 h prior to treating with HOSCN could prevent the decrease in intracellular ATP (Figure 5.12). In the previous experiment, a significant decrease in ATP concentration was observed at 50 µM HOSCN (Figure 5.11), whereas a decrease was only noted at the highest treatment concentration (200 µM) after pre-treatment with CsA (1 µM). This result indicates that the loss of intracellular ATP is significantly affected by the condition of the MPTP.

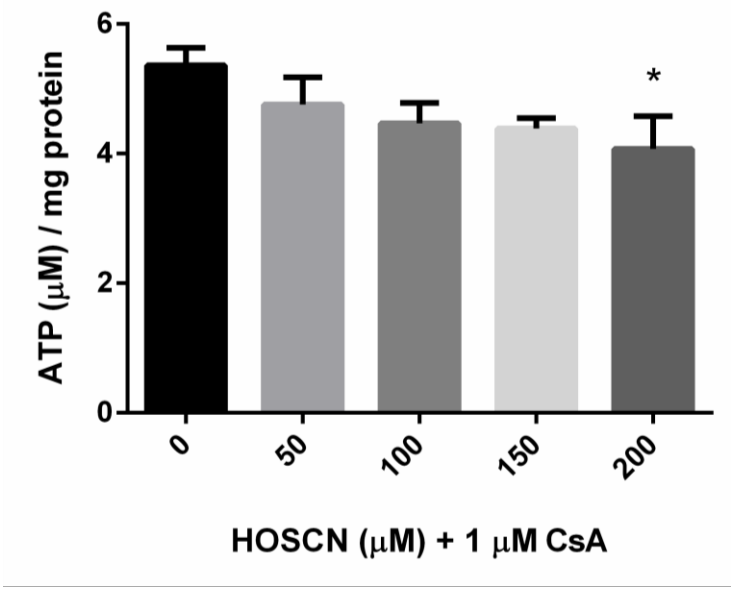

Figure 5.12: Cyclosporin A is able to prevent the loss of intracellular ATP after HOSCN treatment.

*J774A.1 cells (1 × 10^6 cells) were treated with CsA (1 µM) for 1 h before HOSCN (0 – 200 µM) treatment for 1 h at 22 ˚C before being lysed and added to a solution of D-luciferin and luciferase. ATP form the cell lysate is consumed in the reaction which produces visible light (570 nm) allowing for the quantification of intracellular ATP concentration. Results show that the pre-treatment of J774A.1 cells with CsA can help prevent the loss of intracellular ATP caused by HOSCN. Values of the results are the mean ± S.E.M (n = 3). * shows a significant (p < 0.05) decrease compared to the untreated control by Repeated Measures one-way ANOVA with a post-hoc Tukey's test.*

5.4 Discussion

This Thesis has previously shown that HOSCN can induce the formation of sulfenic acids on both cytosolic and mitochondrial proteins in J774A.1 cells. Data have also been presented showing the attenuation of glycolysis in cells exposed to HOSCN. This attenuation of glycolysis ultimately results in the decreased production of the energetic end-product, lactate, consistent with a reduction in pyruvate, the substrate for the tricarboxylic (TCA) cycle. From the TCA cycle, NADH is produced, which is fed into the ETC for oxidative phosphorylation, ultimately yielding ATP for the cell. The results of this Chapter have shown that HOSCN attenuates mitochondrial respiration, increases mitochondrial membrane permeability and reduces the ability of the mitochondria to produce ATP (Figure 5.13).

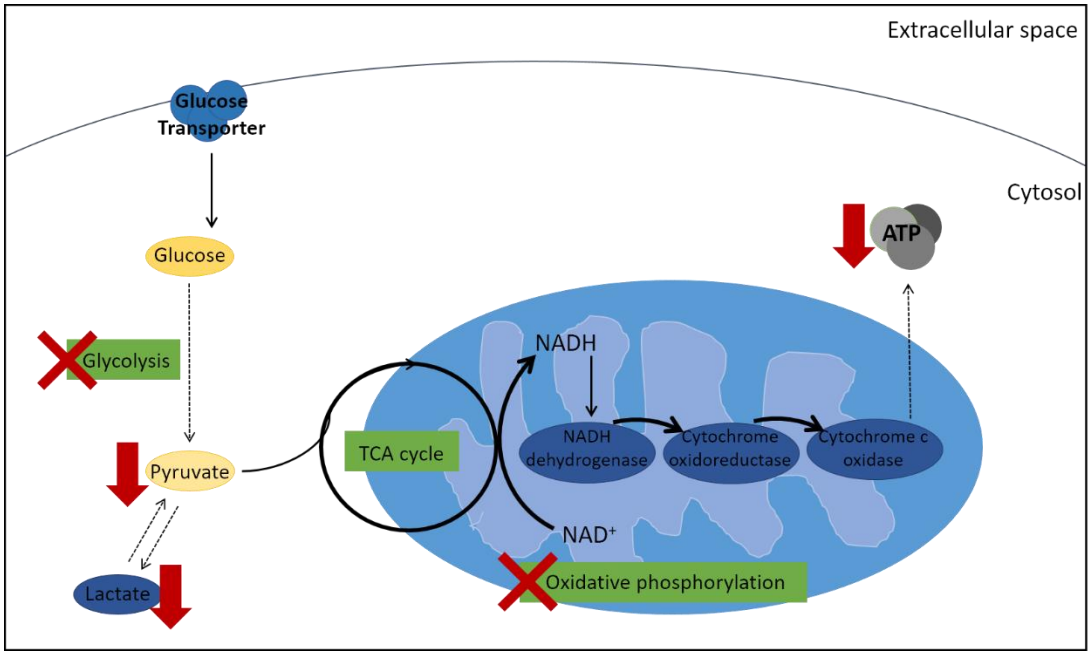

Figure 5.13: The interaction of HOSCN with the metabolic pathways of glycolysis and oxidative phosphorylation.

The inhibition of mitochondrial respiration in cells exposed to HOSCN could occur through two mechanisms, either by direct oxidation of mitochondrial proteins or indirectly via the lack of glycolysis end-product formation. Previously published data have shown that reaction of mitochondrial thiols with diamide (250 µM), which preferentially reacts with small acidic thiols, for 40 min results in a decrease of OCR in rat aortic smooth muscle cells, in a similar

fashion to the results reported in this Chapter [416]. Results have shown that HOSCN is able to form sulfenic acids on mitochondrial proteins in HOSCN treated cells after 1 h. The results of the Seahorse XF assay have shown that baseline respiration can be affected in less than 20 min. There are currently no published data involving mitochondrial protein oxidation and HOSCN. Previous data suggest that HOSCN is able to affect cytosolic proteins in time periods as short as 5 and 15 min, as shown by experiments using ThioGlo-1 and IAF to probe for intracellular thiols [91, 179, 201]. Together, these data support a possible role of HOSCN-mediated mitochondrial thiol oxidation as a pathway to the disruption of mitochondrial respiration and ATP production.

The role of thiol oxidation as a pathway to mitochondrial dysfunction is further highlighted by previous studies that have shown that mitochondrial electron transfer chains can be inhibited the ebselen-induced oxidation of critical thiols in mitochondrial complexes I and II [417, 418], which would cause decreases in ATP production. Similarly, trichlorotelluro-dypnones are able to reduce the number of free protein thiols in rat liver mitochondria, which correlates with a decrease in state 3 and state 4 respiration, reducing the respiratory control ratio (RCR) of the isolated mitochondria [419]. RCR can only be measured in isolated mitochondria, but a decrease in the RCR indicates a decrease in substrate oxidation and ATP turnover, and a high proton leak, supporting the HOSCN data. The results of this study clearly indicate that thiols are critical in the bioenergetic pathway of mitochondria, and that inhibiting them, much in the same way HOSCN inhibits thiols, reduces the ATP turnover within the mitochondria.

The role of thiols in energy production has also been studied using diamide, which causes protein S-glutathionylation by reacting with free GSH. Treatment with diamide caused the loss of free thiols within rat aortic smooth muscle cells [416]. This S-glutathionylation and the subsequent removal of protein thiols from the system led to decreases in the OCR/ECAR ratio, causing the cells to become both less aerobic and less glycolytic. These results corroborate with data obtained in this Chapter. HOSCN causes a loss in free thiols by oxidising them, inhibiting their reductive potential much in the same way as diamide, causing a decrease in the OCR/ECAR ratio, indicating that thiols are critical in oxidative phosphorylation.

A further potential contributor to reduced mitochondrial respiration is a decrease in the mitochondrial membrane potential. Depolarisation of the mitochondria leads to the increased permeability of mitochondria which causes a subsequent loss in small molecules,

such as cytochrome *c* and protons, from the inner mitochondrial space into the cytosol. The loss of the mitochondrial membrane potential becomes significant at the 50 µM HOSCN treatment concentration (Figure 5.9), with the loss of membrane potential decreasing further with increases in the HOSCN concentration. For the positive control, CCCP was used, as it uncouples the ETC to cause a loss in the proton gradient. The results indicate that 200 µM HOSCN is able to disrupt the mitochondrial membrane potential to a similar extent as CCCP (Figure 5.9). This result indicates that HOSCN may act in a similar fashion to CCCP or that the consequences of HOSCN-induced oxidation have a mitochondrial membrane-destabilising side effect. Thus, VDAC, which is located on the outer mitochondrial membrane is crucial for the diffusion of small molecules across the membrane [420, 421], and contains transmembrane cysteine residues that are critical for protein function [215]. HOSCN (100 µM) has been shown to cause a loss in the mitochondrial membrane potential in human coronary artery endothelial cells treated for 2 h [185], which was associated with the release of mitochondrial enzymes cytochrome *c*, apoptosis inducing factor (AIF) and EndoG. Other studies have shown that modifying mitochondrial thiols induces apoptosis and a subsequent mitochondrial depolarisation [192, 422], which supports the idea that HOSCN-induced mitochondrial depolarisation is caused by a change in the level of reduced thiols within the mitochondria, resulting in a leak of small molecules from the mitochondria into the cytosol, which would, in turn, cause a loss in the ATP turnover of mitochondria.

HOSCN was shown to reduce the intracellular ATP concentration in treated J774A.1 cells. ATP, in mammalian cells, is formed primarily through 2 processes. Glycolysis, which has been shown previously to be inhibited by HOSCN treatment and via cellular respiration, which has been shown to be attenuated, either by direct oxidation of associated protein thiols by HOSCN, or due to a decrease in the production of energetic substrates from glycolysis. Results of this Chapter also showed that intracellular ATP levels could be recovered to some extent by pre-treating J774A.1 cells with 1 µM CsA. This was surprising, given the extent of HOSCN-induced perturbation of glycolysis. Further experiments are required to elucidate the process by which CsA protects the intracellular ATP levels.

The inhibition of ATP production has numerous implications, as ATP is the primary energetic currency of cells. Previous data have shown that minor changes in the ADP/ATP ratio of cells can impair cellular growth, causing apoptosis in some cases [412, 413]. ATP is important in cellular growth as cells can undergo cell cycle arrest, activating catabolic metabolism and autophagy when the ability to produce ATP from glucose is impaired [423, 424]. These results

draw comparisons between the lack of ATP production in mammalian cells and the bacteriostatic action of HOSCN. In *E. coli*, when outgrowing from stationary phase, the intracellular concentration of ATP increases significantly, resulting in an increase in rRNA synthesis with subsequent protein synthesis and cellular proliferation, while a decrease in intracellular ATP leads to a decrease in these processes [425, 426]. Studies on bacterial cell growth and HOSCN have shown that while *S. typhimurium* is resistant to cell death after treatment with the LPO/H_2O_2/SCN^- system but is susceptible to the bacteriostatic effect [427]. HOSCN caused decreases in cell growth and proliferation, though, whether this was an ATP dependent process was not investigated, it draws similar conclusions between the results of this study and published data. ATP has been found to be critical to macrophage function and proliferation, by delivering ATP to full-thickness skin wounds, there is a mass activation and subsequent proliferation of macrophages [428]. ATP administration begins the initiation of wound-healing within 24 h, rather than the traditional 3-6 day lag, indicating that ATP is crucial for macrophage proliferation and activation [428, 429] and has been hypothesised to be due to the direct increase of cellular energy supplies.

The effect of HOCl on mitochondrial respiration was not explored in this Chapter. This is because HOCl was found to be too reactive, reacting preferentially with the DMEM used during the respiration experiments, and the Cell-Tak adhesive, rather than the cells. However, it has been reported previously that HOCl activates the MPTP and induces apoptosis in HepG2 cells [187]. Despite its ability to induce the MPTP, it was shown in the previous Chapter that HOCl had no effect on the formation of lactate in J774A.1 cells, implying that it does not attenuate glycolysis. In this setting, HOSCN may be more deleterious to J774A.1 energy production compared to HOCl, as HOSCN attenuates glycolysis by oxidising glycolytic enzymes, reducing the formation of substrates for oxidative phosphorylation, while possibly also oxidising the proteins involved in the ETC.

The implication of HOSCN-induced mitochondrial dysfunction becomes clear, as HOSCN oxidises glycolytic proteins, fewer energetic substrates become available for use during mitochondrial respiration. The mitochondria may also be subjected to protein oxidation by HOSCN, further reducing the ability of the mitochondria to produce ATP, inhibiting cell growth and proliferation while not allowing the macrophages to perform as they should, analogous to the growth inhibition reported in bacteria exposed to this oxidant [379].

5.5 Summary

The results of this Chapter demonstrated that HOSCN has the ability to inhibit mitochondrial function in real time in J774A.1 macrophages at low concentrations of HOSCN (50 μM), while inhibiting ATP turnover and the efficiency of ATP formation at concentrations ≥ 100 μM HOSCN. It is hypothesised that this loss in ATP formation efficiency is due to HOSCN causing an efflux of protons from the mitochondria via changes in the mitochondrial membrane potential. Results using JC-1 indicated that HOSCN does cause mitochondrial depolarisation and a subsequent decrease in intracellular ATP concentrations. This was further verified by pre-treating the cells with CsA, an inhibitor of the MPTP. Results showed that CsA was able to inhibit the opening of the MPTP and therefore reduce the damage caused by HOSCN in regards to mitochondrial membrane permeability and prevent the loss of intracellular ATP. The metabolic profile of the cells and targets of the MPO-derived oxidants in macrophages will be examined further using vibrational spectroscopy, to give a more global overview of the patterns of oxidative damage observed with HOSCN, and how that compares to that seen with HOCl.

6 Identifying Cellular Damage Caused by Hypothiocyanous Acid Using Fourier Transform Infra-Red Spectroscopy

6.1 Introduction

There is a lack of a specific chemical biomarker for HOSCN, which makes accessing the reactivity of this oxidant *in vivo* quite difficult. HOSCN is a hypohalous acid like HOCl and HOBr, except HOSCN has a more limited range of targets with which it interacts with and oxidises [380]. Low-molecular mass thiols such as GSH are targets of HOSCN-induced oxidation, resulting in the formation of unstable sulfenyl thiocyanate (RS-SCN) species and the perturbation of the GSH/GSSG ratio [84, 91, 430]. Another important target of HOSCN-induced oxidation is proteins, as HOSCN favourably oxidises protein thiols [56, 97, 107, 130]. It has been postulated that the reaction of HOSCN and protein thiols creates RS-SCN which are hydrolysed to sulfenic acids or react with another thiol to form a disulfide, all of which are readily reduced in a cellular system [109, 431].

In terms of biomarker development, a problem with HOSCN-induced damage relates to its ability to reversibly oxidise targets [97, 432]. There is a lack of direct evidence for the formation of RS-SCN species on proteins, and the formation of sulfenic acids and disulfides is not only attributable to HOSCN [49, 107, 130]. Fluorescent probes have been used to assess the reactivity of HOSCN with its targets, but there are various limitations imposed on the use of probes, such as probe accessibility to the target and non-specific binding of the probe [433, 434]. Fluorescent probes also have a limitation that reduces the amount of data that can be obtained in an experiment, in that they are specific, only allowing for the determination of the structure or chemical group labelled with the probe, and hence determining the fate of a pathway, such as glycolysis or mitochondrial respiration, can become impractical [434]. A surrogate biomarker is homocitrulline from carbamylation of lysine by cyanate (OCN^-), a decomposition product of HOSCN. However, OCN^- can be produced by other biological pathways, for example, uraemia and hence lacks specificity [81].

To try and overcome these limitations and further investigate the effect of HOSCN in cellular systems, infra-red spectroscopy was utilised to probe cells for HOSCN-induced damage. Fourier transform infra-red (FTIR) spectroscopy allows for non-destructive analysis of biological samples without the need for probes or chemical tagging, but requires the dehydration of cells before scanning, as H_2O is a strong absorber of IR [435]. FTIR allows for the interrogation of a wide number of chemical groups within the cells that can be identified by individual spectral peaks in the mid-IR range [436], allowing for an alternative method for determining HOSCN-induced cell damage. Chemical covalent bonds with an electric dipole

moment that can change via atomic displacement by natural vibrations are IR active and these vibrational modes can be quantitatively measured by FTIR spectroscopy [436]. The use of FTIR in a disease diagnosis and screening setting has been investigated, and exploring the effects of diseases on various tissues has been studied in numerous disease settings including cervical dysplasia [437], coeliac disease [438] and also in determining surgery outcomes in breast cancer cases [439].

6.2 Aim

The aim of the study presented in this Chapter is to use FTIR spectroscopy and multivariate data analysis as techniques to quantify and assess the pattern of HOSCN-induced cellular damage and the inhibition of cellular metabolism.

6.3 Methods

6.3.1 Infra-red spectroscopy

6.3.1.1 Oxidant treatment of J774A.1 cells and plating to silicon nitride plates

For the experiments detailed in this Chapter, cells were plated at 3×10^6 cells/flask in DMEM and allowed to adhere in a 25 cm^2 flask, in an incubator overnight at 5 % CO_2 and 37 ˚C. The next day, cells were washed twice with HBSS prior to incubation with 3 mL of either a control solution (HBSS), HOSCN (50, 100 or 200 µM), decomposed HOSCN (dHOSCN) or HOCl (200 µM) for 1 h at 22 ˚C. Following oxidant treatment, the media was removed from the cells and the cells were washed and resuspended in 1 mL of HBSS (3×10^6 cells/mL) before counting using a haemocytometer in the presence of 0.2% v/v trypan blue. Cells were then centrifuged in an Allegra X-15R centrifuge (Beckman Coulter) at 400 *g* for 5 min at 22 ˚C to form a cell pellet. The pellet was resuspended in HBSS to the required density of cells (1.25×10^6 cells/ 100 µL). After resuspension, 20 µL of the sample was pipetted onto a 96-well silicon nitride plate (Figure 6.1), making sure to load the cells evenly within the well to avoid clumping and uneven layers.

After loading the samples onto the silicon nitride plate in triplicate, the plate was transferred into a desiccator and left overnight at 22 ˚C to remove moisture from the samples [435], before being analysed using the Bruker Tensor 27 HTS-XT.

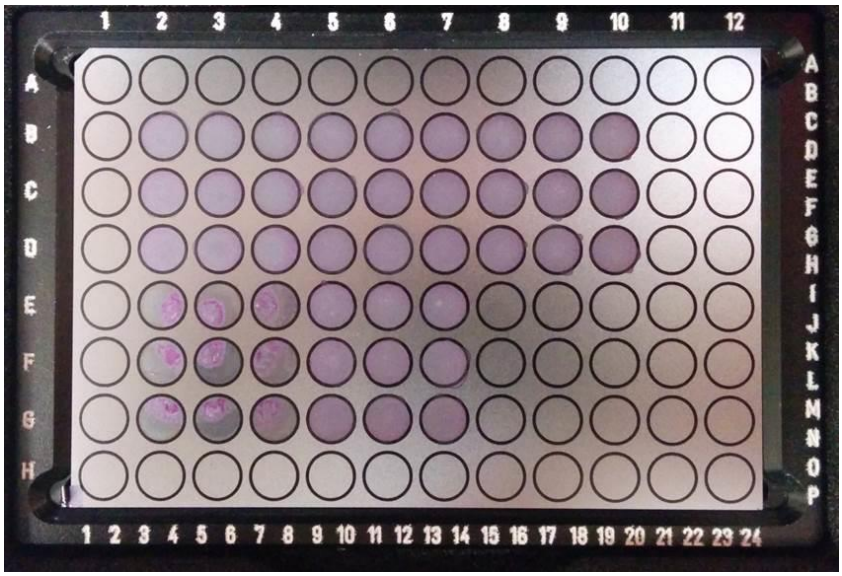

Figure 6.1: Silicon nitride 96-well plate.

The silicon nitride plate is a flat plate, with 96 marked circles marking where the spectrometer takes measurements. The representative image shows how the samples appeared after desiccating overnight at 22 ˚C.

6.3.1.2 Infra-red spectroscopy using the Bruker Tensor 27 HTS-XT

The instrument used for Fourier transform infra-red (FTIR) spectroscopy was a Bruker Tensor 27 FTIR spectrometer coupled to a HTS-XT sampling accessory. The silicon nitride plate containing samples was loaded into the spectrometer and each sample was run in triplicate to ensure reproducibility. Spectra were collected over the mid infra-red region (4000 – 400 cm^{-1}) at a spectral resolution of 4 cm^{-1} with 256 co-added scans and background scans, allowing for greater resolution of the data sets. All the data were recorded using Opus 6.5 (Section 6.3.2.1).

6.3.2 Data analysis

Pre-processing of the spectra was performed on each software package, which both used the same algorithms. The derivatives used were second-order derivatives, calculated using a Savitzky-Golay algorithm with nine smoothing points. All data was normalised to either the CH region (3000 – 2800 cm^{-1}), the protein region (1800 – 1400 cm^{-1}) or the fingerprint region (1400 – 700 cm^{-1}). Other conditions are discussed in the relevant section of the Chapter.

6.3.2.1 Opus 6.5

Opus (version 6.5, Bruker, Germany) was used to control the instrument and collect data. It was also used to consolidate the separate scans to create the average spectra of 256 scans across triplicate samples in 3 separate experiments. After creating the averaged spectra, the peaks could then be normalised to their respective regions using vector normalisation, which calculates the average y-values and divides it by the square root of the sum ('Manipulate' → 'Normalisation'). The peaks could then be compared by using an integration method ('Evaluate' → 'Integration'), which allows for the calculation of peak heights and area by drawing a straight line between the peaks of the two frequency limits defined. Each peak was analysed separately using this method, after which, the peak heights were compared to each other.

6.3.2.2 The Unscrambler X 10.3

The Unscrambler (10.3, Camo, Oslo, Norway) is a chemometrics software program that incorporates numerous algorithms for use in large data analysis. The software is also able to directly import native instrument file formats, such as the Opus spectral files.

In this study, principal component analysis (PCA) was performed on the pre-processed opus data files only. To analyse this data, non-linear partial-least –squares algorithm was employed with a full-cross validation (to determine the number of principal components to retain to account for data variability). Additionally, a Savitzky-Golay convolution algorithm was used to normalise, increase the signal-to-noise ratio, smooth the data and obtain the second order derivatives. In this analysis, only principal components (PC) 1 and 2 were assessed by using the PC scores and loading plots (as determined by full-cross validation).

6.4 Results

Previous Chapters have shown that HOSCN can attenuate the energy producing pathways of glycolysis and mitochondrial respiration in J774A.1 cells. Initial studies were performed to determine if changes in the bioenergetic status of the cells could be determined using FTIR spectroscopy. Mid-infra-red (mid-IR) light (4000 – 400 cm^{-1}) can be used to study fundamental vibrations and rotational-vibrations, by passing IR light through the cells. When the frequency of the IR light is the same as the vibrational frequency of a bond, the light is absorbed. This light is then transmitted by the sample, which reveals how much energy has been absorbed at any particular frequency. For a molecule to be IR active, it must be able to change its dipole moment, and the occurring vibration is called a 'vibrational mode'.

J774A.1 cells (3×10^6 in a 25 cm^2 flask) were treated with either a control solution (HBSS), HOSCN (50, 100 or 200 µM), decomposed HOSCN or HOCl (200 µM) for 1 h at 22 ˚C. One concentration of HOCl was employed as a comparison with HOSCN, as it is known that extensive cellular damage occurs upon treatment of cells with high concentrations of HOCl. The cells were then washed and plated onto a silicon nitride plate at a density of 2.5×10^5 cells/spot and desiccated for 18 h at 22 ˚C before being sampled in the mid-IR range using a Bruker HTS IR spectrometer (256 scans per sample). After sampling, the data were processed using Opus 6.5, the second-order derivative was performed (negative peaks), then each peak could be analysed, and its area determined and compared against other treatments.

6.4.1 HOSCN affects the CH region of J774A.1 cells

The results of the FTIR spectroscopy from J774A.1 cells were analysed over different spectral regions. The first region is the higher wavenumber region (ca. 2800 – 3000 cm^{-1}) that is associated with stretching vibrations of S-H, O-H, N-H and C-H, and will be called the CH region from this point on. Because of cellular hierarchy and its relative abundance, the CH region is usually indicative of changes that occur to phospholipids of the cellular membrane [436].

When observing the CH region (Figure 6.2), it appears that very little change in the spectra is observed as a result of oxidant treatment. This could be due to the abundance of CH_2 and CH_3 bonds relative to the concentration of oxidant used. But after peak integration, the results indicated that HOSCN, dHOSCN and HOCl were unable to influence CH_3 symmetric (s)

or asymmetric (as) stretching (v) (Figure 6.3A & C) while 200 µM HOSCN, 200 µM HOCl and dHOSCN was able to significantly reduce CH_2 asymmetric stretches (vas) (Figure 6.3B) and increase CH_2 symmetric stretches (vs) (Figure 6.3D). This result is consistent with some interaction or reaction of the treatments with the phospholipid bilayer of J774A.1 macrophages.

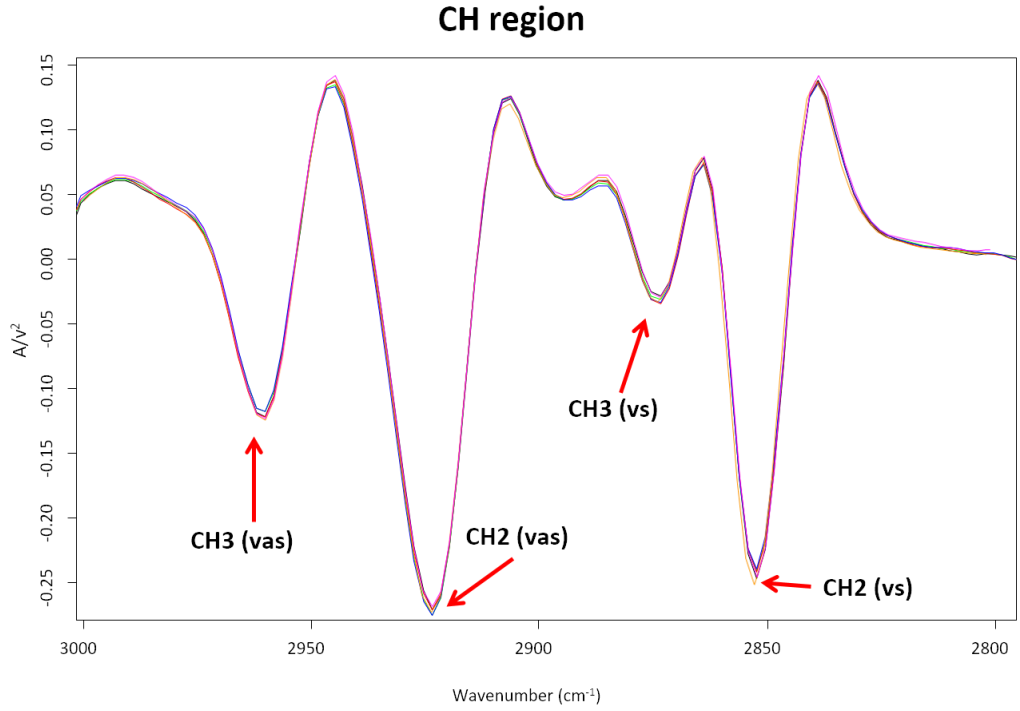

Figure 6.2: The CH region of J774A.1 cells visualised using FTIR.

J774A.1 cells (2.5 × 10^5 cells) were interrogated using a Bruker HTS-XT infra-red spectrometer (256 scans) after being treated with either a control solution (HBSS), HOSCN (50, 100, 200 µM), dHOSCN or HOCl (200 µM) in HBSS for 1 h at 22 ˚C. The CH region (ca. 2800 – 3000 cm^{-1}) has four distinct peaks, CH_2 (vs); 2852 cm^{-1}, CH_3 (vs); 2870 cm^{-1}, CH_2 (vas); 2927 cm^{-1}, CH_3 (vas); 2960 cm^{-1} which can be observed after performing a second derivative Fourier transformation. Each spectrum is the average of triplicates from 3 separate experiments. Control (blue), 50 µM HOSCN (red), 100 µM HOSCN (green), 200 µM HOSCN (black), 200 µM HOCl (orange), dHOSCN (pink).

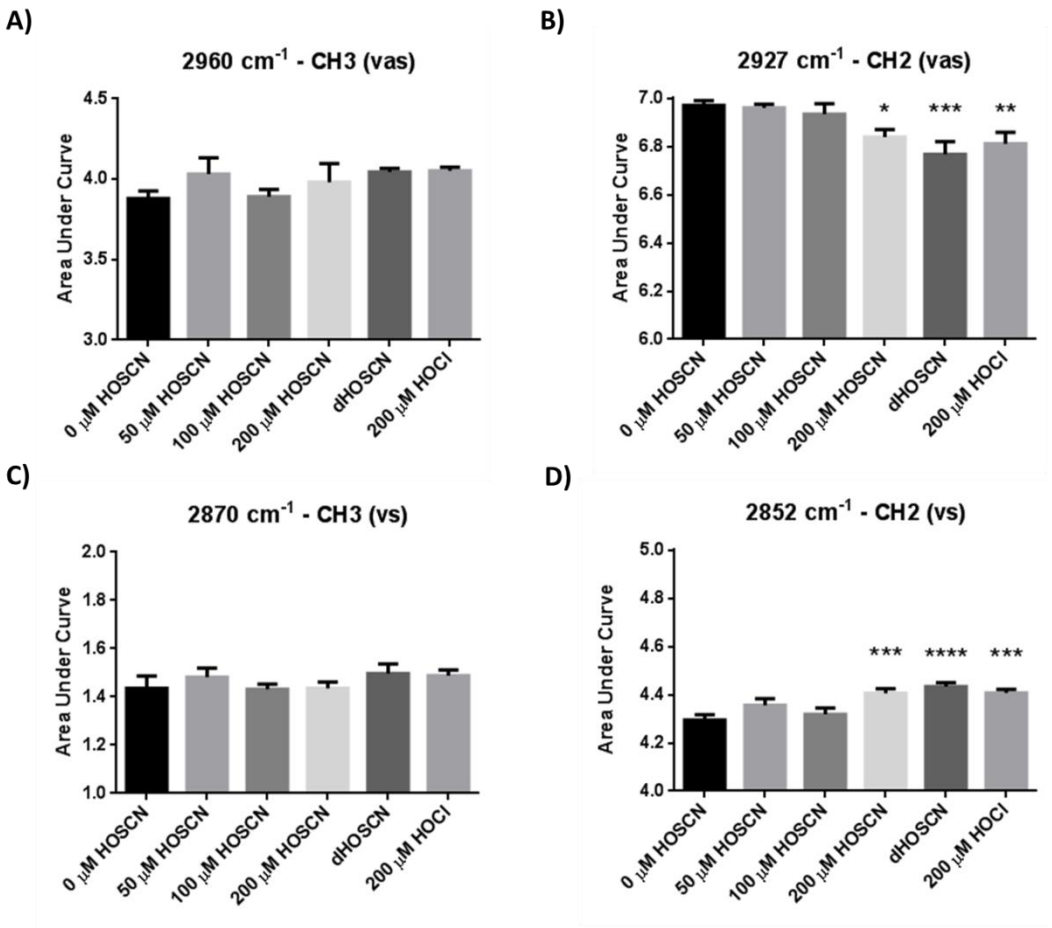

Figure 6.3: Changes to the CH region of J774A.1 cells by hypohalous acids.

*J774A.1 cells (2.5 × 10^5 cells) were interrogated using a Bruker HTS-XT IR spectrometer (256 scans) after being treated with either HBSS, HOSCN (50, 100, 200 µM), dHOSCN or 200 µM HOCl in HBSS for 1 h at 22 ˚C. Second derivative Fourier transformation, peak integration and peak area were determined. Results indicate that none of the treatments influenced CH_3 vibrational modes (A & C) while 200 µM HOSCN, dHOSCN and 200 µM HOCl were able to (B) attenuate the CH_2 (vas) vibrational mode and (D) increase the CH_2 (vs) vibrational mode. All data are the average of 3 separate experiments ± S.E.M. *, **, *** and **** show a significant (p < 0.05, 0.01, 0.001 and 0.0001, respectively) decrease or increase compared to respective controls by Repeated Measures one-way ANOVA with a post-hoc Tukey's test.*

6.4.2 HOSCN affects infra-red spectra of the protein region in J774A.1 cells

The second region within the IR spectra is comprised of wavenumbers from 1800 – 1450 cm^{-1}, and will be called the protein region from this point on. This region contains peaks mainly associated with the stretching and bending bonds of proteins [436].

After J774A.1 cells were treated and interrogated using the Bruker HTS-XT, changes in peak height were easily identifiable upon inspection. Even before peak integration, it was possible to determine that HOSCN, HOCl and to some extent, dHOSCN, was able to influence the vibrational modes of protein bonds. The assignment of bonds is indicated in Figure 6.4 and the respective Figure legend.

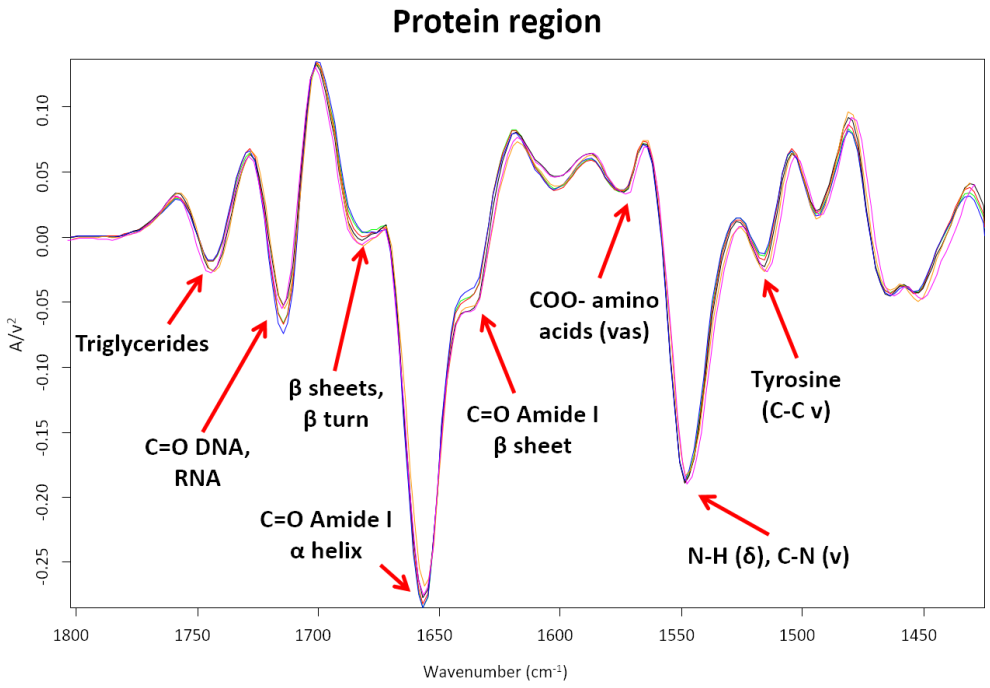

Figure 6.4: The protein region of J774A.1 cells visualised using FTIR.

J774A.1 cells (2.5 × 10^5 cells) were interrogated using a Bruker HTS-XT infra-red spectrometer (256 scans) after being treated with either a control solution (HBSS), HOSCN (50, 100, 200 µM), dHOSCN or HOCl (200 µM) in HBSS for 1 h at 22 ˚C. In the protein region (ca. 1450 – 1800 cm^{-1}), eight peaks could be identified, tyrosine (C-C v); 1515 cm^{-1}, N-H (δ), C-N (v) peptide linkages; 1545 cm^{-1}, COO^- (vas); 1576 cm^{-1}, amide I – beta sheets; 1637 cm^{-1}, amide I – alpha helix; 1656 cm^{-1}, beta sheets and beta turns; 1682 cm^{-1}, DNA and RNA (C=O); 1713 cm^{-1}, triglycerides; 1743 cm^{-1}. Each spectra is the average of triplicates from 3 separate experiments. Control (blue), 50 µM HOSCN (red), 100 µM HOSCN (green), 200 µM HOSCN (black), 200 µM HOCl (orange), dHOSCN (pink).

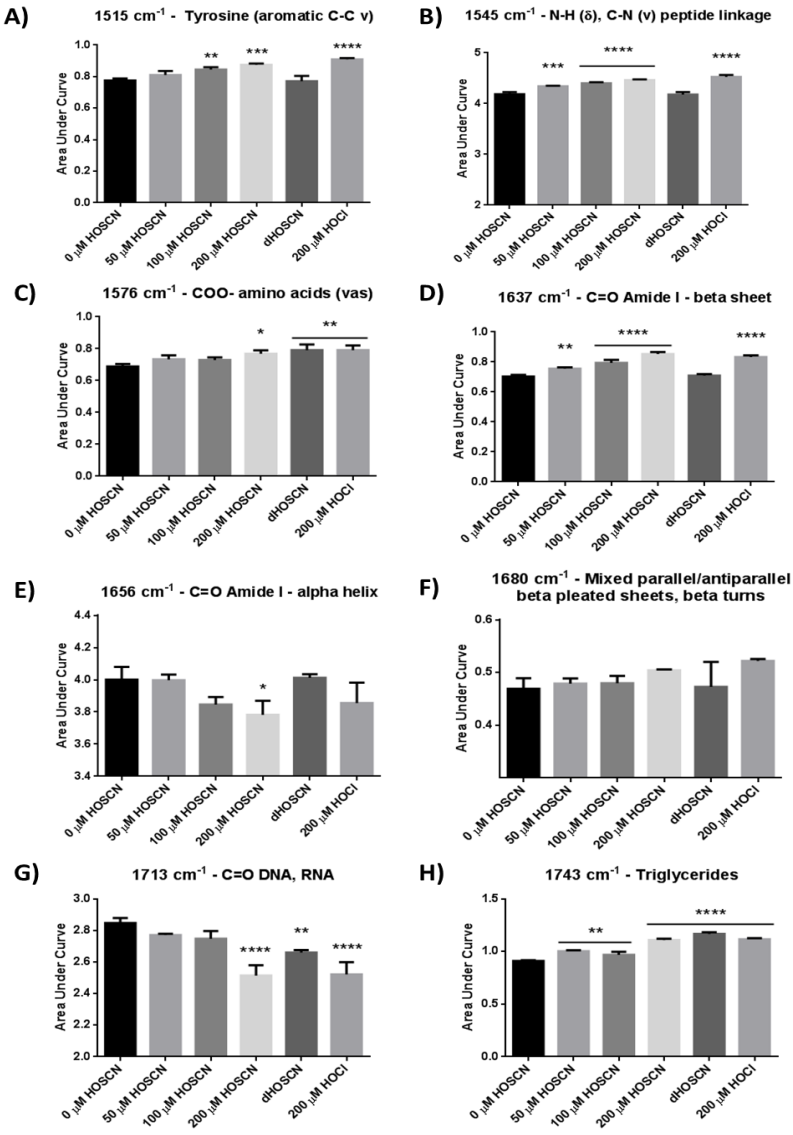

Figure 6.5: Hypohalous acids cause changes to the protein region of J774A.1 cells.

*J774A.1 cells (2.5 × 10^5 cells) were interrogated using a Bruker HTS-XT IR spectrometer (256 scans) after being treated with either HBSS, HOSCN (50, 100, 200 µM), dHOSCN or 200 µM HOCl in HBSS for 1 h at 22 ˚C. Second derivative Fourier transformation, peak integration and peak area were determined. Results indicate that HOSCN influences (A) tyrosine, (B) peptide linkages, (C) COO-, (D) protein beta sheets, (E) alpha helices, (G) DNA/RNA and (H) triglycerides. dHOSCN affects COO-, DNA/RNA, and triglycerides. HOCl affects tyrosine, peptide linkage, COO-, protein beta sheets, DNA/RNA, and triglycerides. No treatment affected (F) mixed parallel beta formations. All data are the average of 3 separate experiments ± S.E.M. *, **, *** and **** show a significant (p < 0.05, 0.01, 0.001 and 0.0001, respectively) decrease or increase compared to respective controls by Repeated Measures one-way ANOVA with a post-hoc Tukey's test.*

After peak analysis using Opus 6.5 was completed, multiple changes in the vibrational modes of protein bonds were identified. The first peak change identified was at 1515 cm^{-1} which was indicative of changes to the vibrational mode of the aromatic C-C bonds of tyrosine (Figure 6.5A). Increases in C-C (ν) vibrations were identified with 100 and 200 µM HOSCN and with 200 µM HOCl. Major changes were identified with (Figure 6.5B) peptide linkages (N-H (δ) and C-N (ν)) (1576 cm^{-1}) and (Figure 6.5D) C=O amide I – beta sheets (1637 cm^{-1}) after treatment with ≥ 50 µM HOSCN and 200 µM HOCl. An increase in (Figure 6.5C) COO^- (vas) was also identified with 200 µM HOSCN, dHOSCN and 200 µM HOCl treatments (1576 cm^{-1}). Concerning the amide I – alpha helices (1656 cm^{-1}), only 200 µM HOSCN induced a significant decrease in the C=O vibrational mode (Figure 6.5E). Finally, there was no significant change in the vibrational mode of mixed parallel/antiparallel beta pleated sheets or beta turns (1680 cm^{-1}) in any of the treatment conditions (Figure 6.5F).

Non-protein related peaks were also identified in this portion of the spectra, the first was a DNA and RNA peak related to the vibrational C=O mode (1713 cm^{-1}), which experienced a significant decrease after treatment with 200 µM HOSCN, dHOSCN and 200 µM HOCl (Figure 6.5G). The second peak was associated with the vibration of triglycerides (1743 cm^{-1}), and increases in the vibrational mode were observed at ≥ 50 µM HOSCN, dHOSCN and 200 µM HOCl (Figure 6.5H).

6.4.3 Reactivity of HOSCN with the fingerprint region

The third region within the IR spectra is comprised of wavenumbers from 1450 – 700 cm^{-1}, and will be called the fingerprint region from this point on. This region contains low-energy peaks mainly associated with bending (δ), stretching and carbon skeleton fingerprint vibrations. This area is quite complex as the peaks can be associated with various different classes of biological chemicals, including lipids, nucleic acids and carbohydrates, resulting in spectra that is unique to specific cells and cell types [436].

After J774A.1 cells were treated, and the IR spectra were interrogated using the Bruker HTS-XT, the collected data were run through an algorithm to determine the second-derivative peaks. Upon inspection of the spectra, differences between treatments were immediately observed, with substantial changes in peak area seen between 1250 – 950 cm^{-1} (Figure 6.6). These peaks were then integrated using Opus 6.5 and compared against

other treatments to quantify the changes in vibrational modes. The vibration of specific bonds is given in Figure 6.6.

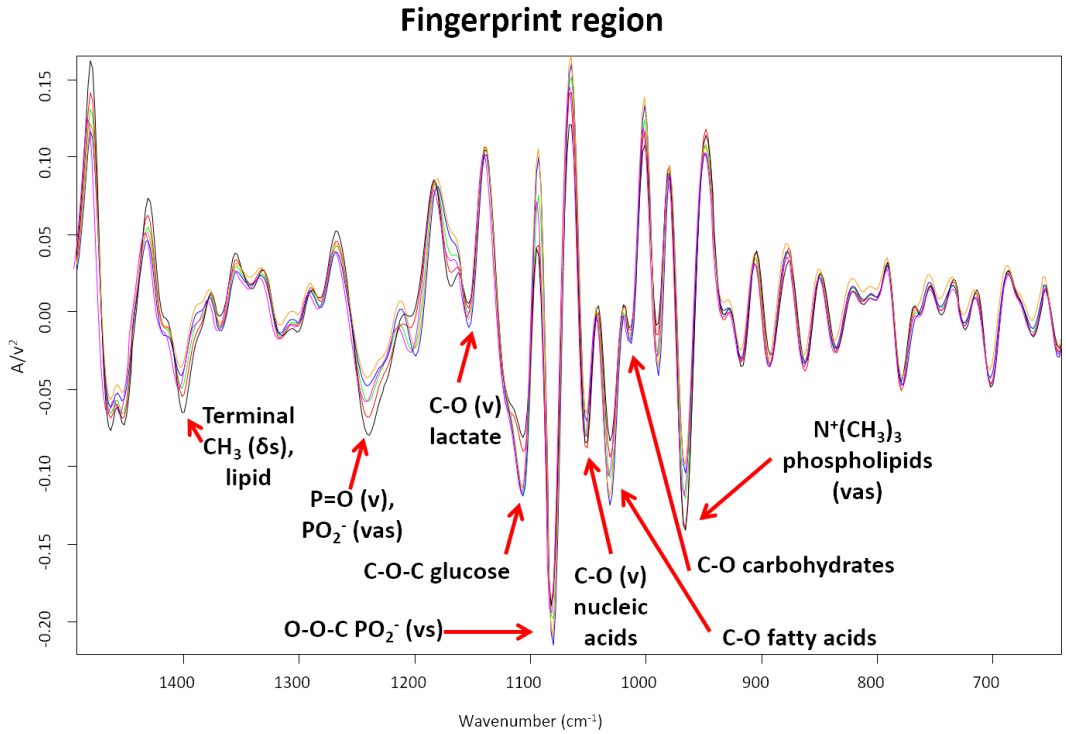

Figure 6.6: The fingerprint region of J774A.1 cells visualised using FTIR.

J774A.1 cells (2.5 × 10^5 cells) were interrogated using a Bruker HTS-XT infra-red spectrometer (256 scans) after being treated with either a control solution (HBSS), HOSCN (50, 100, 200 µM), dHOSCN or HOCl (200 µM) in HBSS for 1 h at 22 ˚C. In the fingerprint region (600 – 1450 cm^{-1}) nine peaks were identified, choline phospholipids (vas); 967 cm^{-1}, carbohydrates; 1011 cm^{-1}, fatty acids; 1031 cm^{-1}, nucleic acids (v); 1052 cm^{-1}, hypophosphite (vs); 1080 cm^{-1}, glucose; 1105 cm^{-1}, lactate; 1152 cm^{-1}, P=O (v) and hypophosphite (vas); 1242 cm^{-1}, and terminal CH_3 (δs) and lipids; 1385 cm^{-1}. Each spectra is the average of triplicates from 3 separate experiments. Control (blue), 50 µM HOSCN (red), 100 µM HOSCN (green), 200 µM HOSCN (black), 200 µM HOCl (orange), dHOSCN (pink).

After peak analysis, numerous changes were identified in this region. An increase in vas vibrational mode of choline phospholipids (967 cm^{-1}) was observed after treatment of the J774A.1 cells with ≥ 100 µM HOSCN and 200 µM HOCl (Figure 6.7A). A decrease in fatty acid C-O (1031 cm^{-1}) vibrations were seen with 100 and 200 µM HOSCN (Figure 6.7B). The C-O (v) vibrational mode of nucleic acids (1052 cm^{-1}) were increased significantly after 200 µM HOSCN treatment (Figure 6.7C). The compound hypophosphinate (PO_2^-) and O-O-C (vs) vibrational modes (1080 cm^{-1}) were decreased by ≥ 100 µM HOSCN treatment and 200 µM HOCl (Figure 6.7D), while an increase in PO_2^- (vas) and P=O (v) (1242 cm^{-1}) were noted with 200 µM HOSCN and HOCl (Figure 6.7E). Finally, there was a significant increase in terminal CH_3 (δ) (1385 cm^{-1}) after 200 µM HOCl treatment (Figure 6.7F).

In support of the data from Chapter 4, changes were also identified in the vibrational modes of various carbohydrates and glycolytic products in J774A.1 cells after treatment with HOSCN. The peak at 1011 cm^{-1} is indicative of the C-O bonds of carbohydrate molecules, and the data show that treatment of J774A.1 cells with ≥ 100 µM HOSCN led to a significant decrease in the vibrational mode of carbohydrates (Figure 6.8A). Glucose was identified due to its C-O-C bond (1105 cm^{-1}), and a significant decrease in the glucose vibration was detected after treatment with 200 µM HOSCN (Figure 6.8B). Finally, lactate (C-O (v) – 1152 cm^{-1}), an end-product of glycolysis whose production was shown to decrease after HOSCN treatment, was significantly decreased after ≥ 100 HOSCN in these experiments (Figure 6.8C).

After completing the analysis of J774A.1 IR spectra using Opus 6.5, the data were analysed using multivariate data analysis. This multivariate data analysis allows for the analysis of large data sets, which in turn, allows a global assessment of cellular damage and the localisation or nature of this damage.

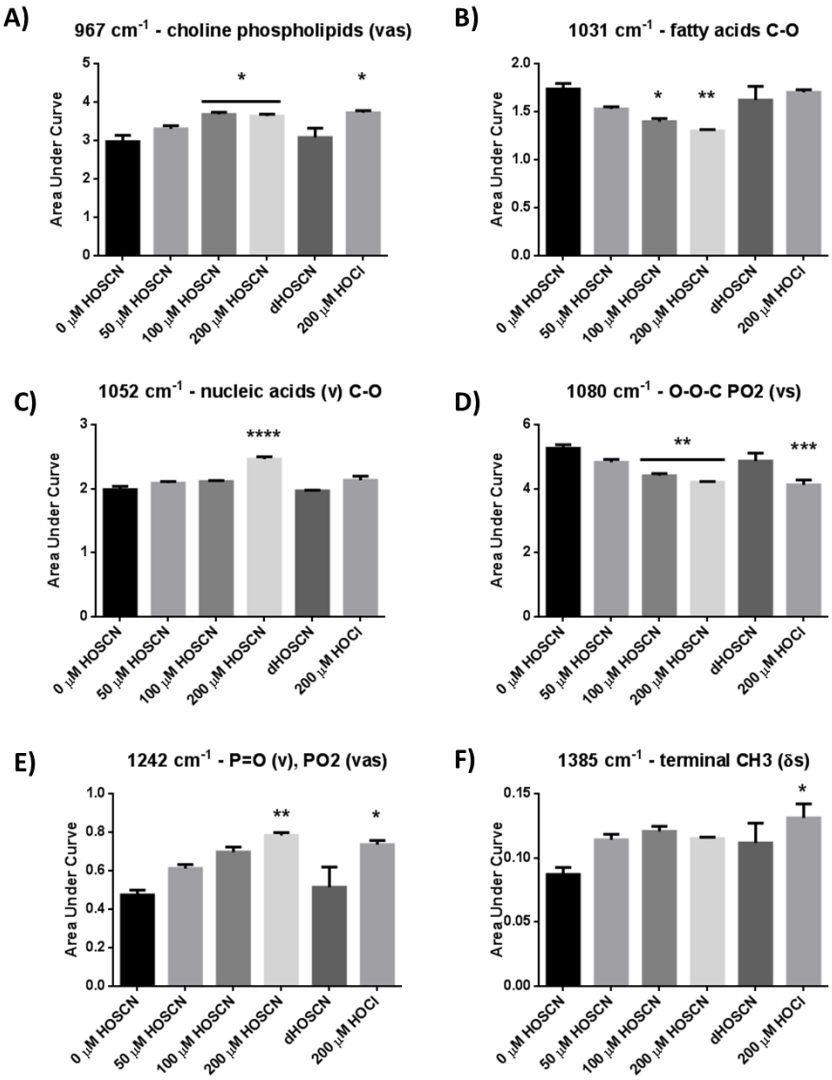

Figure 6.7: Hypohalous acids cause changes to the fingerprint region of FTIR-interrogated J774A.1 cells.

*J774A.1 cells (2.5 × 10^5 cells) were interrogated using a Bruker HTS-XT IR spectrometer (256 scans) after being treated with either HBSS, HOSCN (50, 100, 200 µM), dHOSCN or 200 µM HOCl in HBSS for 1 h at 22 ˚C. Second derivative Fourier transformation, peak integration and peak area were determined. Results indicate that high concentrations of HOSCN were able to significantly influence (A) choline phospholipid (vas), (B) fatty acid (C-O), (C) nucleic acid (C-O v), (D) PO_2 (O-O-C vs), and (E) P=O (v) and PO_2 (vas) vibrations. HOCl was also able to influence phospholipid (vas), PO_2 (O-O-C vs), P=O (v) and PO_2 (vas) and terminal CH_3 (δs). dHOSCN did not influence any vibrational modes in this region. All data are the average of 3 separate experiments ± S.E.M. *, **, *** and **** show a significant ($p < 0.05$, 0.01, 0.001 and 0.0001, respectively) decrease or increase compared to respective controls by Repeated Measures one-way ANOVA with a post-hoc Tukey's test.*

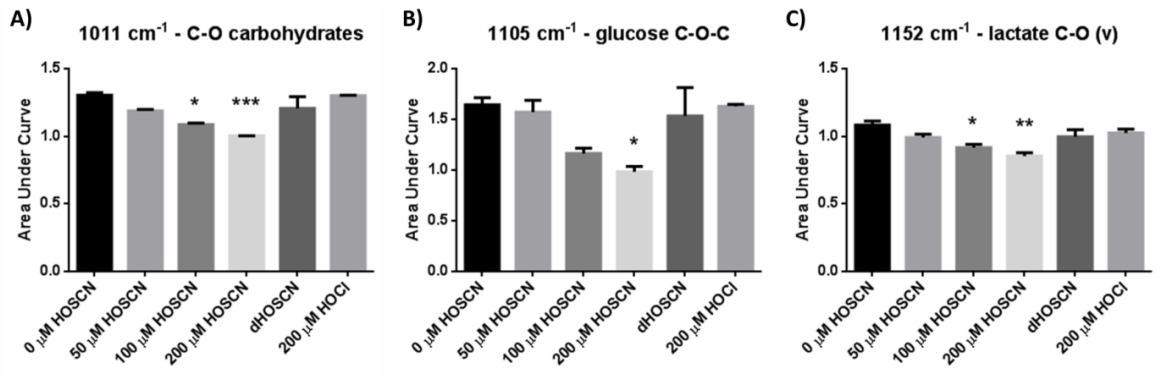

Figure 6.8: HOSCN attenuates the recognition of bioenergetic molecules.

*J774A.1 cells (2.5 × 10^5 cells) were interrogated using a Bruker HTS-XT infra-red spectrometer (256 scans) after being treated with either a control solution (HBSS), HOSCN (50, 100, 200 µM), dHOSCN or HOCl (200 µM) in HBSS for 1 h at 22 ˚C. After second derivative Fourier transformation, the peaks were integrated and the peak area was determined. In the fingerprint region (600 – 1450 cm^{-1}) three peaks were identified that are involved in cellular bioenergetics. The results showed that only higher concentrations of HOSCN were able to attenuate the vibrational modes of (A) carbohydrates, (B) glucose and (C) lactate in J774A.1 macrophages. All data are the average of 3 separate experiments ± S.E.M. *, ** and *** show a significant (p < 0.05, 0.01 and 0.001, respectively) decrease compared to respective controls by Repeated Measures one-way ANOVA with a post-hoc Tukey's test.*

6.4.4 Multivariate data analysis

To further analyse the data gathered by FTIR, multivariate data analysis was performed. To do this, a statistical procedure called 'principal component analysis' (PCA) was employed. In short, the data, which is correlated, is converted into a set of numbered matrices, which are linearly uncorrelated, the variables of which are called 'principal components'. The number of principal components possible is equal to the number of original variables (i.e. the intensity at each wavenumber is the variable), where they are arranged so that the first principal component explains the largest possible variance and each succeeding component has the next largest.

By using this statistical procedure, it is possible to see which chemical groups within the J774A.1 cells are affected the most by oxidant treatment without the need for analysing the peaks. In this way, bias in the data analysis is removed and each point is compared to every other peak within the set. After the completion of the procedure, a PCA scores plot and PCA loadings plot is formed. The scores plot is used as a tool to determine whether the global changes, due to a treatment, causes a change in the cellular chemistry and is determined via a separation in the points of the two groups, while the loadings plot indicate where these changes in the spectra and therefore, the cell, have occurred. The loadings plot also give information about the relative abundance and/or detection of each chemical group, with negative values indicating a decrease, and positive values indicating an increase.

The results of the PCA between the control and 50 µM HOSCN-treated cells revealed that 50 µM HOSCN did alter J774A.1 cell chemistry on a global cellular scale, but the change that occurred was weak. The PCA scores plot (Figure 6.9A) showed a large variation in the control points across both the PC-1 and PC-2 axis, while cells treated with 50 µM HOSCN had a large variation on the PC-1 axis and less on the PC-2. The score plot also showed that the points between these two groups are not totally separated, indicating that the difference between these two conditions is weak. The loadings plot shows the variation on the PC-1 axis (explaining 74% of variation) (Figure 6.9B). The PC-1 axis is explaining some variation between the two treatments, but not enough to determine whether the change seen is caused by HOSCN.

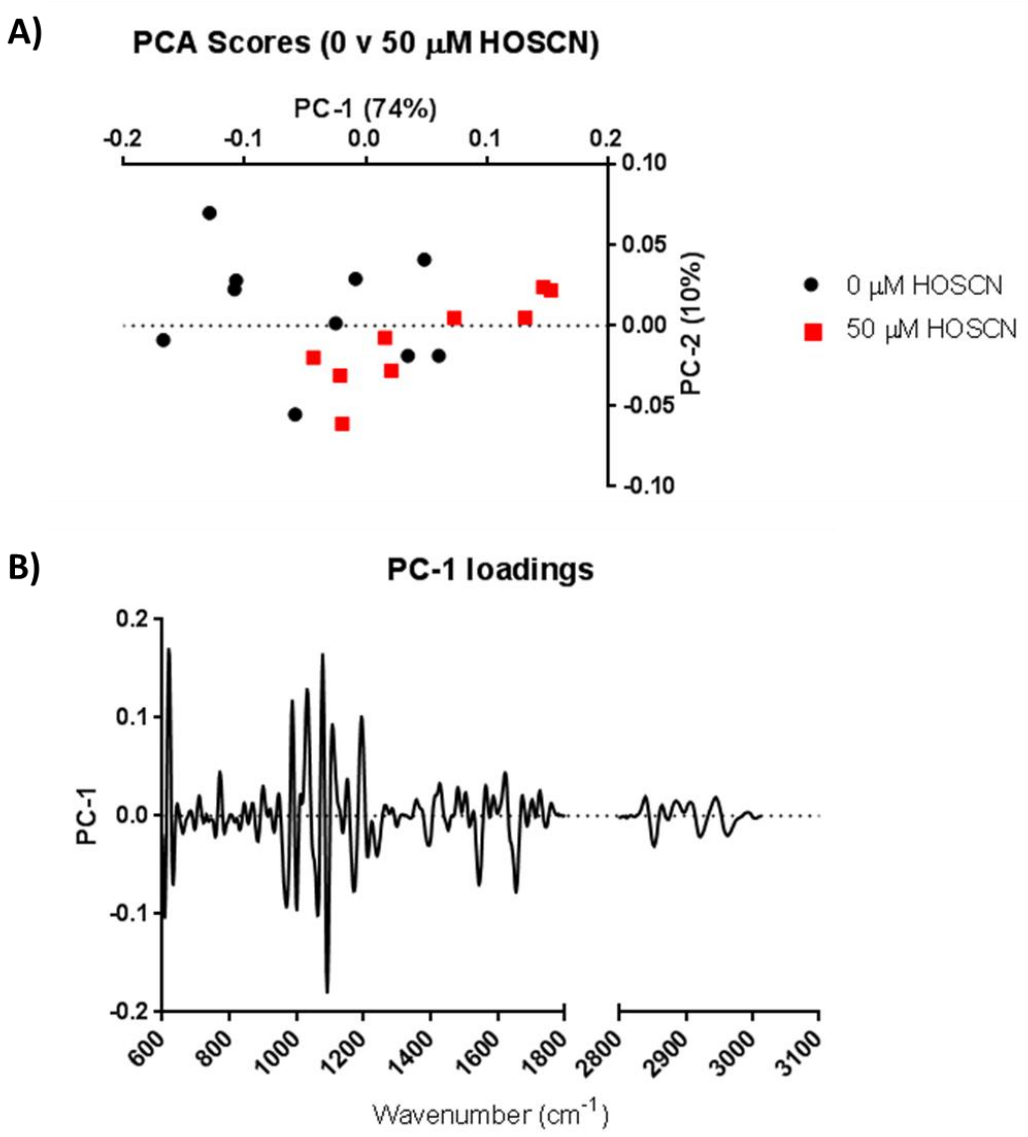

Figure 6.9: PCA of J774A.1 cells treated with 50 µM HOSCN.

Principal component analysis scores and PC-1 loading plots of second derivatives of the spectra (Savitzky-Golay 9 points) comparing control and 50 µM HOSCN treatments. (A) The PCA scores plot comparing control and 50 µM HOSCN on PC-1 and PC-2 axes. (B) The PC-1 loading plot describes where in the spectra the variation occurs. These data show that there is a weak separation between control and 50 µM HOSCN treated cells, indicating that the changes induced by HOSCN at this concentration are minimal on a global cellular level.

The next PCA was performed to determine the changes that occurred to J774A.1 cells after 100 μM HOSCN treatment. The results show that 100 μM HOSCN was able to alter J774A.1 chemistry significantly. The PCA scores plot (Figure 6.10A) showed a large variation of control cells across both the PC-1 and PC-2 axis, while the 100 μM HOSCN treated samples are grouped more tightly, in comparison across both axes, indicating that HOSCN has affected the treated cells in a specific way. In addition, there is an observable difference and separation between the control points and the 100 μM HOSCN treated points, indicating a strong difference between the two. The separation between the control and 100 μM HOSCN treated cells occurs on the PC-1 axis, so a PC-1 loadings plot was generated (Figure 6.10B). This loadings plot indicates which peaks of the spectra are affected the most, causing the separation in the PC-1 axis split between the two treatment conditions. Table 6.1 lists the different peaks identified on the PC-1 loadings plots, which had a clear and observable change in intensity from the baseline.

After the analysis of control and 100 μM HOSCN treated samples, the control and 200 μM HOSCN treated samples were analysed. The results showed that 200 μM HOSCN influenced J774A.1 chemistry very strongly. The PCA scores plot (Figure 6.11A) showed a large separation between control samples and 200 μM HOSCN treated samples across the PC-1 axis, indicating that the variability between the two groups can be primarily explained on the PC-1 loading plot (Figure 6.11B). Interestingly, across the PC-2 axis, there is a very tight grouping of the HOSCN treated group, while the control group is spread across the entire axis (Figure 6.11C), indicating that the natural variation in the control cells can be visualised on the PC-2 loading plot. Tables were constructed to determine which peaks in the spectra were most affected by the 200 μM HOSCN treatment (Table 6.2) with peaks in the fingerprint region, such as nucleic acids, PO_2^-, lactate and carbohydrates found to contribute the most to these differences.

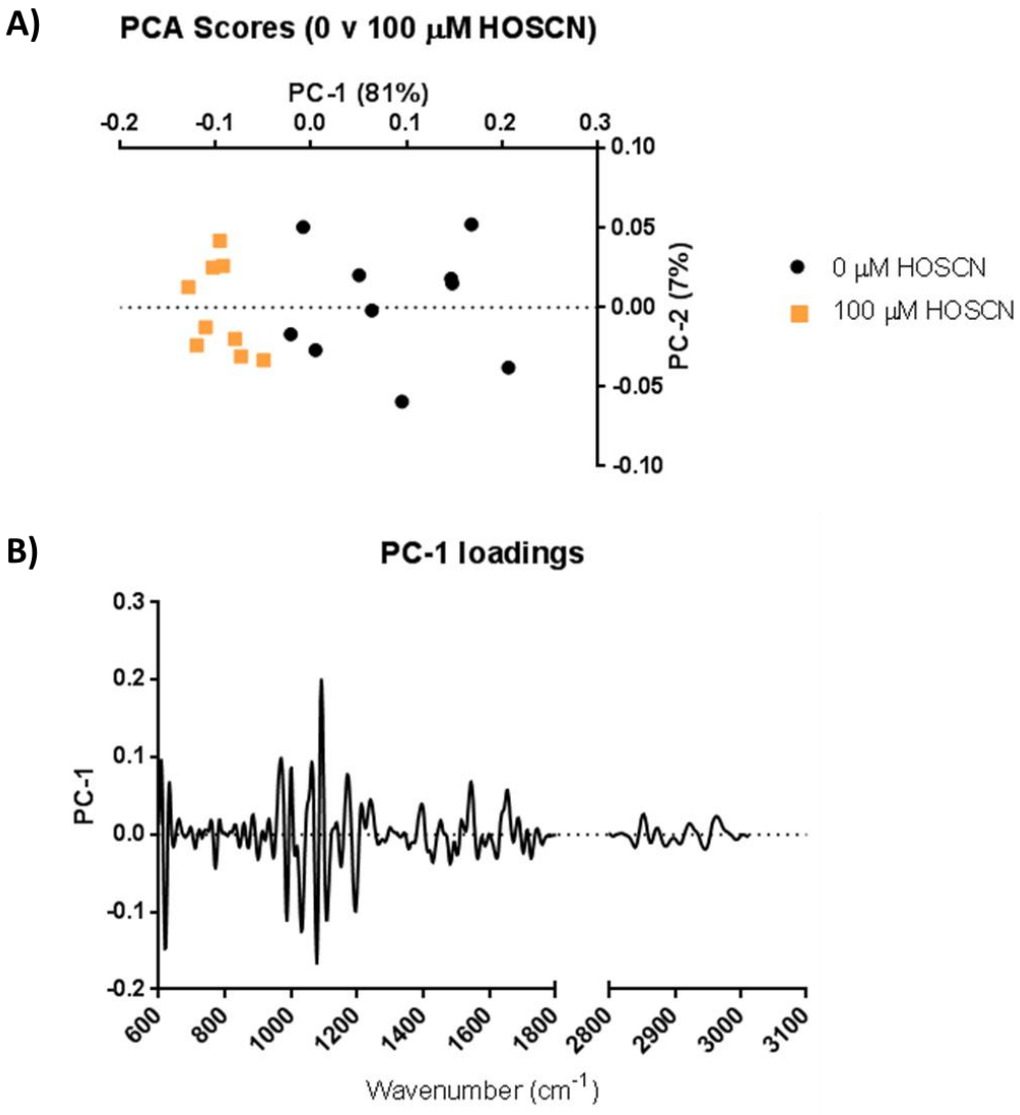

Figure 6.10: PCA of J774A.1 cells treated with 100 µM HOSCN.

Principal component analysis scores and PC-1 loading plots of second derivatives of the spectra (Savitzky-Golay 9 points) comparing control and 100 µM HOSCN treatments. (A) The PCA scores plot comparing control and 100 µM HOSCN on PC-1 and PC-2 axes. (B) The PC-1 loading plot describes where in the spectra the variation occurs. These data show that there is a significant separation between control and 100 µM HOSCN treated cells on the PC-1 axis, indicating that the changes induced by HOSCN at this concentration are significant on a global cellular level.

Table 6.1: Groups identified using PC-1 loadings between control and 100 µM HOSCN treated groups.

Wavenumber (cm^{-1})	Chemical Group
620	N.A. ↓
970	Choline phospholipids (vas) ↓
987	N.A. ↓
1011	Carbohydrates (C-O) ↓
1031	Fatty acids (C-O) ↓
1052	Nucleic acids (C-O) (v) ↓
1080	O-O-C PO_2^- (vs) ↓
1091	N.A. ↑
1105	Glucose (C-O-C) ↓
1152	Lactate (C-O) (v) ↓
1195	N.A. ↓
1400	N.A. ↑
1547	N-H (δ), C-N (v) peptide linkages ↓
1637	Amide I – beta sheet (C=O) ↓

↓ - decrease, ↑ - increase, N.A. – Not available, peak has not yet been identified. Spectral assignments [440-442].

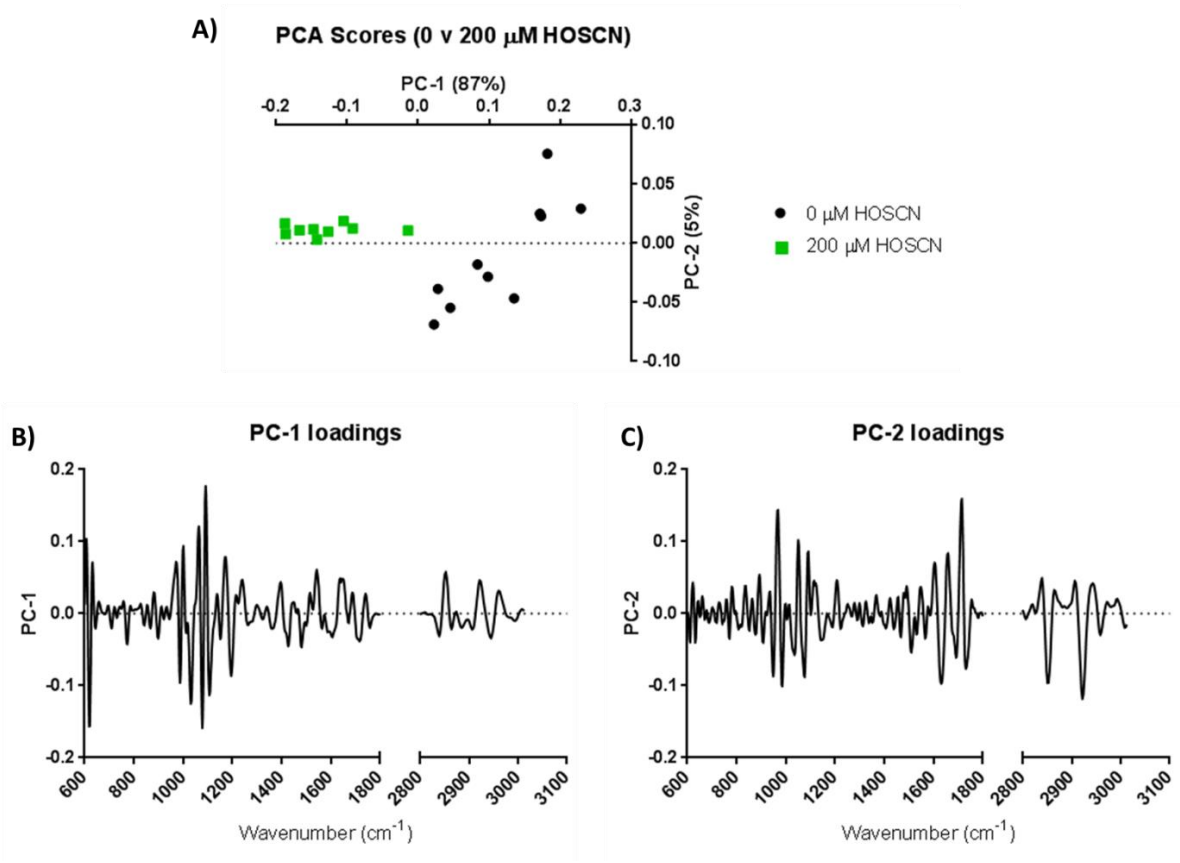

Figure 6.11: PCA score plot of J774A.1 cells treated with 200 µM HOSCN.

Principal component analysis scores and, PC-1 and PC-2 loading plots of second derivatives of the spectra (Savitzky-Golay 9 points) comparing control and 200 µM HOSCN treatments. (A) The PCA scores plot comparing control and 200 µM HOSCN on PC-1 and PC-2 axes. (B) The PC-1 loading plot describes where in the spectra the variation occurs. (C) The PC-2 axis explains the variation in the control data as it is spread across the axis, while 200 µM treated sampes do not move along this axis. These data show that there is a significant separation between control and 200 µM HOSCN treated cells on the PC-1 axis, indicating that the changes induced by HOSCN at this concentration are significant on a global cellular level. The variation on the PC-2 axis explains natural variation across the control cells.

Table 6.2: Groups identified using PC-1 loadings between control and 200 µM HOSCN treated groups.

Wavenumber (cm^{-1})	Chemical Group
620	N.A. ↓
967	Choline phospholipids (vas) ↓
987	N.A. ↓
1011	Carbohydrates (C-O) ↓
1031	Fatty acids (C-O) ↓
1052	Nucleic acids (C-O) (v) ↓
1080	O-O-C PO_2^- (vs) ↓
1091	N.A. ↑
1105	Glucose (C-O-C) ↓
1152	Lactate (C-O) (v) ↓
1195	N.A. ↓
1400	N.A. ↑
1545	N-H (δ), C-N (v) peptide linkages ↓
1637	Amide I – beta sheet (C=O) ↑
1656	Amide I – alpha helix (C=O) ↑
2852	CH_2 (vs) ↑
2927	CH_2 (vas) ↑

↓ - decrease, ↑ - increase, N.A. – Not available, peak has not yet been identified. Spectral assignments [440-442].

Table 6.3: Groups identified using PC-2 loadings between control and 200 µM HOSCN treated groups.

Wavenumber (cm^{-1})	Chemical Group
951	N.A. ↓
967	Choline phospholipids (vas) ↓
987	N.A. ↑
1052	Nucleic acids (C-O) (v) ↓
1080	O-O-C PO_2^- (vs) ↓
1604	N.A. ↑
1637	Amide I – beta sheet (C=O) ↓
1680	Mixed parallel/antiparallel beta sheets/turns ↑
1714	DNA, RNA (C=O) ↑
2852	CH_2 (vs) ↓
2921	c.a. CH_2 (vas) ↓

↓ - decrease, ↑ - increase, N.A. – Not available, peak has not yet been identified; c.a. – approximately. Spectral assignments [440-442].

Interestingly, after generating a PC-2 loading plot for the control and 200 µM HOSCN groups, it was possible to see which peaks in the spectra contributed the most to the natural variation of the control groups, due to their large spread across the PC-2 axis. After generating the PC-2 loading plot (Figure 6.11C), a table was generated listing the major peaks identified in the loadings plot (Table 6.3). The peaks identified indicate that across the untreated J774A.1 cells, the variation occurs across various classes of chemicals, such as the phospholipid membrane, proteins and nucleic acids, with no variation seen in the carbohydrate pool. This suggests that HOSCN is primarily responsible for changes in the carbohydrate, glucose and lactate levels within the J774A.1 cells.

dHOSCN was compared against the control samples using PCA. The data show that there is a cellular response to treatment with dHOSCN with a clear separation between the control and dHOSCN groups on the PC-1 axis. Though, there was one group of dHOSCN treated cells that seemed to be an outlier, appearing in the control sample grouping (Figure 6.12A). The control samples also seemed to be spread across the PC-2 axis, which when analysed

exhibited the same natural variation as the control group from the previous analysis. The PC-1 loadings plot (Figure 6.12B) was generated and Table 6.4 describes which peaks were affected by the dHOSCN treatment, contributing to the separation in the two groups.

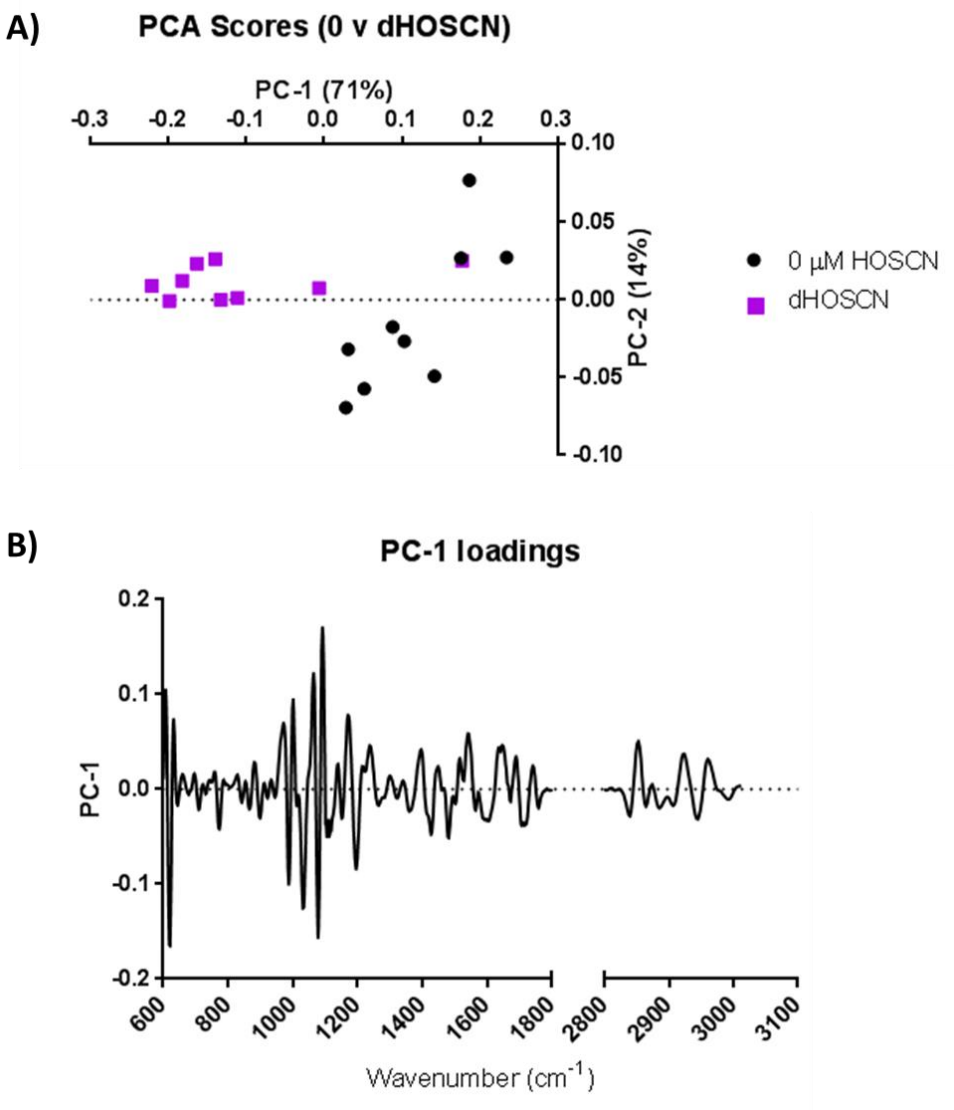

Figure 6.12: PCA scores of J774A.1 cells treated with decomposed HOSCN.

Principal component analysis scores and PC-1 loading plots of second derivatives of the spectra (Savitzky-Golay 9 points) comparing control and decomposed HOSCN treatments. (A) The PCA scores plot comparing control and dHOSCN on PC-1 and PC-2 axes. (B) The PC-1 loading plot describes where in the spectra any variation occurs. These data show that there is a strong separation between control and dHOSCN treated cells on the PC-1 axis, indicating that the changes induced by dHOSCN are significant on a global cellular level.

Table 6.4: Groups identified using PC-1 loadings between control and decomposed HOSCN treated groups.

Wavenumber (cm^{-1})	Chemical Group
620	N.A. ↓
967	Choline phospholipids (vas) ↓
989	N.A. ↑
1033	Fatty acids (C-O) ↓
1080	O-O-C PO_2^- (vs) ↓
1193	N.A. ↑
1385	Terminal CH_3 ↑
1545	N-H (δ), C-N (v) peptide linkages ↑
2852	CH_2 (vs) ↓
2927	CH_2 (vas) ↑
2960	CH_3 (vas) ↑

↓ *- decrease,* ↑ *- increase, N.A. – Not available, peak has not yet been identified. Spectral assignments [440-442].*

After identifying the peaks affected by decomposed HOSCN, it was noted that none of the peaks associated with carbohydrates, glucose or lactate were identified. This corroborates the hypothesis that HOSCN is required to oxidise J774A.1 glycolytic proteins, reducing the level of carbohydrates and lactate within the cell, and it is the oxidative ability of HOSCN that causes this attenuation of glycolysis, and not a latent effect of the non-oxidising components of HOSCN.

Finally, dHOSCN was compared against 200 µM HOSCN. Interestingly, the separation between both treatments occurred on the PC-2 axis, rather than the PC-1 axis (Figure 6.13A). This is indicative of the similarities between both treatments, and the difference on the PC-2 axis is hypothesised to account for the difference in the oxidative ability between both treatments (Figure 6.13B). The differences between 200 µM HOSCN and dHOSCN are primarily attributed to their ability to interact with lipids, proteins and in one case, DNA/RNA. More importantly, the PC-2 axis also shows the ability of 200 µM HOSCN to influence the glucose and lactate concentration in J774A.1 cells. Table 6.5 lists the different peaks

identified on the PC-2 loading plots, which had a clear and observable change in intensity from the baseline.

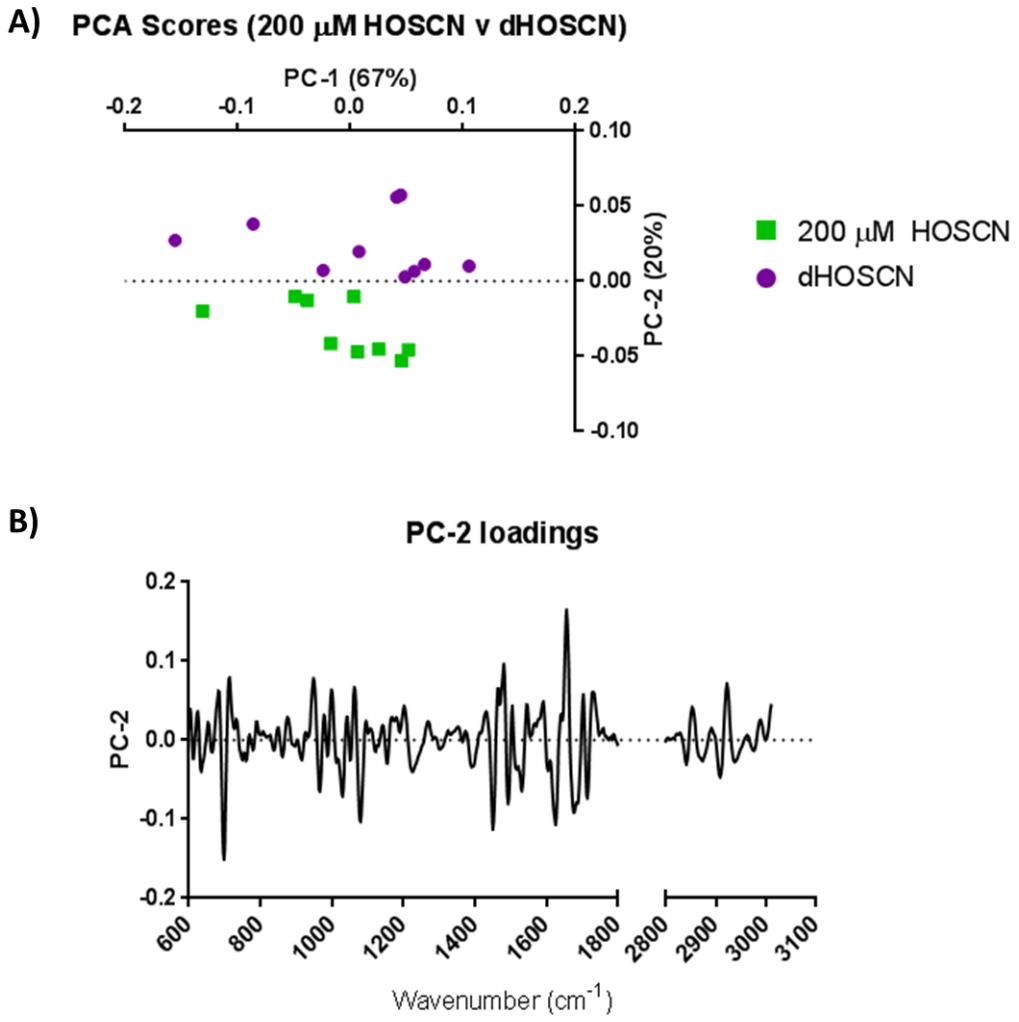

Figure 6.13: PCA scores of J774A.1 cells treated with 200 µM HOSCN or decomposed HOSCN.

Principal component analysis scores and PC-2 loading plots of second derivatives of the spectra (Savitzky-Golay 9 points) comparing 200 µM HOSCN and decomposed HOSCN treatments. (A) The PCA scores plot comparing 200 µM HOSCN and dHOSCN on PC-1 and PC-2 axes. (B) The PC-2 loading plot describes where in the spectra any variation occurs. These data show that there is a separation between 200 µM HOSCN and dHOSCN treated cells on the PC-2 axis, indicating that the differences between both treatments are significant on a global cellular level.

Table 6.5: Groups identified using PC-2 loadings between 200 µM HOSCN and dHOSCN treated groups.

Wavenumber (cm^{-1})	Chemical Group
715	Rocking band of methylene in lipid chains ↓
1080	O-O-C PO_2^- (vs) ↓
1105	Glucose (C-O-C) ↓
1152	Lactate (C-O) (v) ↓
1452	N.A. ↓
1494	N.A. ↓
1637	Amide I – beta sheet (C=O) ↓
1656	Amide I – alpha helix (C=O) ↑
1685	c.a. Mixed parallel/antiparallel beta sheets/turns ↓
1714	DNA, RNA (C=O) ↑
2927	CH_2 (vas) ↓

↓ - decrease, ↑ - increase, N.A. – Not available, peak has not yet been identified. c.a. – approximately. Spectral assignments [440-442].

6.4.4.1 HOCl induces changes to J774A.1 macrophages in a similar manner to HOSCN

PCA was also performed to compare control cells with cells treated with 200 µM HOCl. The data indicate that HOCl also causes significant changes to the chemistry of J774A.1 cells (Figure 6.14A), with a similar pattern of separation between control and 200 µM HOCl, and control and 200 µM HOSCN. Between the control group and the HOCl treatment group, the separation occurs mainly on the PC-1 axis, so a PC-1 loading plot was generated (Figure 6.14B) and the peaks which contributed most to the separation, and therefore were most affect by HOCl were listed in Table 6.6. The control group was spread throughout the PC-2, similar to the 200 µM HOSCN and dHOSCN treatments, and the variation on this axis explains the natural variation between the cells in the control group.

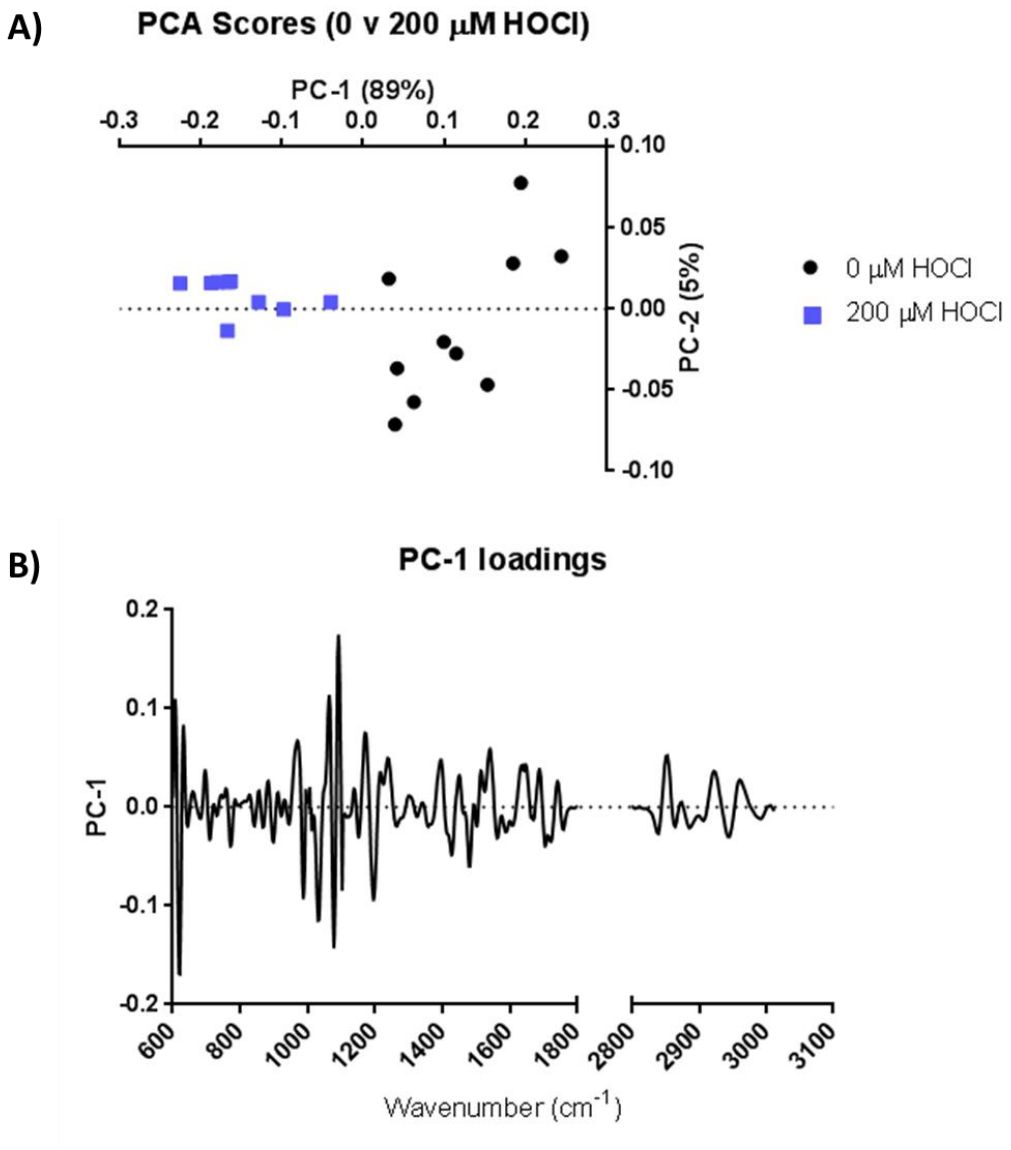

Figure 6.14: PCA score plot of J774A.1 cells treated with 200 µM HOCl.

Principal component analysis scores and PC-1 loading plots of second derivatives of the spectra (Savitzky-Golay 9 points) comparing control and 200 µM HOCl treatments. (A) The PCA scores plot comparing control and 200 µM HOCl on PC-1 and PC-2 axes. (B) The PC-1 loading plot describes where in the spectra any variation occurs. These data show that there is a strong separation between control and 200 µM HOCl treated cells on the PC-1 axis, indicating that the changes induced by 200 µM HOCl are significant on a global cellular level.

Table 6.6: Groups identified using PC-1 loadings between control and 200 µM HOCl treated groups.

Wavenumber (cm^{-1})	Chemical Group
620	N.A. ↓
989	N.A. ↑
1033	Fatty acids (C-O) ↓
1052	Nucleic acids (C-O) (v) ↓
1080	O-O-C PO_2^- (vs) ↓
1093	N.A. ↑
1242	P=O (v), PO_2^- (vas) ↑
1398	N.A. ↓
1483	N.A. ↓
1545	N-H (δ), C-N (v) peptide linkages ↑
1637	Amide I – beta sheet (C=O) ↑
2852	CH_2 (vs) ↑
2927	CH_2 (vas) ↑
2960	CH_3 (vas) ↑

↓ *- decrease,* ↑ *- increase, N.A. – Not available, peak has not yet been identified. Spectral assignments [440-442].*

Once again, after identifying the peaks in the spectra that contributed most to the separation between the control and 200 µM HOCl treatment groups, many of the differences noted between the control and HOCl treated cells occurred to the phospholipid membrane, proteins, nucleic acids and fatty acids. Interestingly the carbohydrates, glucose and lactate were not identified in the control and HOCl principal component analysis, a similar result to the control and dHOSCN principal component analysis. This suggests that HOCl and dHOSCN alter the chemistry of J774A.1 cells in a different manner than HOSCN, in accord with data reported in the previous Chapters. Thus, results are consistent with HOSCN rather than HOCl or the non-oxidative decomposition products of HOSCN causing a loss in glycolytic ability.

6.5 Discussion

This Chapter examined the pattern and the extent of damage caused to J774A.1 macrophages after treatment with HOSCN, HOCl and decomposed HOSCN (dHOSCN). HOCl (200 µM) was used as a comparison for cell damage caused by HOSCN while dHOSCN was used as a non-oxidative (negative) control for HOSCN-induced damage. Exposure of J774A.1 macrophage cells to HOSCN, HOCl and dHOSCN resulted in changes to the biochemistry of the cells, which could be monitored by IR spectroscopy. All the treatments caused some perturbation or changes in the relative abundance of lipids, proteins and nucleic acids, while only HOSCN was able to attenuate the detection and/or abundance of carbohydrate and lactate vibrational modes. Those results do not necessarily indicate a direct reaction of the targets with any of the treatments; the results represent changes in the vibrational mode of specific bonds contained within specific molecules. For example, the decrease in the detection of glucose and lactate correlates with data obtained in previously published studies and in Chapter 4 of this Thesis. However, in Chapter 4, the decrease is the result of an inhibition of glycolytic proteins by HOSCN [199, 201], resulting in a decrease in the formation of glycolytic end-products such and pyruvate and lactate.

The spectra of J774A.1 cells can be analysed as 3 distinct areas. The first is the CH region (ca. 2800 – 3000 cm^{-1}), and changes in CH_2 vibrational modes (both vs and vas) were observed with 200 µM HOSCN, 200 µM HOCl and dHOSCN. These CH_2 peaks correspond with the fatty acyl chain of the phospholipid membrane [443]. Reaction of J774A.1 cells with 200 µM HOCl may result in the formation of fatty acyl chlorohydrins on the cell membrane, as has been shown to occur to red blood cell membrane extracts upon exposure to HOCl [180]. The alteration of CH_2 vibrational modes may also occur after treatment of dHOSCN with the J774A.1 cells, though it is not possible to determine the nature of the modification, as the decomposition products of HOSCN are a complex mixture [75, 76]. It is possible that dHOSCN may cause carbamylation of the phospholipid acyl chain via the formation of cyanate (^{-}OCN) which is a major product of HOSCN decay [77, 93]. The results also indicated that 200 µM HOSCN induced changes to the vibrational mode of CH_2 peaks (both vas and vs), though no data exists indicating that HOSCN would react directly with the CH_2 bonds of phospholipids indicating that this may be a secondary effect of HOSCN oxidation, or indeed a decomposition product of HOSCN.

The second spectral area of the J774A.1 cells is the protein region (1800 – 1450 cm^{-1}), consisting mainly of protein related peaks that relate to protein structure and backbone

chemistry, and two peaks that are not protein related. The PCA loadings and scores, and the FTIR results of this region indicate that HOSCN and HOCl both have a significant effect on J774A.1 protein chemistry and structure, while dHOSCN, though not as effective, also has a role influencing protein stretches and structure. Tyrosine, an aromatic amino acid that plays a role in many signal transduction processes [444], was significantly affected by HOCl treatment. The vibrational mode altered is related to the stretching of the aromatic C-C bonds of tyrosine. The reaction of HOCl with tyrosine results in the addition of a chlorine atom to the 3-position of the aromatic ring, forming 3-chlorotyrosine [299], this new asymmetry in the phenol ring results in an altered vibration. Unexpectedly, increases were also detected in HOSCN-treated samples (≥ 100 µM), though HOSCN demonstrates low reactivity with tyrosine [49]. This increase could be a secondary effect of HOSCN treatment, as previously published data has shown that HOSCN can inhibit protein tyrosine phosphatases (PTPs) via the oxidation of active-site cysteines [179]. Therefore, the result obtained by this experiment could indicate that the increase in tyrosine recognition (via C-C stretching of the phenol ring) is due to a decrease in phosphate removal from tyrosine residues by PTPs, as the phosphate (PO_4^{3-}) would act similarly to the Cl^-, increasing the asymmetry of the C-C bond, resulting in increased detection.

Increases were also detected on the amino and carboxyl group of amino acids. J774A.1 cells treated with ≥ 50 µM HOSCN or 200 µM HOCl saw an increase in the vibrational mode of the N-H (δ) or C-N (ν) peptide linkage, while treatment with 200 µM HOSCN, HOCl or dHOSCN led to a significant increase in the carboxyl vibrational mode. These may indicate some reaction of the oxidants with these groups, though it is unexpected as amino acid side chains, such as cysteine, are more favourable targets [11, 49]. It is likely that the increases in the backbone vibrational modes correlate with changes in the protein secondary structure and the increases in the amide I – β-sheet vibrational mode. Treatment of J774A.1 cells with ≥ 50 µM HOSCN or 200 µM HOCl caused increases in the vibrational intensity, and possibly the formation of structures correlating with β-sheets. The oxidation of cysteine residues by HOSCN or HOCl can cause the formation of inter-strand disulfide bonds [95, 107, 380], and while it is rare to find disulfide bonds in β-sheets, data suggests that the formation of disulfides helps to stabilise and define the extent of β-sheet secondary structure [445]. This disulfide bond formation and β-sheet stabilisation would account for the increase in the amide I - β-sheet vibrational mode. The protein amide I – α-helix also experienced a decrease in vibrational mode after 200 µM HOSCN treatment, which could be attributed to a conformational transition (α-helix to β-sheet) due to oxidant treatment [446-450].

In the third spectral area (1450 – 700 cm^{-1}), the fingerprint region, there are numerous peaks that correspond with many different chemical groups, not all of which have been identified. Of the identified peaks, many were affected by HOSCN or HOCl treatment, while none were affected by dHOSCN. The most interesting changes have been attributed to molecules that are related to the glycolytic pathway, such as carbohydrates, glucose and lactate. After the treatment of J774A.1 cells with HOSCN, decreases were observed in the vibrational modes and PCA loadings of carbohydrates (≥ 100 μM) and glucose (200 μM), which was an unexpected result. Results of the previous Chapter indicate that HOSCN inhibits glycolytic proteins without influencing the uptake of glucose by J774A.1 cells. However, the glucose uptake assay performed in Chapter 4 was performed using a fluorescent glucose analog, 2-NBDG, which cannot be phosphorylated by hexokinase, the first enzyme of glycolysis, which prepares glucose for further catabolic steps. In cells treated with HOSCN, it has been shown that GAPDH, the sixth glycolytic enzyme, is inhibited [201]. The result is the catabolism of glucose by hexokinase and downstream enzymes up until GAPDH, leading to a reduction of carbohydrate and glucose levels, and a build-up in glyceraldehyde 3-phophate levels without a payoff of ATP, pyruvate or NADH. The FTIR also revealed a decrease in the lactate concentration, which corroborates with the data obtained in Chapter 4. A decrease in the lactate concentration can be explained by the inhibition of glycolysis, inhibiting the formation of pyruvate, which is converted to lactate by LDH, serving as a marker for glycolytic activity [334].

After the completion of these experiments it became clear that FTIR and PCA are reliable and accurate measures for determining oxidant damage within cellular systems. The use of principal component analysis allowed for the computation of large data sets without bias. The resulting plots allowed for the determination of treatment efficacy (PCA scores) and favourable targets within the samples (loadings plots). Using these plots, the pattern of damage caused by HOSCN, HOCl and also dHOSCN was clearly visible. Despite the similarities between the treatments used, there were subtle and specific changes that occur, which are dependent on the treatment. Specifically, HOSCN was able to induce changes in the vibrational mode of proteins, lipids, nucleic acids and molecules involved in glycolysis.

6.6 Summary

The study in this Chapter demonstrated that HOSCN and HOCl-induced damage to J774A.1 macrophages can be identified using FTIR spectroscopy and principal component analysis. The results show that the damage caused by HOCl extends to lipids, proteins and nucleic acids while HOSCN is also able to induce changes in the vibrational mode of lipids, proteins, nucleic acids and carbohydrates including glucose, corroborating data from a previous Chapter. Further corroboration was revealed after determining that lactate could be identified using FTIR, and the inhibition of the lactate vibration further supports HOSCN as an inhibitor of glycolysis. The final study of this Thesis will further investigate the role of HOSCN in cellular damage by using Raman spectroscopy and microscopy to image and map the damage caused to cells after HOSCN-induced oxidation.

7 Using Raman Spectroscopy to Image Hypothiocyanous Acid-Induced Damage

7.1 Introduction

A common method of interrogating cells is via the use of microscopy. There are multiple microscopy techniques including bright field microscopy, which uses simple illumination of the sample, dark field microscopy, which is used to improve the contrast of unstained samples, and phase contrast microscopy, which allows for the visualisation of differences in refractive index of a sample as changes in contrast [451-453]. Another widely used microscopy technique is fluorescent microscopy, which requires the use of fluorescent probes or conjugated antibodies. Although a powerful technique, there are some limitations in the use of fluorescent probes in biological studies. For example, fluorophores can undergo photo-bleaching, which occurs as they are illuminated by the microscope light, due to the excitation of electrons during fluorescence [454]. Another limitation of fluorescent microscopy stems from the specificity of the fluorescent probes. Fluorescent microscopy only allows for the observation of structures that have been labelled with the fluorophore, for example, the fluorophore, 4',6-diamidino-2-phenylindole (DAPI) is used widely to image DNA [455]. DAPI only binds to the A-T rich regions of DNA, so only the DNA within the cell is imaged and nothing else about the cell is revealed [456]. Another fluorescent probe is dihydroethidium (DHE), which is used to monitor ROS-induced damage *in vitro* [457, 458]. DHE also has limitations in its use, including auto-oxidation, photo-oxidation and photo-conversion, interfering with oxidant reactivity and the knowledge of the concentration-response relationship between the probe and the substrate [459]. Finally, the target must be known in order to employ the correct probe, therefore the use of this technique to interrogate HOSCN-induced damage is difficult, as the reactivity of HOSCN is limited to thiols. Difficulty assessing damage *in vivo* is also compounded by the lack of a HOSCN-specific biomarker. Unlike 3-chlorotyrosine, which allows for the visualisation of HOCl-induced damage using an antibody approach, there currently is no probe to detect HOSCN-induced damage [460, 461].

Raman spectroscopy is an alternative technique that can be used to map cellular damage with the advantage of no requirement for probes. When monochromatic light interacts with the covalent bonds of a sample, the interaction can result in the shifting of the energy of the light (Stokes Raman scattering; decrease in energy, Anti-Stokes Raman scattering; increase in energy), and the degree of the shift allows for the determination of a chemical bond and group within a sample. By measuring the Raman scattering (inelastic scattering), an entire cell can be interrogated, and the gross chemical make-up or chemical 'fingerprint' can be

determined, along with a visual map of the cell that displays where in the cell certain chemical groups exist [462].

Recently, due to its ability to identify a wide range of chemical groups within a sample, Raman spectroscopy and mapping has been used as a diagnostic tool in every step of disease screening and treatment. For example, Raman spectroscopy has been used in studies analysing the chemical composition of skin, determining the possible pathological state and investigating the kinetics of drug penetration into the various dermal layers [463]. Due to its ability to discriminate between chemical compositions of different samples, Raman spectroscopy has also been used to determine the chemical changes in cancer cell formation, for use in a diagnostic setting [464-466]. Given that Raman spectroscopy can be used to generate image maps in the absence of chemical probes, the method allowed for an alternative way to image HOSCN-induced oxidative damage to macrophages.

7.2 Aims

The aim of the study presented in this Chapter is determine whether HOSCN-induced oxidative damage to J774A.1 macrophages can be visualised using Raman spectroscopy. This proof-of-concept study was also extended to utilising Raman microscopy techniques to gain spatial and qualitative data on J774A.1 cells with and without oxidant treatment.

7.3 Methods

7.3.1 Preparation of J774A.1 macrophages

7.3.1.1 J774A.1 murine macrophage cells

The cell experiments performed in this Chapter were carried out using J774A.1 cells, a murine macrophage-like cell line.

Prior to the experiment, cells were washed with fresh DMEM, followed by scraping from the flasks (175 cm^2) into 10 mL of DMEM and counted using a haemocytometer in the presence of 0.2% v/v trypan blue to exclude dead cells. Cells were then centrifuged in an Allegra X-15R centrifuge (Beckman Coulter) at 400 *g* for 5 min at 22 ˚C to form a cell pellet. The pellet was resuspended in DMEM to the required density of cells (1×10^6 cells mL^{-1}) before being

transferred to a 12-well cell culture plate at a density of 1×10^6 cells/well and incubated in a sterile environment, overnight at 5% CO_2 and 37 ˚C.

7.3.1.2 Oxidant treatment of J774A.1 cells

For the experiments detailed in this Chapter, cells were plated at 1×10^6 cells/well in DMEM and allowed to adhere in a 12-well plate, in an incubator, overnight at 5 % CO_2 and 37 ˚C. The next day, cells were washed twice with HBSS prior to incubation with 3 mL of either a control solution (HBSS) or HOSCN (200 µM) in HBSS for 1 h at 22 ˚C. Following oxidant treatment, the media was removed from the cells and the cells were washed with HBSS to prevent any reactions resulting from residual oxidant of media components.

7.3.1.3 Preparing cells on calcium fluoride slides

Calcium fluoride (Crystran, UK) was chosen as the surface for plating cells as it is transparent over a wide range of light frequencies (single Raman peak at 312 cm^{-1}) and silicon nitride (used for FTIR) can auto-fluoresce in the conditions used for Raman spectroscopy.

After oxidant treatment and washing, the cells were resuspended in 1 mL HBSS:H_2O (1:1) (this ratio was used to reduce the salt concentration within the media) at 1×10^6 cells/mL and counted using a haemocytometer in the presence of 0.2 % v/v trypan blue. Cells were then centrifuged in an Allegra X-15R centrifuge (Beckman Coulter) at 400 *g* for 5 min at 22 ˚C to form a cell pellet. The pellet was then resuspended to the required density of cells (1×10^6 cells/ 500 µL). After resuspension, 10 µL of the sample was pipetted onto the calcium fluoride slide, making sure to keep the slide horizontal, as to avoid movement and clumping of the cells within the sample.

After loading samples onto the calcium fluoride slide, the slide was left to rest in sterile conditions for 20 min at 22 ˚C, before being transferred into a desiccator and left for 1 h at 22 ˚C to remove moisture from the sample, before being analysed, as described below, using a Renishaw inVia Raman microscope.

7.3.2 Raman microscopy and mapping

The instrument used for Raman microscopy was a Renishaw inVia (United Kingdom) coupled to a light microscope to allow for visualisation of the sample before testing. The calcium fluoride slide was placed on the sampling stage and the cell to be sampled was centred in the middle of the viewing area. Before mapping, the Raman laser was set to 785 nm at 50 % power and mapping was performed by sampling the Raman shift between 400 – 3200 cm^{-1}. The resolution used was chosen based on optimisation steps taken, quality and time required to map. 1 µm steps were chosen, with each step taking ca. 3 min (each cell took ca. 3 h to map).

7.3.3 Data processing

Once the data was acquired using the Renishaw inVia, the raw data were processed using WiRE (4.1, Renishaw, United Kingdom). First the maps were loaded onto the software and the data were analysed to remove cosmic rays that interfere with the data acquisition. Using the 'cosmic ray removal' tool. Cosmic rays were removed by identifying them by their characteristically sharp peaks and 'width of features' algorithm was employed and was set to a width parameter = 3 and a height parameter = 15.

After the cosmic rays were removed, vector normalisation, which calculates the average y-values and divides it by the square root of the sum. The peaks could then be compared by using an integration method, which allows for the calculation of peak heights by drawing a straight line between the peaks of the two frequency limits defined. Each peak was analysed separately using this method, after which, the peak heights were compared to each other.

For both the control and HOSCN treated cells, a noise filter level of 3 was chosen, which explained > 99 % of the variance within the data. Once completed, the heat maps were generated, which allowed for the visualisation of data variance and they were analysed by employing a 'signal to baseline' algorithm. After the peak was identified, normalisation was performed by adjusting the 'min' and 'max' states of the look-up table (LUT) between the control and HOSCN treated samples, and setting them equally.

7.4 Results

7.4.1 Optimisation of Raman spectroscopy

7.4.1.1 Determination of cell media salt concentration

To determine the correct conditions required to obtain Raman spectra, various permutations were tested using the Renishaw inVia Raman microscope. Because the samples were living cells, HBSS was used throughout the cell preparation steps. The use of 1 × HBSS caused the formation of large crystals on the slide which caused salt artifacts to occur within the Raman spectra. To determine an optimal salt concentration, serial dilutions of HBSS were prepared with H_2O (1:0, 3:1, 1:1 and 1:3 – HBSS:H_2O) then images were taken. The images show that a ratio of 1:0 and 3:1 (HBSS:H_2O) resulted in extensive crystal formation, leading to cells being trapped within the formed crystals (red arrows) (Figure 7.1A & B). A ratio of 1:1 resulted in the trapping of fewer cells within salt crystals, and fewer salt crystals being formed (Figure 7.1C). Finally, a ratio of 1:3 resulted in minimal salt crystal formation, but resulted in cell blebbing and irregularity in shape (black arrows), which was hypothesised to be a result of the lack of salt within the media, causing an osmotic accumulation of H_2O within the cells (Figure 7.1D).

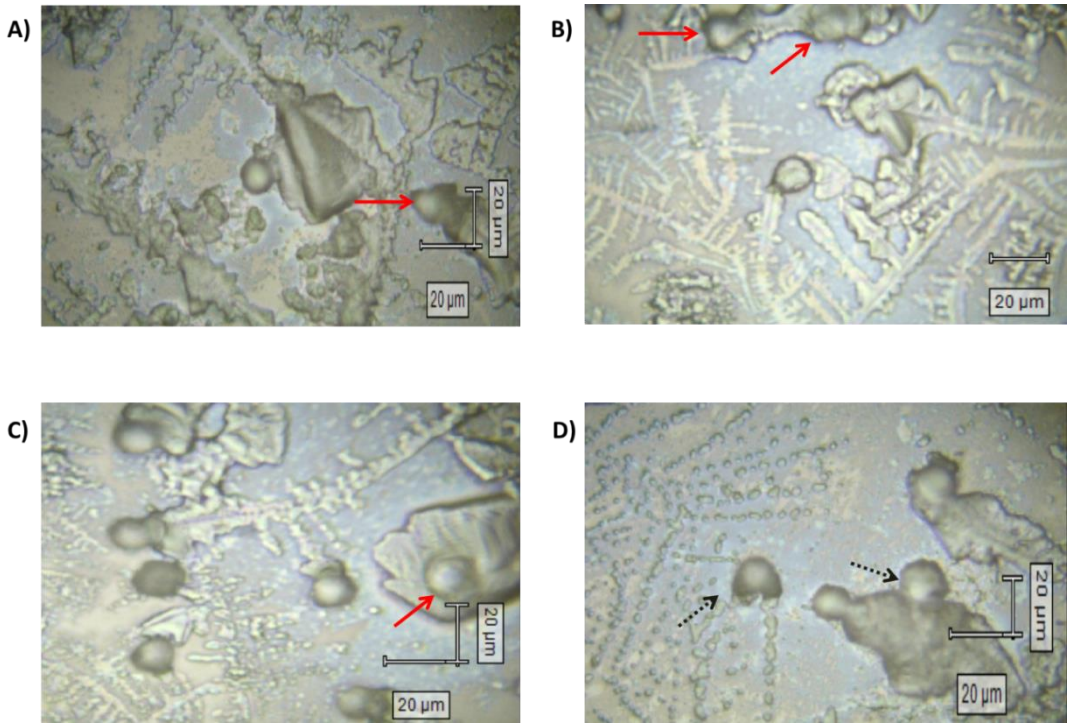

Figure 7.1: Optimisation of HBSS concentration for J774A.1 cell resuspension.

J774A.1 cells were resuspended in various concentrations of HBSS in H_2O to determine the optimal concentration of salt in the resuspension solution, before being plated onto stainless steel slides. A) J774A.1 cells in 100 % HBSS, B) J774A.1 cells in 75 % HBSS, C) J774A.1 cells in 50 % HBSS and D) J774A.1 cells in 25 % HBSS. The image is a representative of 1 experiment run in triplicate. Red arrows indicate cells trapped within salt crystals. Black dashed arrows indicate blebbing and irregularly shaped cells.

7.4.1.2 Optimisation of plating surface material and laser power

After optimising the concentration of HBSS to resuspend cells, stainless steel was chosen as the plating material due to the ease of handling and cost, rather than calcium fluoride, which is markedly more expensive and difficult to handle. To begin, a 512 nm laser was chosen to probe the cells for Raman shift between 600 – 1700 cm^{-1}, but this led to the burning and destruction of cell samples at all the power levels tested (results not shown). A weaker laser was chosen (785 nm) and laser settings were applied to a data optimised mode (DOM), which increased scan time to improve peak identification (3.18 s per point, 100 % laser power). However, preliminary experiments using stainless steel were unsuccessful as spectra were weak, leading to a loss in peak differentiation (Figure 7.2A).

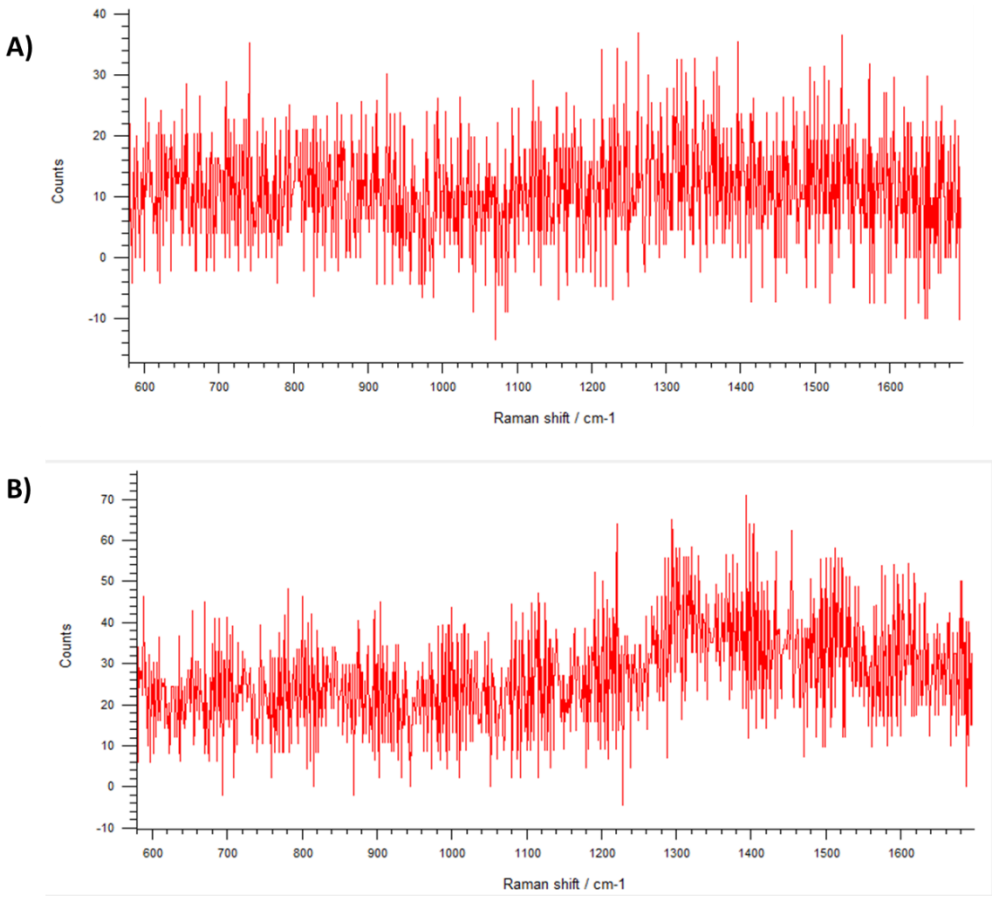

Figure 7.2: A comparison of stainless steel and calcium fluoride.

The raw spectra of single, J774A.1 cells on A) Stainless steel and B) calcium fluoride plating surfaces. The results show very little differentiation and weak intensity of the Raman spectra when J774A.1 cells were plated on stainless steel. When J774A.1 cells were plated on calcium fluoride, both the differentiation and intensity improved using the same laser settings at 785 nm (DOM = 3.18 s per point, 100% laser power).

When J774A.1 cells were plated on calcium fluoride then probed using the same laser setting as previously (785 nm, DOM = 3.18 s per point, 100% laser power), peak intensity (counts) and differentiation improved significantly, which allowed the data to be analysed and the chemical peaks to be extracted using second derivative Fourier transform (not shown) in WiRE 4.0. After determining the correct laser settings and surface material, Raman mapping was performed on cells treated with or without HOSCN.

7.4.2 HOSCN affects the Raman scattering of J774A.1 cells

The previous Chapter has shown that HOSCN-induced changes to cellular components can be identified by using infra-red spectroscopy coupled with principal component analysis. By using these methods, a pattern of the damage caused to J774A.1 cells by HOSCN was identified, including changes to proteins, lipids and the concentration of carbohydrates within the cells, and compared to that seen with decomposed HOSCN and HOCl. The study presented in this Chapter utilises Raman spectroscopy to map and visualise the changes that occur in J774A.1 cells after HOSCN-induced oxidation.

J774A.1 cells (1×10^6 cells/well) were treated with either a control solution (HBSS) or 200 µM HOSCN for 1 h at 22 ˚C. After treatment the cells were washed in HBSS, and then the cells were set onto a calcium fluoride slide before being desiccated for 1 h at 22 ˚C to remove moisture from the sample. The cells were then analysed using a Renishaw inVia Raman spectrometer coupled to a light microscope at 785 nm. The Raman scattering was recorded (400 – 3200 cm^{-1}) at 1 µM spots across the entire cell. The results show gross changes in the Raman scattering between the control and HOSCN-treated samples across the entire spectrum (Figure 7.3). Upon observation, large changes can be seen in the quantity of lipids, proteins, nucleic acids and carbohydrates in the J774A.1 cells. Though it must be mentioned that this data is preliminary with further experiments needed to improve the conditions used for the spectroscopy portion of this experiment.

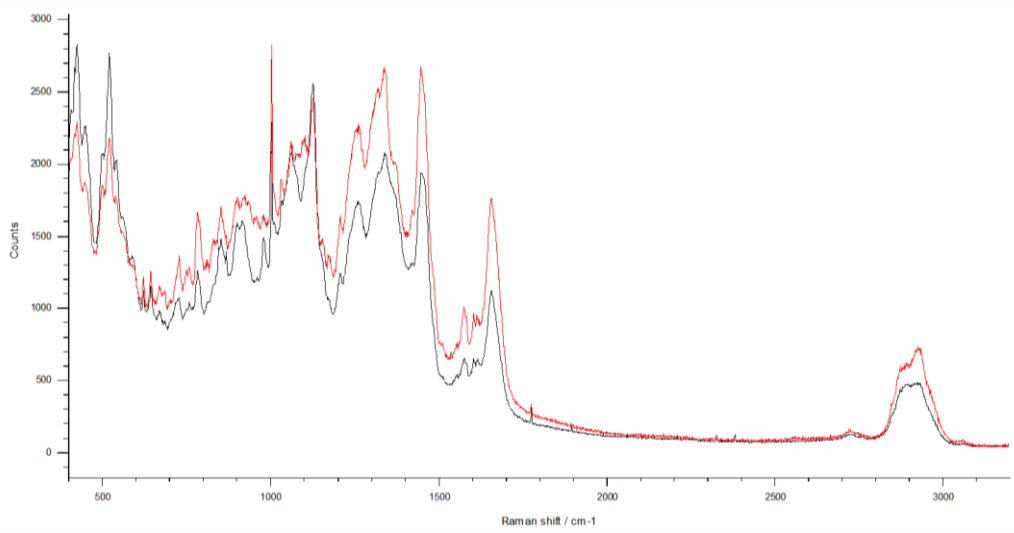

Figure 7.3: The Raman spectra of J774A.1 macrophages is affected by HOSCN

Raw single cell Raman spectra of control (red) and HOSCN (200 µM) (black) treated J774A.1 cells plated on calcium fluoride slides. The spectra were obtained by interrogating the cells with monochromatic light at 785 nm at 50 % power and recording the Raman scattering between 400 – 3200 cm^{-1}, then the individual spectra were averaged and compiled. No normalisation was performed on these spectra as normalisation was performed on a peak-by-peak basis. The presented spectrum is a representative spectrum of 3 different experiments.

7.4.3 HOSCN interacts with and alters lipids in J774A.1 cells

After treating the cells with HOSCN (200 µM), there were numerous changes in lipid composition and location in J774A.1 cells. There were changes in the CH region (2810 – 3026 cm^{-1}) after HOSCN treatment, with a decrease in the heat map density. This is consistent with reaction of HOSCN with the lipid membrane of the J774A.1 cells (Figure 7.4A). The lipid/protein region (2859 – 2901 cm^{-1}) was also affected by HOSCN, the heat map shows the formation of another hot spot (red), indicating that the membrane of the J774A.1 cell is being altered and indicates a change in the shape of the cell after HOSCN treatment (Figure 7.4B). The membrane of mammalian cells contain high levels of unsaturated fatty acids (UFA) [467]. In the non-treated cells, UFA (1624 – 1706 cm^{-1}) can be detected throughout the cell, consistent with localisation of these species to the cell membrane. The results also indicate that treatment with HOSCN greatly reduces the concentration UFAs or alters the environment surrounding UFAs in J774A.1 cells (Figure 7.4C).

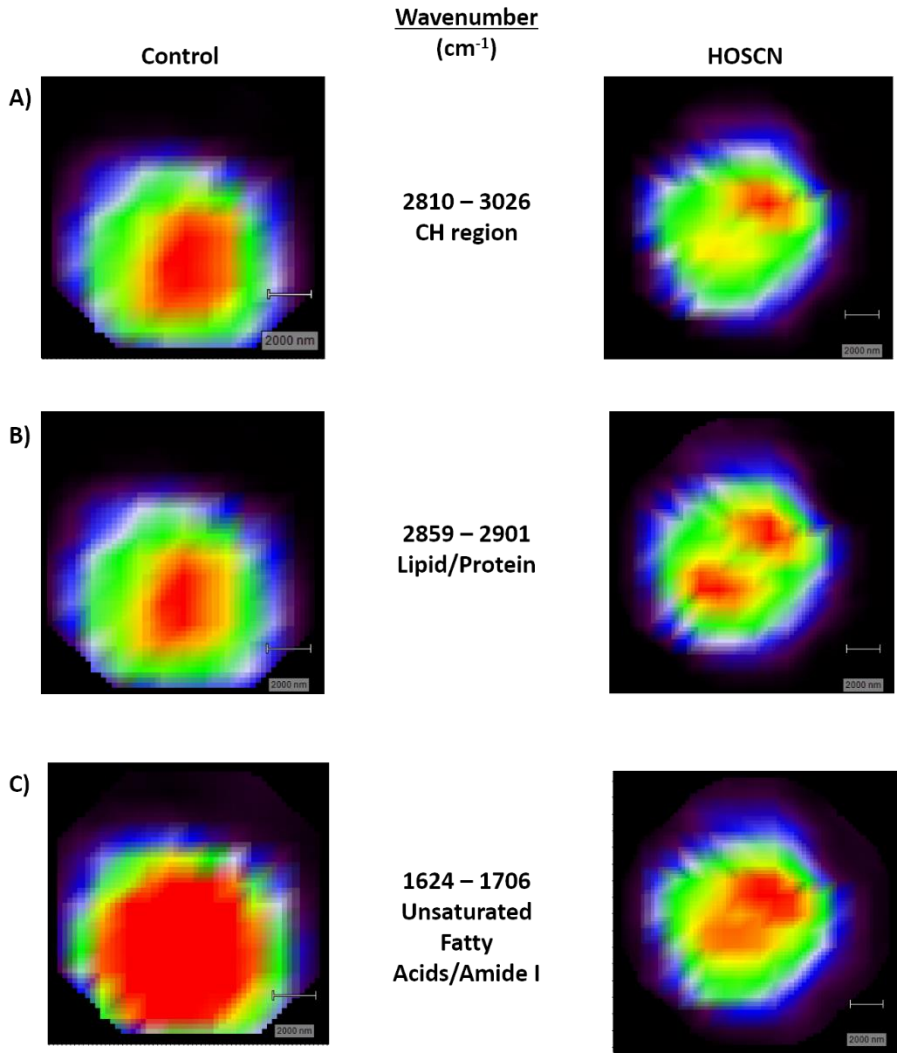

Figure 7.4: Raman heat maps of peaks related to lipids and fatty acids in J774A.1 cells.

J774A.1 cells (1 × 10^6) were treated either with a control solution (HBSS) or HOSCN (200 µM) for 1 h at 22 ˚C before single cells were interrogated with a Renishaw inVia Raman spectrometer and microscope. After performing a cosmic ray removal and principal component analysis (noise filter), a map of the cell was created using peaks to visualise the location and relative concentration of various molecules. (A) The 2810 – 3026 cm^{-1} peak which correlates with scattering of CH bonds. (B) The 2859 – 2901 cm^{-1} peak which correlates with the scattering of lipids and proteins. (C) The 1624 – 1706 cm^{-1} peak which correlates with the scattering of unsaturated fatty acids. The maps are a visualisation of the principal components and representative of the maps generated in 3 separate experiments.

7.4.4 HOSCN interacts and alters the proteins of J774A.1 cells

After J774A.1 cells were treated and interrogated using the Renishaw inVia Raman spectrometer, maps were created to visualise the peaks that correlated to proteins in the cells. Because proteins occur in large concentrations within the cytosol and in the cellular membrane, due to the resolution used in the imaging of the cells, it is currently not possible to determine where the imaged proteins occur within the samples.

Upon analysis of the spectra (Figure 7.3), changes in the protein peaks were easily identified and the maps indicate that HOSCN alters the concentration and localisation of proteins within treated cells. The protein region (2902 – 2954 cm^{-1}) indicates that proteins are located throughout the entire cell in the untreated cells, possibly in the cytosol, due to the decrease in the heat map intensity around the cell border. Treating the cells with HOSCN (200 µM) causes a loss in protein distribution, conversely, because the protein region is related to protein structure, the loss of heat map intensity could indicate a loss in protein structure (Figure 7.5A). This indicates that HOSCN has altered protein structure, in a way that causes a decrease in Raman scattering. After treating the cells with HOSCN (200 µM), a decrease is also seen in the protein/lipid peak (1426 – 1491 cm^{-1}) (Figure 7.5B) in the J774A.1 cells. This is indicative of changes to both intracellular proteins and membrane bound proteins, indicating an interaction of HOSCN with these elements.

The amide III band (1216 – 1280 cm^{-1}) consists of C-N stretching and N-H bending bands and correlates primarily with protein structure. This peak can give information about cellular protein structure, and in non-treated cells the heat map shows a large distribution of protein in the middle of the cell. Exposure of cells to HOSCN results in a decrease in amide III peak intensity, while also altering amide III distribution in J774A.1 cells (Figure 7.5C). This result is consistent with the idea that HOSCN treatment alters protein structure and location within the cell after treatment, while the tighter grouping and splitting of the amide II peak group into two separate groups being consistent with protein aggregation.

Finally, the last peak identified was the peak the correlates with protein disulfide bond stretching (502 – 535 cm^{-1}). The results show that disulfides are present in the untreated cells and treating J774A.1 cells with HOSCN (200 µM) increases disulfide bond distribution within the J774A.1 cells (Figure 7.5D). This result is consistent with the chemistry of HOSCN, as the oxidation of thiols by HOSCN causes the formation of a sulfenyl thiocyanate, this product can react with neighbouring thiols to form a disulfide bridge [62].

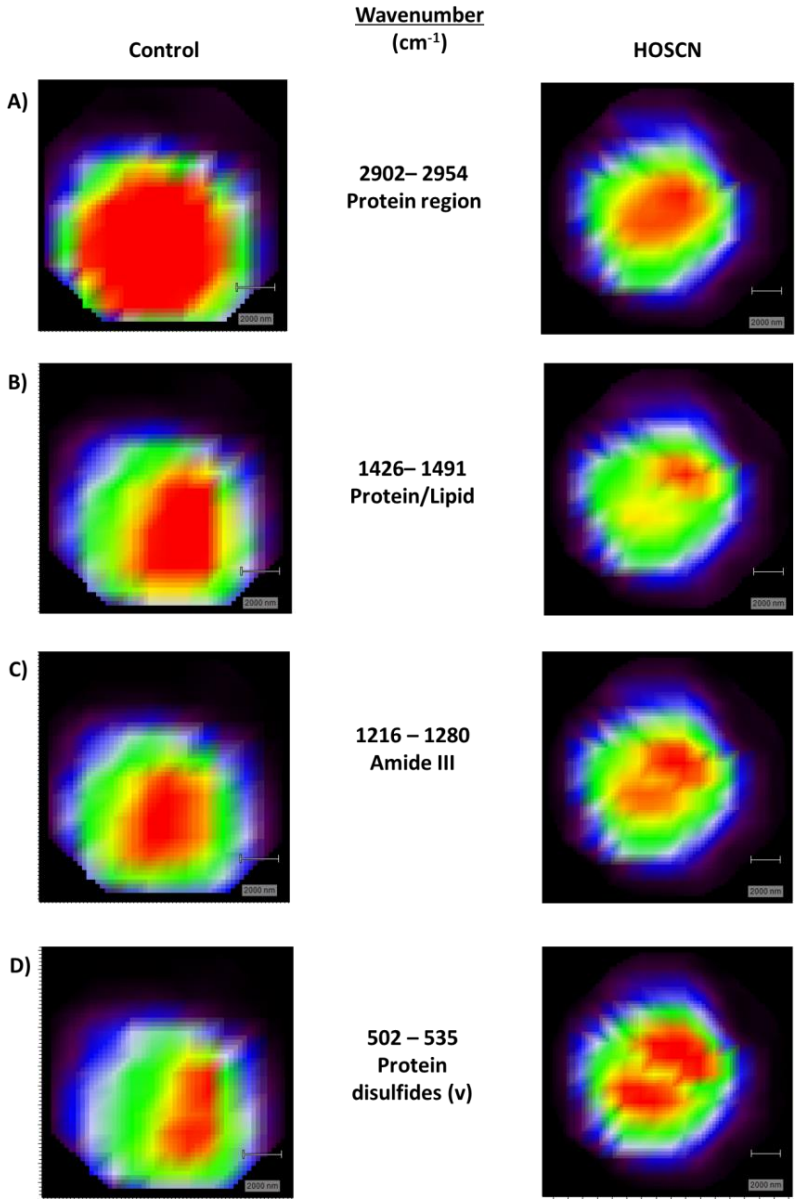

Figure 7.5: Raman heat maps of the peaks associated with proteins in J774A.1 cells.

J774A.1 cells (1×10^6) were treated either with a control solution (HBSS) or HOSCN (200 µM) for 1 h at 22 ˚C before single cells were interrogated with a Renishaw inVia Raman spectrometer and microscope. After performing a cosmic ray removal and principal component analysis (noise filter), a map of the cell was created using peaks to visualise the location and relative concentration of various molecules. (A) The 2902 – 2954 cm^{-1} peak correlates with the scattering of proteins. (B) The 1426 - 1491 cm^{-1} peak that correlates with the scattering of proteins and lipids. (C) The 1216 – 1280 cm^{-1} peak that correlates with the scattering of the amide III region. (D) The 502 – 535 cm^{-1} peak that correlates with the scattering of protein disulfide bonds. The maps are a visualisation of the principal components and representative of the maps generated in 3 separate experiments.

7.4.5 HOSCN interacts with J774A.1 nucleic acids

The nucleic acid region was the next group to be mapped out after analysing the J774A.1 cells using the Renishaw inVia Raman spectrometer. After mapping, there were two peaks of interest that were affected by the treatment of J774A.1 cells by HOSCN (200 μM).

The first peak was the nucleic acid peak (1561 – 1591 cm^{-1}), this peak is confined to the centre of the cell in the control cell, indicating that the majority of the nucleic acids are found in the nucleus of the cell. After treating the J774A.1 cells with HOSCN, a change in nucleic acid location is detected (Figure 7.6A), where the originally tight grouping of the nucleic acids in the non-treated samples becoming dispersed throughout the cell after HOSCN treatment. This result could indicate a structural abnormality of the nucleus or an increase in the formation of mRNA, making its way into the cytosol.

The next peak correlates with the DNA backbone, uracil, thymine and cytosine ring breathing and phosphatidylserine (770 – 800 cm^{-1}). In the control cell, these groups can be seen being confined to the centre of the cell, indicating a high concentration of these within the nucleus of the cell, which is similar in the pattern of distribution as the previous nucleic acid peak. After HOSCN treatment, these DNA and RNA constituents can be found in other parts of the cell, and has been speculated that HOSCN either causes damage to the nuclear envelope, causing a loss in genetic material, or HOSCN-induced oxidation is activating the formation of mRNA that is being sent into the cytosol, and it is the RNA that is being detected (Figure 7.6B).

Interestingly, the peak at 770 – 800 cm^{-1} also correlates with phosphatidylserine, a phospholipid membrane component that plays a key role in apoptosis. Though phosphatidylserine must be exposed on the cell membrane to indicate apoptosis is occurring, this result suggests that HOSCN may play a role in apoptosis. This result may be consistent with early apoptosis as the increased distribution of phosphatidylserine in the 200 μM HOSCN-treated samples may be located on the cellular membrane.

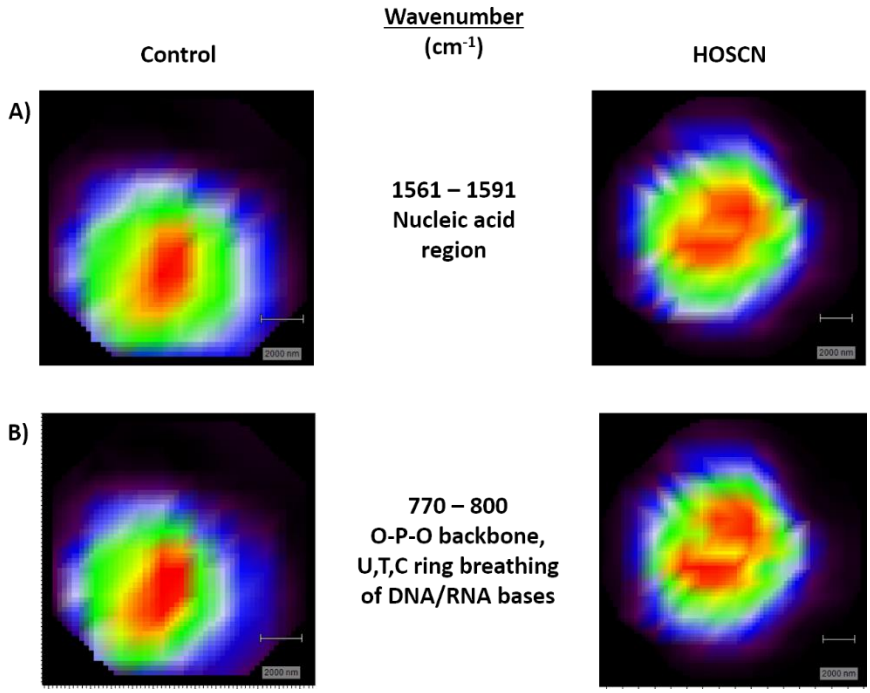

Figure 7.6: Raman heat maps of peaks associated with nucleic acids in J774A.1 cells.

J774A.1 cells (1 × 10^6) were treated either with a control solution (HBSS) or HOSCN (200 µM) for 1 h at 22 ˚C before single cells were interrogated with a Renishaw inVia Raman spectrometer and microscope. After performing a cosmic ray removal and principal component analysis (noise filter), a map of the cell was created using peaks to visualise the location and relative concentration of various molecules. (A) The 1561 – 1591 cm^{-1} peak correlates with nucleic acids. (B) The 770 – 800 cm^{-1} peak correlates with O-P-O backbone and U,T,C ring breathing of DNA/RNA. The maps are a visualisation of the principal components and representative of the maps generated in 3 separate experiments.

7.4.6 HOSCN causes a depletion of molecules involved in J774A.1 bioenergetics

Raman spectroscopy can also be used to assess the distribution of substrates involved in glycolysis and bioenergetics, including glycolysis and NADH [468]. This is important as previous results indicate that HOSCN affects glycolysis, resulting in a decrease in glycolytic end-products. In addition, the FTIR data presented in Chapter 6 are consistent with a decrease in intracellular glucose and lactate concentrations.

The first peak correlated with glucose (1326 – 1349 cm^{-1}), and in the untreated cells, glucose was identified throughout the entire cell. After treating the cells with 200 µM HOSCN a

marked reduction in intracellular glucose was observed (Figure 7.7A). The next peak was a NADH (988 – 997 cm^{-1}), which was observed throughout much of the cell in the untreated samples, while treating the cells with 200 µM HOSCN led to a complete loss in the NADH peak, indicating that no NADH was identified within the cell (Figure 7.7B).

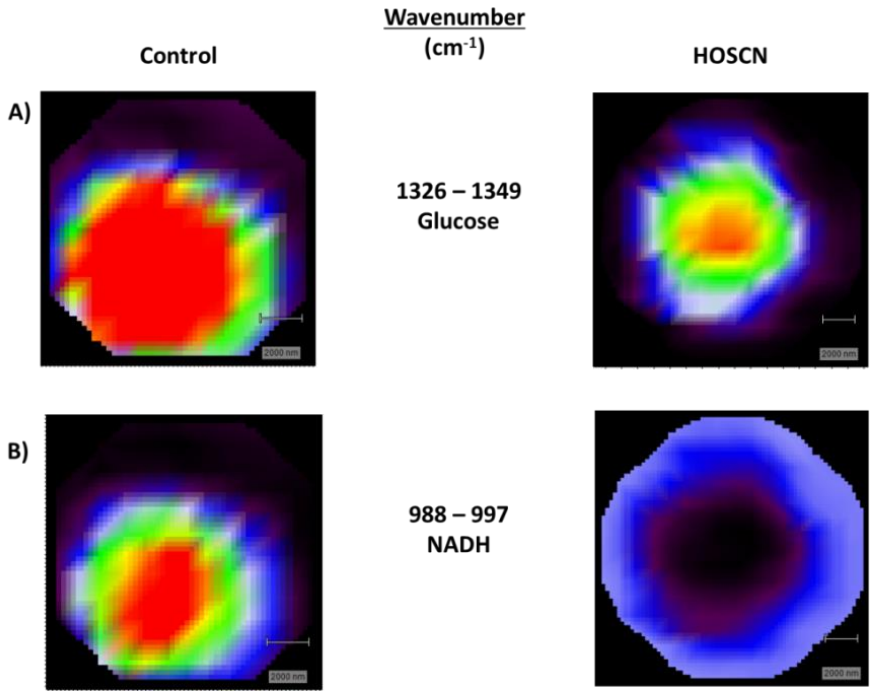

Figure 7.7: Raman heat maps of peaks associated with molecules related to glycolysis in J774A.1 cells.

J774A.1 cells (1 × 10^6) were treated either with a control solution (HBSS) or HOSCN (200 µM) for 1 h at 22 ˚C before single cells were interrogated with a Renishaw inVia Raman spectrometer and microscope. After performing a cosmic ray removal and principal component analysis (noise filter), a map of the cell was created using peaks to visualise the location and relative concentration of various molecules. (A) The 1326 – 1349 cm^{-1} peak correlates with glucose. (B) The 988 - 997 cm^{-1} peak correlates with NADH. The maps are a visualisation of the principal components and representative of the maps generated in 3 separate experiments.

7.5 Discussion

This Chapter was a preliminary study to determine whether HOSCN-induced damage to J774A.1 cells could be visually mapped using Raman spectroscopy. The results of this Chapter support previous data in this Thesis, and are consistent with HOSCN induction of extensive changes in the biochemistry of cells exposed to this oxidant. Changes in the concentration and location of lipids, proteins, nucleic acids and molecules involved in cellular energy production were observed.

HOSCN induced changes to lipid peaks of the Raman spectra as assessed by measuring changes in the CH region (2310 – 3026 cm^{-1}), lipid/protein region (2859 – 2901 cm^{-1}) and unsaturated fatty acid region (1624 – 1706 cm^{-1}). Data are consistent with HOSCN interacting directly or indirectly with the lipids of J774A.1 macrophages. The CH region corresponds with fatty acyl chains of the lipid membrane [443]. However, no data exists that would explain the interaction of HOSCN with the fatty acyl groups of the membrane. Instead, this may be a secondary interaction, as one of the many decomposition products of HOSCN may cause the carbamylation of fatty acyl groups, which could explain the observed changes in the CH region. Changes were also seen in the lipid/protein region, which would most likely indicate an interaction between HOSCN and protein, rather than lipid. Decreases were also seen in the unsaturated fatty acid (UFA) peak throughout the cell, indicating a loss in recognition. No data currently exists to explain this phenomenon, as this type of chemistry is not known to exist between HOSCN and UFAs, though data has been shown that HOSCN can react with cholesteryl esters to form lipid hydroperoxides, 9-hydroxy-10,12-octadecadienoic acid (9-HODE) and F2-isoprostanes [142]. This loss in recognition would be expected upon treatment with HOCl, as HOCl can cause the formation of chlorohydrins upon reaction with UFA in phospholipids [143], this result is most likely due to a secondary reaction.

HOSCN caused numerous changes in the protein peaks (protein region, 2902 – 2954 cm^{-1}; protein/lipid, 1426 – 1491 cm^{-1}; amide III, 1216 – 1280 cm^{-1} and protein disulfides, 502 – 535 cm^{-1}) detected by Raman spectroscopy. The first was a decrease in the recognition of the protein peak, the protein/lipid peak and the amide III peak, consistent with multiple chemical and structural changes to protein folding and secondary structure [469, 470]. The oxidation of cysteine residues by HOSCN could induce changes to protein structure in the cell, which could cause the aggregation of proteins within the cytosol. There is considerable evidence showing that the oxidation and reduction of cysteine residues constitutes a redox switch that

controls the structure and function of proteins, indicating that HOSCN may play a role in redox signaling [471].

The next peak identified was the disulfide peak, because symmetrical bonds tend to be better Raman scatterers, disulfide bonds can be quite easily observed. The results show that HOSCN causes an increase in the formation of disulfide bonds on proteins in the J774A.1 cells. This result is indicative of the chemistry of HOSCN with cysteine residues. When HOSCN oxidises thiols a sulfenyl thiocyanate product is formed, which can react with a neighbouring thiol to form a disulfide bond [62, 101, 102]. This result also complements the data acquired in Chapter 3, outlining that HOSCN-induced oxidation of thiols are reversible.

Raman mapping was also used to examine the effect of HOSCN on nucleic acids. In non-treated cells, the nucleic acids were confined entirely at the centre of the cell, indicating their location within the nucleus. Upon HOSCN treatment, both the nucleic acid peak and the peak associated with the DNA backbone, and the U, T and C rings were located in other locations of the cell. This result could indicate one of two possibilities, the first being that HOSCN causes structural abnormalities in the nuclear envelope, causing a leak in the genetic material. This may be unlikely, as no data exists corroborating the interaction of HOSCN with the nuclear envelope or DNA, even at concentrations exceeding the requirement to produce an antibacterial effect [134]. It is also possible that HOSCN-induced oxidation of J774A.1 cells causes an increase in transcription, leading to an increase in mRNA within the cytosol. This is supported by previous data, where HOSCN has been shown to inhibit protein tyrosine phosphatases, resulting in the hyperphosphorylation of MAPK [176, 179], which can lead to the increase in transcription factor activation, and potentially increase mRNA synthesis [472].

The Raman data also reflect a decrease in the intracellular glucose concentration in HOSCN-treated cells. Previous results in this Thesis show that glucose transport is not inhibited in HOSCN-treated cells. The decrease in intracellular glucose concentration could reflect a reduced rate of glycolysis in HOSCN treated cells, supported by data in Chapters 4 and 6, showing a reduction in intracellular lactate concentration. Studies with a fluorescent glucose analog (2-NBDG), employed to determine glucose uptake, and showed a similar extent of fluorescence in the presence and absence of HOSCN. However, 2-NBDG is unable to be phosphorylated by hexokinase, and used in glycolysis, and is only suitable for determining glucose uptake in cells, rather than as a measure of intracellular glucose concentration. Thus, the decrease in the intracellular glucose concentration in HOSCN-treated cells is

hypothesised to be a feedback loop due to the decreased activity of glycolysis, as discussed in Chapter 6.

NADH, a co-enzyme that plays a key role in redox reactions by shuttling electrons was identified, though further experiments and analysis are required to support this result [473]. In the control cells, NADH is distributed throughout much of the cell. However, on exposure of the cells to HOSCN (200 μM), a dramatic loss of NADH was seen, shown by the absence of this peak and the shift in the heat map. This may reflect that glycolysis was completely inhibited in J774A.1 cells after treatment with 200 μM HOSCN. Glycolysis is a process in which the free energy formed is used to create the high-energy products of ATP, pyruvate and NADH [158, 474]. With the inhibition of NADH formation, import redox reactions are unable to occur, such as oxidative phosphorylation and ATP formation, which ultimately leads to cellular dysfunction, and the inhibition of cell growth and proliferation [404, 406, 475, 476].

After analysis, it was concluded that the data obtained in this Chapter compared well with data obtained using FTIR, and with the data of the glycolytic stress test. However, these data were only preliminary, but they outline the potential advantages of this technique, including the large amount of biochemical information that can be probed via the use of Raman spectroscopy. To further establish the effect of HOSCN on J774A.1 cells, further concentrations should be tested, along with a decomposed HOSCN treatment and HOCl treatment. To further improve on the data quality, the limitations must be reduced, for example, a sampling method should be further trialled, as to increase the resolution and spatial quality of images obtained while decreasing the time taken to map the samples.

7.6 Summary

The study in this Chapter was a proof-of-concept experiment that attempted to use Raman spectroscopy to visually map the damage caused to J774A.1 cells by HOSCN-induced oxidation. The results show that the concentration of HOSCN used was able to induce changes to the concentration and location of lipids, proteins, disulfide bonds and nucleic acids in the cell. These preliminary data also corroborated previous results reported in this Thesis, supporting data that HOSCN was able to completely inhibit glycolysis after mapping and visualising the concentration of the co-factor, NADH. This study confirms the data of previous sections and presents a novel method to detect hypohalous acid-induced damage to cells *in vitro*.

8 Discussion, Future Studies and Concluding Remarks

8.1 Discussion

The role of hypohalous acids is primarily in the innate immune system, as they are utilised by neutrophils to oxidise and destroy invading pathogens [19, 49, 432]. This Thesis has explored the role of hypohalous acid-induced oxidation on the function of macrophages. A major target of hypohalous acid-induced oxidation is the thiols contained on the free Cys residues of proteins and low molecular weight species such as GSH [95]. Essential cellular processes such as glycolysis, mitochondrial energy production, the formation of insulin by β-cells and phosphate uptake require thiols [477-480]. Although uncommon residues, only making up ca. 2% of all known human proteins [481], thiols are susceptible to oxidation by many ROS. Upon reaction with ROS, a number of post-translational modifications are formed, some of which have been explored in this Thesis, including, but not limited to, inter- and intra-protein disulfides, sulfenic, sulfinic and sulfonic acids, sulfenyl halides and s-glutathionylated species. This allows Cys residues to have a diverse effect on important regulatory roles in enzyme function [102, 135, 329, 353, 367, 431]. Enzymes with active site cysteine residues typically employ the deprotonated, thiolate (RS^-) form and activity can be enhanced by the microenvironment, especially by neighbouring amino acids that reduce the usually high pK_a of Cys (ca. 8.5) to a value lower than the pK_a at neutral pH [482].

Enzymes with low pK_a Cys are more readily oxidised, meaning that proteins requiring the use of Cys for function can be easily altered by oxidants such as H_2O_2, HOCl, $ONOO^-$ and HOSCN [483, 484]. Phosphorylation of Tyr plays an important part in many cellular processes including signal transduction, apoptosis, metabolic processes and cell cycle progression, with the reversibility of phosphorylation playing a major part [485, 486]. Protein tyrosine phosphatases (PTPs) contain an active-site Cys with a low pK_a that dephosphorylates its substrate generating a cysteinyl phosphate, which becomes hydrolysed to reform the original thiol, and its activity has been shown to be inhibited by HOSCN, resulting in the hyperphosphorylation of cellular proteins [179, 487]. Another group of enzymes that contain important Cys residues are thiol proteases such as caspases and cathepsins [488]. These enzymes catalyse proteolysis using the Cys thiolate as the attacking nucleophile, and the activity of these enzymes has been shown to be modulated via the formation of sulfenic acids by H_2O_2 and NO donors, and caspase activity has been shown to be inhibited by HOSCN in cells exposed for ≥ 2 h [91, 92, 489, 490]. Conversely caspase activation has been observed in HUVECs exposed to HOCl [191].

The most studied of the hypohalous acids, HOCl, can react with mammalian cells, oxidising numerous biomolecules, particularly proteins, to alter their function and perturb cellular function [62, 66, 70, 96]. The reaction of HOCl with DNA can cause the formation of chloramines, which causes a loss in the of hydrogen-bonding and the dissociation of the DNA double-bonds [66]. The oxidation of DNA bases with HOCl causes the formation of numerous chlorinated products such as, 5-chlorocytosine, 5-chlorouracil, 8-chloroadenosine and 8-chloroguanosine [132, 135, 137, 296]. HOCl also reacts readily with unsaturated fatty acids and cholesterol to form chlorohydrins, to destabilise cell membranes and cause cell lysis, and with antioxidants such as GSH, which result in the alteration of cell function [135, 143, 145, 180, 181, 491]. The alteration of these molecules is important in the progression of diseases, such as atherosclerosis, and the reaction of HOCl with the amino acid Tyr can lead to the formation of the biomarker, 3-chlorotyrosine [125, 299, 492]. The use of this biomarker has allowed for the probing of HOCl-induced damage and the determination of the role of this oxidant in disease progression *in vivo*. On the contrary, there is no biomarker for HOSCN-induced oxidative damage, partially because the oxidation products formed by HOSCN are not unique to this oxidant [432]. Because the reactivity of HOSCN and HOCl is different, the lack of biomarker means that the exact role of HOSCN in disease progression is currently unclear.

The difference in the reactivity between HOSCN and HOCl was explored in Chapter 3, ThioGlo-1, a fluorescent maleimide, was used to assay HOSCN- and HOCl-treated cells for the concentration of free thiols. This method does not determine the oxidative species formed on the thiol after treatment, but by using sulfenic acid-specific probes, sulfenic acids were observed to be a major species formed upon treatment of cells with HOSCN, but not HOCl, where non-reversible oxidation of thiols was observed. While these methods allow for a determination of the state of intracellular thiols, they give very little information on the secondary or alternate effects of HOSCN/HOCl-induced oxidation of cells. Another complication of identifying hypohalous acid-induced damage in cells is the lack of a HOSCN-specific biomarker. HOCl-induced oxidation can be identified via the determination of 3-chlorotyrosine levels, and has been used to identify the role of MPO and HOCl in the progression of atherosclerosis [299, 316]. At this point in time, no such marker exists to identify HOSCN-induced damage to cells *in vivo* or *in vitro*, due to the oxidative nature of HOSCN and the reversible products formed by HOSCN, which are either unstable or also formed by numerous other oxidants including HOCl, NO and H_2O_2 [201, 489, 493, 494]. Protein carbamylation of Lys residues by OCN^- and the formation of homocitrulline has been

used as a surrogate biomarker to implicate HOSCN as playing a role in the progression of atherosclerosis [81]. However, the use of homocitrulline as a biomarker for HOSCN-induced damage in atherosclerosis has limitations, particularly on analysis of plasma samples obtained from uremic patients, as protein carbamylation is a phenomenon of uraemia due to elevated OCN^-.

Apart from its ability to form reversibly oxidised Cys oxyforms, the role and activity of HOSCN in cellular systems is somewhat different to HOCl, as it is usually regarded as a milder oxidant, with a different pattern of reactivity [19]. It has been hypothesised that the presence of SCN^- and the formation of HOSCN is protective in some conditions, as it removes more damaging oxidants, such as HOCl, from the cellular environment [495, 496]. In contrast to HOCl, HOSCN is bacteriostatic rather than bactericidal as HOSCN is known to inhibit bacterial growth and proliferation rather than causing bacterial cell death [427]. The results of this Thesis show that HOSCN is more potent than HOCl at inhibiting glycolysis in J774A.1 macrophages [56, 198, 379]. The method by which HOSCN inhibits bacterial cell growth is via the oxidation of glycolytic enzymes that contain critical thiol groups, such as bacterial GAPDH, hexokinase, aldolase, glucose 6-phosphate dehydrogenase and glucose transporters, which results in the inhibition of glycolysis [56, 198-200, 385, 390]. For decades, the production of HOSCN was postulated to be normal and healthy for the host as it was thought that HOSCN only affected bacteria [54]. But due to the targeting of thiols, HOSCN may be detrimental to the host under inflammatory conditions, as shown by recently published data, showing that HOSCN can potentially perpetuate inflammation, deplete GSH and inhibit a wide array of proteins such as PTPs, GAPDH and ATPases [84, 91, 174, 179, 185, 201].

This Thesis explored the attenuation of energy production in macrophages after exposure to HOSCN as GAPDH contains an active-site Cys, which is reported to be a key target for oxidants including HOSCN and HOCl [185, 201]. This enzyme plays an important role in glycolysis, and ultimately, energy production, by converting glyceraldehyde 3-phosphate to glycerate 1, 3-bisphosphate. Its activity has been reported to be inhibited by HOSCN-induced sulfenic acid formation, while it has also been shown to be susceptible NO and to the formation of S-glutathionylated species [201, 497, 498]. The inhibition of the GAPDH has interesting modulatory effects on the protein, as the formation of a sulfenic acid at the active-site Cys not only inhibits its dehydrogenase activity, but switches the enzyme to acyl phosphatase activity [499]. In essence, GAPDH begins to catalyse the reverse reaction, uncoupling glycolysis from the production of ATP at the reactions that follow in the glycolytic pathway

[498, 499]. Along with its metabolic role, GAPDH has been shown to move between the cytosol and nucleus to activate transcription, implicating a role between the metabolic state of the cell and transcription [500]. This modulation in GAPDH activity has a pivotal consequence on the cell, with results from the functional glycolysis assays showing that treatment of J774A.1 macrophages with low concentrations (≥ 25 μM) of HOSCN was enough to significantly reduce the ability of the cells to metabolise glucose at baseline conditions. The attenuation of glycolysis results in a dynamic reduction of substrates for oxidative phosphorylation including pyruvate and NADH (shown in Chapter 7). This results in the alteration of the cellular metabolic state and could also have serious implications for gene transcription [500].

Because glucose metabolism and ATP production via oxidative phosphorylation is a connected and dynamic process, it was hypothesised that the inhibition of glycolysis and reduction of glycolytic end-products would inhibit mitochondrial oxidative phosphorylation. Results also showed that HOSCN oxidises mitochondrial thiols forming sulfenic acids and inhibits mitochondrial respiration. These results correlate with previously published data showing that the removal of thiols from the mitochondria inhibits mitochondrial function and respiration [192, 213, 416]. The data of this Thesis indicate that HOSCN affects mammalian bioenergetics via multiple pathways, indicating a systemic influence of HOSCN on macrophage energy production. The inhibiting of glycolysis has numerous consequences for cells, with these consequences having been trialled in treatment for cancer. Reports have shown that the inhibition of glycolysis in cancer cells with mitochondrial defects (analogous to the HOSCN-induced mitochondrial damage observed in Chapter 5), causes a severe depletion of ATP and the dephosphorylation of Bcl-2-associated death promoter. This causes a relocation of Bcl-2-associated X protein to the mitochondria causing cell death [501]. By a similar process of influencing the energy producing pathways in macrophages, HOSCN could also propagate lesion development in atherosclerosis.

In addition, by the inhibition of glycolysis and mitochondrial respiration in macrophages, HOSCN could also promote foam cell formation seen in early atherosclerotic lesions. After treating J774A.1 cells with HOSCN, glucose is no longer able to be utilised for energy production and the cells must begin using another substrate for energy production [502]. A major energetic substrate found within the atherosclerotic lesion is lipoprotein-cholesterol, which can be taken up by macrophages [503-505]. Once taken up by the macrophages, the lipids undergo lipolysis to liberate glycerol and fatty acids, and it is the free fatty acids that

the cells could use for energy production after the inhibition of glycolysis by HOSCN [506]. The process by which fatty acids are catabolised for energy production is called 'β-oxidation', where, through a series of enzymatic steps, acetyl-CoA is formed [507]. Interestingly, this process takes place entirely within the mitochondria, which the results of this Thesis have shown, is heavily influenced by HOSCN-induced oxidation, indicating that much like the glycolytic pathway, the substrate is able to enter the pathway but the energetic end-product is unable to be formed due to the HOSCN-induced oxidation of a critical enzyme.

Experiments were performed to determine whether the damage caused by HOSCN, such as the attenuation of energy production, could be alleviated using inhibitors and reducing agents. Results indicated that CsA could reverse the mitochondrial depolarisation caused by HOSCN, consistent with the interaction of the oxidant with the mitochondrial-permeability transition pore (MPTP) [508]. CsA also restored ATP levels within the treated cells, though the mechanism involved remains unclear. While thiol loss has explained the attenuation of glycolysis and mitochondrial respiration, previous data have shown that a loss in mitochondrial respiration due to thiol modification could be completely repaired after treating rat aortic smooth muscle cells with DTT [416].

Perturbation of bioenergetics and cellular dysfunction was supported by the use of FTIR, and this damage could be mapped visually using Raman spectroscopy techniques. The results of the FTIR and Raman also allows for a novel method of detecting HOSCN-induced damage which is significant in light of the lack of a chemical biomarker. These methods allow for the visualisation of HOSCN-induced damage by interrogating the change in chemical bond vibrations, which can then be analysed using PCA. By using PCA, the changes at each point in the spectra were compared to changes in other treatment groups, allowing for gross chemical changes within the cell to be identified with a unique spectral fingerprint [509, 510]. The results of both the FTIR and Raman mapping showed reduction in the intracellular glucose concentration and the glycolytic by-products, lactate and NADH, which is an energetic substrate required for oxidative phosphorylation. Furthermore, changes in the protein peaks determined that HOSCN caused structural and locational changes to proteins, indicating that HOSCN caused protein aggregation and increases in disulfide bond formation, which correlates with the chemistry of HOSCN [511]. The results of the Raman mapping also showed a reduction in the intracellular concentration of unsaturated fatty acids, which is hypothesised to be due to the reduction in glycolysis, as the cells require a new energy source, they undergo β-oxidation, which could be a trigger for foam-cell formation. The

results of this study implicate a role of HOSCN in the formation and progression of atherosclerotic lesions, particularly in smokers who have been shown to have increased plasma SCN^-, the precursor of HOSCN [83].

The use of FTIR and Raman spectroscopy are interesting and novel methods by which oxidant damage to cells can be studied. The advantages include the large amounts of information that can be obtained, without the restrictions of fluorescent probes, which only allow the visualisation of tagged substrate, and in some cases, can alter the function of the substrate of interest. But there are limitations to the FTIR and Raman methods used in this Thesis, including the need to dehydrate the sample and the long sampling times required for Raman mapping. By using these techniques and with further optimisation, methods can be developed to identify HOSCN-induced damage throughout atherosclerotic disease progression, as various biochemical changes occur to cells contained within the lesion over time, such as the increase in LDL cholesterol [512]. The use of this method is further strengthened as it has been used in recent years to identify cellular changes in disease processes like cancer and metabolic disorders [439, 513, 514].

Taken together, the data in this Thesis with isolated HOSCN and macrophages support a role for this oxidant in promoting dysfunction and potentially disease, which may be more relevant for smokers with elevated plasma SCN^-. This supports data showing correlations between plasma SCN^- and early markers of macrophage dysfunction and lipid uptake [515, 516]. However, data have also shown that patients with a previous myocardial infarct (MI) had better survival rates when plasma MPO was below median and SCN^- was above median, while patients with the worst survival rate had above median MPO levels and below median SCN^- over a period of ca. 12 years. However, the study included deaths from all causes, so mortality may be unrelated to cardiovascular disease [517]. The investigators hypothesised that the patients with above median SCN^- and below median MPO had higher survival rates resulting from a decrease in HOCl-induced oxidation due to the formation of HOSCN, via the reaction of HOCl with the excess SCN^-. These results are open for interpretation, primarily due to the lack of a HOSCN-specific biomarker, as the group with the lowest survival rates had high levels of plasma MPO and low levels of SCN^-. These results also conflict with the results of a previous study, which linked high plasma protein-carbamylation via MPO oxidation of SCN^-, with a positive relation to future myocardial infarction, stroke and death [81]. Knowing that these patients are survivors of a previous MI implies a chronic inflammatory condition and the constant formation of hypohalous acids. Kinetic data have

shown that the specificity of SCN^- for MPO is much higher than that of Cl^- for MPO (730:1) [48, 49, 518]. Upon extrapolation, these results may reflect that the reduction of plasma SCN^- is an effect of the increased formation of HOSCN (high MPO, low SCN^-), and that this is the cause of the reduced survival increased in this condition, rather than the increased survival being a result of HOCl being preferentially formed by MPO then reacting with SCN^- to form HOSCN.

8.2 Future studies

This Thesis showed, for the first time, that HOSCN can target mitochondrial proteins to form sulfenic acids. The results also showed that, unlike previously thought, HOSCN is able to inhibit glycolysis and oxidative phosphorylation in mammalian cells, and that HOSCN-induced damage could be visualised and quantified using FTIR and Raman spectroscopy.

The first and key future direction of this work would be to identify both the cytosolic and mitochondrial proteins affected by HOSCN-induced sulfenic acid formation. Proteomic analysis has been considered, using methods such as tandem mass spectrometry and matrix-assisted desorption/ionisation (MALDI) would allow for the identification and characterisation of the proteins oxidised by HOSCN in J774A.1 macrophages, and whether these proteins are involved in cellular energy producing pathways.

HOSCN has previously been shown to inhibit GAPDH, and this study saw a functional effect on glycolysis after HOSCN treatment [201]. Because GAPDH has been found to influence a link between metabolism and gene transcription, future studies could also attempt to determine the changes that occur to gene expression after HOSCN treatment, especially those involved in the S-phase of the cell cycle [500]. Though, despite HOSCN attenuating glycolysis and mitochondrial oxidative phosphorylation, very little cell death was observed as a function of cell lysis in the LDH activity assays. It was hypothesised that perhaps the cells after a 1 h treatment with HOSCN were not dying, or were in the early stages of apoptosis as implied by increases in the recognition of phosphatidylserine in the Raman mapping experiments. By using flow cytometry, further studies could identify a link between the inhibition of glycolysis and oxidative phosphorylation with increases in apoptosis and necrosis.

In regard to the mitochondrial dysfunction and inhibition of oxidative phosphorylation induced by HOSCN treatment, it was proposed that the uncoupling of the electron transport chain would cause an increase in ROS within the mitochondria. This could be measured using an HPLC method and dihydroethidium, which is oxidised to a specific product, 2-hydroxyethidine by $O_2^{\bullet-}$ [519]. This method would also allow for the determination of the feasibility of antioxidants as a treatment to prevent HOSCN-induced damage. A previous report showed that MitoQ, which uses ubiquinone as the active antioxidant, was able to prevent HOCl-induced mitochondrial damage and cell death [520].

Another hypothesis that appeared throughout this Thesis, which was proposed due to the lack of cell death observed after the LDH assays, was that the cells are switching their primary energy producing pathway to lipolysis and β-oxidation after HOSCN treatment. This would have interesting implications on the formation of foam cells in atherosclerosis. There is an assay kit available by Seahorse Bioscience, which probes cells for fatty acid oxidation. It has been hypothesised that, because β-oxidation occurs in the mitochondria and the mitochondria are influenced by HOSCN-induced sulfenic acid formation, the XF fatty acid oxidation assay would help to connect the role of cellular bioenergetics with the progression of atherosclerosis.

The Raman spectroscopy allowed for a visualisation of HOSCN-induced oxidation in J774A.1 cells and in regards to the proof-of-concept study the data obtained was invaluable, but further analysis was not performed due to the time constraints. Further studies could continue optimising the assay, which would allow for quicker preparation of the cells and faster imaging, while increasing the quality of the images taken. This could be achieved by further optimising the laser power, for example, using a wavelength such as 633 nm, may allow for quicker imaging and better spectral resolution, without burning samples. One of the hopes of this study was to image organelles within the J774A.1 macrophages, allowing for the determination of chemical changes within different cellular compartments upon treatment with HOSCN or HOCl. Increasing the number of treatment concentrations would first allow for a comparative study to visualise the progression of HOSCN-induced damage, while the use of a synchrotron would give high-quality, high resolution data.

The results of this Thesis have also extended the knowledge of the role of HOSCN in a cellular model. HOSCN's ability to modulate metabolic function has consequences that can be further studied and elucidated, allowing for further understanding about the involvement of HOSCN in atherosclerosis and other diseases where oxidative stress plays a key role.

8.3 Concluding remarks

This Thesis explored the involvement of HOCl and HOSCN in regards to thiol oxidation in J774A.1 cells. The results indicate that HOCl induces thiol loss in an irreversible manner, while HOSCN induced the formation of reversible products, including sulfenic acids on protein thiols in the cytosol and mitochondria. The formation of these reversible species was investigated in regards to the functional aspects of glycolysis and mitochondrial oxidative phosphorylation. The study concluded that HOSCN induces glycolytic inhibition, and that the reduction in glycolytic end-products ultimately affects the function of the mitochondrial electron transport chain and the formation of the energetic end-product, ATP. The results of the lactate assay also indicate that this process is not reversible upon the reculture of cells in the absence of HOSCN, despite the reversible nature of HOSCN-induced oxidation. The gross effects of HOSCN and HOCl were also investigated using FTIR, Raman spectroscopy and PCA, and the results indicate that both oxidants affect multiple cellular components, including proteins, DNA/RNA, lipids, while HOSCN was also able to attenuate the levels of carbohydrates within the cell. These data strengthen the argument that HOSCN could play a role in the progression of inflammatory disease, including atherosclerosis. This helps to rationalise why smokers, who have elevated plasma SCN^-, exhibit increased inflammatory conditions within the large arteries and have higher incidences of atherosclerosis. However, the lack of a HOSCN-specific biomarker limits the ability of researchers to fully understand the role of HOSCN-induced oxidation of biological targets *in vivo*, which means further investigations into the targets and patterns of damage caused by HOSCN must performed.

9 References

1. Sies, H., *Role of reactive oxygen species in biological processes.* Klin Wochenschr, 1991. **69**(21-23): p. 965-8.
2. Davies, M.J., *The oxidative environment and protein damage.* Biochimica Et Biophysica Acta-Proteins and Proteomics, 2005. **1703**(2): p. 93-109.
3. Babior, B.M., *NADPH oxidase.* Curr Opin Immunol, 2004. **16**(1): p. 42-7.
4. Babior, B.M., *Phagocytes and oxidative stress.* Am J Med, 2000. **109**(1): p. 33-44.
5. Simpson, J.A., et al., *Long-lived reactive species on free-radical-damaged proteins.* Biochem J, 1992. **282 (Pt 3)**: p. 621-4.
6. Dean, R.T., et al., *Biochemistry and pathology of radical-mediated protein oxidation.* Biochem J, 1997. **324 (Pt 1)**: p. 1-18.
7. Tainer, J.A., et al., *Structure and mechanism of copper, zinc superoxide dismutase.* Nature, 1983. **306**(5940): p. 284-7.
8. Giorgio, M., et al., *Hydrogen peroxide: a metabolic by-product or a common mediator of ageing signals?* Nat Rev Mol Cell Biol, 2007. **8**(9): p. 722-8.
9. Veal, E.A., A.M. Day, and B.A. Morgan, *Hydrogen peroxide sensing and signaling.* Mol Cell, 2007. **26**(1): p. 1-14.
10. Groeger, G., C. Quiney, and T.G. Cotter, *Hydrogen peroxide as a cell-survival signaling molecule.* Antioxid Redox Signal, 2009. **11**(11): p. 2655-71.
11. Davies, M.J., et al., *Mammalian heme peroxidases: from molecular mechanisms to health implications.* Antioxid Redox Signal, 2008. **10**(7): p. 1199-234.
12. Reiter, R.J., et al., *A review of the evidence supporting melatonin's role as an antioxidant.* J Pineal Res, 1995. **18**(1): p. 1-11.
13. Muller, F., *The nature and mechanism of superoxide production by the electron transport chain: Its relevance to aging.* J Am Aging Assoc, 2000. **23**(4): p. 227-53.
14. Kim, H.J., et al., *Reactive oxygen species induce antiviral innate immune response through IFN-lambda regulation in human nasal epithelial cells.* Am J Respir Cell Mol Biol, 2013. **49**(5): p. 855-65.
15. Mittal, M., et al., *Reactive oxygen species in inflammation and tissue injury.* Antioxid Redox Signal, 2014. **20**(7): p. 1126-67.
16. Ferrero-Miliani, L., et al., *Chronic inflammation: importance of NOD2 and NALP3 in interleukin-1beta generation.* Clin Exp Immunol, 2007. **147**(2): p. 227-35.
17. Sorokin, L., *The impact of the extracellular matrix on inflammation.* Nat Rev Immunol, 2010. **10**(10): p. 712-23.
18. Lau, D. and S. Baldus, *Myeloperoxidase and its contributory role in inflammatory vascular disease.* Pharmacol Ther, 2006. **111**(1): p. 16-26.
19. Rayner, B.S., D.T. Love, and C.L. Hawkins, *Comparative reactivity of myeloperoxidase-derived oxidants with mammalian cells.* Free Radic Biol Med, 2014. **71**: p. 240-55.
20. Hoy, A., et al., *Growing significance of myeloperoxidase in non-infectious diseases.* Clin Chem Lab Med, 2002. **40**(1): p. 2-8.
21. Sugiyama, S., et al., *Macrophage myeloperoxidase regulation by granulocyte macrophage colony-stimulating factor in human atherosclerosis and implications in acute coronary syndromes.* Am J Pathol, 2001. **158**(3): p. 879-91.
22. Van Der Vliet, A., et al., *Myeloperoxidase and protein oxidation in cystic fibrosis.* Am J Physiol Lung Cell Mol Physiol, 2000. **279**(3): p. L537-46.
23. Winterbourn, C.C., *Comparative reactivities of various biological compounds with myeloperoxidase-hydrogen peroxide-chloride, and similarity of the oxidant to hypochlorite.* Biochim Biophys Acta, 1985. **840**(2): p. 204-10.
24. Hernandez-Aguilera, A., et al., *Mitochondrial dysfunction: a basic mechanism in inflammation-related non-communicable diseases and therapeutic opportunities.* Mediators Inflamm, 2013. **2013**: p. 135698.

25. Wallace, D.C., *A mitochondrial paradigm of metabolic and degenerative diseases, aging, and cancer: a dawn for evolutionary medicine.* Annu Rev Genet, 2005. **39**: p. 359-407.
26. Tawakol, A., et al., *HIF-1alpha and PFKFB3 Mediate a Tight Relationship Between Proinflammatory Activation and Anerobic Metabolism in Atherosclerotic Macrophages.* Arterioscler Thromb Vasc Biol, 2015.
27. Freemerman, A.J., et al., *Metabolic reprogramming of macrophages: glucose transporter 1 (GLUT1)-mediated glucose metabolism drives a proinflammatory phenotype.* J Biol Chem, 2014. **289**(11): p. 7884-96.
28. Han, D., E. Williams, and E. Cadenas, *Mitochondrial respiratory chain-dependent generation of superoxide anion and its release into the intermembrane space.* Biochem J, 2001. **353**(Pt 2): p. 411-6.
29. Wallace, D.C., *A mitochondrial paradigm for degenerative diseases and ageing.* Novartis Found Symp, 2001. **235**: p. 247-63; discussion 263-6.
30. Hayflick, L., *The future of ageing.* Nature, 2000. **408**(6809): p. 267-9.
31. Madamanchi, N.R. and M.S. Runge, *Mitochondrial dysfunction in atherosclerosis.* Circ Res, 2007. **100**(4): p. 460-73.
32. Lesnefsky, E.J., et al., *Mitochondrial dysfunction in cardiac disease: ischemia--reperfusion, aging, and heart failure.* J Mol Cell Cardiol, 2001. **33**(6): p. 1065-89.
33. Chung, H.Y., et al., *Molecular inflammation: underpinnings of aging and age-related diseases.* Ageing Res Rev, 2009. **8**(1): p. 18-30.
34. Suh, Y.A., et al., *Cell transformation by the superoxide-generating oxidase Mox1.* Nature, 1999. **401**(6748): p. 79-82.
35. Dunn, W.B., J.H. Hardin, and S.S. Spicer, *Ultrastructural localization of myeloperoxidase in human neutrophil and rabbit heterophil and eosinophil leukocytes.* Blood, 1968. **32**(6): p. 935-44.
36. Conner, G.E., M. Salathe, and R. Forteza, *Lactoperoxidase and hydrogen peroxide metabolism in the airway.* Am J Respir Crit Care Med, 2002. **166**(12 Pt 2): p. S57-61.
37. Klebanoff, S.J., *Iodination of bacteria: a bactericidal mechanism.* J Exp Med, 1967. **126**(6): p. 1063-78.
38. Bainton, D.F. and M.G. Farquhar, *Differences in enzyme content of azurophil and specific granules of polymorphonuclear leukocytes. I. Histochemical staining of bone marrow smears.* J Cell Biol, 1968. **39**(2): p. 286-98.
39. Borregaard, N., O.E. Sorensen, and K. Theilgaard-Monch, *Neutrophil granules: a library of innate immunity proteins.* Trends Immunol, 2007. **28**(8): p. 340-5.
40. Brumell, J.H., et al., *Subcellular distribution of docking/fusion proteins in neutrophils, secretory cells with multiple exocytic compartments.* J Immunol, 1995. **155**(12): p. 5750-9.
41. Thomas, E.L., M.B. Grisham, and M.M. Jefferson, *Preparation and characterization of chloramines.* Methods Enzymol, 1986. **132**: p. 569-85.
42. Thomas, E.L., *Products of lactoperoxidase-catalyzed oxidation of thiocyanate and halides*. Immunology Series. Vol. 27. 1985. 31-53.
43. Harrison, J.E. and J. Schultz, *Studies on the chlorinating activity of myeloperoxidase.* J Biol Chem, 1976. **251**(5): p. 1371-4.
44. Ueda, T., et al., *Molecular cloning and characterization of the chromosomal gene for human lactoperoxidase.* Eur J Biochem, 1997. **243**(1-2): p. 32-41.
45. Furtmuller, P.G., U. Burner, and C. Obinger, *Reaction of myeloperoxidase compound I with chloride, bromide, iodide, and thiocyanate.* Biochemistry, 1998. **37**(51): p. 17923-30.

46. Marquez, L.A. and H.B. Dunford, *Kinetics of oxidation of tyrosine and dityrosine by myeloperoxidase compounds I and II. Implications for lipoprotein peroxidation studies.* J Biol Chem, 1995. **270**(51): p. 30434-40.
47. Marquez, L.A. and H.B. Dunford, *Interaction of acetaminophen with myeloperoxidase intermediates: optimum stimulation of enzyme activity.* Arch Biochem Biophys, 1993. **305**(2): p. 414-20.
48. van Dalen, C.J., et al., *Thiocyanate and chloride as competing substrates for myeloperoxidase.* Biochem J, 1997. **327 (Pt 2)**: p. 487-92.
49. Pattison, D.I., M.J. Davies, and C.L. Hawkins, *Reactions and reactivity of myeloperoxidase-derived oxidants: Differential biological effects of hypochlorous and hypothiocyanous acids.* Free Radic Res, 2012.
50. Chandler, J.D. and B.J. Day, *Thiocyanate: a potentially useful therapeutic agent with host defense and antioxidant properties.* Biochem Pharmacol, 2012. **84**(11): p. 1381-7.
51. Chapman, A.L., et al., *Chlorination of bacterial and neutrophil proteins during phagocytosis and killing of Staphylococcus aureus.* J Biol Chem, 2002. **277**(12): p. 9757-62.
52. Hampton, M.B., A.J. Kettle, and C.C. Winterbourn, *Inside the neutrophil phagosome: oxidants, myeloperoxidase, and bacterial killing.* Blood, 1998. **92**(9): p. 3007-17.
53. Reeves, E.P., et al., *Reassessment of the microbicidal activity of reactive oxygen species and hypochlorous acid with reference to the phagocytic vacuole of the neutrophil granulocyte.* J Med Microbiol, 2003. **52**(Pt 8): p. 643-51.
54. Ashby, M.T., *Inorganic chemistry of defensive peroxidases in the human oral cavity.* J Dent Res, 2008. **87**(10): p. 900-14.
55. Pruitt, K.M., et al., *Lactoperoxidase-catalyzed oxidation of thiocyanate: polarographic study of the oxidation products.* Biochemistry, 1982. **21**(3): p. 562-7.
56. Thomas, E.L. and T.M. Aune, *Lactoperoxidase, peroxide, thiocyanate antimicrobial system: correlation of sulfhydryl oxidation with antimicrobial action.* Infect Immun, 1978. **20**(2): p. 456-63.
57. Morris, J.C., *The acid ionization constant of HOCl from 5 to 35 degrees celsius.* Journal of Physical Chemistry, 1966. **70**(12): p. 3798-&.
58. Prutz, W.A., et al., *On the irreversible destruction of reduced nicotinamide nucleotides by hypohalous acids.* Arch Biochem Biophys, 2000. **380**(1): p. 181-91.
59. Thomas, E.L., *Lactoperoxidase-catalyzed oxidation of thiocyanate: equilibria between oxidized forms of thiocyanate.* Biochemistry, 1981. **20**(11): p. 3273-80.
60. Hazen, S.L., et al., *Human neutrophils employ chlorine gas as an oxidant during phagocytosis.* J Clin Invest, 1996. **98**(6): p. 1283-9.
61. Spalteholz, H., O.M. Panasenko, and J. Arnhold, *Formation of reactive halide species by myeloperoxidase and eosinophil peroxidase.* Arch Biochem Biophys, 2006. **445**(2): p. 225-34.
62. Hawkins, C.L., D.I. Pattison, and M.J. Davies, *Hypochlorite-induced oxidation of amino acids, peptides and proteins.* Amino Acids, 2003. **25**(3-4): p. 259-274.
63. Weiss, S.J., et al., *Brominating oxidants generated by human eosinophils.* Science, 1986. **234**(4773): p. 200-3.
64. Thomas, E.L., et al., *Oxidation of bromide by the human leukocyte enzymes myeloperoxidase and eosinophil peroxidase. Formation of bromamines.* J Biol Chem, 1995. **270**(7): p. 2906-13.
65. Hayatsu, H., S. Pan, and T. Ukita, *Reaction of sodium hypochlorite with nucleic acids and their constituents.* Chem Pharm Bull (Tokyo), 1971. **19**(10): p. 2189-92.

66. Hawkins, C.L. and M.J. Davies, *Hypochlorite-induced damage to nucleosides: formation of chloramines and nitrogen-centered radicals.* Chem Res Toxicol, 2001. **14**(8): p. 1071-81.
67. Hawkins, C.L. and M.J. Davies, *The role of reactive N-bromo species and radical intermediates in hypobromous acid-induced protein oxidation.* Free Radic Biol Med, 2005. **39**(7): p. 900-12.
68. Pattison, D.I. and M.J. Davies, *Kinetic analysis of the reactions of hypobromous acid with protein components: implications for cellular damage and use of 3-bromotyrosine as a marker of oxidative stress.* Biochemistry, 2004. **43**(16): p. 4799-809.
69. Trogolo, D. and J.S. Arey, *Benchmark thermochemistry of chloramines, bromamines, and bromochloramines: halogen oxidants stabilized by electron correlation.* Phys Chem Chem Phys, 2015. **17**(5): p. 3584-98.
70. Hawkins, C.L. and M.J. Davies, *Inactivation of protease inhibitors and lysozyme by hypochlorous acid: role of side-chain oxidation and protein unfolding in loss of biological function.* Chem Res Toxicol, 2005. **18**(10): p. 1600-10.
71. Hawkins, C.L., D.I. Pattison, and M.J. Davies, *Reaction of protein chloramines with DNA and nucleosides: evidence for the formation of radicals, protein-DNA cross-links and DNA fragmentation.* Biochem J, 2002. **365**(Pt 3): p. 605-15.
72. Pruitt, K.M. and J. Tenovuo, *Kinetics of hypothiocyanite production during peroxidase-catalyzed oxidation of thiocyanate.* Biochim Biophys Acta, 1982. **704**(2): p. 204-14.
73. Pruitt, K.M., et al., *Steady-state kinetics of thiocyanate oxidation catalyzed by human salivary peroxidase.* Biochemistry, 1988. **27**(1): p. 240-5.
74. Slungaard, A. and J.R. Mahoney, Jr., *Thiocyanate is the major substrate for eosinophil peroxidase in physiologic fluids. Implications for cytotoxicity.* J Biol Chem, 1991. **266**(8): p. 4903-10.
75. Barnett, J.J., M.L. McKee, and D.M. Stanbury, *Acidic aqueous decomposition of thiocyanogen.* Inorg Chem, 2004. **43**(16): p. 5021-33.
76. Nagy, P., K. Lemma, and M.T. Ashby, *Kinetics and mechanism of the comproportionation of hypothiocyanous acid and thiocyanate to give thiocyanogen in acidic aqueous solution.* Inorg Chem, 2007. **46**(1): p. 285-92.
77. Kalmar, J., et al., *Mechanism of decomposition of the human defense factor hypothiocyanite near physiological pH.* J Am Chem Soc, 2011. **133**(49): p. 19911-21.
78. Okafor, P.N., C.O. Okorowkwo, and E.N. Maduagwu, *Occupational and dietary exposures of humans to cyanide poisoning from large-scale cassava processing and ingestion of cassava foods.* Food Chem Toxicol, 2002. **40**(7): p. 1001-5.
79. Han, H. and H. Kwon, *Estimated dietary intake of thiocyanate from Brassicaceae family in Korean diet.* J Toxicol Environ Health A, 2009. **72**(21-22): p. 1380-7.
80. Saloojee, Y., et al., *Carboxyhaemoglobin and plasma thiocyanate: complementary indicators of smoking behaviour?* Thorax, 1982. **37**(7): p. 521-5.
81. Wang, Z., et al., *Protein carbamylation links inflammation, smoking, uremia and atherogenesis.* Nat Med, 2007. **13**(10): p. 1176-84.
82. Husgafvel-pursiainen, K., et al., *Passive smoking at work: biochemical and biological measures of exposure to environmental tobacco smoke.* International Archives of Occupational and Environmental Health, 1987. **59**(4): p. 337-345.
83. Morgan, P.E., et al., *High plasma thiocyanate levels in smokers are a key determinant of thiol oxidation induced by myeloperoxidase.* Free Radic Biol Med, 2011. **51**(9): p. 1815-22.

84. Arlandson, M., et al., *Eosinophil peroxidase oxidation of thiocyanate. Characterization of major reaction products and a potential sulfhydryl-targeted cytotoxicity system.* J Biol Chem, 2001. **276**(1): p. 215-24.
85. Figlar, J.N. and D.M. Stanbury, *Thiocyanogen as an intermediate in the oxidation of thiocyanate by hydrogen peroxide in acidic aqueous solution.* Inorg Chem, 2000. **39**(22): p. 5089-94.
86. Lovaas, E., *Free radical generation and coupled thiol oxidation by lactoperoxidase/SCN-/H2O2.* Free Radic Biol Med, 1992. **13**(3): p. 187-95.
87. Exner, M., et al., *Thiocyanate catalyzes myeloperoxidase-initiated lipid oxidation in LDL.* Free Radic Biol Med, 2004. **37**(2): p. 146-55.
88. van Dalen, C.J. and A.J. Kettle, *Substrates and products of eosinophil peroxidase.* Biochem J, 2001. **358**(Pt 1): p. 233-9.
89. Nagy, P., J.L. Beal, and M.T. Ashby, *Thiocyanate is an efficient endogenous scavenger of the phagocytic killing agent hypobromous acid.* Chem Res Toxicol, 2006. **19**(4): p. 587-93.
90. Ashby, M.T., A.C. Carlson, and M.J. Scott, *Redox buffering of hypochlorous acid by thiocyanate in physiologic fluids.* J Am Chem Soc, 2004. **126**(49): p. 15976-7.
91. Lloyd, M.M., et al., *Hypothiocyanous acid is a more potent inducer of apoptosis and protein thiol depletion in murine macrophage cells than hypochlorous acid or hypobromous acid.* Biochem J, 2008. **414**(2): p. 271-80.
92. Bozonet, S.M., et al., *Hypothiocyanous acid is a potent inhibitor of apoptosis and caspase 3 activation in endothelial cells.* Free Radic Biol Med, 2010. **49**(6): p. 1054-63.
93. Ashby, M.T., *Hypothiocyanate*, in *Advances in Inorganic Chemistry, Vol 64: Inorganic Bioinorganic Reaction Mechanisms*, R. VanEldik, Editor. 2012, Elsevier Academic Press Inc: San Diego. p. 263-303.
94. Barnett, J.J. and D.M. Stanbury, *Formation of trithiocyanate in the oxidation of aqueous thiocyanate.* Inorg Chem, 2002. **41**(2): p. 164-6.
95. Pattison, D.I. and M.J. Davies, *Reactions of myeloperoxidase-derived oxidants with biological substrates: gaining chemical insight into human inflammatory diseases.* Curr Med Chem, 2006. **13**(27): p. 3271-90.
96. Pattison, D.I. and M.J. Davies, *Absolute rate constants for the reaction of hypochlorous acid with protein side chains and peptide bonds.* Chem Res Toxicol, 2001. **14**(10): p. 1453-64.
97. Hawkins, C.L., et al., *Tryptophan residues are targets in hypothiocyanous acid-mediated protein oxidation.* Biochem J, 2008. **416**(3): p. 441-52.
98. Skaff, O., D.I. Pattison, and M.J. Davies, *Hypothiocyanous acid reactivity with low-molecular-mass and protein thiols: absolute rate constants and assessment of biological relevance.* Biochem J, 2009. **422**(1): p. 111-7.
99. Skaff, O., et al., *Selenium-containing amino acids are targets for myeloperoxidase-derived hypothiocyanous acid: determination of absolute rate constants and implications for biological damage.* Biochemical Journal, 2012. **441**: p. 305-316.
100. Hazell, L.J. and R. Stocker, *Oxidation of low-density lipoprotein with hypochlorite causes transformation of the lipoprotein into a high-uptake form for macrophages.* Biochem J, 1993. **290 (Pt 1)**: p. 165-72.
101. Davies, M.J. and C.L. Hawkins, *Hypochlorite-induced oxidation of thiols: formation of thiyl radicals and the role of sulfenyl chlorides as intermediates.* Free Radic Res, 2000. **33**(6): p. 719-29.
102. Lemma, K. and M.T. Ashby, *Reactive sulfur species: kinetics and mechanism of the equilibrium between cysteine sulfenyl thiocyanate and cysteine thiosulfinate ester in acidic aqueous solution.* J Org Chem, 2008. **73**(8): p. 3017-23.

103. Yang, Y.T., M. Whiteman, and S.P. Gieseg, *Intracellular glutathione protects human monocyte-derived macrophages from hypochlorite damage.* Life Sci, 2012. **90**(17-18): p. 682-8.
104. Ghezzi, P., *Regulation of protein function by glutathionylation.* Free Radic Res, 2005. **39**(6): p. 573-80.
105. Fernandes, A.P. and A. Holmgren, *Glutaredoxins: glutathione-dependent redox enzymes with functions far beyond a simple thioredoxin backup system.* Antioxid Redox Signal, 2004. **6**(1): p. 63-74.
106. Dalle-Donne, I., et al., *Protein S-glutathionylation: a regulatory device from bacteria to humans.* Trends Biochem Sci, 2009. **34**(2): p. 85-96.
107. Aune, T.M. and E.L. Thomas, *Oxidation of protein sulfhydryls by products of peroxidase-catalyzed oxidation of thiocyanate ion.* Biochemistry, 1978. **17**(6): p. 1005-10.
108. Poole, L.B., *Formation and functions of protein sulfenic acids.* Curr Protoc Toxicol, 2004. **Chapter 17**: p. Unit17 1.
109. Poole, L.B., P.A. Karplus, and A. Claiborne, *Protein sulfenic acids in redox signaling.* Annu Rev Pharmacol Toxicol, 2004. **44**: p. 325-47.
110. Paulsen, C.E. and K.S. Carroll, *Chemical dissection of an essential redox switch in yeast.* Chem Biol, 2009. **16**(2): p. 217-25.
111. Levine, R.L., J. Moskovitz, and E.R. Stadtman, *Oxidation of methionine in proteins: roles in antioxidant defense and cellular regulation.* IUBMB Life, 2000. **50**(4-5): p. 301-7.
112. Levine, R.L., et al., *Methionine residues as endogenous antioxidants in proteins.* Proc Natl Acad Sci U S A, 1996. **93**(26): p. 15036-40.
113. Brot, N., et al., *Enzymatic reduction of protein-bound methionine sulfoxide.* Proc Natl Acad Sci U S A, 1981. **78**(4): p. 2155-8.
114. Lee, B.C., et al., *Functions and evolution of selenoprotein methionine sulfoxide reductases.* Biochim Biophys Acta, 2009. **1790**(11): p. 1471-7.
115. Riddles, P.W., R.L. Blakeley, and B. Zerner, *Reassessment of Ellman's reagent.* Methods Enzymol, 1983. **91**: p. 49-60.
116. Fernstrom, J.D., *Role of precursor availability in control of monoamine biosynthesis in brain.* Physiol Rev, 1983. **63**(2): p. 484-546.
117. Fu, X., et al., *Hypochlorous acid generated by myeloperoxidase modifies adjacent tryptophan and glycine residues in the catalytic domain of matrix metalloproteinase-7 (matrilysin): an oxidative mechanism for restraining proteolytic activity during inflammation.* J Biol Chem, 2003. **278**(31): p. 28403-9.
118. Bhaskar, B., et al., *A novel heme and peroxide-dependent tryptophan-tyrosine cross-link in a mutant of cytochrome c peroxidase.* J Mol Biol, 2003. **328**(1): p. 157-66.
119. van de Weert, M., et al., *Mass spectrometric analysis of oxidized tryptophan.* Journal of Mass Spectrometry, 1998. **33**(9): p. 884-891.
120. Derosa, M. and J.L.T. Alonso, *STUDIES OF MECHANISM OF CHLORINATION OF INDOLES - DETECTION OF N-CHLOROINDOLE AND 3-CHLORO-INDOLE-H-3 AS INTERMEDIATES.* Journal of Organic Chemistry, 1978. **43**(13): p. 2639-2643.
121. Hadfield, K.A., et al., *Myeloperoxidase-derived oxidants modify apolipoprotein A-I and generate dysfunctional high-density lipoproteins: comparison of hypothiocyanous acid (HOSCN) with hypochlorous acid (HOCl).* Biochem J, 2013. **449**(2): p. 531-42.
122. Bonifay, V., et al., *Tryptophan oxidation in proteins exposed to thiocyanate-derived oxidants.* Arch Biochem Biophys, 2014. **564**: p. 1-11.

123. Fu, S., et al., *Reactions of hypochlorous acid with tyrosine and peptidyl-tyrosyl residues give dichlorinated and aldehydic products in addition to 3-chlorotyrosine.* J Biol Chem, 2000. **275**(15): p. 10851-8.
124. Schieven, G.L., H. de Fex, and L. Stephenson, *Hypochlorous acid activates tyrosine phosphorylation signal pathways leading to calcium signaling and TNFalpha production.* Antioxid Redox Signal, 2002. **4**(3): p. 501-7.
125. Winterbourn, C.C. and A.J. Kettle, *Biomarkers of myeloperoxidase-derived hypochlorous acid.* Free Radic Biol Med, 2000. **29**(5): p. 403-9.
126. Kettle, A.J., *Neutrophils convert tyrosyl residues in albumin to chlorotyrosine.* FEBS Lett, 1996. **379**(1): p. 103-6.
127. Wu, W., et al., *3-Bromotyrosine and 3,5-dibromotyrosine are major products of protein oxidation by eosinophil peroxidase: potential markers for eosinophil-dependent tissue injury in vivo.* Biochemistry, 1999. **38**(12): p. 3538-48.
128. Prutz, W.A., et al., *On the oxidation of cytochrome c by hypohalous acids.* Arch Biochem Biophys, 2001. **389**(1): p. 110-22.
129. Kopple, J.D. and M.E. Swendseid, *Evidence that histidine is an essential amino acid in normal and chronically uremic man.* J Clin Invest, 1975. **55**(5): p. 881-91.
130. Aune, T.M., E.L. Thomas, and M. Morrison, *Lactoperoxidase-catalyzed incorporation of thiocyanate ion into a protein substrate.* Biochemistry, 1977. **16**(21): p. 4611-5.
131. Hazell, L.J., J.J. van den Berg, and R. Stocker, *Oxidation of low-density lipoprotein by hypochlorite causes aggregation that is mediated by modification of lysine residues rather than lipid oxidation.* Biochem J, 1994. **302 (Pt 1)**: p. 297-304.
132. Whiteman, M., A. Jenner, and B. Halliwell, *Hypochlorous acid-induced base modifications in isolated calf thymus DNA.* Chem Res Toxicol, 1997. **10**(11): p. 1240-1246.
133. van Rensburg, C.E., et al., *Hypochlorous acid potentiates hydrogen peroxide-mediated DNA-strand breaks in human mononuclear leucocytes.* Mutat Res, 1992. **265**(2): p. 255-61.
134. White, W.E., Jr., K.M. Pruitt, and B. Mansson-Rahemtulla, *Peroxidase-thiocyanate-peroxide antibacterial system does not damage DNA.* Antimicrob Agents Chemother, 1983. **23**(2): p. 267-72.
135. Prutz, W.A., *Hypochlorous acid interactions with thiols, nucleotides, DNA, and other biological substrates.* Arch Biochem Biophys, 1996. **332**(1): p. 110-20.
136. Kawai, Y., et al., *Endogenous formation of novel halogenated 2 '-deoxycytidine - Hypohalous acid-mediated DNA modification at the site of inflammation.* Journal of Biological Chemistry, 2004. **279**(49): p. 51241-51249.
137. Henderson, J.P., J. Byun, and J.W. Heinecke, *Chlorination of nucleobases, RNA and DNA by myeloperoxidase: a pathway for cytotoxicity and mutagenesis by activated phagocytes.* Redox Report, 1999. **4**(6): p. 319-320.
138. Takeshita, J., et al., *Myeloperoxidase generates 5-chlorouracil in human atherosclerotic tissue - A potential pathway for somatic mutagenesis by macrophages.* Journal of Biological Chemistry, 2006. **281**(6): p. 3096-3104.
139. Lao, V.V., et al., *Incorporation of 5-chlorocytosine into mammalian DNA results in heritable gene silencing and altered cytosine methylation patterns.* Carcinogenesis, 2009. **30**(5): p. 886-93.
140. Zhang, R.L., et al., *Defects in leukocyte-mediated initiation of lipid peroxidation in plasma as studied in myeloperoxidase-deficient subjects: systematic identification of multiple endogenous diffusible substrates for myeloperoxidase in plasma.* Blood, 2002. **99**(5): p. 1802-1810.

141. Collins, P., et al., *17 beta-Estradiol attenuates acetylcholine-induced coronary arterial constriction in women but not men with coronary heart disease.* Circulation, 1995. **92**(1): p. 24-30.
142. Ismael, F.O., et al., *Comparative reactivity of the myeloperoxidase-derived oxidants HOCl and HOSCN with low-density lipoprotein (LDL): Implications for foam cell formation in atherosclerosis.* Arch Biochem Biophys, 2015. **573**: p. 40-51.
143. Carr, A.C., J.J.M. vandenBerg, and C. Winterbourn, *Chlorination of cholesterol in cell membranes by hypochlorous acid.* Arch Biochem Biophys, 1996. **332**(1): p. 63-69.
144. Carr, A.C., C.C. Winterbourn, and J.J.M. vandenBerg, *Peroxidase-mediated bromination of unsaturated fatty acids to form bromohydrins.* Arch Biochem Biophys, 1996. **327**(2): p. 227-233.
145. Winterbourn, C.C., et al., *Chlorohydrin formation from unsaturated fatty acids reacted with hypochlorous acid.* Arch Biochem Biophys, 1992. **296**(2): p. 547-55.
146. Heinecke, J.W., et al., *Cholesterol chlorohydrin synthesis by the myeloperoxidase-hydrogen peroxide-chloride system: potential markers for lipoproteins oxidatively damaged by phagocytes.* Biochemistry, 1994. **33**(33): p. 10127-36.
147. van den Berg, J.J., C.C. Winterbourn, and F.A. Kuypers, *Hypochlorous acid-mediated modification of cholesterol and phospholipid: analysis of reaction products by gas chromatography-mass spectrometry.* J Lipid Res, 1993. **34**(11): p. 2005-12.
148. Yuan, X.M., et al., *Lysosomal destabilization during macrophage damage induced by cholesterol oxidation products.* Free Radic Biol Med, 2000. **28**(2): p. 208-18.
149. Vissers, M.C., A.C. Carr, and C.C. Winterbour, *Fatty acid chlorohydrins and bromohydrins are cytotoxic to human endothelial cells.* Redox Rep, 2001. **6**(1): p. 49-55.
150. Moser, A.B., et al., *Human and great ape red blood cells differ in plasmalogen levels and composition.* Lipids Health Dis, 2011. **10**: p. 101.
151. Gorgas, K., et al., *The ether lipid-deficient mouse: tracking down plasmalogen functions.* Biochim Biophys Acta, 2006. **1763**(12): p. 1511-26.
152. Nagan, N. and R.A. Zoeller, *Plasmalogens: biosynthesis and functions.* Prog Lipid Res, 2001. **40**(3): p. 199-229.
153. Albert, C.J., et al., *Reactive brominating species produced by myeloperoxidase target the vinyl ether bond of plasmalogens: disparate utilization of sodium halides in the production of alpha-halo fatty aldehydes.* J Biol Chem, 2002. **277**(7): p. 4694-703.
154. Albert, C.J., et al., *Eosinophil peroxidase-derived reactive brominating species target the vinyl ether bond of plasmalogens generating a novel chemoattractant, alpha-bromo fatty aldehyde.* J Biol Chem, 2003. **278**(11): p. 8942-50.
155. Thukkani, A.K., et al., *Myeloperoxidase-derived reactive chlorinating species from human monocytes target plasmalogens in low density lipoprotein.* J Biol Chem, 2003. **278**(38): p. 36365-72.
156. Thukkani, A.K., et al., *Neutrophil-mediated accumulation of 2-ClHDA during myocardial infarction: 2-ClHDA-mediated myocardial injury.* Am J Physiol Heart Circ Physiol, 2005. **288**(6): p. H2955-64.
157. Flitsch, S.L. and R.V. Ulijn, *Sugars tied to the spot.* Nature, 2003. **421**(6920): p. 219-20.
158. Romano, A.H. and T. Conway, *Evolution of carbohydrate metabolic pathways.* Res Microbiol, 1996. **147**(6-7): p. 448-55.
159. Reeves, R.E., et al., *Pyrophosphate:D-fructose 6-phosphate 1-phosphotransferase. A new enzyme with the glycolytic function of 6-phosphofructokinase.* J Biol Chem, 1974. **249**(24): p. 7737-41.
160. Woods, A.A. and M.J. Davies, *Fragmentation of extracellular matrix by hypochlorous acid.* Biochem J, 2003. **376**(Pt 1): p. 219-27.

161. Storkey, C., et al., *Preventing protein oxidation with sugars: scavenging of hypohalous acids by 5-selenopyranose and 4-selenofuranose derivatives.* Chem Res Toxicol, 2012. **25**(11): p. 2589-99.
162. Pullar, J.M., M.C. Vissers, and C.C. Winterbourn, *Living with a killer: the effects of hypochlorous acid on mammalian cells.* IUBMB Life, 2000. **50**(4-5): p. 259-66.
163. Berridge, M.J., P. Lipp, and M.D. Bootman, *The versatility and universality of calcium signalling.* Nat Rev Mol Cell Biol, 2000. **1**(1): p. 11-21.
164. Eley, D.W., et al., *Calcium homeostasis in rabbit ventricular myocytes. Disruption by hypochlorous acid and restoration by dithiothreitol.* Circ Res, 1991. **69**(4): p. 1132-8.
165. !!! INVALID CITATION !!!
166. Favero, T.G., et al., *Hypochlorous acid modifies calcium release channel function from skeletal muscle sarcoplasmic reticulum.* J Appl Physiol (1985), 2003. **94**(4): p. 1387-94.
167. Periasamy, M. and A. Kalyanasundaram, *SERCA pump isoforms: their role in calcium transport and disease.* Muscle Nerve, 2007. **35**(4): p. 430-42.
168. Lipskaia, L., J.S. Hulot, and A.M. Lompre, *Role of sarco/endoplasmic reticulum calcium content and calcium ATPase activity in the control of cell growth and proliferation.* Pflugers Arch, 2009. **457**(3): p. 673-85.
169. Tong, X., A. Evangelista, and R.A. Cohen, *Targeting the redox regulation of SERCA in vascular physiology and disease.* Curr Opin Pharmacol, 2010. **10**(2): p. 133-8.
170. Cook, N.L., et al., *Myeloperoxidase-derived oxidants inhibit sarco/endoplasmic reticulum Ca2+-ATPase activity and perturb Ca2+ homeostasis in human coronary artery endothelial cells.* Free Radic Biol Med, 2012. **52**(5): p. 951-61.
171. Manning, G., et al., *The protein kinase complement of the human genome.* Science, 2002. **298**(5600): p. 1912-34.
172. Pearson, G., et al., *Mitogen-activated protein (MAP) kinase pathways: regulation and physiological functions.* Endocr Rev, 2001. **22**(2): p. 153-83.
173. Midwinter, R.G., M.C. Vissers, and C.C. Winterbourn, *Hypochlorous acid stimulation of the mitogen-activated protein kinase pathway enhances cell survival.* Arch Biochem Biophys, 2001. **394**(1): p. 13-20.
174. Wang, J.G., et al., *Thiocyanate-dependent induction of endothelial cell adhesion molecule expression by phagocyte peroxidases: a novel HOSCN-specific oxidant mechanism to amplify inflammation.* J Immunol, 2006. **177**(12): p. 8714-22.
175. Wang, J.G., et al., *The principal eosinophil peroxidase product, HOSCN, is a uniquely potent phagocyte oxidant inducer of endothelial cell tissue factor activity: a potential mechanism for thrombosis in eosinophilic inflammatory states.* Blood, 2006. **107**(2): p. 558-65.
176. Jung, K.J., et al., *Significance of protein tyrosine kinase/protein tyrosine phosphatase balance in the regulation of NF-kappaB signaling in the inflammatory process and aging.* Free Radic Biol Med, 2009. **47**(7): p. 983-91.
177. Rao, V.N. and E.S. Reddy, *elk-1 proteins interact with MAP kinases.* Oncogene, 1994. **9**(7): p. 1855-60.
178. Whiteman, M., et al., *Nitrite-mediated protection against hypochlorous acid-induced chondrocyte toxicity: a novel cytoprotective role of nitric oxide in the inflamed joint?* Arthritis Rheum, 2003. **48**(11): p. 3140-50.
179. Lane, A.E., et al., *The myeloperoxidase-derived oxidant HOSCN inhibits protein tyrosine phosphatases and modulates cell signalling via the mitogen-activated protein kinase (MAPK) pathway in macrophages.* Biochem J, 2010. **430**(1): p. 161-9.
180. Carr, A.C., et al., *Modification of red cell membrane lipids by hypochlorous acid and haemolysis by preformed lipid chlorohydrins.* Redox Rep, 1997. **3**(5-6): p. 263-71.

181. Pullar, J.M., C.C. Winterbourn, and M.C. Vissers, *Loss of GSH and thiol enzymes in endothelial cells exposed to sublethal concentrations of hypochlorous acid.* Am J Physiol, 1999. **277**(4 Pt 2): p. H1505-12.
182. Cantin, A.M., *Taurine modulation of hypochlorous acid-induced lung epithelial cell injury in vitro. Role of anion transport.* J Clin Invest, 1994. **93**(2): p. 606-14.
183. Hawkins, C.L., B.E. Brown, and M.J. Davies, *Hypochlorite- and hypobromite-mediated radical formation and its role in cell lysis.* Arch Biochem Biophys, 2001. **395**(2): p. 137-45.
184. Schraufstatter, I.U., et al., *Mechanisms of hypochlorite injury of target cells.* J Clin Invest, 1990. **85**(2): p. 554-62.
185. Lloyd, M.M., et al., *Comparative reactivity of the myeloperoxidase-derived oxidants hypochlorous acid and hypothiocyanous acid with human coronary artery endothelial cells.* Free Radic Biol Med, 2013. **65**: p. 1352-62.
186. Englert, R.P. and E. Shacter, *Distinct modes of cell death induced by different reactive oxygen species: amino acyl chloramines mediate hypochlorous acid-induced apoptosis.* J Biol Chem, 2002. **277**(23): p. 20518-26.
187. Whiteman, M., et al., *Hypochlorous acid-mediated mitochondrial dysfunction and apoptosis in human hepatoma HepG2 and human fetal liver cells: role of mitochondrial permeability transition.* Free Radic Biol Med, 2005. **38**(12): p. 1571-84.
188. Sugiyama, S., et al., *Hypochlorous acid, a macrophage product, induces endothelial apoptosis and tissue factor expression: involvement of myeloperoxidase-mediated oxidant in plaque erosion and thrombogenesis.* Arterioscler Thromb Vasc Biol, 2004. **24**(7): p. 1309-14.
189. Xiang, J., D.T. Chao, and S.J. Korsmeyer, *BAX-induced cell death may not require interleukin 1 beta-converting enzyme-like proteases.* Proc Natl Acad Sci U S A, 1996. **93**(25): p. 14559-63.
190. Yang, Y.T., M. Whiteman, and S.P. Gieseg, *HOCl causes necrotic cell death in human monocyte derived macrophages through calcium dependent calpain activation.* Biochim Biophys Acta, 2012. **1823**(2): p. 420-9.
191. Vissers, M.C., J.M. Pullar, and M.B. Hampton, *Hypochlorous acid causes caspase activation and apoptosis or growth arrest in human endothelial cells.* Biochem J, 1999. **344 Pt 2**: p. 443-9.
192. Marchetti, P., et al., *Redox regulation of apoptosis: impact of thiol oxidation status on mitochondrial function.* Eur J Immunol, 1997. **27**(1): p. 289-96.
193. Wagner, B.A., et al., *Role of thiocyanate, bromide and hypobromous acid in hydrogen peroxide-induced apoptosis.* Free Radic Res, 2004. **38**(2): p. 167-75.
194. Hanssen, F.S., *The bactericidal property of milk.* British Journal of Experimental Pathology, 1924. **5**(5): p. 271-280.
195. Wright, R.C. and J. Tramer, *Factors influencing the activity of cheese starters - The role of milk peroxidase.* Journal of Dairy Research, 1958. **25**(1): p. 104-118.
196. Klebanoff, S.J., W.H. Clem, and R.G. Luebke, *The peroxidase-thiocyanate-hydrogen peroxide antimicrobial system.* Biochim Biophys Acta, 1966. **117**(1): p. 63-72.
197. Thomas, E.L., et al., *Inhibition of Streptococcus mutans by the lactoperoxidase antimicrobial system.* Infection and Immunity, 1983. **39**(2): p. 767-778.
198. Carlsson, J., M.B.K. Edlund, and L. Hanstrom, *Bactericidal and cytotoxic effects of hypothiocyanite-hydrogen peroxide mixtures.* Infection and Immunity, 1984. **44**(3): p. 581-586.
199. Oram, J.D. and B. Reiter, *The inhibition of streptococci by lactoperoxidase, thiocyanate and hydrogen peroxide. The oxidation of thiocyanate and the nature of the inhibitory compound.* Biochem J, 1966. **100**(2): p. 382-8.

200. Mickelson, M.N., *Antibacterial action of lactoperoxidase-thiocyanate-hydrogen peroxide on Streptococcus agalactiae.* Appl Environ Microbiol, 1979. **38**(5): p. 821-6.
201. Barrett, T.J., et al., *Inactivation of thiol-dependent enzymes by hypothiocyanous acid: role of sulfenyl thiocyanate and sulfenic acid intermediates.* Free Radic Biol Med, 2012. **52**(6): p. 1075-85.
202. Henze, K. and W. Martin, *Evolutionary biology: essence of mitochondria.* Nature, 2003. **426**(6963): p. 127-8.
203. McBride, H.M., M. Neuspiel, and S. Wasiak, *Mitochondria: more than just a powerhouse.* Curr Biol, 2006. **16**(14): p. R551-60.
204. Hardy, L., et al., *Reoxygenation-dependent decrease in mitochondrial NADH:CoQ reductase (Complex I) activity in the hypoxic/reoxygenated rat heart.* Biochem J, 1991. **274 (Pt 1)**: p. 133-7.
205. Ballinger, S.W., et al., *Hydrogen peroxide- and peroxynitrite-induced mitochondrial DNA damage and dysfunction in vascular endothelial and smooth muscle cells.* Circ Res, 2000. **86**(9): p. 960-6.
206. MacMillan-Crow, L.A., J.P. Crow, and J.A. Thompson, *Peroxynitrite-mediated inactivation of manganese superoxide dismutase involves nitration and oxidation of critical tyrosine residues.* Biochemistry, 1998. **37**(6): p. 1613-22.
207. Dupuy, J., et al., *Crystal structure of human iron regulatory protein 1 as cytosolic aconitase.* Structure, 2006. **14**(1): p. 129-39.
208. Lauble, H., et al., *Crystal structures of aconitase with trans-aconitate and nitrocitrate bound.* J Mol Biol, 1994. **237**(4): p. 437-51.
209. Yankovskaya, V., et al., *Architecture of succinate dehydrogenase and reactive oxygen species generation.* Science, 2003. **299**(5607): p. 700-4.
210. Tomitsuka, E., et al., *Direct evidence for two distinct forms of the flavoprotein subunit of human mitochondrial complex II (succinate-ubiquinone reductase).* J Biochem, 2003. **134**(2): p. 191-5.
211. Carroll, J., et al., *Bovine complex I is a complex of 45 different subunits.* J Biol Chem, 2006. **281**(43): p. 32724-7.
212. Kurowski, B. and B. Ludwig, *The genes of the Paracoccus denitrificans bc1 complex. Nucleotide sequence and homologies between bacterial and mitochondrial subunits.* J Biol Chem, 1987. **262**(28): p. 13805-11.
213. Nesci, S., et al., *Thiol oxidation of mitochondrial F0-c subunits: a way to switch off antimicrobial drug targets of the mitochondrial ATP synthase.* Med Hypotheses, 2014. **83**(2): p. 160-5.
214. Subedi, K.P., et al., *Voltage-dependent anion channel 2 modulates resting Ca(2)+ sparks, but not action potential-induced Ca(2)+ signaling in cardiac myocytes.* Cell Calcium, 2011. **49**(2): p. 136-43.
215. Zeth, K., *Structure and evolution of mitochondrial outer membrane proteins of beta-barrel topology.* Biochim Biophys Acta, 2010. **1797**(6-7): p. 1292-9.
216. Sies, H., *Oxidative stress: oxidants and antioxidants.* Exp Physiol, 1997. **82**(2): p. 291-5.
217. Davies, K.J., *Oxidative stress: the paradox of aerobic life.* Biochem Soc Symp, 1995. **61**: p. 1-31.
218. McCord, J.M. and I. Fridovich, *Superoxide dismutase: the first twenty years (1968-1988).* Free Radic Biol Med, 1988. **5**(5-6): p. 363-9.
219. Zelko, I.N., T.J. Mariani, and R.J. Folz, *Superoxide dismutase multigene family: a comparison of the CuZn-SOD (SOD1), Mn-SOD (SOD2), and EC-SOD (SOD3) gene structures, evolution, and expression.* Free Radic Biol Med, 2002. **33**(3): p. 337-49.

220. Borgstahl, G.E., et al., *The structure of human mitochondrial manganese superoxide dismutase reveals a novel tetrameric interface of two 4-helix bundles.* Cell, 1992. **71**(1): p. 107-18.
221. Auchere, F. and C. Capeillere-Blandin, *Oxidation of Cu, Zn-superoxide dismutase by the myeloperoxidase/hydrogen peroxide/chloride system: functional and structural effects.* Free Radic Res, 2002. **36**(11): p. 1185-98.
222. Chelikani, P., I. Fita, and P.C. Loewen, *Diversity of structures and properties among catalases.* Cell Mol Life Sci, 2004. **61**(2): p. 192-208.
223. Gaetani, G.F., et al., *Predominant role of catalase in the disposal of hydrogen peroxide within human erythrocytes.* Blood, 1996. **87**(4): p. 1595-9.
224. Gabaldon, T., *Peroxisome diversity and evolution.* Philos Trans R Soc Lond B Biol Sci, 2010. **365**(1541): p. 765-73.
225. Wanders, R.J. and H.R. Waterham, *Biochemistry of mammalian peroxisomes revisited.* Annu Rev Biochem, 2006. **75**: p. 295-332.
226. Circu, M.L. and T.Y. Aw, *Glutathione and modulation of cell apoptosis.* Biochim Biophys Acta, 2012. **1823**(10): p. 1767-77.
227. Jones, D.P., et al., *Redox state of glutathione in human plasma.* Free Radic Biol Med, 2000. **28**(4): p. 625-35.
228. Pompella, A., et al., *The changing faces of glutathione, a cellular protagonist.* Biochem Pharmacol, 2003. **66**(8): p. 1499-503.
229. Meister, A., *Glutathione metabolism and its selective modification.* J Biol Chem, 1988. **263**(33): p. 17205-8.
230. Carr, A.C. and C.C. Winterbourn, *Oxidation of neutrophil glutathione and protein thiols by myeloperoxidase-derived hypochlorous acid.* Biochem J, 1997. **327 (Pt 1)**: p. 275-81.
231. Tatsumi, T. and H. Fliss, *Hypochlorous acid and chloramines increase endothelial permeability: possible involvement of cellular zinc.* Am J Physiol, 1994. **267**(4 Pt 2): p. H1597-607.
232. Vissers, M.C. and C.C. Winterbourn, *Oxidation of intracellular glutathione after exposure of human red blood cells to hypochlorous acid.* Biochem J, 1995. **307 (Pt 1)**: p. 57-62.
233. Epp, O., R. Ladenstein, and A. Wendel, *The refined structure of the selenoenzyme glutathione peroxidase at 0.2-nm resolution.* Eur J Biochem, 1983. **133**(1): p. 51-69.
234. Aruoma, O.I. and B. Halliwell, *Action of hypochlorous acid on the antioxidant protective enzymes superoxide dismutase, catalase and glutathione peroxidase.* Biochem J, 1987. **248**(3): p. 973-6.
235. Townsend, D.M., *S-glutathionylation: indicator of cell stress and regulator of the unfolded protein response.* Mol Interv, 2007. **7**(6): p. 313-24.
236. Fujii, J. and Y. Ikeda, *Advances in our understanding of peroxiredoxin, a multifunctional, mammalian redox protein.* Redox Rep, 2002. **7**(3): p. 123-30.
237. Hall, A., et al., *Structure-based insights into the catalytic power and conformational dexterity of peroxiredoxins.* Antioxid Redox Signal, 2011. **15**(3): p. 795-815.
238. Chae, H.Z., S.J. Chung, and S.G. Rhee, *Thioredoxin-dependent peroxide reductase from yeast.* J Biol Chem, 1994. **269**(44): p. 27670-8.
239. Stacey, M.M., et al., *Protein thiol oxidation and formation of S-glutathionylated cyclophilin A in cells exposed to chloramines and hypochlorous acid.* Arch Biochem Biophys, 2012. **527**(1): p. 45-54.
240. Stacey, M.M., M.C. Vissers, and C.C. Winterbourn, *Oxidation of 2-cys peroxiredoxins in human endothelial cells by hydrogen peroxide, hypochlorous acid, and chloramines.* Antioxid Redox Signal, 2012. **17**(3): p. 411-21.

241. Holmgren, A., *Thioredoxin and glutaredoxin systems.* J Biol Chem, 1989. **264**(24): p. 13963-6.
242. Gilbert, H.F., *Thiol/disulfide exchange equilibria and disulfide bond stability.* Methods Enzymol, 1995. **251**: p. 8-28.
243. Nordberg, J. and E.S. Arner, *Reactive oxygen species, antioxidants, and the mammalian thioredoxin system.* Free Radic Biol Med, 2001. **31**(11): p. 1287-312.
244. El Hadri, K., et al., *Thioredoxin-1 promotes anti-inflammatory macrophages of the M2 phenotype and antagonizes atherosclerosis.* Arterioscler Thromb Vasc Biol, 2012. **32**(6): p. 1445-52.
245. Mustacich, D. and G. Powis, *Thioredoxin reductase.* Biochem J, 2000. **346 Pt 1**: p. 1-8.
246. Benzie, I.F., *Vitamin C: prospective functional markers for defining optimal nutritional status.* Proc Nutr Soc, 1999. **58**(2): p. 469-76.
247. Justi, K.C., et al., *Nutritional composition and vitamin C stability in stored camu-camu (Myrciaria dubia) pulp.* Arch Latinoam Nutr, 2000. **50**(4): p. 405-8.
248. Lonn, M.E., J.M. Dennis, and R. Stocker, *Actions of "antioxidants" in the protection against atherosclerosis.* Free Radic Biol Med, 2012.
249. Banhegyi, G. and J. Mandl, *The hepatic glycogenoreticular system.* Pathol Oncol Res, 2001. **7**(2): p. 107-10.
250. Carr, A.C., T. Tijerina, and B. Frei, *Vitamin C protects against and reverses specific hypochlorous acid- and chloramine-dependent modifications of low-density lipoprotein.* Biochem J, 2000. **346 Pt 2**: p. 491-9.
251. Satoh, K. and H. Sakagami, *Effect of metal ions on radical intensity and cytotoxic activity of ascorbate.* Anticancer Res, 1997. **17**(2A): p. 1125-9.
252. McGregor, G.P. and H.K. Biesalski, *Rationale and impact of vitamin C in clinical nutrition.* Curr Opin Clin Nutr Metab Care, 2006. **9**(6): p. 697-703.
253. Ames, B.N., et al., *Uric acid provides an antioxidant defense in humans against oxidant- and radical-caused aging and cancer: a hypothesis.* Proc Natl Acad Sci U S A, 1981. **78**(11): p. 6858-62.
254. Maxwell, S.R., et al., *Antioxidant status in patients with uncomplicated insulin-dependent and non-insulin-dependent diabetes mellitus.* Eur J Clin Invest, 1997. **27**(6): p. 484-90.
255. Davies, K.J., et al., *Uric acid-iron ion complexes. A new aspect of the antioxidant functions of uric acid.* Biochem J, 1986. **235**(3): p. 747-54.
256. Leake, D.S., *Does an acidic pH explain why low density lipoprotein is oxidised in atherosclerotic lesions?* Atherosclerosis, 1997. **129**(2): p. 149-57.
257. Kand'ar, R. and P. Zakova, *Allantoin as a marker of oxidative stress in human erythrocytes.* Clin Chem Lab Med, 2008. **46**(9): p. 1270-4.
258. Stamp, L.K., et al., *Myeloperoxidase and oxidation of uric acid in gout: implications for the clinical consequences of hyperuricaemia.* Rheumatology (Oxford), 2014. **53**(11): p. 1958-65.
259. Meotti, F.C., et al., *Urate as a physiological substrate for myeloperoxidase: implications for hyperuricemia and inflammation.* J Biol Chem, 2011. **286**(15): p. 12901-11.
260. Kettle, A.J. and C.C. Winterbourn, *Mechanism of inhibition of myeloperoxidase by anti-inflammatory drugs.* Biochem Pharmacol, 1991. **41**(10): p. 1485-92.
261. Kettle, A.J., C.A. Gedye, and C.C. Winterbourn, *Mechanism of inactivation of myeloperoxidase by 4-aminobenzoic acid hydrazide.* Biochem J, 1997. **321 (Pt 2)**: p. 503-8.

262. Queiroz, R.F., S.M. Vaz, and O. Augusto, *Inhibition of the chlorinating activity of myeloperoxidase by tempol: revisiting the kinetics and mechanisms.* Biochem J, 2011. **439**(3): p. 423-31.
263. Rees, M.D., et al., *Inhibition of myeloperoxidase-mediated hypochlorous acid production by nitroxides.* Biochem J, 2009. **421**(1): p. 79-86.
264. Sliskovic, I., et al., *Analysis of the mechanism by which tryptophan analogs inhibit human myeloperoxidase.* Free Radic Biol Med, 2009. **47**(7): p. 1005-13.
265. Tiden, A.K., et al., *2-thioxanthines are mechanism-based inactivators of myeloperoxidase that block oxidative stress during inflammation.* J Biol Chem, 2011. **286**(43): p. 37578-89.
266. Forbes, L.V., et al., *Potent reversible inhibition of myeloperoxidase by aromatic hydroxamates.* J Biol Chem, 2013. **288**(51): p. 36636-47.
267. Forbes, L.V., et al., *Isoniazid as a substrate and inhibitor of myeloperoxidase: identification of amine adducts and the influence of superoxide dismutase on their formation.* Biochem Pharmacol, 2012. **84**(7): p. 949-60.
268. Carr, A.C., et al., *Myeloperoxidase binds to low-density lipoprotein: potential implications for atherosclerosis.* FEBS Lett, 2000. **487**(2): p. 176-80.
269. Daugherty, A., et al., *Myeloperoxidase, a catalyst for lipoprotein oxidation, is expressed in human atherosclerotic lesions.* J Clin Invest, 1994. **94**(1): p. 437-44.
270. Klebanoff, S.J., *Myeloperoxidase: contribution to the microbicidal activity of intact leukocytes.* Science, 1970. **169**(3950): p. 1095-7.
271. Hirche, T.O., et al., *Myeloperoxidase plays critical roles in killing Klebsiella pneumoniae and inactivating neutrophil elastase: effects on host defense.* J Immunol, 2005. **174**(3): p. 1557-65.
272. Aratani, Y., et al., *Severe impairment in early host defense against Candida albicans in mice deficient in myeloperoxidase.* Infect Immun, 1999. **67**(4): p. 1828-36.
273. Rosen, H., J.R. Crowley, and J.W. Heinecke, *Human neutrophils use the myeloperoxidase-hydrogen peroxide-chloride system to chlorinate but not nitrate bacterial proteins during phagocytosis.* J Biol Chem, 2002. **277**(34): p. 30463-8.
274. Ihalin, R., et al., *The effects of different (pseudo)halide substrates on peroxidase-mediated killing of Actinobacillus actinomycetemcomitans.* J Periodontal Res, 1998. **33**(7): p. 421-7.
275. Conner, G.E., et al., *The lactoperoxidase system links anion transport to host defense in cystic fibrosis.* FEBS Lett, 2007. **581**(2): p. 271-8.
276. Moskwa, P., et al., *A novel host defense system of airways is defective in cystic fibrosis.* Am J Respir Crit Care Med, 2007. **175**(2): p. 174-83.
277. Wijkstrom-Frei, C., et al., *Lactoperoxidase and human airway host defense.* Am J Respir Cell Mol Biol, 2003. **29**(2): p. 206-12.
278. Gerson, C., et al., *The lactoperoxidase system functions in bacterial clearance of airways.* Am J Respir Cell Mol Biol, 2000. **22**(6): p. 665-71.
279. Minarowski, L., et al., *Thiocyanate concentration in saliva of cystic fibrosis patients.* Folia Histochem Cytobiol, 2008. **46**(2): p. 245-6.
280. Xu, Y., S. Szep, and Z. Lu, *The antioxidant role of thiocyanate in the pathogenesis of cystic fibrosis and other inflammation-related diseases.* Proc Natl Acad Sci U S A, 2009. **106**(48): p. 20515-9.
281. Thong, Y.H., *How important is the myeloperoxidase microbicidal system of phagocytic cells?* Med Hypotheses, 1982. **8**(3): p. 249-54.
282. Segal, A.W., *How neutrophils kill microbes.* Annu Rev Immunol, 2005. **23**: p. 197-223.
283. Gaut, J.P., et al., *Neutrophils employ the myeloperoxidase system to generate antimicrobial brominating and chlorinating oxidants during sepsis.* Proc Natl Acad Sci U S A, 2001. **98**(21): p. 11961-11966.

284. Henderson, J.P., et al., *The eosinophil peroxidase-hydrogen peroxide-bromide system of human eosinophils generates 5-bromouracil, a mutagenic thymine analogue.* Biochemistry, 2001. **40**(7): p. 2052-2059.
285. Schultz, C.P., et al., *Thiocyanate levels in human saliva: quantitation by Fourier transform infrared spectroscopy.* Anal Biochem, 1996. **240**(1): p. 7-12.
286. Tenovuo, J., et al., *Antimicrobial factors of saliva in relation to dental caries and salivary levels of mutans streptococci.* Journal de Biologie Buccale, 1992. **20**(2): p. 85-90.
287. Tenovuo, J., et al., *Inhibition of dental plaque acid production by the salivary lactoperoxidase antimicrobial system.* Infect Immun, 1981. **34**(1): p. 208-14.
288. Cao, C.F. and Q.T. Smith, *Crevicular fluid myeloperoxidase at healthy, gingivitis and periodontitis sites.* Journal of Clinical Periodontology, 1989. **16**(1): p. 17-20.
289. Yankaskas, J.R., et al., *Cystic fibrosis adult care: consensus conference report.* Chest, 2004. **125**(1 Suppl): p. 1S-39S.
290. Ratjen, F. and G. Doring, *Cystic fibrosis.* Lancet, 2003. **361**(9358): p. 681-9.
291. Brown, R.K., et al., *Pulmonary dysfunction in cystic fibrosis is associated with oxidative stress.* Eur Respir J, 1996. **9**(2): p. 334-9.
292. Kettle, A.J., et al., *Myeloperoxidase and protein oxidation in the airways of young children with cystic fibrosis.* Am J Respir Crit Care Med, 2004. **170**(12): p. 1317-23.
293. Saude, E.J., et al., *NMR analysis of neutrophil activation in sputum samples from patients with cystic fibrosis.* Magn Reson Med, 2004. **52**(4): p. 807-14.
294. Dawson, D.C., S.S. Smith, and M.K. Mansoura, *CFTR: mechanism of anion conduction.* Physiol Rev, 1999. **79**(1 Suppl): p. S47-75.
295. Valinluck, V., et al., *5-halogenated pyrimidine lesions within a CpG sequence context mimic 5-methylcytosine by enhancing the binding of the methyl-CpG-binding domain of methyl-CpG-binding protein 2 (MeCP2).* Nucleic Acids Res, 2005. **33**(9): p. 3057-64.
296. Stanley, N.R., D.I. Pattison, and C.L. Hawkins, *Ability of hypochlorous acid and N-chloramines to chlorinate DNA and its constituents.* Chem Res Toxicol, 2010. **23**(7): p. 1293-302.
297. Pal, B.C., et al., *Environmental pollutant 5-chlorouracil is incorporated in mouse liver and testes DNA.* Mutat Res, 1981. **91**(4-5): p. 395-401.
298. Pero, R.W., et al., *Hypochlorous acid/N-chloramines are naturally produced DNA repair inhibitors.* Carcinogenesis, 1996. **17**(1): p. 13-8.
299. Hazen, S.L. and J.W. Heinecke, *3-Chlorotyrosine, a specific marker of myeloperoxidase-catalyzed oxidation, is markedly elevated in low density lipoprotein isolated from human atherosclerotic intima.* J Clin Invest, 1997. **99**(9): p. 2075-81.
300. Choi, D.K., et al., *Ablation of the inflammatory enzyme myeloperoxidase mitigates features of Parkinson's disease in mice.* J Neurosci, 2005. **25**(28): p. 6594-600.
301. Robinson, J.G., et al., *Atherosclerosis profile and incidence of cardiovascular events: a population-based survey.* BMC Cardiovasc Disord, 2009. **9**: p. 46.
302. Hansson, G.K., P. Libby, and I. Tabas, *Inflammation and plaque vulnerability.* J Intern Med, 2015.
303. Stary, H.C., *Evolution of atherosclerotic plaques in the coronary-arteries of young adults.* Arteriosclerosis, 1983. **3**(5): p. A471-A471.
304. Libby, P., *Inflammation in atherosclerosis.* Nature, 2002. **420**(6917): p. 868-74.
305. Diaz, M.N., et al., *Antioxidants and atherosclerotic heart disease.* N Engl J Med, 1997. **337**(6): p. 408-16.
306. Finn, A.V., et al., *Concept of vulnerable/unstable plaque.* Arterioscler Thromb Vasc Biol, 2010. **30**(7): p. 1282-92.

307. Haberland, M.E., C.L. Olch, and A.M. Folgelman, *Role of lysines in mediating interaction of modified low density lipoproteins with the scavenger receptor of human monocyte macrophages.* J Biol Chem, 1984. **259**(18): p. 11305-11.
308. Goldstein, J.L., et al., *Binding site on macrophages that mediates uptake and degradation of acetylated low density lipoprotein, producing massive cholesterol deposition.* Proc Natl Acad Sci U S A, 1979. **76**(1): p. 333-7.
309. Malle, E., et al., *Immunohistochemical evidence for the myeloperoxidase/H2O2/halide system in human atherosclerotic lesions: colocalization of myeloperoxidase and hypochlorite-modified proteins.* Eur J Biochem, 2000. **267**(14): p. 4495-503.
310. Heinecke, J.W., *Pathways for oxidation of low density lipoprotein by myeloperoxidase: tyrosyl radical, reactive aldehydes, hypochlorous acid and molecular chlorine.* Biofactors, 1997. **6**(2): p. 145-55.
311. Marsche, G., et al., *Class B scavenger receptors CD36 and SR-BI are receptors for hypochlorite-modified low density lipoprotein.* J Biol Chem, 2003. **278**(48): p. 47562-70.
312. Hotamisligil, G.S., *Endoplasmic reticulum stress and atherosclerosis.* Nat Med, 2010. **16**(4): p. 396-9.
313. Lin, J., V. Kakkar, and X. Lu, *The role of interleukin 35 in atherosclerosis.* Curr Pharm Des, 2015.
314. Tavora, F.R., et al., *Monocytes and neutrophils expressing myeloperoxidase occur in fibrous caps and thrombi in unstable coronary plaques.* BMC Cardiovasc Disord, 2009. **9**: p. 27.
315. Libby, P., P.M. Ridker, and A. Maseri, *Inflammation and atherosclerosis.* Circulation, 2002. **105**(9): p. 1135-43.
316. Hazen, S.L., et al., *Mass spectrometric quantification of 3-chlorotyrosine in human tissues with attomole sensitivity: a sensitive and specific marker for myeloperoxidase-catalyzed chlorination at sites of inflammation.* Free Radic Biol Med, 1997. **23**(6): p. 909-16.
317. Brennan, M.L., et al., *Prognostic value of myeloperoxidase in patients with chest pain.* N Engl J Med, 2003. **349**(17): p. 1595-604.
318. Kutter, D., et al., *Consequences of total and subtotal myeloperoxidase deficiency: risk or benefit ?* Acta Haematol, 2000. **104**(1): p. 10-5.
319. Bergt, C., et al., *Lysine residues direct the chlorination of tyrosines in YXXK motifs of apolipoprotein A-I when hypochlorous acid oxidizes high density lipoprotein.* J Biol Chem, 2004. **279**(9): p. 7856-66.
320. Bergt, C., et al., *Human neutrophils employ the myeloperoxidase/hydrogen peroxide/chloride system to oxidatively damage apolipoprotein A-I.* Eur J Biochem, 2001. **268**(12): p. 3523-31.
321. Zheng, L., et al., *Localization of nitration and chlorination sites on apolipoprotein A-I catalyzed by myeloperoxidase in human atheroma and associated oxidative impairment in ABCA1-dependent cholesterol efflux from macrophages.* J Biol Chem, 2005. **280**(1): p. 38-47.
322. Malle, E., et al., *Myeloperoxidase-mediated oxidation of high-density lipoproteins: fingerprints of newly recognized potential proatherogenic lipoproteins.* Arch Biochem Biophys, 2006. **445**(2): p. 245-55.
323. Eyer, P., et al., *Molar absorption coefficients for the reduced Ellman reagent: reassessment.* Anal Biochem, 2003. **312**(2): p. 224-7.
324. Hawkins, C.L., P.E. Morgan, and M.J. Davies, *Quantification of protein modification by oxidants.* Free Radic Biol Med, 2009. **46**(8): p. 965-88.

325. McDonagh, B. and D. Sheehan, *Effects of oxidative stress on protein thiols and disulphides in Mytilus edulis revealed by proteomics: actin and protein disulphide isomerase are redox targets.* Mar Environ Res, 2008. **66**(1): p. 193-5.
326. Clark, H.M., T.D. Hagedorn, and L.M. Landino, *Hypothiocyanous acid oxidation of tubulin cysteines inhibits microtubule polymerization.* Arch Biochem Biophys, 2013.
327. Leonard, S.E. and K.S. Carroll, *Chemical 'omics' approaches for understanding protein cysteine oxidation in biology.* Curr Opin Chem Biol, 2011. **15**(1): p. 88-102.
328. Leonard, S.E., K.G. Reddie, and K.S. Carroll, *Mining the Thiol Proteome for Sulfenic Acid Modifications Reveals New Targets for Oxidation in Cells.* ACS Chemical Biology, 2009. **4**(9): p. 783-799.
329. Claiborne, A., et al., *Protein-sulfenic acids: diverse roles for an unlikely player in enzyme catalysis and redox regulation.* Biochemistry, 1999. **38**(47): p. 15407-16.
330. Kolb, H.C., M.G. Finn, and K.B. Sharpless, *Click Chemistry: Diverse Chemical Function from a Few Good Reactions.* Angew Chem Int Ed Engl, 2001. **40**(11): p. 2004-2021.
331. Kumar, B., et al., *Oxidative stress is inherent in prostate cancer cells and is required for aggressive phenotype.* Cancer Res, 2008. **68**(6): p. 1777-85.
332. Han, J., et al., *Interrelated roles for Mcl-1 and BIM in regulation of TRAIL-mediated mitochondrial apoptosis.* J Biol Chem, 2006. **281**(15): p. 10153-63.
333. Knowles, J.R., *Enzyme-catalyzed phosphoryl transfer reactions.* Annu Rev Biochem, 1980. **49**: p. 877-919.
334. Griffin, J.L. and J.P. Shockcor, *Metabolic profiles of cancer cells.* Nat Rev Cancer, 2004. **4**(7): p. 551-61.
335. Demetrius, L.A., J.F. Coy, and J.A. Tuszynski, *Cancer proliferation and therapy: the Warburg effect and quantum metabolism.* Theor Biol Med Model, 2010. **7**: p. 2.
336. Govers, R., *Cellular regulation of glucose uptake by glucose transporter GLUT4.* Adv Clin Chem, 2014. **66**: p. 173-240.
337. Zor, T. and Z. Selinger, *Linearization of the Bradford protein assay increases its sensitivity: theoretical and experimental studies.* Anal Biochem, 1996. **236**(2): p. 302-8.
338. Tal, M., A. Silberstein, and E. Nusser, *Why does Coomassie Brilliant Blue R interact differently with different proteins? A partial answer.* J Biol Chem, 1985. **260**(18): p. 9976-80.
339. Smith, P.K., et al., *Measurement of protein using bicinchoninic acid.* Anal Biochem, 1985. **150**(1): p. 76-85.
340. Stoscheck, C.M., *Quantitation of protein.* Methods Enzymol, 1990. **182**: p. 50-68.
341. Lowry, O.H., et al., *Protein measurement with the Folin phenol reagent.* J Biol Chem, 1951. **193**(1): p. 265-75.
342. Ihalin, R., V. Loimaranta, and J. Tenovuo, *Origin, structure, and biological activities of peroxidases in human saliva.* Arch Biochem Biophys, 2006. **445**(2): p. 261-8.
343. Kettle, A.J., C.A. Gedye, and C.C. Winterbourn, *Superoxide is an antagonist of antiinflammatory drugs that inhibit hypochlorous acid production by myeloperoxidase.* Biochem Pharmacol, 1993. **45**(10): p. 2003-10.
344. Weiss, S.J., et al., *Chlorination of taurine by human neutrophils. Evidence for hypochlorous acid generation.* J Clin Invest, 1982. **70**(3): p. 598-607.
345. Pattison, D.I., C.L. Hawkins, and M.J. Davies, *Hypochlorous acid-mediated oxidation of lipid components and antioxidants present in low-density lipoproteins: absolute rate constants, product analysis, and computational modeling.* Chem Res Toxicol, 2003. **16**(4): p. 439-49.
346. Hamann, M., et al., *Quantitation of protein sulfinic and sulfonic acid, irreversibly oxidized protein cysteine sites in cellular proteins.* Methods Enzymol, 2002. **348**: p. 146-56.

347. Denu, J.M. and K.G. Tanner, *Specific and reversible inactivation of protein tyrosine phosphatases by hydrogen peroxide: evidence for a sulfenic acid intermediate and implications for redox regulation.* Biochemistry, 1998. **37**(16): p. 5633-42.
348. Gallogly, M.M. and J.J. Mieyal, *Mechanisms of reversible protein glutathionylation in redox signaling and oxidative stress.* Curr Opin Pharmacol, 2007. **7**(4): p. 381-91.
349. Paulsen, C.E. and K.S. Carroll, *Orchestrating Redox Signaling Networks through Regulatory Cysteine Switches.* ACS Chemical Biology, 2009. **5**(1): p. 47-62.
350. Wright, S.K. and R.E. Viola, *Evaluation of methods for the quantitation of cysteines in proteins.* Anal Biochem, 1998. **265**(1): p. 8-14.
351. Reddie, K.G. and K.S. Carroll, *Expanding the functional diversity of proteins through cysteine oxidation.* Curr Opin Chem Biol, 2008. **12**(6): p. 746-54.
352. Carballal, S., et al., *Sulfenic acid in human serum albumin.* Amino Acids, 2007. **32**(4): p. 543-51.
353. Johansson, M. and M. Lundberg, *Glutathionylation of beta-actin via a cysteinyl sulfenic acid intermediary.* BMC Biochem, 2007. **8**: p. 26.
354. Fratelli, M., et al., *Identification by redox proteomics of glutathionylated proteins in oxidatively stressed human T lymphocytes.* Proc Natl Acad Sci U S A, 2002. **99**(6): p. 3505-10.
355. Casagrande, S., et al., *Glutathionylation of human thioredoxin: a possible crosstalk between the glutathione and thioredoxin systems.* Proc Natl Acad Sci U S A, 2002. **99**(15): p. 9745-9.
356. Garcia, J., et al., *Regulation of mitochondrial glutathione redox status and protein glutathionylation by respiratory substrates.* J Biol Chem, 2010. **285**(51): p. 39646-54.
357. Grek, C.L., et al., *S-glutathionylated serine proteinase inhibitors as plasma biomarkers in assessing response to redox-modulating drugs.* Cancer Res, 2012. **72**(9): p. 2383-93.
358. Riordan, J.F. and B.L. Vallee, *Reactions with N-ethylmaleimide and p-mercuribenzoate.* Methods Enzymol, 1972. **25**: p. 449-56.
359. Giustarini, D., et al., *S-glutathionylation: from redox regulation of protein functions to human diseases.* J Cell Mol Med, 2004. **8**(2): p. 201-12.
360. Li, N., et al., *Relative quantification of proteasome activity by activity-based protein profiling and LC-MS/MS.* Nat Protoc, 2013. **8**(6): p. 1155-68.
361. Cook, N.L., D.I. Pattison, and M.J. Davies, *Myeloperoxidase-derived oxidants rapidly oxidize and disrupt zinc-cysteine/histidine clusters in proteins.* Free Radic Biol Med, 2012. **53**(11): p. 2072-80.
362. Summers, F.A., A. Forsman Quigley, and C.L. Hawkins, *Identification of proteins susceptible to thiol oxidation in endothelial cells exposed to hypochlorous acid and N-chloramines.* Biochem Biophys Res Commun, 2012. **425**(2): p. 157-61.
363. Pullar, J.M., M.C. Vissers, and C.C. Winterbourn, *Glutathione oxidation by hypochlorous acid in endothelial cells produces glutathione sulfonamide as a major product but not glutathione disulfide.* J Biol Chem, 2001. **276**(25): p. 22120-5.
364. Yoshitake, S., et al., *Possible differences in the regenerative roles played by thioltransferase and thioredoxin for oxidatively damaged proteins.* J Biochem, 1994. **116**(1): p. 42-6.
365. Claiborne, A., et al., *Protein-sulfenic acid stabilization and function in enzyme catalysis and gene regulation.* FASEB J, 1993. **7**(15): p. 1483-90.
366. Azevedo, D., et al., *Two redox centers within Yap1 for H2O2 and thiol-reactive chemicals signaling.* Free Radic Biol Med, 2003. **35**(8): p. 889-900.
367. van Montfort, R.L., et al., *Oxidation state of the active-site cysteine in protein tyrosine phosphatase 1B.* Nature, 2003. **423**(6941): p. 773-7.

368. Salmeen, A., et al., *Redox regulation of protein tyrosine phosphatase 1B involves a sulphenyl-amide intermediate.* Nature, 2003. **423**(6941): p. 769-73.
369. Wang, P.F., et al., *An unusually low pK(a) for Cys282 in the active site of human muscle creatine kinase.* Biochemistry, 2001. **40**(39): p. 11698-705.
370. Pineda-Molina, E., et al., *Glutathionylation of the p50 subunit of NF-kappaB: a mechanism for redox-induced inhibition of DNA binding.* Biochemistry, 2001. **40**(47): p. 14134-42.
371. Mieyal, J.J., et al., *Molecular mechanisms and clinical implications of reversible protein S-glutathionylation.* Antioxid Redox Signal, 2008. **10**(11): p. 1941-88.
372. Sitia, R. and S.N. Molteni, *Stress, protein (mis)folding, and signaling: the redox connection.* Sci STKE, 2004. **2004**(239): p. pe27.
373. Xie, L., C.N. Chesterman, and P.J. Hogg, *Control of von Willebrand factor multimer size by thrombospondin-1.* J Exp Med, 2001. **193**(12): p. 1341-9.
374. Thornton, J.M., *Disulphide bridges in globular proteins.* J Mol Biol, 1981. **151**(2): p. 261-87.
375. Eaton, P., et al., *Glyceraldehyde phosphate dehydrogenase oxidation during cardiac ischemia and reperfusion.* J Mol Cell Cardiol, 2002. **34**(11): p. 1549-60.
376. Mallis, R.J., et al., *Irreversible thiol oxidation in carbonic anhydrase III: protection by S-glutathiolation and detection in aging rats.* Biol Chem, 2002. **383**(3-4): p. 649-62.
377. Nulton-Persson, A.C., et al., *Reversible inactivation of alpha-ketoglutarate dehydrogenase in response to alterations in the mitochondrial glutathione status.* Biochemistry, 2003. **42**(14): p. 4235-42.
378. Ravichandran, V., et al., *S-thiolation of glyceraldehyde-3-phosphate dehydrogenase induced by the phagocytosis-associated respiratory burst in blood monocytes.* J Biol Chem, 1994. **269**(40): p. 25010-5.
379. Lenander-Lumikari, M., et al., *Combined inhibitory effect of fluoride and hypothiocyanite on the viability and glucose metabolism of Streptococcus mutans, serotype c.* Oral Microbiol Immunol, 1997. **12**(4): p. 231-5.
380. Hawkins, C.L., *The role of hypothiocyanous acid (HOSCN) in biological systems.* Free Radic Res, 2009. **43**(12): p. 1147-58.
381. Yamagishi, K., et al., *Smoking raises the risk of total and ischemic strokes in hypertensive men.* Hypertens Res, 2003. **26**(3): p. 209-17.
382. Jastroch, M., et al., *Mitochondrial proton and electron leaks.* Essays Biochem, 2010. **47**: p. 53-67.
383. Hao, W., et al., *Oligomycin-induced bioenergetic adaptation in cancer cells with heterogeneous bioenergetic organization.* J Biol Chem, 2010. **285**(17): p. 12647-54.
384. Lardy, H.A., D. Johnson, and M.W. Mc, *Antibiotics as tools for metabolic studies. I. A survey of toxic antibiotics in respiratory, phosphorylative and glycolytic systems.* Arch Biochem Biophys, 1958. **78**(2): p. 587-97.
385. Mickelson, M.N., *Glucose transport in Streptococcus agalactiae and its inhibition by lactoperoxidase-thiocyanate-hydrogen peroxide.* J Bacteriol, 1977. **132**(2): p. 541-8.
386. Madern, D., *Molecular evolution within the L-malate and L-lactate dehydrogenase super-family.* J Mol Evol, 2002. **54**(6): p. 825-40.
387. Richards, D.M., R.T. Dean, and W. Jessup, *Membrane proteins are critical targets in free radical mediated cytolysis.* Biochim Biophys Acta, 1988. **946**(2): p. 281-8.
388. Decker, T. and M.L. Lohmann-Matthes, *A quick and simple method for the quantitation of lactate dehydrogenase release in measurements of cellular cytotoxicity and tumor necrosis factor (TNF) activity.* J Immunol Methods, 1988. **115**(1): p. 61-9.

389. Weidmann, E., et al., *Lactate dehydrogenase-release assay: a reliable, nonradioactive technique for analysis of cytotoxic lymphocyte-mediated lytic activity against blasts from acute myelocytic leukemia.* Ann Hematol, 1995. **70**(3): p. 153-8.
390. Hoogendoorn, H., et al., *Hypothiocyanite ion; the inhibitor formed by the system lactoperoxidase-thiocyanate-hydrogen peroxide. I. Identification of the inhibiting compound.* Caries Res, 1977. **11**(2): p. 77-84.
391. O'Leary, V. and M. Solberg, *Effect of sodium nitrite inhibition on intracellular thiol groups and on the activity of certain glycolytic enzymes in Clostridium perfringens.* Appl Environ Microbiol, 1976. **31**(2): p. 208-12.
392. Tenovuo, J., et al., *Antibacterial effect of myeloperoxidase against Streptococcus mutans.* Oral Microbiol Immunol, 1988. **3**(2): p. 68-71.
393. Kundig, W., et al., *Restoration of active transport of glycosides in Escherichia coli by a component of a phosphotransferase system.* J Biol Chem, 1966. **241**(13): p. 3243-6.
394. Garcia-Alles, L.F., et al., *Mechanism-based inhibition of enzyme I of the Escherichia coli phosphotransferase system. Cysteine 502 is an essential residue.* J Biol Chem, 2002. **277**(9): p. 6934-42.
395. Postma, P.W., J.W. Lengeler, and G.R. Jacobson, *Phosphoenolpyruvate:carbohydrate phosphotransferase systems of bacteria.* Microbiol Rev, 1993. **57**(3): p. 543-94.
396. Saier, M.H., Jr., *The Bacterial Phosphotransferase System: New Frontiers 50 Years after Its Discovery.* J Mol Microbiol Biotechnol, 2015. **25**(2-3): p. 73-8.
397. Pessin, J.E. and G.I. Bell, *Mammalian facilitative glucose transporter family: structure and molecular regulation.* Annu Rev Physiol, 1992. **54**: p. 911-30.
398. Mueckler, M., *Facilitative glucose transporters.* Eur J Biochem, 1994. **219**(3): p. 713-25.
399. Bone, W., et al., *Effect of ornidazole on fertility of male rats: inhibition of a glycolysis-related motility pattern and zona binding required for fertilization in vitro.* J Reprod Fertil, 2000. **118**(1): p. 127-35.
400. Gatenby, R.A. and R.J. Gillies, *Why do cancers have high aerobic glycolysis?* Nat Rev Cancer, 2004. **4**(11): p. 891-9.
401. Ramanathan, R., et al., *Covalent binding of 4-hydroxy-2-nonenal to lactate dehydrogenase decreases NADH formation and metmyoglobin reducing activity.* J Agric Food Chem, 2014. **62**(9): p. 2112-7.
402. Tilton, W.M., et al., *Regulation of glycolysis in the erythrocyte: role of the lactate/pyruvate and NAD/NADH ratios.* J Lab Clin Med, 1991. **118**(2): p. 146-52.
403. Denton, R.M., et al., *Regulation of mammalian pyruvate dehydrogenase.* Mol Cell Biochem, 1975. **9**(1): p. 27-53.
404. Rich, P.R., *The molecular machinery of Keilin's respiratory chain.* Biochem Soc Trans, 2003. **31**(Pt 6): p. 1095-105.
405. Porter, R.K. and M.D. Brand, *Mitochondrial proton conductance and H+/O ratio are independent of electron transport rate in isolated hepatocytes.* Biochem J, 1995. **310 (Pt 2)**: p. 379-82.
406. Bartolome, F. and A.Y. Abramov, *Measurement of mitochondrial NADH and FAD autofluorescence in live cells.* Methods Mol Biol, 2015. **1264**: p. 263-70.
407. Schwartz, J.P., et al., *The effect of growth conditions on NAD+ and NADH concentrations and the NAD+:NADH ratio in normal and transformed fibroblasts.* J Biol Chem, 1974. **249**(13): p. 4138-43.
408. Yagi, T. and Y. Hatefi, *Thiols in oxidative phosphorylation: inhibition and energy-potentiated uncoupling by monothiol and dithiol modifiers.* Biochemistry, 1984. **23**(11): p. 2449-55.

409. Yagi, T. and Y. Hatefi, *Thiols in oxidative phosphorylation: thiols in the F0 of ATP synthase essential for ATPase activity.* Arch Biochem Biophys, 1987. **254**(1): p. 102-9.
410. Schinder, A.F., et al., *Mitochondrial dysfunction is a primary event in glutamate neurotoxicity.* J Neurosci, 1996. **16**(19): p. 6125-33.
411. White, R.J. and I.J. Reynolds, *Mitochondrial depolarization in glutamate-stimulated neurons: an early signal specific to excitotoxin exposure.* J Neurosci, 1996. **16**(18): p. 5688-97.
412. Izyumov, D.S., et al., *"Wages of fear": transient threefold decrease in intracellular ATP level imposes apoptosis.* Biochim Biophys Acta, 2004. **1658**(1-2): p. 141-7.
413. Vander Heiden, M.G., et al., *Bcl-xL prevents cell death following growth factor withdrawal by facilitating mitochondrial ATP/ADP exchange.* Mol Cell, 1999. **3**(2): p. 159-67.
414. Buki, A., et al., *Cytochrome c release and caspase activation in traumatic axonal injury.* J Neurosci, 2000. **20**(8): p. 2825-34.
415. Forkink, M., et al., *Complex I and complex III inhibition specifically increase cytosolic hydrogen peroxide levels without inducing oxidative stress in HEK293 cells.* Redox Biol, 2015. **6**: p. 607-616.
416. Hill, B.G., et al., *Regulation of vascular smooth muscle cell bioenergetic function by protein glutathiolation.* Biochim Biophys Acta, 2010. **1797**(2): p. 285-95.
417. Puntel, R.L., et al., *Mitochondrial electron transfer chain complexes inhibition by different organochalcogens.* Toxicol In Vitro, 2013. **27**(1): p. 59-70.
418. Puntel, R.L., et al., *Organochalcogens inhibit mitochondrial complexes I and II in rat brain: possible implications for neurotoxicity.* Neurotox Res, 2013. **24**(2): p. 109-18.
419. Yokomizo, C.H., et al., *Effects of Trichlorotelluro-dypnones on Mitochondrial Bioenergetics and Their Relationship to the Reactivity with Protein Thiols.* Chem Res Toxicol, 2015. **28**(6): p. 1167-75.
420. Benz, R., *Permeation of hydrophilic solutes through mitochondrial outer membranes: review on mitochondrial porins.* Biochim Biophys Acta, 1994. **1197**(2): p. 167-96.
421. Mannella, C.A., *The 'ins' and 'outs' of mitochondrial membrane channels.* Trends Biochem Sci, 1992. **17**(8): p. 315-20.
422. Henry-Mowatt, J., et al., *Role of mitochondrial membrane permeabilization in apoptosis and cancer.* Oncogene, 2004. **23**(16): p. 2850-60.
423. Shaw, R.J., et al., *The tumor suppressor LKB1 kinase directly activates AMP-activated kinase and regulates apoptosis in response to energy stress.* Proc Natl Acad Sci U S A, 2004. **101**(10): p. 3329-35.
424. Lum, J.J., et al., *Growth factor regulation of autophagy and cell survival in the absence of apoptosis.* Cell, 2005. **120**(2): p. 237-48.
425. Murray, H.D., D.A. Schneider, and R.L. Gourse, *Control of rRNA expression by small molecules is dynamic and nonredundant.* Mol Cell, 2003. **12**(1): p. 125-34.
426. Gaal, T., et al., *Transcription regulation by initiating NTP concentration: rRNA synthesis in bacteria.* Science, 1997. **278**(5346): p. 2092-7.
427. Purdy, M.A., et al., *Effect of growth phase and cell envelope structure on susceptibility of Salmonella typhimurium to the lactoperoxidase-thiocyanate-hydrogen peroxide system.* Infect Immun, 1983. **39**(3): p. 1187-95.
428. Wang, J., et al., *Intracellular adenosine triphosphate delivery enhanced skin wound healing in rabbits.* Ann Plast Surg, 2009. **62**(2): p. 180-6.
429. Wang, J., et al., *Intracellular delivery of adenosine triphosphate enhanced healing process in full-thickness skin wounds in diabetic rabbits.* Am J Surg, 2010. **199**(6): p. 823-32.

430. Grisham, M.B. and E.M. Ryan, *Cytotoxic properties of salivary oxidants.* Am J Physiol, 1990. **258**(1 Pt 1): p. C115-21.
431. Roos, G. and J. Messens, *Protein sulfenic acid formation: from cellular damage to redox regulation.* Free Radic Biol Med, 2011. **51**(2): p. 314-26.
432. Barrett, T.J. and C.L. Hawkins, *Hypothiocyanous acid: benign or deadly?* Chem Res Toxicol, 2012. **25**(2): p. 263-73.
433. Kalyanaraman, B., et al., *Measuring reactive oxygen and nitrogen species with fluorescent probes: challenges and limitations.* Free Radic Biol Med, 2012. **52**(1): p. 1-6.
434. Jensen, E.C., *Use of fluorescent probes: their effect on cell biology and limitations.* Anat Rec (Hoboken), 2012. **295**(12): p. 2031-6.
435. Krafft, C., *Bioanalytical applications of Raman spectroscopy.* Anal Bioanal Chem, 2004. **378**(1): p. 60-2.
436. Baker, M.J., et al., *Using Fourier transform IR spectroscopy to analyze biological materials.* Nat Protoc, 2014. **9**(8): p. 1771-91.
437. Shaw, R.A., et al., *Analysis of biomedical spectra and images: from data to diagnosis.* Journal of Molecular Structure: THEOCHEM, 2000. **500**(1–3): p. 129-138.
438. de Carvalho, F.K., et al., *Oral aspects in celiac disease children: clinical and dental enamel chemical evaluation.* Oral Surg Oral Med Oral Pathol Oral Radiol, 2015. **119**(6): p. 636-43.
439. Tian, P., et al., *Intraoperative detection of sentinel lymph node metastases in breast carcinoma by Fourier transform infrared spectroscopy.* Br J Surg, 2015.
440. Gault, N. and J.L. Lefaix, *Infrared microspectroscopic characteristics of radiation-induced apoptosis in human lymphocytes.* Radiat Res, 2003. **160**(2): p. 238-50.
441. Gault, N., et al., *Infrared microspectroscopy study of gamma-irradiated and H2O2-treated human cells.* Int J Radiat Biol, 2005. **81**(10): p. 767-79.
442. Meade, A.D., et al., *Growth substrate induced functional changes elucidated by FTIR and Raman spectroscopy in in-vitro cultured human keratinocytes.* Anal Bioanal Chem, 2007. **387**(5): p. 1717-28.
443. Wolkers, W.F. and H. Oldenhof, *In situ FTIR studies on mammalian cells.* Journal of Spectroscopy, 2010. **24**(5): p. 525-534.
444. Kato, H., et al., *Role of tyrosine kinase activity in signal transduction by the insulin-like growth factor-I (IGF-I) receptor. Characterization of kinase-deficient IGF-I receptors and the action of an IGF-I-mimetic antibody (alpha IR-3).* J Biol Chem, 1993. **268**(4): p. 2655-61.
445. Almeida, A.M., R. Li, and S.H. Gellman, *Parallel beta-sheet secondary structure is stabilized and terminated by interstrand disulfide cross-linking.* J Am Chem Soc, 2012. **134**(1): p. 75-8.
446. Litvinov, R.I., et al., *The alpha-helix to beta-sheet transition in stretched and compressed hydrated fibrin clots.* Biophys J, 2012. **103**(5): p. 1020-7.
447. Sethuraman, A., et al., *Protein unfolding at interfaces: Slow dynamics of α-helix to β-sheet transition.* Proteins: structure, function, and bioinformatics, 2004. **56**(4): p. 669-678.
448. Miller, J.A., et al., *Oxidative refolding of insulin-like growth factor 1 yields two products of similar thermodynamic stability: a bifurcating protein-folding pathway.* Biochemistry, 1993. **32**(19): p. 5203-13.
449. Uversky, V.N., et al., *Methionine oxidation inhibits fibrillation of human α-synuclein in vitro.* FEBS Letters, 2002. **517**(1–3): p. 239-244.
450. Palaniappan, P. and V. Vijayasundaram, *FTIR study of arsenic induced biochemical changes on the liver tissues of fresh water fingerlings Labeo rohita.* Rom J Biophys, 2008. **18**: p. 135-144.

451. Zernike, F., *How I discovered phase contrast.* Science, 1955. **121**(3141): p. 345-9.
452. Onder, D., S. Zengin, and S. Sarioglu, *A review on color normalization and color deconvolution methods in histopathology.* Appl Immunohistochem Mol Morphol, 2014. **22**(10): p. 713-9.
453. Verebes, G.S., et al., *Hyperspectral enhanced dark field microscopy for imaging blood cells.* J Biophotonics, 2013. **6**(11-12): p. 960-7.
454. Bernas, T., et al., *Loss of image quality in photobleaching during microscopic imaging of fluorescent probes bound to chromatin.* J Biomed Opt, 2005. **10**(6): p. 064015.
455. Bass, H.W., et al., *Defining multiple, distinct, and shared spatiotemporal patterns of DNA replication and endoreduplication from 3D image analysis of developing maize (Zea mays L.) root tip nuclei.* Plant Mol Biol, 2015.
456. Kapuscinski, J., *DAPI: a DNA-specific fluorescent probe.* Biotech Histochem, 1995. **70**(5): p. 220-33.
457. Zhao, H., et al., *Superoxide reacts with hydroethidine but forms a fluorescent product that is distinctly different from ethidium: potential implications in intracellular fluorescence detection of superoxide.* Free Radic Biol Med, 2003. **34**(11): p. 1359-68.
458. Bindokas, V.P., et al., *Superoxide production in rat hippocampal neurons: selective imaging with hydroethidine.* J Neurosci, 1996. **16**(4): p. 1324-36.
459. Yazdani, M., *Concerns in the application of fluorescent probes DCDHF-DA, DHR 123 and DHE to measure reactive oxygen species in vitro.* Toxicol In Vitro, 2015.
460. Robaszkiewicz, A., G. Bartosz, and M. Soszynski, *Detection of 3-chlorinated tyrosine residues in human cells by flow cytometry.* J Immunol Methods, 2011. **369**(1-2): p. 141-5.
461. Mu, H., et al., *Chlorotyrosine promotes human aortic smooth muscle cell migration through increasing superoxide anion production and ERK1/2 activation.* Atherosclerosis, 2008. **201**(1): p. 67-75.
462. Gardiner, D.J., P.R. Graves, and H.J. Bowley, *Practical Raman spectroscopy*. 1989, Berlin ; New York: Springer-Verlag. viii, 157 p.
463. Franzen, L. and M. Windbergs, *Applications of Raman spectroscopy in skin research - From skin physiology and diagnosis up to risk assessment and dermal drug delivery.* Adv Drug Deliv Rev, 2015. **89**: p. 91-104.
464. Ramos, I.R., A. Malkin, and F.M. Lyng, *Current Advances in the Application of Raman Spectroscopy for Molecular Diagnosis of Cervical Cancer.* Biomed Res Int, 2015. **2015**: p. 561242.
465. Kourkoumelis, N., et al., *Advances in the in Vivo Raman Spectroscopy of Malignant Skin Tumors Using Portable Instrumentation.* Int J Mol Sci, 2015. **16**(7): p. 14554-70.
466. De Luca, A.C., K. Dholakia, and M. Mazilu, *Modulated Raman Spectroscopy for Enhanced Cancer Diagnosis at the Cellular Level.* Sensors (Basel), 2015. **15**(6): p. 13680-704.
467. Hulbert, A.J., *Life, death and membrane bilayers.* J Exp Biol, 2003. **206**(Pt 14): p. 2303-11.
468. Naumann, D., *FT-INFRARED AND FT-RAMAN SPECTROSCOPY IN BIOMEDICAL RESEARCH.* Applied Spectroscopy Reviews, 2001. **36**(2-3): p. 239-298.
469. Maiti, N.C., et al., *Raman spectroscopic characterization of secondary structure in natively unfolded proteins: alpha-synuclein.* J Am Chem Soc, 2004. **126**(8): p. 2399-408.
470. Oshokoya, O.O. and R.D. JiJi, *"Parallel factor analysis of multi-excitation ultraviolet resonance Raman spectra for protein secondary structure determination".* Anal Chim Acta, 2015. **892**: p. 59-68.
471. Hogg, P.J., *Disulfide bonds as switches for protein function.* Trends Biochem Sci, 2003. **28**(4): p. 210-4.

472. Rehani, T., A. Jonas, and A. Slungaard, *The Major Phagocyte Peroxidase-Derived Oxidant HOSCN Stimulates Gene-Specific p38 MAPK- Dependent, NF-kappa b-Mediated Activation of Tissue Factor, VCAM-1 and ICAM-1 Expression In Endothelium.* Blood, 2010. **116**(21): p. 633-633.
473. Pollak, N., C. Dolle, and M. Ziegler, *The power to reduce: pyridine nucleotides--small molecules with a multitude of functions.* Biochem J, 2007. **402**(2): p. 205-18.
474. Li, X.B., J.D. Gu, and Q.H. Zhou, *Review of aerobic glycolysis and its key enzymes - new targets for lung cancer therapy.* Thorac Cancer, 2015. **6**(1): p. 17-24.
475. Schafer, F.Q. and G.R. Buettner, *Redox environment of the cell as viewed through the redox state of the glutathione disulfide/glutathione couple.* Free Radic Biol Med, 2001. **30**(11): p. 1191-212.
476. Lin, S.J. and L. Guarente, *Nicotinamide adenine dinucleotide, a metabolic regulator of transcription, longevity and disease.* Curr Opin Cell Biol, 2003. **15**(2): p. 241-6.
477. Borg, L.A., *Effects of alloxan on the islets of langerhans: why does alloxan not stimulate insulin release?* Ups J Med Sci, 1981. **86**(2): p. 189-95.
478. Cleland, W.W., *Dithiothreitol, a New Protective Reagent for Sh Groups.* Biochemistry, 1964. **3**: p. 480-2.
479. Fonyo, A. and S.P. Bessman, *The action of oligomycin and of para-hydroxymercuribenzoate on mitochondrial respiration stimulated by ADP, arsenate and calcium.* Biochem Biophys Res Commun, 1966. **24**(1): p. 61-6.
480. Haugaard, N., et al., *The role of sulfhydryl groups in oxidative phosphorylation and ion transport by rat liver mitochrondia.* Biochim Biophys Acta, 1969. **172**(2): p. 198-204.
481. Qu, Z., et al., *NitroDIGE analysis reveals inhibition of protein S-nitrosylation by epigallocatechin gallates in lipopolysaccharide-stimulated microglial cells.* J Neuroinflammation, 2014. **11**: p. 17.
482. Nagahara, N., *Catalytic site cysteines of thiol enzyme: sulfurtransferases.* J Amino Acids, 2011. **2011**: p. 709404.
483. Kim, J.-R., et al., *Identification of Proteins Containing Cysteine Residues That Are Sensitive to Oxidation by Hydrogen Peroxide at Neutral pH.* Analytical Biochemistry, 2000. **283**(2): p. 214-221.
484. Chung, H.S., et al., *Cysteine oxidative posttranslational modifications: emerging regulation in the cardiovascular system.* Circ Res, 2013. **112**(2): p. 382-92.
485. Chiarugi, P. and F. Buricchi, *Protein tyrosine phosphorylation and reversible oxidation: two cross-talking posttranslation modifications.* Antioxid Redox Signal, 2007. **9**(1): p. 1-24.
486. den Hertog, J., A. Ostman, and F.D. Bohmer, *Protein tyrosine phosphatases: regulatory mechanisms.* FEBS J, 2008. **275**(5): p. 831-47.
487. Denu, J.M. and J.E. Dixon, *Protein tyrosine phosphatases: mechanisms of catalysis and regulation.* Curr Opin Chem Biol, 1998. **2**(5): p. 633-41.
488. Lalmanach, G., et al., *Cysteine cathepsins and caspases in silicosis.* Biol Chem, 2006. **387**(7): p. 863-70.
489. Allison, W.S., *Formation and reactions of sulfenic acids in proteins.* Accounts of Chemical Research, 1976. **9**(8): p. 293-299.
490. Percival, M.D., et al., *Inhibition of cathepsin K by nitric oxide donors: evidence for the formation of mixed disulfides and a sulfenic acid.* Biochemistry, 1999. **38**(41): p. 13574-83.
491. Winterbourn, C.C. and S.O. Brennan, *Characterization of the oxidation products of the reaction between reduced glutathione and hypochlorous acid.* Biochem J, 1997. **326 (Pt 1)**: p. 87-92.

492. Bergt, C., et al., *The myeloperoxidase product hypochlorous acid oxidizes HDL in the human artery wall and impairs ABCA1-dependent cholesterol transport.* Proc Natl Acad Sci U S A, 2004. **101**(35): p. 13032-7.
493. Poole, L.B., et al., *Fluorescent and affinity-based tools to detect cysteine sulfenic acid formation in proteins.* Bioconjug Chem, 2007. **18**(6): p. 2004-17.
494. Saurin, A.T., et al., *Widespread sulfenic acid formation in tissues in response to hydrogen peroxide.* Proc Natl Acad Sci U S A, 2004. **101**(52): p. 17982-7.
495. Das, D., P.K. De, and R.K. Banerjee, *Thiocyanate, a plausible physiological electron donor of gastric peroxidase.* Biochem J, 1995. **305 (Pt 1)**: p. 59-64.
496. Hanstrom, L., A. Johansson, and J. Carlsson, *Lactoperoxidase and thiocyanate protect cultured mammalian cells against hydrogen peroxide toxicity.* Med Biol, 1983. **61**(5): p. 268-74.
497. Brandes, N., S. Schmitt, and U. Jakob, *Thiol-based redox switches in eukaryotic proteins.* Antioxid Redox Signal, 2009. **11**(5): p. 997-1014.
498. Ishii, T., et al., *Critical role of sulfenic acid formation of thiols in the inactivation of glyceraldehyde-3-phosphate dehydrogenase by nitric oxide.* Biochem Pharmacol, 1999. **58**(1): p. 133-43.
499. Schmalhausen, E.V., et al., *Mildly oxidized GAPDH: the coupling of the dehydrogenase and acyl phosphatase activities.* FEBS Lett, 1999. **452**(3): p. 219-22.
500. Zheng, L., R.G. Roeder, and Y. Luo, *S phase activation of the histone H2B promoter by OCA-S, a coactivator complex that contains GAPDH as a key component.* Cell, 2003. **114**(2): p. 255-66.
501. Xu, R.H., et al., *Inhibition of glycolysis in cancer cells: a novel strategy to overcome drug resistance associated with mitochondrial respiratory defect and hypoxia.* Cancer Res, 2005. **65**(2): p. 613-21.
502. Leverve, X., C. Batandier, and E. Fontaine, *Choosing the right substrate.* Novartis Found Symp, 2007. **280**: p. 108-21; discussion 121-7, 160-4.
503. Yang, L., et al., *Recent advances in lipidomics for disease research.* J Sep Sci, 2015.
504. Aviram, M., *Macrophage foam cell formation during early atherogenesis is determined by the balance between pro-oxidants and anti-oxidants in arterial cells and blood lipoproteins.* Antioxid Redox Signal, 1999. **1**(4): p. 585-94.
505. Falk, E., *Pathogenesis of atherosclerosis.* J Am Coll Cardiol, 2006. **47**(8 Suppl): p. C7-12.
506. Lass, A., et al., *Lipolysis - a highly regulated multi-enzyme complex mediates the catabolism of cellular fat stores.* Prog Lipid Res, 2011. **50**(1): p. 14-27.
507. Stahl, A., *A current review of fatty acid transport proteins (SLC27).* Pflugers Arch, 2004. **447**(5): p. 722-7.
508. Altschuld, R.A., et al., *Cyclosporin inhibits mitochondrial calcium efflux in isolated adult rat ventricular cardiomyocytes.* Am J Physiol, 1992. **262**(6 Pt 2): p. H1699-704.
509. Hori, R. and J. Sugiyama, *A combined FT-IR microscopy and principal component analysis on softwood cell walls.* Carbohydrate Polymers, 2003. **52**(4): p. 449-453.
510. Boydston-White, S., et al., *Cell-cycle-dependent variations in FTIR micro-spectra of single proliferating HeLa cells: Principal component and artificial neural network analysis.* Biochimica et Biophysica Acta (BBA) - Biomembranes, 2006. **1758**(7): p. 908-914.
511. Ashby, M.T. and H. Aneetha, *Reactive sulfur species: aqueous chemistry of sulfenyl thiocyanates.* J Am Chem Soc, 2004. **126**(33): p. 10216-7.
512. Oh, J., et al., *Endoplasmic reticulum stress controls M2 macrophage differentiation and foam cell formation.* J Biol Chem, 2012. **287**(15): p. 11629-41.

513. Banerjee, S., et al., *Fourier-transform-infrared-spectroscopy based spectral-biomarker selection towards optimum diagnostic differentiation of oral leukoplakia and cancer.* Anal Bioanal Chem, 2015.
514. Lacombe, C., et al., *Rapid screening of classic galactosemia patients: a proof-of-concept study using high-throughput FTIR analysis of plasma.* Analyst, 2015. **140**(7): p. 2280-6.
515. Botti, T.P., et al., *A comparison of the quantitation of macrophage foam cell populations and the extent of apolipoprotein E deposition in developing atherosclerotic lesions in young people: high and low serum thiocyanate groups as an indication of smoking. PDAY Research Group. Pathobiological Determinants of Atherosclerosis in Youth.* Atherosclerosis, 1996. **124**(2): p. 191-202.
516. Scanlon, C.E., et al., *Evidence for more extensive deposits of epitopes of oxidized low density lipoprotein in aortas of young people with elevated serum thiocyanate levels. PDAY Research Group.* Atherosclerosis, 1996. **121**(1): p. 23-33.
517. Nedoboy, P.E., et al., *High plasma thiocyanate levels are associated with enhanced myeloperoxidase-induced thiol oxidation and long-term survival in subjects following a first myocardial infarction.* Free Radic Res, 2014. **48**(10): p. 1256-66.
518. Wilson, A.M., M.C. Ryan, and A.J. Boyle, *The novel role of C-reactive protein in cardiovascular disease: risk marker or pathogen.* Int J Cardiol, 2006. **106**(3): p. 291-7.
519. Fink, B., et al., *Detection of intracellular superoxide formation in endothelial cells and intact tissues using dihydroethidium and an HPLC-based assay.* Am J Physiol Cell Physiol, 2004. **287**(4): p. C895-902.
520. Whiteman, M., et al., *Do mitochondriotropic antioxidants prevent chlorinative stress-induced mitochondrial and cellular injury?* Antioxid Redox Signal, 2008. **10**(3): p. 641-50.